THERMAL HOMOGENEITY AND ENERGY EFFICIENCY IN SINGLE SCREW EXTRUSION OF POLYMERS

J.Vera-Sorroche

PhD

UNIVERSITY OF BRADFORD

2014

THERMAL HOMOGENEITY AND ENERGY EFFICIENCY IN SINGLE SCREW EXTRUSION OF POLYMERS

The use of in-process metrology to quantify the effects of process conditions, polymer rheology, screw geometry and extruder scale on melt temperature and specific energy consumption

Javier Vera-Sorroche

Submitted for the degree of Doctor of Philosophy

Faculty of Engineering and Informatics

University of Bradford

2014

to my parents

Carmen Sorroche-López and Mariano Vera-Mula

my brother and Sonia Graser

THERMAL HOMOGENEITY AND ENERGY EFFICIENCY IN SINGLE SCREW EXTRUSION OF POLYMERS

Javier VERA-SORROCHE

Keywords: Polymer extrusion, infrared thermometry, rheology, scale up, melt temperature measurement, extruder screw geometry, energy efficiency, thermocouple

Abstract

Polymer extrusion is an energy intensive process whereby the simultaneous action of viscous shear and thermal conduction are used to convert solid polymer to a melt which can be formed into a shape. To optimise efficiency, a homogeneous melt is required with minimum consumption of process energy. In this work, in-process monitoring techniques have been used to characterise the thermal dynamics of the single screw extrusion process with real-time quantification of energy consumption. Thermocouple grid sensors were used to measure radial melt temperatures across the melt flow at the entrance to the extruder die. Moreover, an infrared sensor flush mounted at the end of the extruder barrel was used to measure non-invasive melt temperature profiles across the width of the screw channel in the metering section of the extruder screw. Both techniques were found to provide useful information concerning the thermal dynamics of the extrusion process; in particular this application of infrared thermometry could prove useful for industrial extrusion process monitoring applications.

Extruder screw geometry and extrusion variables should ideally be tailored to suit the properties of individual polymers but in practise this is rarely achieved due the lack of understanding. Here, LDPE, LLDPE, three grades of HDPE, PS, PP and PET were extruded using three geometries of extruder screws at several set temperatures and screw rotation speeds.

Extrusion data showed that polymer rheology had a significant effect on the thermal efficiency on the extrusion process. In particular, melt viscosity was found to have a significant effect on specific energy consumption and thermal homogeneity of the melt.

Extruder screw geometry, set extrusion temperature and screw rotation speed were also found to have a direct effect on energy consumption and melt consistency. Single flighted extruder screws exhibited poorer temperature homogeneity and larger fluctuations than a barrier flighted screw with a spiral mixer. These results highlighted the importance of careful selection of processing conditions and extruder screw geometry on melt homogeneity and process efficiency.

Extruder scale was found to have a significant influence on thermal characteristics due to changes in surface area of the screw, barrel and heaters which consequently affect the effectiveness of the melting process and extrusion process energy demand. In this thesis, the thermal and energy characteristics of two single screw extruders were compared to examine the effect of extruder scale and processing conditions on measured melt temperature and energy consumption. Extrusion thermal dynamics were shown to be highly dependent upon extruder scale whilst specific energy consumption compared more favourably, enabling prediction of a process window from lab to industrial scale within which energy efficiency can be optimised.

Overall, this detailed experimental study has helped to improve understanding of the single screw extrusion process, in terms of thermal stability and energy consumption. It is hoped that the findings will allow those working in this field to make more informed decisions regarding set conditions, screw geometry and extruder scale, in order to improve the efficiency of the extrusion process.

Conferences and papers

Abeykoon C., Kelly A.L., Brown E.C., Vera-Sorroche J., Coates P.D., Harkin-Jones E., Howell K.B., Deng J., Li K and Price M. (2014) "Investigation of the process energy demand in polymer extrusion: A brief review and an experimental study" *Applied Energy,**136** 726-737*

Abeykoon C., Kelly A.L., Vera-Sorroche J., Brown E.C., Coates P.D., Deng J., Li K Harkin-Jones E and Price M. (2014) "Process efficiency in polymer extrusion: Correlation between the energy demand and melt thermal stability" *Applied Energy,**135** 560-571*

Vera-Sorroche J., Kelly A.L., Brown E.C and Coates P.D. (2014) "Infrared melt temperature measurement of single screw extrusion "*Polymer Engineering & Science;* accepted in press

Abeykoon C., Kelly A.L., Vera-Sorroche J., Brown E.C and Coates P.D. (2014) "Monitoring and Modelling of the Energy Consumption in Polymer Extrusion" *European Control Conference (ECC*), *June 24-27*

Deng J., Li K., Harkin-Jones E., Price M., Karnachi N., Kelly A.L., Vera-Sorroche J., Coates P.D., Brown E.C and Fei M. (2014) " Energy monitoring and quality control of a single screw extruder" *Applied Energy, **113** 1775-1785*

Deng J., Li K., Harkin-Jones E., Price M., Fei M., Kelly A.L., Vera-Sorroche J., Coates P.D and Brown E.C. (2014) "Low-cost process monitoring for polymer extrusion" *Transactions of the Institute of Measurement and Control,**36**(3)382-390*

Vera-Sorroche J., Kelly A.L., Brown E.C., Gough T., Abeykoon C., Coates P.D., Deng J., Li K., Harking-Jones E and Price M. (2014) "The Effect of Melt Viscosity on Thermal Efficiency for Single Screw Extrusion", *Chemical Engineering Research and Design, **92** (11) 2404-2412*

Abeykoon C., Kelly A.L., Vera-Sorroche J., Brown E.C and Coates P.D. (2013) "Investigation of Correlations between Process Thermal Stability and Energy Demand in Polymer Extrusion" *International Conference of the Polymer Processing Society (PPS)", paper No: 486*

Vera-Sorroche J., Abeykoon C., Kelly A.L., Brown E.C and Coates P.D. (2013) "The Effect of Molecular Weight on Thermal Efficiency for Single Screw Extrusion of HDPE" *International Conference of the Polymer Processing Society (PPS)", paper No: 485*

Vera-Sorroche J., Kelly A.L., Brown E.C., Coates P.D., Karnachi N., Harking-Jones E., Li K and Deng J. (2013) "Thermal optimisation of polymer extrusion using in-process monitoring techniques", *Applied Thermal Engineering, **53** (2) 405-413*

Vera-Sorroche J., Kelly A.L., Brown E.C and Coates P.D. (2012) "Monitoring of Thermal Homogeneity in Single Screw Extrusion using Infrared Temperature Sensors" *Annual Technical Conference of the Society of Plastics Engineers (SPE ANTEC), 2172-2179*

Kelly A.L., Vera-Sorroche J., Brown E.C and Coates P.D. (2012) "Improving Thermal Efficiency of Single Screw Extrusion" *Annual Technical Conference of the Society of Plastics Engineers (SPE ANTEC), 1080-1088*

Vera-Sorroche J., Kelly A.L., Brown E.C., Coates P.D., Karnachi N., Harking-Jones E., Li K and Deng J. (2011) "Thermal optimisation of polymer extrusion using in-process monitoring techniques" *Sustainable Thermal Energy Management in the Process Industries (SusTEM), 301-309*

Karnachi N., Harkin-Hones E., Price M., Li K., Kelly A.L., Brown E.C., Coates P.D and Vera-Sorroche J. (2011) "A holistic Approach for Energy Management in Polymer Processing Industry" *Polymer Process Engineering (PPE),16-41*

Table of Contents

List of Figures

List of Tables

List of Abbreviations

A	Surface area of each heater
a	width of the transition between the zero shear viscosity region and the power law region
AC	Alternative current
BF	Barrier flighted screw
c	Screw clearance
CM	Continuous mixer
$C_{p,air}$	Specific heat capacity of air
C_p	Specific heat capacity
C_s	Specific heat of the solid bed at its average temperature and pressure
D	Barrel diameter
Ds	Screw diameter
D_1	Diameter of small extruder
D_2	Diameter of large extruder
DC	Direct current
DSC	Differential scanning calorimeter
e	Screw flight width
e	Equivalent length of die that represents the extra entrance pressure drop
ECT	Electrical capacitance tomography
EMF	Electromotive force
F_d	Feed section depth
FV	Free volume
h	Flight depth
h_d	Channel depth
h_1	Enthalpy of feed material
h_2	Enthalpy of the final product
h_f	Feed depth
h_m	Metering depth
H_1	Channel depth of small extruder
H_2	Channel depth of large extruder
H_1	Channel height in feed section

H_2	Channel height in metering section
HD	High density
HDPE	High density polyethylene
HSR	High stress region
Hz	Hertz
I	Current
IR	Infra-red
kg	Kilograms
kW	Kilowatts
LDPE	Low density polyethylene
LLDPE	Linear low density polyethylene
L_a	Length of the screw axis
$\underline{L}$	Pitch
L	Barrel length
L_h	Length of the heating element
L_o	Screw axis length in compression section
L_1	Screw axis length in feed section
L_2	Screw axis length in metering section
L_{die}	Die length
M	Axial length
MFI	Melt flow index
$\dot{m}_{air}$	Mass air flow
$\dot{M}_{p1}$	Plasticating capacity of small extruder
$\dot{M}_{s1}$	Solid conveying rate of small extruder
$\dot{M}_{p2}$	Plasticating capacity of large extruder
$\dot{M}_{s2}$	Solid conveying rate of large extruder
NMR	Nuclear magnetic resonance
N	Screw speed
n	Power law index
N_1	Screw speed of small extruder
N_2	Screw speed of large extruder
N_{cool}	Number of cooling fans
N_h	Number of heaters

PET	Polyethylene terephthalate
P	Power consumption over the entire length of the screw
PA6	Polyamide 6
P_{cool}	Energy removed from the cooling system
P_h	Thermal energy from the heaters
P_h	Power consumption of the heaters
P_{in}	Input energy
P_{loss}	Net of the energy losses
P_m	Mechanical energy provided by the drive motor and imparted to the polymer by the rotational motion of the screw
P_{out}	Output energy
P_{th}	Theoretical power required in an extruder
PP	Polypropylene
PS	Polystyrene
PVC	Polyvinyl chloride
Q	Volumetric flow rate
r	Viscous relaxation time
SBAP	Solid bed acceleration parameter
SCR	Silicon control rectified
SEDC	Separately excited current motor
SMEs	Small and medium-sized enterprises
ST	Stepped compression screw
TA	Tapered compression screw
TC	Thermocouple
T_b	Temperature of the barrel surface
T_{cf}	Critical flow temperature
T_{ex}	Extrusion temperature
T_m	Melting point of the plastic
T_r	Initial temperature of the barrel surface
T_{ro}	Room temperature
t_1	Residence time of small extruder
t_2	Residence time of large extruder
U_z	Velocity of fluid in z direction

$\dot{V}_1$	Output rate of small extruder
V_{sy}	Velocity of the solid face into the interface
V_{bx}	Velocity of the barrel in x direction
V_{b1}	Circumferential speed
$\dot{V}_2$	Output rate of large extruder
V_{b2}	Circumferential speed of large extruder
W	Width of the screw channel
W_1	Channel width of small extruder
W_2	Channel width of large extruder
$\dot{W}_f$	Power consumption in the feed section
$\dot{W}_c$	Power consumption in the compression section
$\dot{W}_m$	Power consumption in the metering section
X	Width of the solid bed
X_c	Degree of crystallinity
Z_0	Screw channel depth in compression section
Z_1	Screw power of small extruder
$\bar{Z}_1$	Screw channel depth in feed section
$\hat{Z}_1$	Specific energy consumption of small extruder
Z_2	Screw power of large extruder
$\bar{Z}_2$	Screw channel depth in metering section
$\hat{Z}_2$	Specific energy consumption of large extruder
δ	Film thickness
θ_b	Helix angle
ω	Rate of melting per unit length in the down channel
ΔV_b	Vector substraction, defined as the difference between velocity of the barrel and velocity of the solid bed in z direction
ρ_m	Density of the melt at the average temperature and pressure of the molten film
μ	Apparent viscosity of the melt at the average temperature and pressure of the molten film, and at a shear rate calculated at average thickness of the latter
$\dot{\gamma}_1$	Shear rate of small extruder
$\dot{\gamma}_2$	Shear rate of large extruder

ρ_r	Resistivity of the heater
ΔT	Variation of temperature
Δ_{hf}	Heat of fusion
ΔP	Pressure rise
$\bar{\mu}$	Average viscosity
φ	Helix angle
δ	Screw flight clearance
θ	Helix angle of the screw
ϕ	Inclination angle in metering section of the screw channel
τ_ω	Apparent wall shear stress
ΔP_{die}	Pressure drop along the capillary
$\dot{\gamma}_w$	Apparent wall shear rate
η_o	Zero-shear viscosity
η_h	Viscous heting
ΔH_m	Enthalpy of melting
ΔH_o	Theoretical enthalpy of melting
J/g	Joule per gram
β	Coefficient of temperature sensitivity

Acknowledgments

I would first like to thank Professor Phil Coates for giving me the opportunity to work with him and his group. I would also like to express my deepest thanks to my two supervisors, Dr. Adrian Kelly and Dr. Elaine Brown. Their advice and support were key motivations throughout my PhD.

I wish to thank sincerely Dr. Tim Gough for his constant support and co-operation.

Special thanks to Mr. Steve Brook, Mr. Ken Howell, Mr. Glen Thompson and Mr. John Wyborn for their technical assistance.

I would like to thank the Engineering and Physical Sciences Research Council, for providing me the funding which allowed me to undertake this research work.

Thanks to Cayetano and colleagues: Gabriela, Dimitris, Bushra, Emma and Max.

CHAPTER ONE

1.1 Introduction

Consumption of polymeric materials has greatly increased over the past few decades due to their use in diverse industrial sectors. Plastics are in high demand in the packaging, construction, automotive, electrical and electronics industries, in addition to many other diverse applications. The extruder is arguably the single most important piece of polymer processing machinery. Single screw extruders are controlled by setting barrel and die temperatures and screw rotation speed. The quality of extruded polymer is highly dependent upon the homogeneity of the molten polymer being fed into the die, which should ideally be supplied at a constant pressure, temperature and throughput.

Melt temperature is important for achieving a successful extrusion process as it has a significant impact on product quality. However, most extruders are commonly supplied with thermocouples flush mounted at the extruder die wall which are shown to provide a melt measurement strongly affected by temperature of the metal wall (Yazbaz & Diraddo, 1993, Sabota et al., 1995). These sensors measure a point or bulk melt temperature and therefore do not provide detailed information of the melt temperature across the die channel. One of the aims of this work was to assess the thermal dynamics of the extrusion process using advanced melt temperature techniques such as thermocouple grid sensors and infrared thermometry. Thermocouple grid sensors allowed measurements of radial melt temperature profiles and levels of temperature variation across the die flow path. Infrared thermometry was used to measure melt temperature across the width of the screw channel at the end of the extruder barrel. The rapid dynamic response of both techniques provided information relating to short term melt temperature changes, allowing examination of the thermal homogeneity of the extrusion process.

Variations in melt temperature that occur when the extruder is operated at high throughputs have been reported to be associated with melting instabilities. Screw design has been found to have a direct effect on melt homogeneity and hence quality of the final product (Kelly et al., 2006). Extrusion variables should be then tailored to suit the performance of each individual extruder screw and polymer being processed.

In this thesis, three screw geometries and three set temperatures were used for each material at different screw rotation speeds to examine the effect of processing conditions on extrusion performance.

Historically, there has been little interest in operating with process energy consumption in mind and as a result extruders were not commonly equipped with energy monitoring equipment. This has led to poor understanding of the links between processing conditions and energy consumption. In this work, energy meters were used to monitor in real-time quantification of energy consumption. These energy measurements combined with measured temperatures from the thermocouple mesh and the infrared sensor allowed investigation of the thermal efficiency of the process.

In single screw extrusion, the viscosity of the polymer generally exhibits non-Newtonian pseudoplastic flow behaviour. It has been reported that examination of the viscous behaviour is essential to assess better polymer processability, leading to optimal extruder screw designs and improved process stability (Giles et al., 2005, Eslami, 2014).

In this thesis, the effect of polymer rheology on the thermal dynamics and specific energy consumption of the extrusion process was examined using a wide range of polymer types such as LDPE, LLDPE, three grades of HDPE, PS, PP and PET to gain sound knowledge of rheological properties and their relationship to the process.

Extruder scale is important due to the need to transfer optimised extrusion processing conditions from laboratory scale to industrial production, maintaining the same extrusion performance. Here, two single screw extruders of different screw diameter were used to investigate extrusion scale and quantify its effect on melt quality and energy consumption.

This reported study forms part of a wider research project which aimed to provide the polymer industry with an energy management tool to optimise energy use and quality in extrusion.

1.2 Aims and Objectives

The main aim of this work was to use in-process monitoring techniques to characterise the thermal dynamics of the extrusion process combined with real-time quantification of energy consumption in an attempt to investigate the thermal efficiency in single screw extrusion of polymers. The overall objectives of this research were to:

1. Employ real-time melt temperature techniques, such as a thermocouple grid sensor and an infrared temperature sensor to provide quantification of the thermal homogeneity of the single screw extrusion process.

2. Attempt to prove that infra-red thermometry could be particularly suited to use in production applications.

3. Monitor real-time quantification of energy consumption using energy meters.

4. Examine the effects of extruder screw geometry, set extrusion temperatures and screw rotation speeds on measured melt temperatures and energy consumption.

5. Investigate the effect of polymer rheology and thermal properties on process energy consumption and thermal extrusion performance.

6. Examine the effect of extruder scale on the effectiveness of the melting process, its direct influence on melt homogeneity, and extrusion process energy demand.

1.3 Scope of Research

This thesis is divided into eight chapters. Chapter 2 introduces classification, production and application of polymers to provide general information relevant to the research carried out, including fundamental principles of polymer extrusion. This chapter focuses on single screw extrusion and details the basic components of the extruder. Extruder screw geometries are described in detail, with particular attention paid to examine the differences in design between non-barrier and barrier screws and their effect on the melting performance. Critical reviews of relevant research concerning melt temperature measurements and melting mechanisms are given throughout the chapter to examine the level of detailed thermal information provided by these sensors and describe the most important analysis of the polymer behaviour in the plasticating zone of the extruder. A review of the scale-up factors for single screw extrusion is also presented to examine the efficiency of the existing methods and their inherent problems in terms of extrusion process performance. Additionally, an analysis of the energy consumption in single screw extrusion is given to highlight its dependence upon set processing conditions and screw geometry. Finally, an examination of the rheological and thermal properties of polymers is provided. Capillary rheometry and Differential Scanning Calorimetry are described in detail. The importance of polymer rheology and thermal analysis on the extrusion performance is highlighted.

Chapter 3 describes the polymers processed during the experimental work, and provides information regarding their structure and applications. This chapter details the equipment and experimental procedure carried out in this work. A Davis Standard BC60 with screw diameter 63.5mm and a Davis Standard Betol BK38 with screw diameter 38mm were used in this study. An instrumented die adaptor used to monitor in real-time temperature and pressure is described, with temperature and pressure measurements and energy meters. Set temperatures used for each material are detailed, with schematic representations of the screw designs used in both extrusion processes. In addition, rheological and thermal characterisation techniques are also described.

Rheological results and thermal properties of the polymers used throughout this work are presented and discussed in chapter 4. A comparison of shear viscosity for each polymer at three set temperatures is made, together with quantification of shear and temperature sensitivity. Extrusion measurements on the large scale extruder are presented and discussed to show the effects of extruder screw geometry, set extrusion temperatures, screw rotation speeds, polymer rheology and thermal properties on throughput, measured melt temperatures, melt homogeneity, die pressure, and energy consumptions for the process, motor and heaters/cooling fans.

Extrusion measurements on the small scale extruder are presented and discussed in chapter 5. These results are also used to show the effects of extruder screw geometry, set extrusion temperatures, screw rotation speeds, polymer rheology and thermal properties on throughput, measured melt temperatures, melt homogeneity, die pressure, and energy consumptions for the process, motor and heaters/cooling fans. In addition, a comparison between the extrusion measurements on large and small scale extruders is provided to discuss the effect of extruder scale on temperature and energy measurements.

Infrared measurements made in the large and small scale extruder are presented in chapter 6, to show the suitability of infra-red thermometry to quantify the thermal dynamics of single screw extrusion. The effect of extruder screw geometry, set extrusion temperatures, screw rotation speeds, polymer type and extruder scale on the measured infrared temperature are examined.

Finally, overall conclusions are presented in chapter 7, with recommendations for further work.

CHAPTER TWO

2 BACKGROUND AND LITERATURE REVIEW

2.1 Introduction

In this section background information about polymers and their classification is provided according to their thermal processing behaviour in order to relate this information to polymer microstructure and its thermo-responsive characteristics. An analysis of the latest European plastics production and demand is also presented to highlight the major uses of polymers and their applications in the present market. In addition, fundamental principles of single screw extrusion are presented, providing information of the equipment and its basic components and the role that screw design plays on extrusion performance. Finally, critical reviews of melt temperature measurement methods, melting and extruder scale are given in conjunction with an evaluation of the energy consumption of the extrusion process. Moreover, polymer melt rheology and thermal properties of polymers are discussed.

2.2 Polymers and classification

A polymer is a long-chained molecule that is built up from smaller units (monomers) covalently bonded together. The architecture of the large molecule is a complex molecular structure that can vary extensively depending on chemistry, molecular composition and structure, crystallisation behaviour and processing characteristics.

Depending on their thermal processing behaviour polymers are most commonly classified as thermoplastics and thermosetting materials. The architecture of thermoplastic materials is linear or slightly branched in which the molecules are bonded by relatively weak intermolecular forces. Examples of these polymers relevant to this work include polyethylene (LDPE, LLDPE and HDPE), polypropylene (PP), polystyrene (PS), polyethylene terephthalate (PET) and their molecular structures are shown in Figure 2.1.

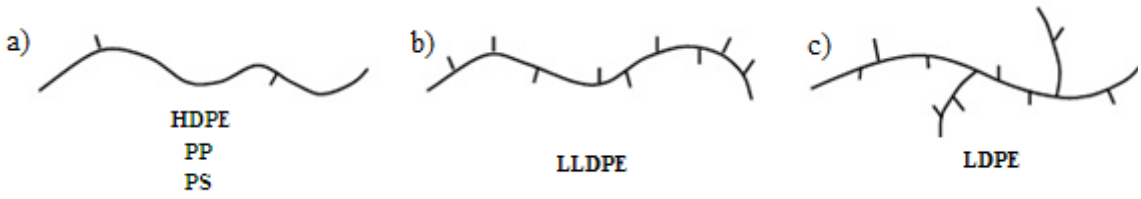

Figure 2.1 Basic molecular structures a) linear polymer chain b) high degree of short-chain branching c) high degree of short-chain branching and long-chain branching

Thermoplastics are polymers that become liquid when heated and solidify upon cooling. Due to their memory effect this cycle of heating and cooling can be repeated numerous times for reprocessing, making them widely used in a range of application such as packaging, building and construction, automotive, electrical & electronics, agriculture, etc.

Thermoplastics are grouped into three categories based on their polymer chain conformation or morphology:

A. Liquid crystalline thermoplastics: polymers that preserve their ordered molecular arrangements in both the melt and the solid states. These are extremely rigid and have a high degree of chemical resistance.

B. Semi-crystalline thermoplastics: these polymers preserve their crystal structure until the melt temperature of the material is reached, at which point the molecular structure becomes random or amorphous. Here, examples of standard semi-crystalline thermoplastics are polyethylenes (HDPE, LDPE, and LLDPE), polypropylene (PP) and engineering plastics such as polyethylene terephthalate (PET).

C. Amorphous thermoplastics: polymers that have irregular structures; upon heating their molecules become disentangled and change from a rigid solid to a viscous liquid. These polymers are softer than crystalline thermoplastics and have a lower degree of chemical resistance. Standards amorphous thermoplastics include polystyrene (PS), polyvinyl chloride (PVC), acrylonitrile butadiene styrene (ABS), etc.

Thermosetting materials are three-dimensional molecular networks with a cross-linked structure and mainly as a result of step polymerisation reactions. Once the polymerisation is completed, they reach a three dimensional insoluble network stage and become a hard and infusible material which cannot be recycled by heating. Examples of thermosetting plastics include polyurethanes and phenolic, amino, polyester, silicon and epoxy resins.

The microstructure and conformation of these polymers and their dependence on heating and cooling are shown in Figure 2.2.

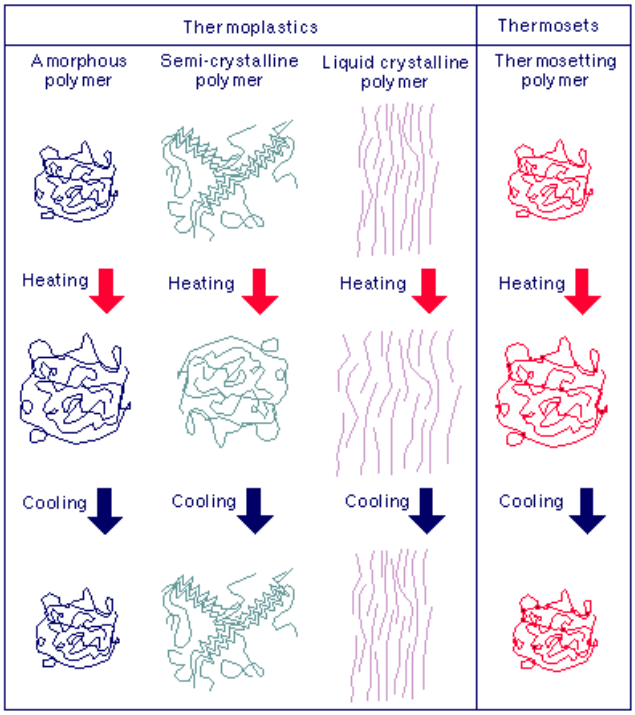

Figure 2.2 Effect of heating and cooling on the microstructures of thermoplastics and thermosetting (Classes of plastics, 2006)

2.3 Plastics production and demand

Europe ranked second in the world plastics production with 20.4% of the total production in 2012, at approximately 41.2 million tonnes (Figure 2.3). In Europe alone it is estimated that approximately 1.4 million people work in the plastics industry in over 50000 companies, many in SMEs (small and medium-sized enterprises), generating turnover in the region of 87 billion euro for plastics producers and 202 billion euro for converters.

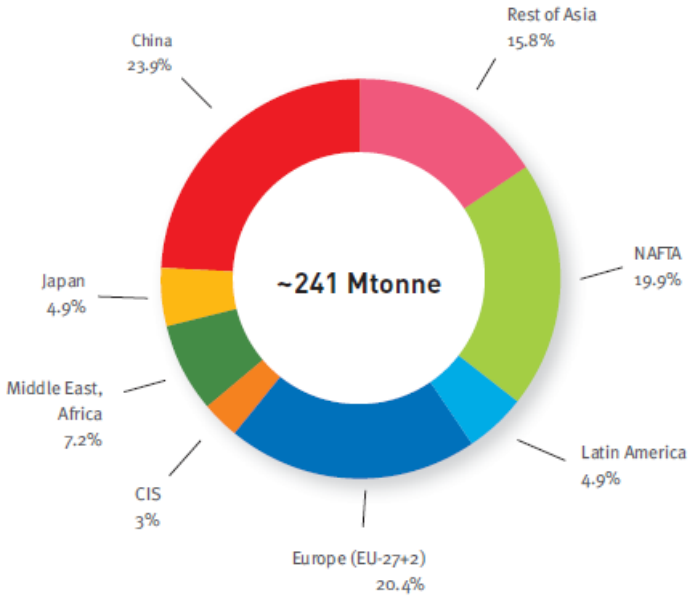

Figure 2.3 World plastics materials production 2012 (PlasticsEurope, 2013)

Thermoplastics were among the most demanded polymers in Europe with approximately 78.9 % of the European total plastics demand (Figure 2.4). Most common were the polyolefins (LDPE, LLDPE, HDPE and PP) in sectors such as packaging, building and construction, representing the highest demands in the plastics market.

With properties such as flexibility, high impact strength, light weight, stability, impermeability and easy sterilisation polyolefins are extremely versatile in their applications. Polyethylene terephthalate (PET), polystyrene (PS) and polyvinyl chloride (PVC) also had extensive demand in Europe with applications in packaging, particularly PET bottles, and building (PlasticsEurope, 2013).

However, thermosetting materials represented only 8.25% of the demand, mainly due to the lack of market for recyclates as these plastics are much harder to adapt to recycling than thermoplastics.

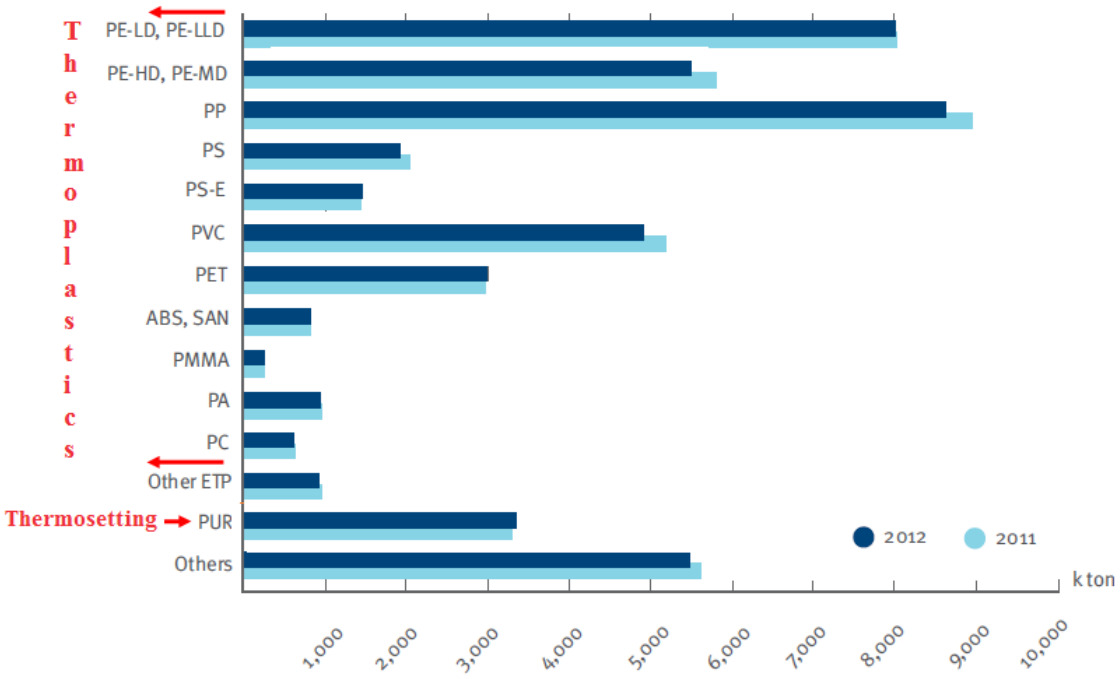

Figure 2.4 European plastics demand by polymer type

2.4 Fundamentals of polymer extrusion

Plastic extrusion is an integrated process for manufacturing finished plastic products for industrial or consumer applications, in which simultaneous operations take place to convert solid polymers to viscous masses by thermal conduction, viscous shearing and pressure.

Single and twin-screw extruders are the most widely used polymer processing machines and acknowledged as being the most important operation units. It has been reported that an optimum use of extruders will determine the quality of the final product as long as the process is run at constant melt pressure and uniform temperature and employs tailored screw geometries that suit the properties of individual polymers (Giles et al., 2005).

Single screw extruders are chosen to manufacture plastic sheets or films, pipes and profiles when virgin raw materials are generally used. Twin screw extruders are more suitable for compounding operations where achieving high level of mixing is necessary with improved performances in heat transfer and residence time distributions. When compared with twin screw extruders, single screw extruders are mechanically fairly simple, relatively easy to operate and maintain and are less expensive. In terms of production, these machines provide higher throughputs and are more energetically favourable.

Therefore, appropriate selection of single screw or twin screw technology can become a long and arduous process that will depend on the desired operation and product selection based on capital investment, maintenance, product yield and capacity.

2.4.1 Single screw extruder equipment

A single screw extruder consists basically of an Archimedean screw, driven by a variable speed motor, which is situated inside a cylindrical heated barrel with just sufficient clearance to allow its rotation. The main components of a single screw extruder include: drive and feed systems, screw, barrel and heaters, head and die assembly and control system, as shown in Figure 2.5.

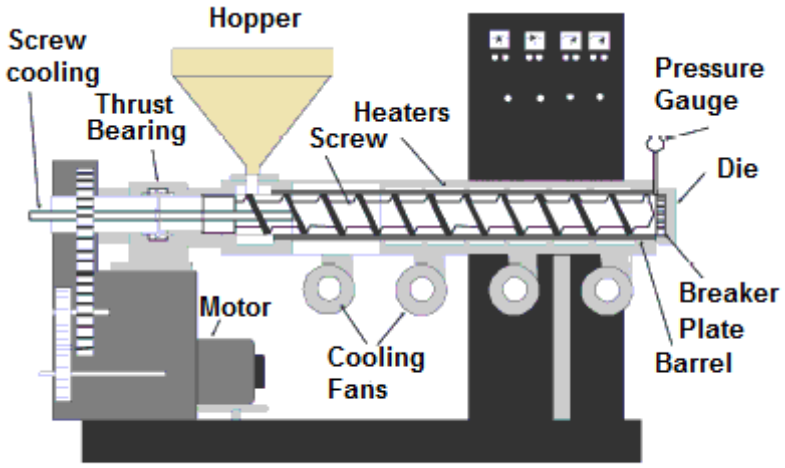

Figure 2.5 Single screw extruder (Giles et al., 2005)

2.4.1.1 Drive system

The drive system in single screw extruders compromises the motor, gear box, bull gear, and thrust bearing assembly. The principal function of the drive system consists in turning the screw at the required rotating speed, minimizing the fluctuations in screw speed and torque.

There are three basic types of drive systems that are currently used in extruders: alternating current (AC), direct current (DC) and hydraulic. Among them, DC silicon control rectified (SCR) and AC adjustable frequency drives are known to be the most widely employed by polymer extruder manufacturers (Harper & Petrie, 2003).

AC motors are used in small extruders and can generate maximum torque without having to run at maximum screw speed. DC motors are found in large scale extruders and in contrast to AC motors, these need to reach maximum screw speed to achieve peak torque (Giles et al., 2005).

2.4.1.2 Feed hopper

Feed hoppers are used to store the material that is fed into the extruder through the feed throat in either powder or granule form. Basically, there are four hopper feeding systems: flood, starve, crammer and melt (Giles et al., 2005). In flood and starve feed systems polymer feedstock flows by gravity and the hopper sits over the feed throat opening. The section of the feed throat is machined directly into the barrel and cooled by a water jacket to prevent bridging and premature melting.

Extruders are commonly operated with flood feeding systems (Figure 2.6) where the hopper is kept filled with polymer causing the throughput to be determined by screw speed. In starve feeding systems, however, the material is fed into the extruder through use of a feeder and as a result the throughput rate is controlled by the feed rate rather than screw speed.

Starve feeding requires a feeder but when compared to flood systems there is no accumulation of material in the hopper (Figure 2.7). Rauwendaal, (2001) observed that lower pressure was then generated along the extruder which reduced agglomeration and temperature, enabling broader process control. However, starve feeding was reported to be more favourable only when used on large extruders.

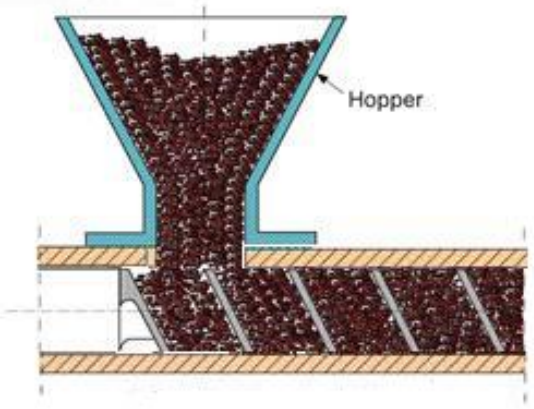

Figure 2.6 Flood feeding (Rauwendaal, 2010)

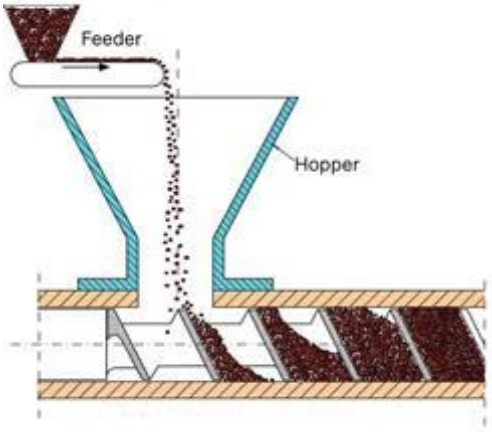

Figure 2.7 Starve feeding (Rauwendaal, 2010)

In crammer feeding systems a screw mechanism is incorporated and mounted vertically in the hopper to force the raw material into the extruder (Figure 2.8). While increasing throughput rates special caution should be taken during start-up of the extruder to prevent overfeeding (Giles et al., 2005).

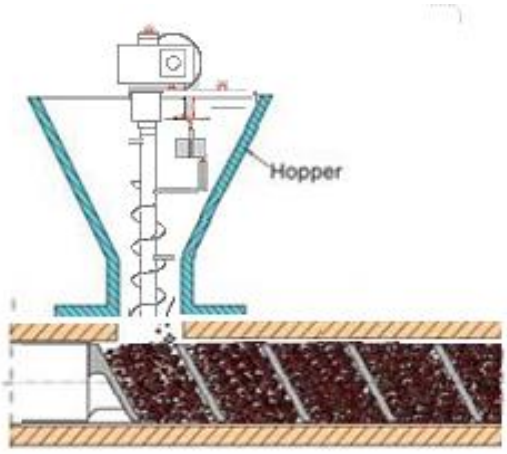

Figure 2.8 Crammer feeding system (Rauwendaal, 2010)

Melt feeding systems are used in post-reactor processing. Melt-fed extruders are operated with plastics that have been already melted and compounded in either a batch mixer (e.g., Banbury-type internal mixer) or a continuous mixer (CM), as shown in Figure 2.9. Melt- fed extruders are thus shorter in length as the polymer is not melted after feeding. These extruders are basically a pump that provides improved melt consistency and uniform pressures (Tadmor & Gogos, 2006).

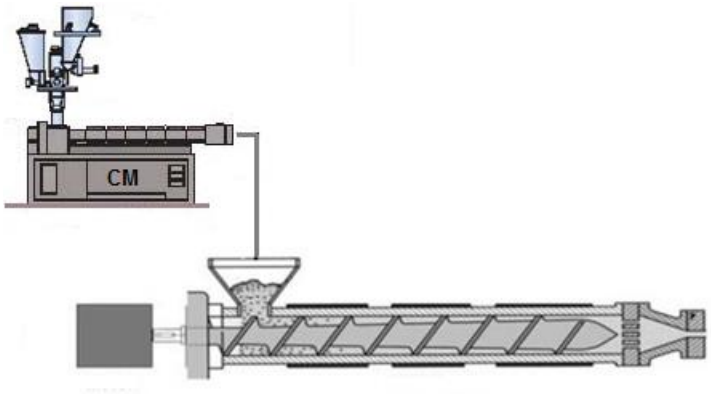

Figure 2.9 Melt-fed extruder

2.4.1.3 Screw, barrel and heaters

When material comes in contact with the screw it is dragged forward to the end of the extruder barrel where finally converges into the die and acquires its final shape. The material along the barrel is thus gradually melted, conveyed forward and mixed. These operations are achieved at three different sections of the screw: feed section, compression and metering. Compression occupies the major portion of the screw length and it is the section where melting occurs. A more detailed discussion of extruder screw geometries and melting mechanisms can be found in sections 2.5.1 and 2.7 respectively.

The melting of the polymer is carried out by heaters (external source) and internal heat from viscous energy dissipation via shearing. Therefore, it is clear that an optimal combination between screw speed and barrel set temperatures appear to be crucial for thermal optimisation of the extrusion process.

Heaters are normally placed along the barrel arranged in zones with auxiliary air cooling systems mounted under each zone (Figure 2.5). When necessary, cooling systems remove heat by blowing air over their surfaces. Besides, the ribbed spacers around the barrel provide additional surface areas that enhance the cooling effect (Figure 2.10). The heat is normally transferred into the atmosphere and rarely exploited.

Water cooling systems are used when greater heat extraction is needed. Compared to air, water is a more efficient cooling medium that exhibits greater heat transfer characteristics and control (Figure 2.10). Water cooling, however, requires recirculation and water treatments raising the price of total installation costs.

The barrel is defined as a long thick-walled tube of steel. Extruder set temperatures along the barrel are controlled with temperature sensors embedded in the wall. These measurements are made as close as possible to the inner barrel wall to allow accurate control of melt temperature. Most extruders operate with electric heating since it has been widely recognised as easy to operate, clean and maintain with lower installation costs (Rauwendaal, 1994). A critical review of melt temperature measurement methods for polymer processing will be discussed in section 2.6.1.

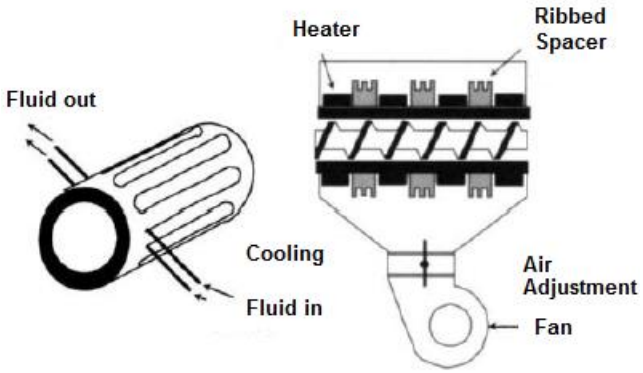

Figure 2.10 Water and air cooling systems on an extruder barrel (Giles et al., 2005)

2.4.1.4 Extrusion head assembly

The construction of the extrusion head assembly implies the use of several components such as an adaptor, die and breaker plate (Figure 2.11). The adaptor is used to connect the die assembly to the extruder barrel.

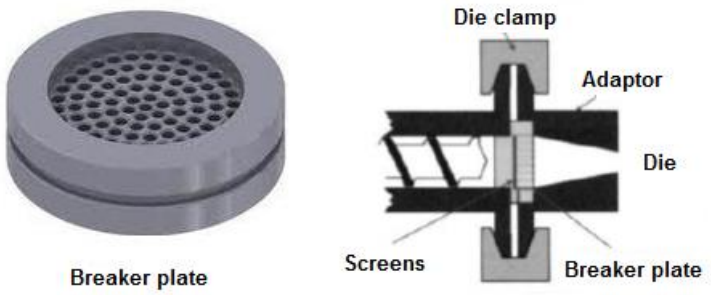

Figure 2.11 Extruder head assembly (Giles et al., 2005)

The extrusion head assembly is of paramount importance to the entire extrusion process. Giles et al., (2005) reported that an efficient design of the head assembly enabled manufacturing process improvements such as desired cross-section at the specified rate, good melt homogeneity and lower pressure drops.

The extrusion head assembly contains three functional zones: the entrance, the adaptor (or transition zone) and the parallel zone. In the entrance zone, a breaker plate is inserted between the end of the extruder and the die assembly. The breaker plate is a round thick disk which contains many holes. The breaker plate is used to arrest the spiralling motion of the flow and convert it into axial flow to prevent the extrudate distortion. It improves melt quality by filtering contaminants and unmolten polymer and enables a better mixing capability by increasing back pressure (Reliance, 2012) . The filtration is accomplished by placing screens in front of the breaker plate such as wire mesh or metal fibres.

In the adaptor (or transition zone), the circular cross-section of the channel gradually reaches the shape of the die lips. The melt acquires its final shape at the parallel zone, a location before the exit die that enables control on the degree of die swell and polymer melt temperature (Covas & Stevens, 1995).

2.4.1.5 Control system

Process control allows easy optimisation of the extrusion process by selecting appropriate operating conditions, such as barrel temperature, extruder load, screw speed, melt temperature and pressure. Advanced control techniques based on empirical models and linear approaches have been shown to facilitate opportunities to the plastics industry to improve both quality and energy efficiency (Abeykoon et al., 2010, Abeykoon et al., 2011). However, the extrusion process is highly non-linear and therefore alternative controllers based on fuzzy logic have been recently developed, providing satisfactory accuracy in processes with different extruder machines, geometries and processing materials (Deng et al., 2014).

2.5 Screw design

The extruder screw is widely acknowledged as being the most important mechanical element of a single screw extruder. The design of the screw is of paramount importance for optimisation of the extrusion process and quality of the extruded polymer.

Recently, Kelly et al., (2006) studied the dependence of the melting mechanism on screw geometry and its effect on melt temperature. It was found that melt temperatures were more influenced by melting at higher throughputs leading to a high dependence of homogeneity on screw geometry. These results clearly confirmed that screw design needed to be matched to polymer type to minimise melting instabilities and reduce pressure inconsistencies. In addition, the dependence of energy consumption on screw geometry and set process conditions was also shown. In this section, therefore, detailed information regarding screw designs is provided to highlight the important role that screw geometry plays on the examination of the extrusion performance.

2.5.1 Sections of the screw and major functions

The major functions of a conventional extruder screw are achieved at different sections of the screw which may vary in length and configuration depending upon operation and polymer type being processed. In general, these functions are: solids conveying, plastication and pressure generation (pumping), as shown in Figure 2.12

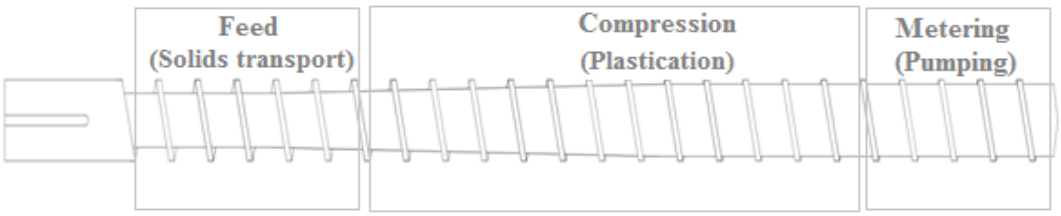

Figure 2.12 Sections of the extruder screw

- Feed (solids transport): brings the feedstock into the extruder and moves the material along the screw. The polymer is then conveyed forward and compressed. This section is usually confined to the first few turns.

- Compression (plastication): comprises the major portion of the screw in which the polymer is gradually melted by simultaneous application of external heating from the barrel and internal viscous shear. An explanation and a critical review of the melting mechanism can be found in section 2.7

- Metering (pumping): usually confined to the last few turns on the screw where the uniformity of the melt is increased. In this section, the melt acquires the required pressure to flow through the section of the die.

2.5.2 Single flighted extruder screws

The standard or conventional extruder screw is widely acknowledged as being the simplest design used in polymer extrusion operations. The configuration of this screw is shown in Figure 2.13 and the main design parameters are discussed below.

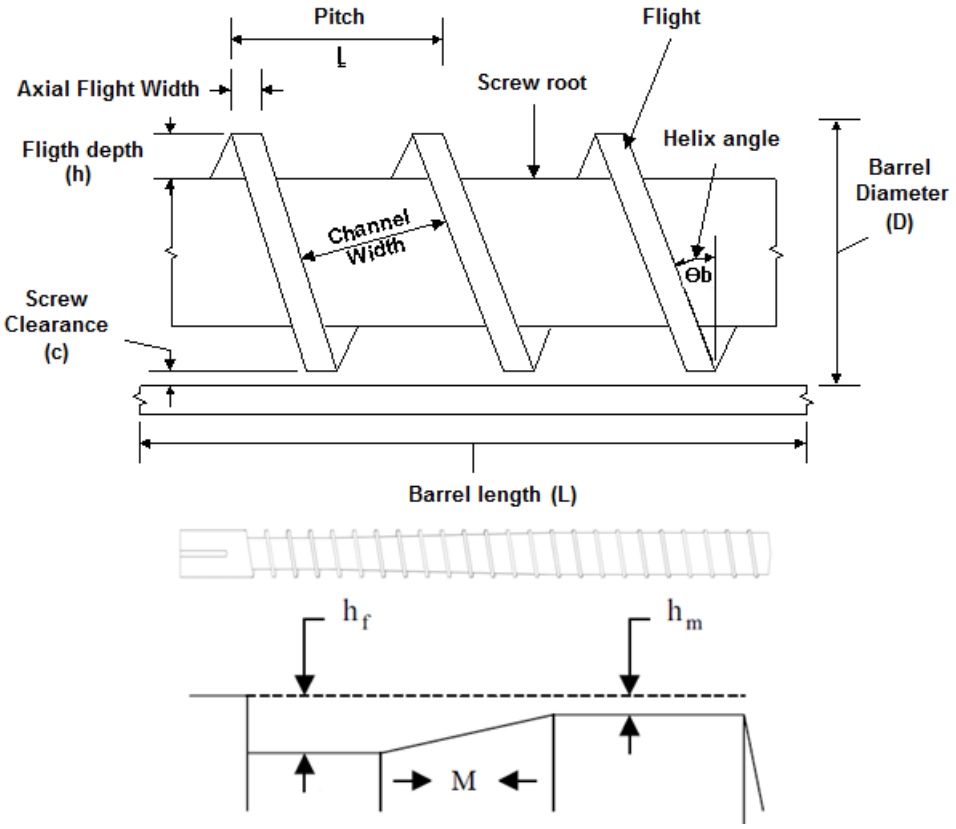

Figure 2.13 The key dimensions of a conventional extruder screw

L/D Ratio

L/D ratio (barrel length/ screw diameter) is the most referenced term of the basic components of a conventional extruder screw. It is closely related to the effectiveness of the process, being calculated based on type of operation and polymer used.

Feed section- Depths and Lengths

Womer, (2000) reported that the depth of the feed section of a screw should not be deeper than:

$$F_{dmax} = 0.2 \times D \qquad (2.1)$$

in order to reduce the risk of twisting the screw in half due to over-torquing whereas the length of the feed section is normally four or five times the diameter of the screw.

Compression ratio- Compression rate

Compression ratio and rate are important parameters for designing screw geometries since these affect the melting mechanism that occurs in the transition section of the screw. Compression ratio is defined as the ratio between the depths in both the feed and the metering section. Compression rate is used to measure the change in depth across the plastication section of the screw. From Figure 2.13 compression ratio and compression rate are defined respectively by the following equations:

$$\text{Compression Ratio} = \frac{h_f}{h_m} \qquad (2.2)$$

$$\text{Compression Rate} = \frac{(h_f - h_m)\sin\theta_b}{M} \qquad (2.3)$$

where h_f is the feed depth, h_m is the metering depth, M is the axial length of the compression section of the screw and θ_b is the helix angle at the barrel wall.

It is well known that extruders with conventional screw designs are often operated at conservative rates to minimise variations in melt temperature that highly affect process stability and product quality. When higher production rates are required, standard screws are found to become less efficient because of the phenomenon called “break up of the solid bed” (Kelly et al., 2006).

This occurs when the melting rate in the extruder is not fast enough, and therefore, the break-up of the solid bed causes solid polymer fragments to be discharged from the extruder. Myers & Barr, (2002) highlighted that this phenomenon deteriorated pumping stability and melt quality performances.

2.5.3 Barrier flighted extruder screws

From the early 1960's barrier flighted screws have been used to provide better performance for the polymer extrusion industry, recognizing the inherent problems and limitations associated with conventional extruder screws. The first barrier flighted screw was designed by Maillefer (Dray, 2002). The design allowed elimination of solid bed break-up by incrementing the melting area relative to a conventional design. This enabled higher production rates and improved melt quality as a result of greater melting performance.

Barrier screws emerged, therefore, to prevent solid bed break-up and improve melting performance. The barrier screw design introduces at the beginning of the melting section a barrier flight into the screw channels, which divides solid and melt.

The clearance over the barrier flight is designed in such a manner that only allows melt to flow over the flight. The melt is then confined into a separate melt channel whilst the solid bed is located at the active side of the barrier flight. This is shown in Figure 2.14.

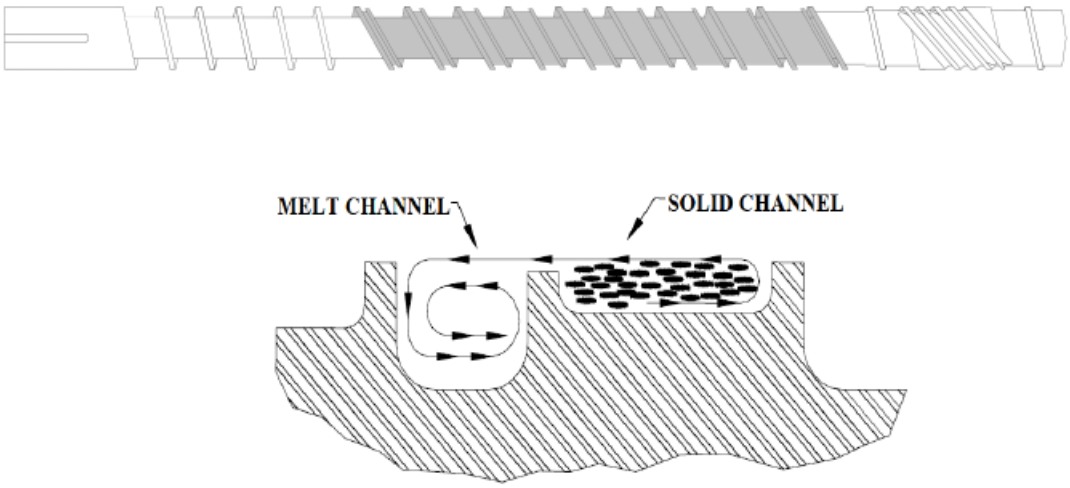

Figure 2.14 Barrier screw channel flow (Myers & Barr, 2002)

Steward, (2002) reported that the placement of the barrier flight, length and depth along the screw should be carefully selected when designing the barrier screw. An optimal selection was found to minimise melting instabilities, optimise pressure stability along the screw and improve consistency of pumping through the die.

Rauwendaal, (1994) summarised the characteristics of various barrier extruder screws in the following Table 2.1:

Table 2.1 Characteristics of various barrier extruders screws (Rauwendaal, 1994)

	MELT CONVEYING CAPABILITY	EASE OF MANUFACTURE	REQUIRED GROOVED BARREL SECTION
MAILLEFER	Good	Good	No
BARR	Moderate	Fair	No
DL	Fair	Fair	No
KIM	Fair	Difficult	No
INGEN HOUSZ	Poor	Difficult	Yes
DFM	Good	Good	No
COMPRESSION (4:1) SINGLE FLIGHTED	Good	Excellent	No
COMPRESSION (4:1) DOUBLE FLIGHTED	Good	Excellent	No

2.5.4 Mixing screws

The mixing mechanism in single screw extrusion is a complex processing phenomenon that affects the quality of the extruded polymer. Conventional extruder screws have been found to have a poor mixing capability (Rauwendaal et al., 1998). As a result, new designs of mixing sections have been installed into the channel to disrupt the melt flow patterns. In single screw extrusion there are two types of mixing, namely distributive and dispersive depending on the process. Dispersive mixing elements are characterised by a high stress region (HSR) that exposes the material to high stresses. In this region, the stress generated by elongational flow is large enough to break down the particles of the melt. It is used for agglomerates or gels when a fine level of dispersion is required.

The fluted or splined mixing section is the most widely used. It was invented by LeRoy and popularised by Maddock (Rauwendaal, 1994, Rauwendaal et al., 1998). This is shown in Figure 2.15.

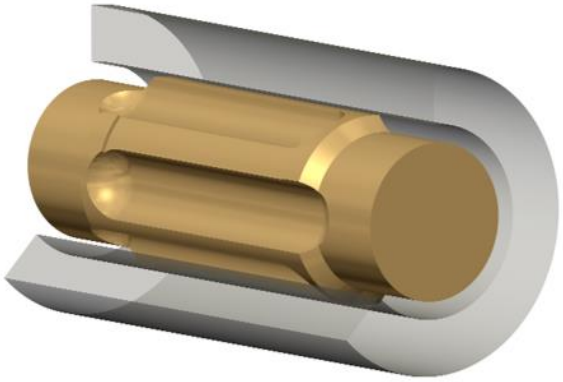

Figure 2.15 Fluted mixer (Compuplast Inc, 2011)

Although fluted mixing sections are popular due to their low pressure drop and good streamlining other dispersive sections have been subsequently patented. For example, Gregory and Street invented the helically fluted section. This was found to improve extrusion performance in terms of throughput and it was shown to cause less degradation (Rauwendaal, 1994).

Distributive mixing elements rely on strain rates that spread out and homogenise different polymers into a uniform melt. In these elements, high strains take place to increase the interfacial area between the two or more phases and reduce the second phase striation thickness (Rios et al., 2000)

Figure 2.16 shows the commonly used “pineapple” mixing element. Pin mixing sections provide good mixing by causing disturbances in the velocity profile. In the literature, there have been a significant number of papers studying the mixing capability of different screws in single screw extrusion. Among them, Wong et al., (2000) used a visualisation technique to compare different mixing elements. The experimental results showed that an optimum location of the mixing section on the screw was required to enhance the mixing capability. Results also demonstrated that Maddock’s screw (Dae Han et al., 1991) provided the highest performance when compared to other geometries.

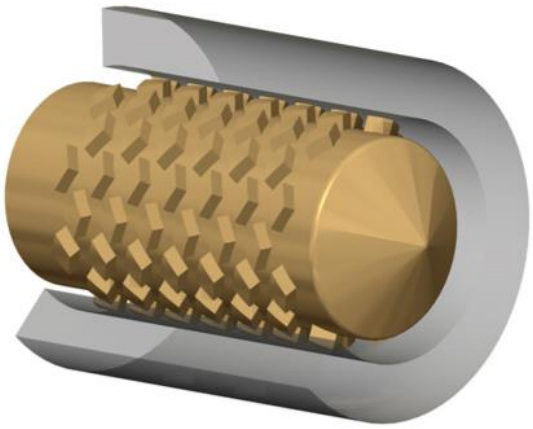

Figure 2.16 Pineapple mixing element (Compuplast Inc, 2011)

2.6 Review of melt temperature in polymer processing

Investigation of melt temperature and its effect on process stability and product quality is essential for understanding the thermal efficiency of the polymer extrusion process. Melt temperature is one of the key variables in extrusion as it has a direct effect on throughput, melt pressure, energy consumption and quality of the final product. Highly accurate melt temperature measurements are required to achieve good control of the process. However, it is often difficult to measure and is generally poorly controlled in industry. This section aims to review techniques used to measure the melt temperature in polymer extrusion in an attempt to generate detailed information concerning to the sensors, operation, accuracy of measurements and improvements that finally enabled characterisation of the extrusion thermal dynamics.

2.6.1 Temperature measurement methods for single screw extrusion

2.6.1.1 Single thermocouples

The first attempt to investigate the ability of standard thermocouples for measuring the temperature of flowing polymeric melts in plastifying equipment was initiated by (Leeuwen, 1967). He examined the effects of conduction errors, inertia and shear heat on stock temperature probes and concluded that an up-stream parallel-to-flow thermocouple was the desired configuration for measuring melt temperature profiles in flowing molten polymer systems.

Figure 2.17 shows most popular thermocouple configurations used to measure melt temperature in polymer extrusion. The principle of a thermocouple is shown in Figure 2.18. Thermocouples are mainly made with a pair of wires of dissimilar metals. They are basically a pair of junctions, one maintained at constant temperature (reference temperature) and the other at the temperature to be measured (hot junction or sensing junction). When these junctions are at different temperature then a voltage can be detected by conversion of thermal energy into electrical energy (Seebeck effect).

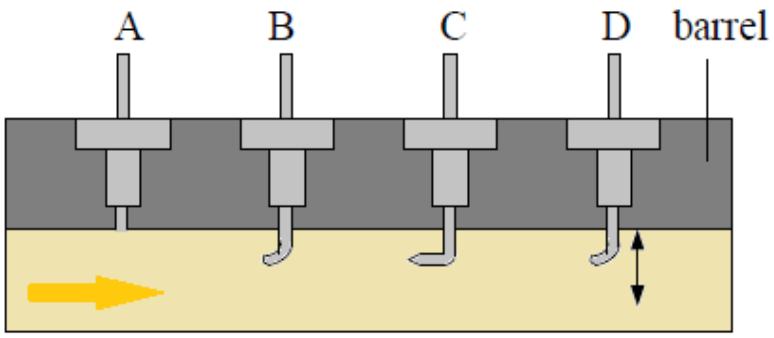

Figure 2.17 Melt temperature thermocouples (Yang, 2008)

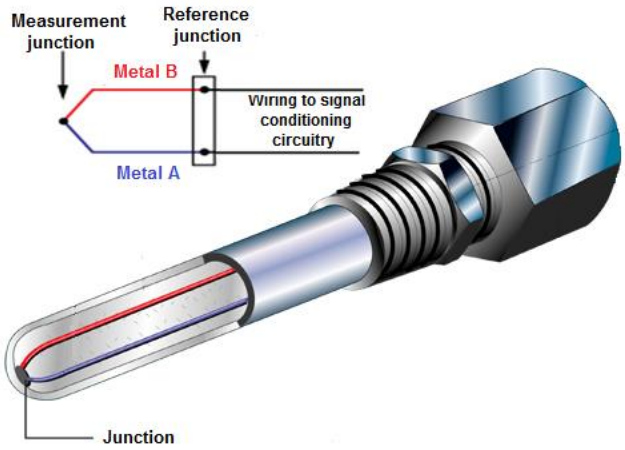

Figure 2.18 Thermocouple (Tutco, 2015)

A flush mounted thermocouple is shown in Figure 2.17A. This thermocouple provides melt temperature measurements at the boundary of the wall without disrupting the melt flow. However, it is widely accepted that this cannot provide precise temperature control since the measurement is heavily influenced by the temperature of the metal wall (Yazbak & Diraddo, 1993).

Protruding thermocouples have been used to provide temperature profiles across flowing melts (Figure 2.17 B and C). Kim & Collins, (1971) developed a temperature probe system that enabled measurements of radial melt temperature profiles in a rod die by using two thermocouples located in the upstream and the downstream locations.

These studies, however, did not consider the development of temperature profiles with increasing axial length. By developing a multi-parallel-to-flow probe suitable for extrusion operations, Saltuk et al., (1972) were able to measure temperature profiles as a function of axial flow length of flowing polymer melts.

This work was an extension of the study developed by (Forsyth & Murphy, 1969) and based on temperature profiles, in which flow disturbances and viscous heating were minimised by using smaller thermocouples.

Later, Bruker et al., (1987) measured radial melt temperature profiles for power law fluids at the end of the screw in a single screw extruder. The extruder was equipped with a ring- bar melt temperature unit on which ten thermocouples were mounted in radial position, opposite to the flow and downstream of the screw-tip.

Shen et al., (1992) measured melt uniformity across the die channel using an autotraversing melt thermocouple that enabled adjustable r/R temperature measurements (Figure 2.17 D). More recently, Kelly et al., (2002) used a motor driven extendible melt thermocouple for measuring temperature across the section of the die. Results were then compared to those obtained with a thermocouple grid sensor to provide concise information of temperature fields in flowing melts.

Such sensors are able to provide useful data relating to the extrusion process but these measurements adversely affect the melt flow and are subject to conduction errors along their lengths or shear heating around the sensor tip. Thermocouples described above are only capable of measuring the temperature at one point in the melt flow and therefore do not provide information regarding thermal dynamics of the extrusion process.

2.6.1.2 Thermocouple mesh devices

Thermocouples meshes or grids were developed in an attempt to provide 2D profiles of temperature of a flowing melt. First studies were initiated by (Judeh, 1989, Wood, 1996) and resulted in the design of a novel thermocouple array capable of measuring melt flow temperature profiles in extrusion or injection applications.

The thermocouple junctions were formed by twisting wires of one polarity around a wire of opposing polarity. This work was later extended by (Rasid & Wood, 2003) to investigate the effect of processing variables on extrusion thermal performance. They found that the metering section barrel temperature had the major effect on melt temperature when compared to compression and feed barrel set temperatures.

Brown et al., (2004) used a thermocouple mesh device modelled on prototypes developed by (Wood, 1996). The thermocouple mesh device enabled monitoring in real time of melt temperature profiles in single screw extrusion. Wires of opposing polarity were fused together at crossing points to form thermocouple junctions, which could be computer monitored (Figure 2.19).

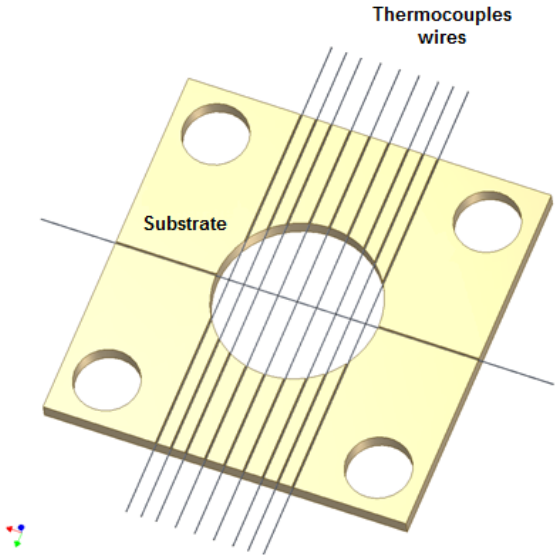

Figure 2.19 Thermocouple mesh (Brown et al., 2004)

The mesh was placed in a region prior to the entrance die, in an instrumented adaptor section. They found that melt temperature profiles became more pointed in the centre of the flow at higher screw speeds whilst these were flat in shape at low screw speeds. Another study by (Kelly et al., 2006) highlighted the effect of screw geometry on melt temperature profiles. They observed a strong effect of screw geometry on melt temperature as a result of the dependence of melting performance on extruder screw speed.

Abeykoon et al., (2011) also examined the effects of screw speed and barrel temperatures on die melt temperature profiles. They found that highest temperature fluctuations existed a few millimetres away from the die wall when the extruder was operated at high screw speeds.

Thermocouple meshes enabled examination of the thermal dynamics of the extrusion process collecting information relating to short-term melt temperature changes. However, these devices cannot be used to measure temperature inside the extruder barrel. Esseghir & Sernas, (1994) developed a mechanical cam driven thermocouple to measure temperatures inside the screw channel of a single screw extruder. The mechanical system allowed measurements of radial melt temperature distribution in the screw channel by the insertion and retraction of a probe through a barrel wall.

2.6.1.3 Infra-red devices

Infrared sensors offer a non-intrusive method of temperature measurement (Haberstroh et al., 2002, Anger et al., 2009). Infrared thermometers can be used to measure the temperature of a polymer by detecting the thermal radiation of a molten polymer (source) via a glass or sapphire window along optical fibers and consequently transformation of the received infrared radiation into an electrical signal (Figure 2.20).

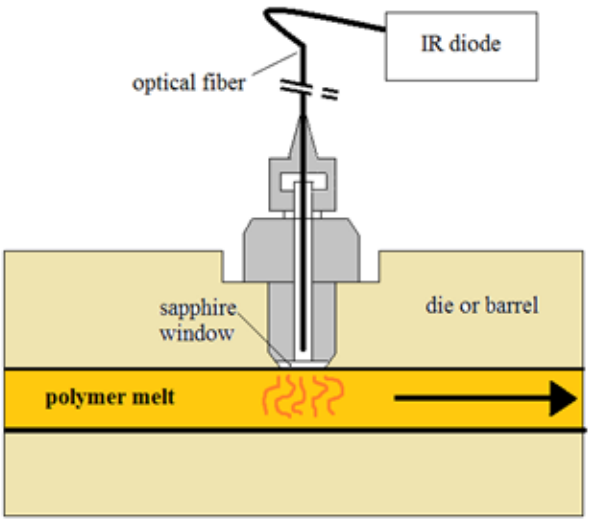

Figure 2.20 An infrared melt temperature sensor

The non-invasive nature and rapid dynamic response (10 ms) of infra-red thermometry make it particularly suitable for extrusion applications and it has been used to provide temperature measurements of polymer melt inside the screw channel (Bendada & Lamontagne, 2004). In addition, the sensor itself is sensitive to changes in surface emissivity which enables measurements of residence time distributions (Nietsch et al., 1997).

Recently, novel IR thermometers with an axially shiftable measuring tip have been used to measure radial temperatures profiles inside the screw channel of a single screw extruder using a tapered compression screw with a shearing and mixing zone. Several points of measurement along the axis with the barrel were used to build the temperature profile over the length of the screw (Anger et al., 2009).

However, the precise area or volume of melt measured by infra-red sensors is unclear and known to be material dependent and, therefore, the operating distances of these devices are limited (Bur et al., 2004). When located in the extruder die adaptor, infrared sensors have been shown to detect temperature fluctuations related to melting instabilities but these were small in magnitude due the large diameter (38 mm) of the region of measurement compared to the relatively small effective penetration of the sensor (Kelly et al., 2003).

2.6.1.4 Ultrasound devices

Ultrasound provides another potentially useful non- intrusive, fast response method for temperature measurements in extrusion processes. The velocity of propagation of an ultrasonic signal passing through a polymer melt is dependent upon temperature and pressure conditions. This suggested that ultrasonic velocity measurement could be used as a temperature and pressure measurement solution for the extrusion process. Chen et al., (1999) presented an ultrasonic temperature measurement device consisting of a piezoelectric transducer and an ultrasonic waveguide. The sensor was installed near the exit of the die and enabled measurements of the die surface temperature.

Results from the ultrasonic device were compared to those obtained from a commercial thermocouple. It was shown that ultrasound temperatures gave faster responses and were in good agreement with the thermocouple temperatures. Later, Brown et al., (1999), Brown et al., (2000) and Franca et al., (2000) showed that ultrasound transducers were suitable for in-line monitoring of extrusion and injection moulding applications.

Brown et al., (2000) highlighted that ultrasonic velocities could be readily employed to monitor the extrusion process providing useful data relating to bulk polymer melt temperature. To provide a comparison to the ultrasound data, Kelly et al., (2002) used thermocouple meshes and infra-red sensors. Bulk ultrasonic measurements and average temperatures measured by thermocouples grids were in good agreement. Results also showed that ultrasonic measurements and infra-red temperatures exhibited similar trends over time.

2.6.1.5 Other methods

Other techniques have been employed to provide measurements of melt temperature distribution. Migler & Bur, (1998) and Bur et al., (2004) developed a novel non-invasive temperature-sensitive fluorescent dye method to measure temperature profiles from the barrel wall to the core of the screw in a single screw extruder. The method allowed temperature measurements of the polymer without interference from the surrounding metal parts. Results showed that fluorescence temperatures when compared to infra-red temperatures exhibited similar trends over time and differed by less than 3 °C.

Electrical capacitance tomography (ECT) is a technique that enables determination of permittivity distributions in a cross section. Knowing that the permittivity of a polymer is a function of the temperature (Neagu et al., 2000), Yang, (2008) presented a feasible non-invasive, non-intrusive electrical capacitance tomography technique capable of measuring melt temperature distributions in polymer extrusion. An 8-electrode ECT sensor was designed for this purpose flush mounted to the internal die surface. However, no further studies were undertaken and therefore more examination is needed.

A summary of the techniques described above is shown in Table 2.2

Table 2.2 Summary of temperature measurements

	Comments	Intrusive	Dynamic response
Wall mounted TC	Bulk measurement, dominated by wall temperature	NO	~1s
Protruding TC	Temperature profile, interruptions of the melt flow, conduction error in length and shear heating around the tip	YES	>1s
Traversing TC	Temperature profile, subject to conduction and shear heating errors	YES	~1s
TC mesh	Multiple readings, provide a 2D profile of the temperature	YES	~0.1s
Infra-red	Bulk measurement over a conical volume near to the wall, measurement dependent upon material type	NO	10ms
Ultrasound	Bulk measurement across the centreline of entire flow, requires careful calibration due to changes with pressure and material type	NO	~1ms
Fluorescence	Temperature profile, dependent upon material type	NO	~0.5s

2.7 Review of extrusion melting mechanism

Melting is a major step in single screw extruders as it contributes to screw design and directly affects melt quality. There has been an enormous interest in developing theoretical analyses that could be useful for refining extrusion operations and maximise any advantage.

Most basic single screw extruders were developed originally to mix and extrude natural rubbers. The extruders were very short (3 -5 L/D) as there was no need for melting the rubber (White & Potente, 2003). The investigation of the melt conveying theory began in 1922 whilst it was not until the late 1950s and early 1960s when the first studies of solids transport and metering were initiated. These studies contributed to the improved design of melt fed extruders and screw pumps. However, although significant advances were made in extrusion research and development, the melting mechanism remained under investigation.

This situation changed dramatically after the first qualitative description of the melting process, which was worked out by (Maddock, 1959). He experimentally studied the melting mechanism in single screw extruders using a polymer with a high degree of crystallinity (e.g. polyethylene). The experiment, which was called the "Cooling experiment", was carried out by visual examinations of screw extractions; slices of solidified plastic taken at various positions along the length of the screw after abruptly stopping the extruder during operation at steady conditions, cooling the barrel and pushing out the screw. To visualise these slices, a tracer was previously introduced within the feed operation. It was found that much of the melting occurs in the upper melt film as a result of viscous heat generation by the contact of solid particles with the barrel hot surface.

It was observed that polymer particles were transported by the action of the screw down the screw channel and formed a solid bed. This was assumed to deform freely. Part of the melt film, defined as the thickness of which can exceed the clearance between the flight and the barrel surface, was dragged towards the leading flight flank. As a result the melt was collected generating the melt pool as shown in Figure 2.21.

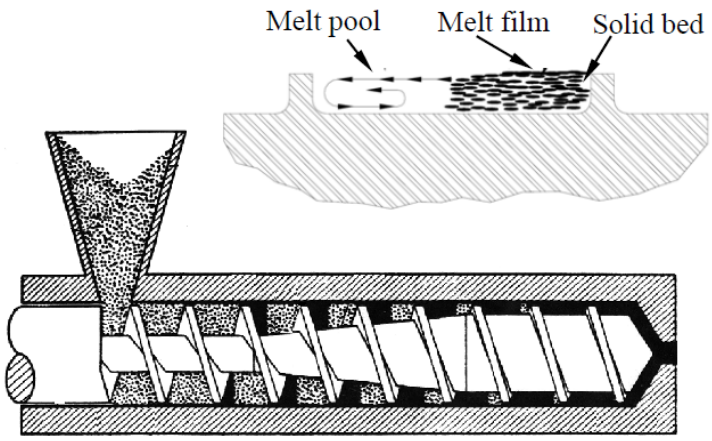

Figure 2.21 Maddock's melting mechanism (Donovan, 1971)

This experimental study revolutionised the analysis of single screw extruders. Based on Maddock's interpretation, Tadmor, (1966) developed the first quantitative description of the melting mechanism. To describe the model, Tadmor, (1966) assumed the existence of thermal and pressure steady state conditions, suggesting that the solid-bed interface remained at the same position in time. Additionally, he considered that the molten polymer in the melt film exhibited a Newtonian behaviour. The solid bed was defined with a rectangular cross section, homogeneous and continuous. In contrast to Street's experimental study (Street, 1961), Tadmor, (1966) assumed that the down channel velocity of the solid bed remained constant throughout the extruder.

The idealised melting mechanism of Tadmor was described by the following assumptions:

- Thermal conduction from the barrel surface through the moving film to the solid-melt interface
- Viscous dissipation in the melt film
- Neglected conduction and convection in the down channel direction
- Melting takes places only at the interface
- The rate of melting remains constant across the section and depends on the rate of heat transfer to and away from the interface
- The fluid is assumed to be Newtonian
- Constant physical properties

Figure 2.22 shows the temperature profile in the molten film and the solid bed.

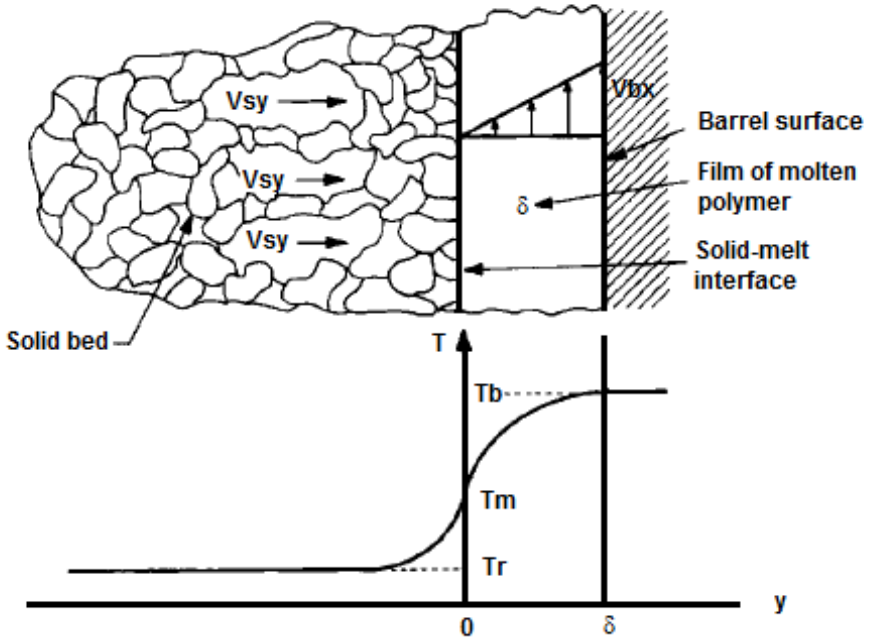

Figure 2.22 Temperature profile in the molten film and solid bed (Tadmor, 1966)

where V_{sy} is the velocity of the solid face into the interface, V_{bx} is the velocity of the barrel in the x direction, δ is the film thickness, T_b is the temperature of the barrel surface, T_m is the melting point of the polymer and T_r is the initial temperature of the barrel surface.

Taking into consideration the boundary conditions for the whole system as:

$T = T_m$ $\qquad$ $y = 0$

$T \rightarrow T_r$ $\qquad$ $y = -\infty$

and considering that the rate of melting per unit interface area is the difference between the rate of heat conducted into/out of the interface and the rate of melting per unit length is defined as the difference between the rate of mass flow of the solid bed into the interface and the rate of mass flow of melt to the rear of the channel, both per unit length, Tadmor defined the film thickness (δ) and the rate of melting per unit length (ω) by the following equations:

$$\text{Film thickness } (\delta) = \left\{\frac{[2K_m\,(T_b - T_m) + \mu(\Delta V_b)^2]X}{V_{bx}\rho_m[C_s(T_m - T_r) + \Delta_{hf}]}\right\}^{1/2} \tag{2.4}$$

$$\text{Rate of melting } (\omega) = \left\{\frac{V_{bx}\rho_m\left[k_m(T_b - T_m) + \frac{\mu}{2}(\Delta V_b)^2\right]X}{2[C_s(T_m - T_r) + \Delta_{hf}]}\right\}^{1/2} \tag{2.5}$$

where K_m is the thermal conductivity of the melt at average temperature and pressure of the molten film, T_b is the temperature of the barrel surface, T_m is the melting point of the polymer, μ is the apparent viscosity of the melt at the average temperature and pressure of the molten film, and at a shear rate calculated at the average thickness of the latter, ΔV_b is V_b-V_{sz} (vector substraction, defined as the difference between velocity of the barrel and velocity of the solid bed in z direction), X is the solid bed width, ρ_m is the density of the melt at the average temperature and pressure of the molten film, C_s is the specific heat of the solid bed at its average temperature and pressure, T_r is the initial temperature of the solid bed and Δ_{hf} is the heat of fusion.

This study led to a systematic investigation of the melting mechanism that takes place along the screw and as a result many models were described and numerous theories were proposed. This section reviews the most important analyses of the melting process. Developments based on Maddock's melting mechanism are presented to give valuable information of the polymer behaviour in the plastication zone of the extruder. The models are divided into three generations. The first and second generations are based on the analysis of Lindt (Lindt, 1985).

The third generation includes recent analyses which were developed in an attempt to explain new concepts such as the incorporation of the effect of rheology into the analysis, introduction of more complex screw geometries, amorphous thermoplastics, polymers being processed in powder form and the use of dynamic observations.

2.7.1 First generation of melting models

Tadmor et al., (1967) modified the melt flow analysis of the original model by considering the polymer melt as a temperature dependent power law fluid. They improved the energy balance of the melt film and introduced external procedures for estimating pressure changes along the melting zone. The experiments were carried out with only one screw and therefore the model was further modified with the use of flight clearance and channel curvature effects (Tadmor & Klein, 1970)

Donovan introduced one of the most significant versions of Tadmor's concept (Donovan, 1971). Carrying out experimental observations, he introduced a solid bed acceleration parameter (SBAP) into Tadmor's solid bed analysis. Additionally, he used exact solutions for both momentum and energy equations of the melt film and solid bed which allowed a heat exchange between the solid bed and the screw. This modification enabled use of a wide variety of screw designs, extruder sizes and polymers.

Mondvai et al., (1973) made an extension of the previous work developed by Tadmor. Although the flow and the heat transfer in the molten films were described containing no pressure terms he made a new contribution by introducing the presence of a molten film at the screw surface.

Lindt, (1985) proposed that the models described above could be grouped into a first generation of melting models. Both Newtonian (Tadmor, 1966, Mondvai et al., 1973) and power law fluids (Tadmor et al., 1967, Donovan, 1971) were useful in predicting melting capacity of a single screw extruder. The second generation of melting models, which are presented below, was characterised by a new analysis of the melt flow that incorporated the presence of pressure terms in the fundamental flow equations.

2.7.2 Second generation of melting models

Edmondson & Fenner, (1975), Shapiro et al., (1976) developed similar models for studying melting in extruders. They made some improvements on the theoretical analysis of the process, including pressure gradients into the melt flow analysis. The solid bed was assumed to deform freely and move at a uniform acceleration which implied that the solid bed velocities did not remain constant along the screw. In addition, this analysis also allowed the formation of a melt film between the unmolten solid bed and the screw.

However, the model did not give satisfactory predictions of the pressure gradients. According to the authors, major limitations were caused due to the oversimplified flow analysis by assuming isothermal Newtonian behaviour of the melt pool and pure drag flow of a temperature dependent power-law fluid in the molten films. These limitations suggested that a comprehensive mathematical model was required for a successful description of the melting mechanism in single screw extruders.

Among the many researchers who modelled the melting behaviour, Lindt and co-workers developed the most sophisticated melting theory. The assumption of an isothermal Newtonian fluid behaviour of the melt pool was replaced by a non-Newtonian analysis. In addition, pressure gradients were included in the melt flow analysis of the molten films and the option of using either the rigid or freely deformable solid bed concept (Shapiro et al., 1976, Lindt, 1981, Lindt, 1985)

A schematic representation of the screw channel cross section in the melting zone is shown in Figure 2.23.

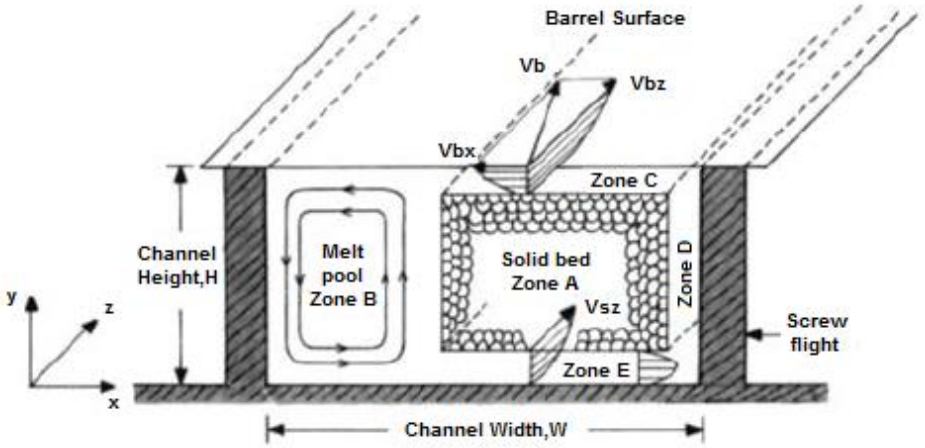

Figure 2.23 Screw channel cross section of Maddock melting mechanism (Lindt, 1985)

In this model, the temperatures of both the barrel and screw surfaces exceed the melting point of the polymer. The screw channel cross section was divided into five zones that denoted the overall transport pattern that prevails in the channel. Each zone was treated as a building block with distinct momentum and energy transport. The zones were interrelated by geometrical constraints and by force, heat and mass balance.

As shown in Figure 2.23, the solid bed, zone A, was described by a rectangular cross-section which is surrounded by relatively thin layers of molten polymer. A thin melt film between the barrel surface and the solid bed, zone C; a thin melt film between the screw flight and the solid bed, zone D; and a thin melt film between the screw surface and the solid bed (zone E). Although the solid bed is melted by conduction from the barrel and screw surfaces, most of the melting occurs in the upper melt film (Zone C) where the barrel heaters are placed and intensive viscous heat generation takes place.

The flow analysis is described by a z-direction bulk of mass flow that takes place in the solid bed and in the melt pool. In the melt pool, zone B, the flow was described by a combination of circulation and downstream motion that generated simultaneous actions of pressure and drag forces. The lower film (zones D and E) that is in contact with the screw surface was treated as a two dimensional flow.

This analysis was later improved by including cross-channel circulation. It was reported that the cross-channel circulation had an important effect on the overall flow and heat transfer pattern in the melting zone, leading to superior results when attempting to simulate accurately the performance of the melting zone.

2.7.3 Third generation of melting models

On the basis of this work, Lee & Han, (1990) introduced a new concept of the solid-bed deformation into the analysis of (Lindt, 1985). They developed a new model that included the rheology of the solid bed with the assumption of a linear relationship between the stress and strain. The model improved the energy analysis by incorporating a convective heat transfer term for the melt pool and the thin melt films. It was confirmed that the assumption of a cross-channel velocity in the thin melt films was essential to predict axial pressure profiles and more realistic melt temperatures in the screw channel.

Zhu & Chen, (1991) presented a dynamic observation method, which was based upon on-line observations. The experiment was carried out with a windowed extruder barrel to observe and record the whole extrusion process. It was noticed that the “solid plug”, an assumption generally adopted by previous researchers to describe the motion of the solid granules in the screw channel, did not correspond with the experimental observations. They observed relative movements and clearances among the solid granules instead of a rigid body.

Zhu & Chen, (1991) proposed, therefore, a non–plug flow solid conveying model in order to describe the movements of the polymer granules. Furthermore, when the screw was not cooled and the screw speed was high, they visualised the solid bed moving from the trailing side of the screw flight to the middle of the screw channel, as predicted by (Lindt, 1976). However, when the screw was cooled the solid bed profile behaved as (Tadmor, 1966) and no acceleration was observed. This implies that break-up of the solid bed did not occur.

Rauwendaal, (1989) put forward an improved analytical melting theory for single screw extruders using an analytical solution obtained for a temperature dependent power law fluid from the analysis of the temperature and pressure profile of the drag flow. This allowed accurate evaluation of the effect of barrel temperature on melting performance.

The above studies of the melting mechanism are mainly based on Maddock's melting mechanism. There are many special screws that incorporate unique mix melting sections. Experiments carried out with these screws have reported that the solid bed may be broken up into a series of solid particles which are dispersed into the melt.

Huang & Peng, (1993) developed a theoretical model, "dispersive melting mechanism", to describe the melting process in single screw extruders that operated with unique mix melting section screws. The melting process was divided into three sequential stages: Maddock's melting, dissipative mix-melting, and dispersive melting stage. In contrast with Maddock's melting model, the dispersive melting model has the following advantages: a greater decrease of the mechanical power consumption, the temperature profile was more uniform with lower mean temperature and the length of melting was shortened by acceleration of the melting rate.

Cox et al., (1981) carried out experimental work conducted on a single screw extruder running with polyethylene in granular and powder form. The aim was to investigate whether the melting mechanism varies with particulate feedstock. It was noticed that two types of melting mechanism may operate; defined as type A or type B. Type A was observed with granule processing and is a classic Maddock's type, previously described in this chapter. In powder extrusion, type A and type B were found. In type B, the relative position of solid bed and melt pool was the reverse of that for type A, and both are illustrated in Figure 2.24.

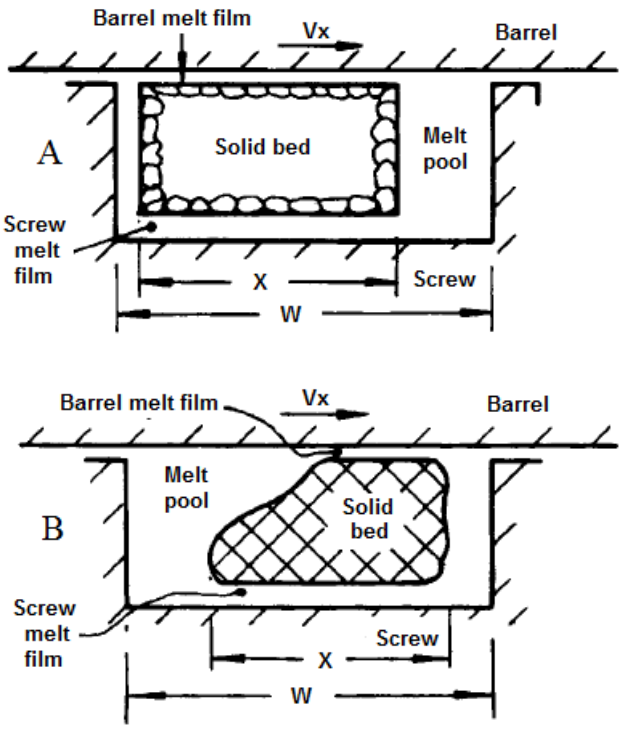

Figure 2.24 Types of melting mechanism (Cox et al., 1981)

The results were summarised as follows:

- In general, lower pressure, output rates and specific power consumptions were associated with the processing of powder.
- Granules melted according to the type A. Powders could melt, in some cases, according to type B.
- The initiation of melting occurred much earlier and more rapidly for powder compared with granules.
- "Cooling" of the barrel delayed melt initiation and was associated with higher generation of pressure and output rates and could change the melting form from type B to type A

Previous efforts were made in developing mathematical models to describe the melting mechanism in single screw extrusion of semi-crystalline polymers. Han et al., (1996) developed a study for analysing the performance of the plasticating extrusion of amorphous polymers. They modified the melting mechanism of Lee & Han, (1990) since amorphous polymers do not have a melting point. They introduced the concept of "critical flow temperature" (T_{cf}) allowing them to define the interface of the thin melt films surrounding the solid bed and the interface between the solid bed and the melt pool. By doing this, Han and Lee were able to define the melt pool for amorphous polymers in the screw channel as shown in Figure 2.25.

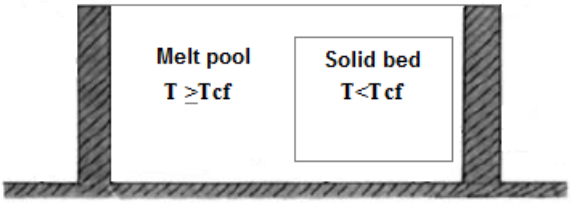

Figure 2.25 Definition of critical flow temperature (T_{cf}) for amorphous polymers (Han et al., 1996)

The models reviewed previously, were developed for performing Maddock's type experiments with homopolymers using a single screw extruder. Cunha et al., (2009), more recently, carried out an experimental study for describing the melting mechanism of polymer blends using PA6/PP. The work reported a more complex melting mechanism that combined the features of Tadmor and the melting mechanism developed by (Rauwendaal, 1989).

Noriega et al., (2004) presented an in-line non-invasive optical measuring technique for extrusion applications that allowed verification of mathematical melting models and computer simulations. The experimental observations showed a delay in the formation of the melt pool that could be included into Tadmor's analysis, enabling the proposed model to improve agreement with experimental data.

2.8 Review of fully predictive extrusion models

In order to describe the single screw extrusion process, Závadský & Karniš, (1985) formulated a mathematical model in which the extruder was divided into five zones; the zone under the hopper, the solids conveying, the delay, the melting and the melt conveying zone. Based on mathematical treatments for describing the processes associated with each individual zone, the capability of the program allowed the design of different types of extruders and an analysis of the influence of processing conditions on properties such as melt temperature and pressure at the end of the extruder.

Acur & Vlachopoulos, (1982) developed a fully predictive steady model of a single screw plasticating extrusion to assess the entire extrusion process, taking into account all the extrusion steps from the feed hopper to the die exit, as shown in Figure 2.26.

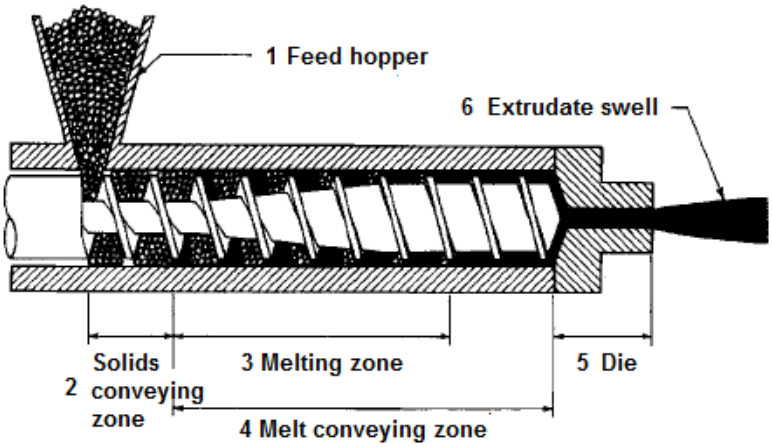

Figure 2.26 Schematic diagram of a single screw extruder showing the components of the computer model (Acur & Vlachopoulos, 1982)

The computational model included: the feed hopper, solids conveying, melting and melt conveying zones, die and swelling of the extrudate at the die exit. Once the material, polymer rheology, screw and extrusion parameters were defined, the extruder model was able to predict flow rate, pressure and temperature profiles in either the extruder screw channel and die sections, and extrudate swell at the die exit.

Amellal et al., (1991) presented a steady state computational model where the analysis of the single screw extrusion process was represented by three zones: the solids conveying section, the melting zone and the metering zone. Experimental work was carried out on an extruder using conventional and barrier screws with different dies. The model was able to predict extrusion performance and optimisation of screw design and operation conditions.

Wilczyński, (1996) presented another fully predictive computer model for single screw extrusion. The model was developed by dividing the extruder into six interdependent sections: the hopper, the solids-conveying zone, the delay zone, the melting, and the melt-conveying zone. The simulations allowed predictions of mass flow rate, pressure and temperature profiles in the screw channel and die, solid bed profile and power consumption. Moreover, degree of mixing, temperature fluctuations and viscoelastic properties of the polymer could be estimated. This model was later extended to simulate extrusion processes with non-conventional screws at different operating conditions (Wilczyñski, 2001)

Although the extruder models described above were suitable for analysing the plasticating process, the computational demand was often very high and, therefore, there was a need for a simpler less time consuming process. Lai & Yu, (2000) developed a new mathematical model that did not involve the use of partial differential equations and hence did not require numerical solution techniques. This work provided a level of accuracy comparable with more complex 3D models but with less demand of computational efforts. Control volumes were used to divide the extruder into a number of circular segments to analyse the plasticating process. This is shown in Figure 2.27. The model enabled prediction of the solid-bed width and pressure profiles, temperature and pressure of the melt at the extruder exit and power consumption.

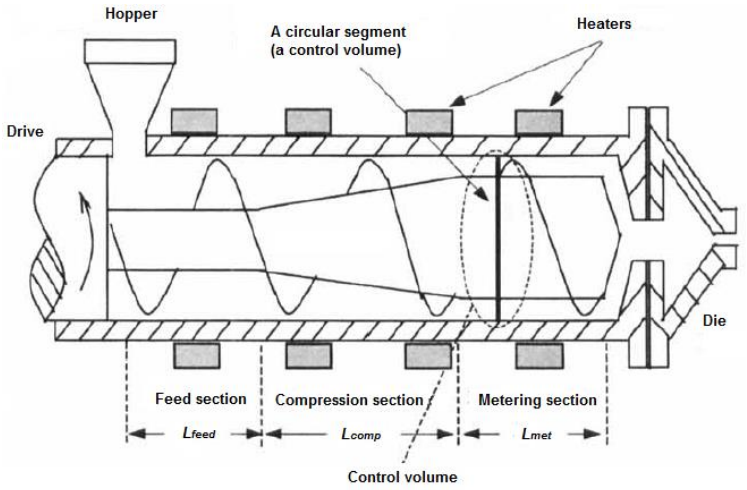

Figure 2.27 Schematic of a single screw extruder (Lai & Yu, 2000)

2.9 Energy consumption in single screw extrusion

2.9.1 Energy usage considerations within extrusion operations

Polymer processing is an energy intensive industrial sector, due to the need to melt, mix, form and solidify polymeric materials in large quantities at high throughputs. The majority of polymer processing operations involve extrusion and this stage typically represents around 50% of the total process energy.

In single screw extrusion, the energy is supplied to the polymer feedstock by the dual action of electrical heaters along the length of the barrel and the drive system, principally in the form of viscous shearing by the motion of the screw. It is therefore clear that an analysis of these two primary energy sources, the heaters and motor, is essential for the optimisation of the extrusion process. For each kg of polymer processed it is necessary to supply, on average, 0.3 kW/kg/h (Kent, 2008). However, there has been little interest in operating with process energy consumption in mind and so the effects of processing conditions on energy consumption have not been well understood.

Often, in the polymer processing industry extruders are operated with extruder screw geometries which are not suited to the polymer being used, either through lack of understanding or financial restrictions. The driver to operate efficiently within industry has tended to link with production outputs rather than optimisation of process energy consumption. Extrusion machines are not commonly equipped with energy monitoring equipment, and as a result there has been little understanding of the links between processing conditions and energy consumption.

However, recently, it has been shown that extruder heaters consume less energy per unit mass when the extruders are operated at higher screw speeds (Kantor, 2010). It has also been found that single screw extruders should be operated at the highest screw speeds to maximise efficiency, whilst the screw geometry should be carefully chosen to optimise melt temperature (Abeykoon, Kelly, Brown, et al., 2014).

For a typical UK plastics company, the electricity bill is usually between 1 and 3% of turnover, which amounts to £380 million per annum for the UK in electricity costs. Therefore, an understanding of the energy consumption in single screw extrusion and its relationship to set process conditions, screw geometry and the polymer being processed may result in potential energy savings. It has been shown by (Kent, 2008) that simple no cost or low cost energy practices can reduce energy consumption by between 10 and 20%, which would result in product cost savings of £38 million per annum.

2.9.2 Balance of energy

Figure 2.28 shows an energy balance for a single screw extruder which is represented as a block diagram. The polymer feedstock is usually fed via the hopper at room temperature and ambient pressure and by energy-consuming processes is transformed into a melt which is conveyed along the screw, generating the required pressure to flow through a shaped die and form the final product, normally at room temperature. There are three energy inputs to the extrusion process: enthalpy of the feed material (h_1), mechanical energy provided by the drive motor and imparted to the polymer by the rotational motion of the screw (P_m) and thermal energy from the heaters (P_h).

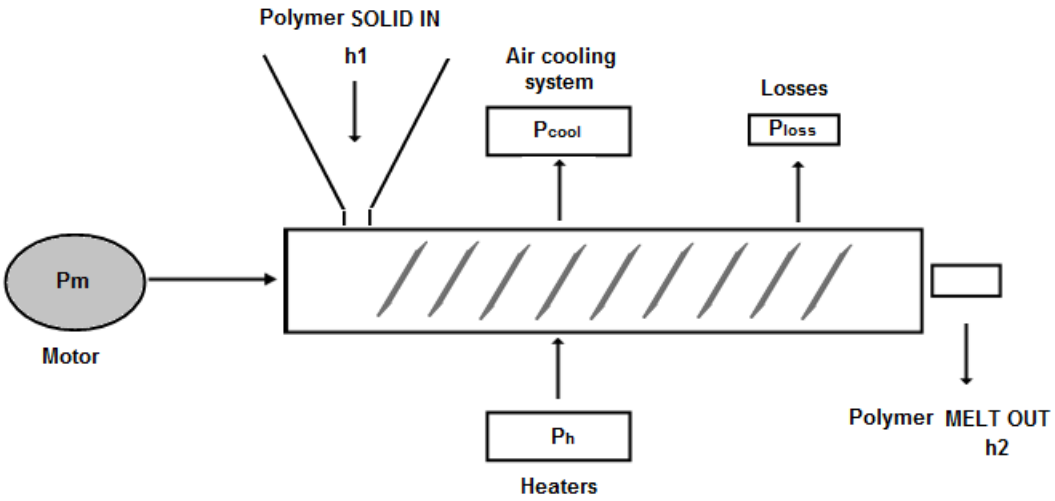

Figure 2.28 Energy balance for a single screw extruder

The energy outputs are the enthalpy of the final product (h_2), net of the losses (P_{loss}) that occur in the system and the energy removed from the cooling system (P_{cool}).

Under a steady state operation, the energy balance can be expressed as:

$$P_m + h_1 + P_h = h_2 + P_{cool} + P_{loss} \qquad (2.6)$$

It has been shown that power consumption required from the barrel heaters represents less than 25% of the power needed to raise the temperature and melt the polymer (Vlachopoulos & Struut, 2003). For a number of heaters placed along the extruder barrel, the total power consumption (P_h) for heaters can be calculated as:

$$P_h = N_h * (V * I) = N * (I^2/R) = N * \left(I^2 * \frac{A}{\rho_r * L_h} \right) \qquad (2.7)$$

where N_h is the number of heaters, I is the current, A is the surface area of each heater, ρ_r is the resistivity of the heater and L_h is the length of the heating element.

With auxiliary air cooling systems mounted under each heater surface for removing heat and transfer it into the ambient when the melt overheats above the barrel set point, the total cooling power consumption (P_{cool}) is defined by the equation:

$$P_{cool} = N_{cool} * (\dot{m}_{air} * C_{p,air} * \Delta T) \quad (2.8)$$

where N_{cool} is the number of cooling fans, $\dot{m}_{air}$ is the mass air flow, $C_{p,air}$ is the specific heat capacity of air, and ΔT is the variation of temperature. This term is normally included as a negative input P_h.

The term P_{loss} represents the net of the losses; convective and radiation heat losses from the barrel, die and heaters and conduction losses from barrel and any die attachments.
The mechanical power (P_m) is the major energy input (Vlachopoulos & Struut, 2003) and it represents the electrical energy that the drive motor converts to mechanical power. This is used to drive the screw, convey the polymer along the screw and build up the pressure. In addition, it is also partially converted into heat by internal friction which in turn is used to heat and melt the material.

If the extrusion process does not involve chemical reactions (Vlachopoulos & Struut, 2003, Hsieh, 2003, Covas & Stevens, 1995), it is commonly accepted that:

$$P_{in} = P_{out} \quad (2.9)$$

$$P_{out} = P_{th} + P_{loss} \quad (2.10)$$

and then the theoretical power required in an extruder (P_{th}) can be expressed by the following equation (Vlachopoulos & Struut, 2003):

$$P_{th} = \overbrace{\rho_m * Q * C_p}^{\text{heating}} * (T_{ex} - T_r) + \overbrace{\rho_m * Q * \Delta_{hf}}^{\text{fusion}} + \overbrace{\Delta P * Q}^{\text{pumping}} \quad (2.11)$$

where ρ_m is the melt density, Q is the volumetric flow rate, C_p is the specific heat capacity, T_{ex} is the extrusion temperature, T_{ro} is the room temperature, Δ_{hf} is the heat of fusion and ΔP is the pressure rise.

In equation (2.11), the first term represents the power transferred to the polymer in the form of heat from room temperature to the extrusion temperature, the second term represents the power required to melt the polymer (heat of fusion) and the third term is the power needed to pump the molten polymer.

Mallouk & McKelvey, (1953) derived an equation for the energy consumption in melt extruders in terms of screw dimensions, screw speed, die pressure and melt viscosity, considering isothermal Newtonian melt flow behaviour and constant screw channel dimensions. The power consumption over the entire length of the screw at steady conditions was then calculated as follows:

$$P = \frac{\pi^3 * Ds^3 * N^2 * \mu * L_a}{h} + \frac{Q * \Delta P}{\cos^2\varphi} + \frac{\pi^2 * Ds^2 * N * e * \mu * L_a}{\delta * \tan\varphi} \quad (2.12)$$

where Ds is the screw diameter, N is the screw speed, μ is the viscosity of the melt, L_a is the length of the screw axis, h is the channel depth, φ is the helix angle, δ is the screw flight clearance and e is the screw flight width.

In the case of polymer melts with non-Newtonian pseudoplastic flow behaviour, the authors introduced an average viscosity ($\bar{\mu}$) into the melt flow analysis:

$$\bar{\mu} = \frac{\int_0^{L_a} \mu * d\lambda}{L_a} \quad (2.13)$$

and hence, the power consumption expression became:

$$P = \left(\frac{\pi^3 * Ds^3 * N^2}{h}\right) + L_a * \bar{\mu} + \frac{Q_D * \Delta P}{\cos^2\varphi} + \left(\frac{\pi^2 * Ds^2 * N^2 * e}{\delta * \tan\varphi}\right) * L_a * \bar{\mu} \quad (2.14)$$

Mallouk & McKelvey, (1953) concluded that the power consumption was the sum of the energy consumed in the helical screw channel and that dissipated between the screw lands and the barrel wall. The expression was found to be useful for designing and examination of performance on melt extruders.

Kim et al., (1982) studied the geometrical and process factors that affect extrusion process energy consumption. Using steady state conditions at constant temperature, they developed power consumption expressions at each individual section of the extruder: feed section, compression and metering section (Figure 2.29).

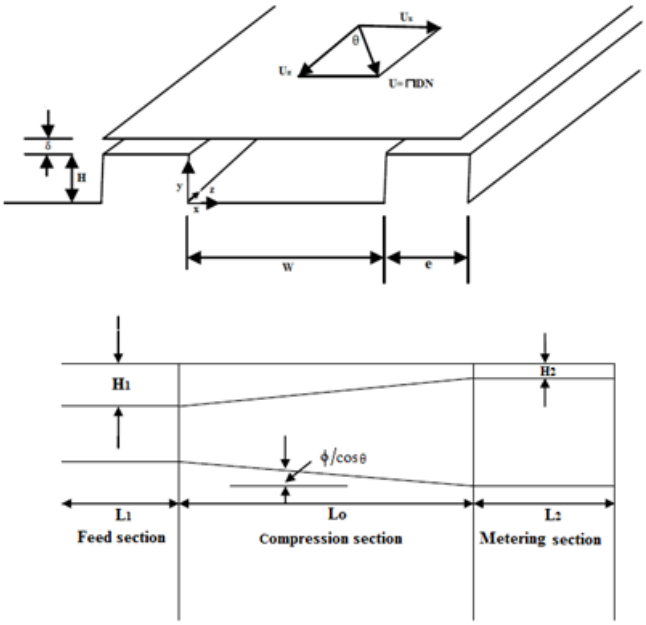

Figure 2.29 Geometry of single parallel screw extruder (Kim et al., 1982)

Ignoring the energy required for melting the polymer and considering the viscosity of the polymer as a constant, the equations were calculated as follows:

$$\dot{W}_f = \frac{\mu * U^2{}_z * W * Z_1}{H_1} * \left[4 * (1 + \tan^2\theta) - \frac{6 * Q}{U_z * W * H_1}\right] + \mu * \frac{U^2{}_z * e * Z_1}{\delta * \cos^2\theta} \quad (2.15)$$

$$\dot{W}_c = \frac{\mu * U^2{}_z * W}{\tan\phi} * \left[4 * (1 + \tan^2\theta) \ln\frac{H_1}{H_2} - \frac{6 * Q}{U_z * W} * \left(\frac{1}{H_2} - \frac{1}{H_1}\right)\right] + \mu * \frac{U^2{}_z * e * Z_0}{\delta * \cos^2\theta} \quad (2.16)$$

$$\dot{W}_m = \mu * U^2{}_{z*} W * \frac{Z_2}{H_2} * \left[4 * (1 + \tan^2\theta) - \frac{6 * Q}{U_z * W * H_2}\right] + \mu * \frac{U^2{}_z * e * Z_2}{\delta * \cos^2\theta} \quad (2.17)$$

where $\dot{W}_f$, $\dot{W}_c$ and $\dot{W}_m$ are the power consumptions in the feed, compression and metering sections, μ is the viscosity of the melt, U_z is the velocity of the fluid in z-direction of the screw channel, W is the width of the screw channel, Z_0, Z_1 and Z_2 are the screw channel lengths corresponding to screw axis lengths L_o, $L_1$and L_2, Q is the volumetric flow rate, H_1 and H_2 are the channel heights at the feed and metering sections, e is screw flight width, θ is the helix angle of the screw, ϕ is the inclination angle in the metering section of the screw channel $(H_1 - H_2)/Z_o$, δ is the screw flight clearance.

They found that the extrusion process was more efficient with increasing screw helix angle, height in channel and clearance whilst it was less efficient as L/D increased. They also examined the effects of screw speed and pressure on energy efficiency. They concluded that efficiency increased with decreasing screw speed and with pressure increase.

More recently, a number of authors have developed mathematical models for analysing energy consumption in single screw extrusion based on process settings (Lai & Yu, 2000, Abeykoon et al., 2010). Abeykoon et al., (2010) presented a new model to calculate motor power consumption by selecting different extrusion processing conditions and materials. Screw rotation speed and barrel set temperatures were found to have a significant effect on power consumption.

This study enabled better selection of individual process variables for improving energy efficiency of single screw extrusion (Abeykoon et al., 2014). However, these models are based on the geometry of the extruder and materials used and may not be particularly suitable for different extrusion machines and experimental conditions.

Deng et al., (2014) presented new methods for real-time monitoring of both motor power and thermal energy consumption, independent of the geometry of the extruder machine and polymer type. These methods based on temperature and motor controller outputs were shown to be accurate and reliable monitoring approaches for polymer processing when compared to power meters (Deng et al., 2014).

Power meters offer another real-time quantification of energy consumption for polymer extrusion. Kelly et al., (2006) showed that extruder screw geometry and screw rotation speed had a direct effect on energy consumption. The demand of energy was found to be heavily dependent upon the rheological and thermal properties of the polymer being processed. These results were in line with the experimental studies carried out by (Kantor, 2010). In both studies a similar relationship was shown between specific energy consumption and extruder screw and its dependence on polymer type. Overall, specific energy consumption was found to decrease as screw speed increased.

2.10 Polymer melt rheology

2.10.1 The role of rheology in polymer extrusion

Rheology has been defined as the science of material deformation and flow. In the plastic extrusion process, melt flow is exposed to the forces of deformation and shear in the screw channel and hence exhibits viscoelastic behaviour under processing conditions. The rheological behaviour of the polymer melt is a crucial parameter when examining polymer processability in extrusion operations (Dealy & Wissbrun, 1999, Giles et al., 2005). In single screw extrusion, melt viscosity is clearly affected by shear and changes nonlinearly with shear rate. The viscosity of the polymer generally exhibits non-Newtonian pseudoplastic flow behaviour, as shown in Figure 2.30.

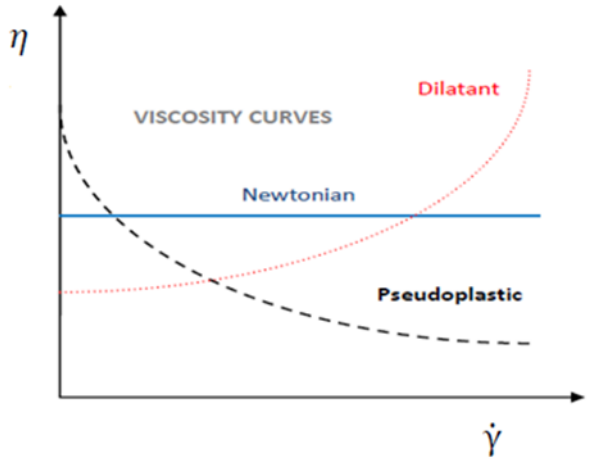

Figure 2.30 Non-newtonian pseudoplastic flow behaviour

Temperature, pressure, shear and thermal history will have a significant effect on the rheological characteristics of the melt flow. For example, at higher screw rotation speeds the molten polymer is exposed to high shear and experiences a corresponding decrease in melt viscosity due to the dependence of melt temperature on viscous energy dissipation via shearing.

The examination of the viscoelasticity earlier, is therefore, essential to assess better polymer processability in extrusion processes and achieve improved stability by evaluation of the effects of processing temperature and pressure on melt viscosity (Giles et al., 2005). Understanding the importance of the melt viscosity and its role in screw design will also help in determining the optimal design of screw geometries. It is well known that the length of the sections of the screw, design of barrier or mixing elements and geometrical dimensions, such as channel depth, helix angle, pitch and flight clearance are carefully calculated based on the viscous behaviour of the polymer being processed (Eslami, 2014).

2.10.2 Capillary rheometry

Capillary rheometers are used to examine the role of high shear rates on the rheological properties of polymer melts. The rheometer consists of a vertical heated barrel which is fitted at the bottom with a capillary die. The polymer melt is pushed through the capillary of constant cross section by the action of a piston which is driven at constant speed. This keeps a constant flow rate which allows determination of shear rate. A pressure transducer is situated at the base of the barrel to measure the generated pressure by the motion of the piston and determines the shear stress, as shown in Figure 2.31

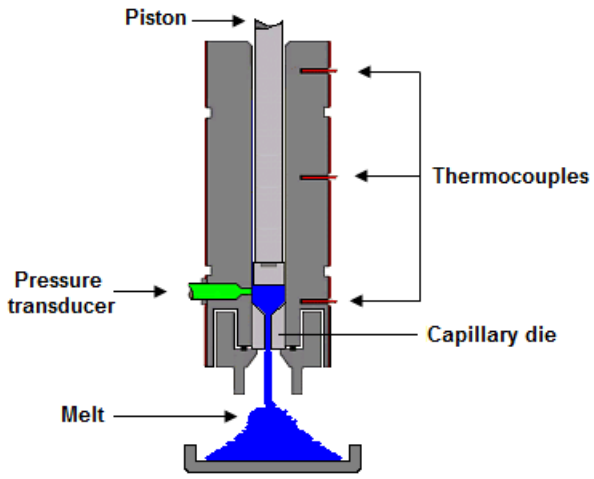

Figure 2.31 Schematic diagram of capillary rheometer (Gammadot, 2015)

The apparent wall shear stress can be calculated as follows:

$$\tau_{\omega} = \frac{R}{2}\left(\frac{\Delta P_{die}}{L_{die}}\right) \tag{2.18}$$

where R is the radius of the capillary die, ΔP_{die} is the pressure drop along the capillary and L_{die} is the die length.

The apparent wall shear rate is given by the following expression:

$$\dot{\gamma}_{\omega} = \frac{4Q}{\pi R^3} \tag{2.19}$$

where Q is the volumetric flow rate.

Hagen and Poiseuille found that the pressure drop, ΔP, in a capillary at a volume flow rate, Q, depends on shear viscosity. The capillary rheometer analysis can be then applied for measuring apparent shear viscosity by the following equation:

$$\eta = \frac{\tau_{\omega}}{\dot{\gamma}_{\omega}} = \frac{\pi(\Delta P)R^4}{8LQ} \tag{2.20}$$

In the previous analysis it is assumed that the pressure drop corresponds to that in the capillary die. However, when polymers melts converge into the capillary entrance, the exiting velocity profile in the main body of the barrel is disrupted and as a result a pressure drop is generated (Figure 2.32).

Figure 2.32 Flow line disturbances (Bagley, 1957)

2.10.2.1 Shear stress correction

Bagley, (1957) studied the losses in driving pressure in the region above the capillary entrance and noticed that plots of pressure versus capillary length to radius ratio at constant shear rate were linear with positive intercepts which were equal to the entrance pressure losses. The experiments were conducted with polyethylene and the L/R of the capillaries ranged from zero to thirty. Equation (2.18) was then corrected by adding an effective extension to the length of the die (end correction, (e)) equivalent to the intercept on the zero pressure axes.

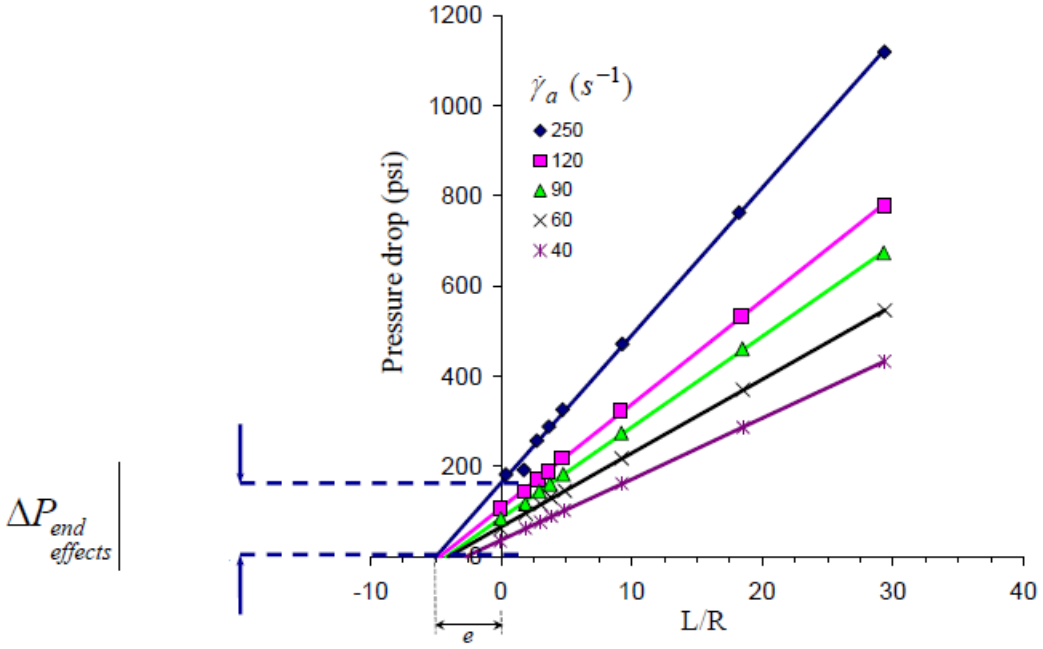

Figure 2.33 Bagley correction length (Bagley, 1957)

In the new analysis the corrected shear stress becomes:

$$\tau_\omega = \frac{\Delta P}{2\left[{}^{L}/_{R} + e\right]} \qquad (2.21)$$

where *e* is the equivalent length of die that represents the extra entrance pressure drop.

2.10.2.2 Shear rate correction

The use of a Newtonian behaviour in the analysis of the melt flow implies that the wall shear rate of equation (2.18) is generally lower than for a non-Newtonian fluid. When analysing polymers that exhibit pseudoplastic flow behaviour, a Weissenberg/ Rabinowitsch correction is necessary to describe more accurately the non-parabolic velocity profiles that occur in the die (Figure 2.34).

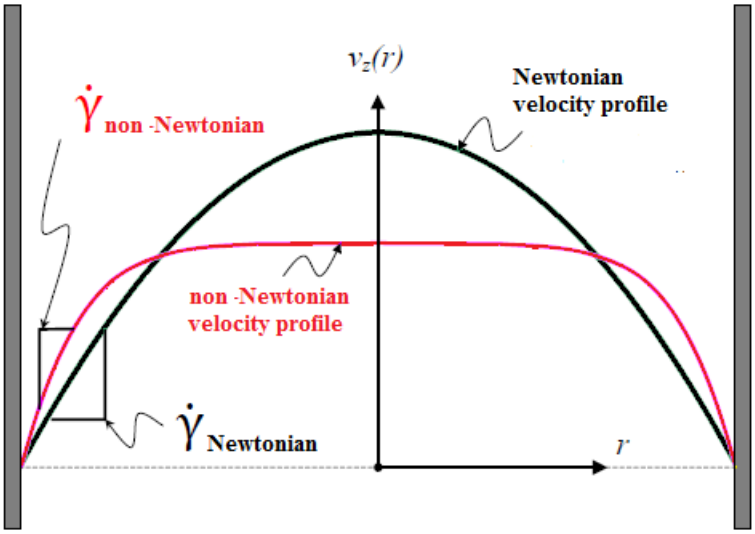

Figure 2.34 Non-parabolic velocity profile

The true shear rate becomes in the form:

$$\dot{\gamma}_{\text{true}} = \frac{4Q}{\pi \times R^3}\frac{3n+1}{4n} \tag{2.22}$$

which means that the velocity profile is a function of the power law index, *n*.

As mentioned before, polymer melts exhibit shear thinning or pseudoplastic flow behaviour in extrusion operations whereby an increase in shear rate causes a decrease in melt viscosity. Figure 2.35 shows a plot of log (shear viscosity) against log (shear rate) to illustrate the general viscous behaviour of the melt flow. The flow curve is divided into three different regions. At low shear rate, in region I, polymers usually exhibit a Newtonian plateau which is commonly called zero-shear rate viscosity (η_o). In region II or region of transition, the viscosity changes non-linearly with shear rate and is then followed by region III, in which the viscosity decreases with increasing shear rate, exhibiting shear thinning behaviour.

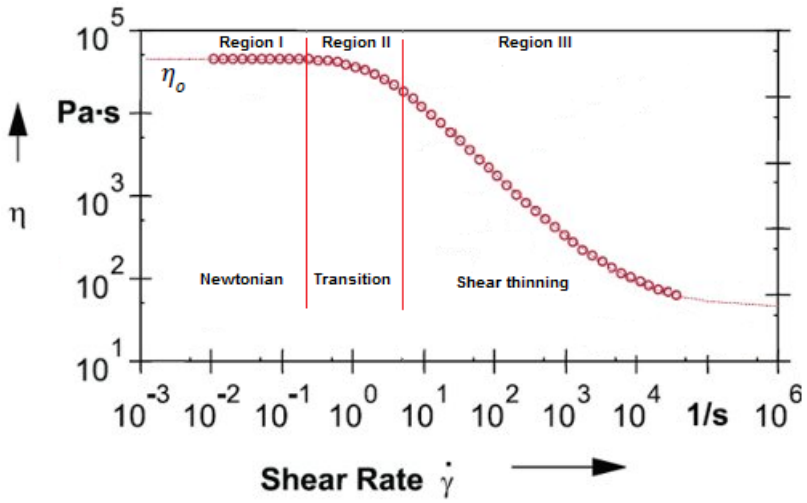

Figure 2.35 Variation of shear viscosity with shear rate for polymer melts

The figure also shows that the viscosity curve can be approximated by a straight line. A simple way to fit viscosity data of polymer melts is the Ostwald-de Waele model or Power- law expression (Scott.Blair et al., 1939), which is defined as:

$$\eta = m * \dot{\gamma}^{n-1} \qquad (2.23)$$

The variable m is a measure of consistency and the power law index (n) is defined as the slope of the curve in this region and represents the sensitivity of the polymer to shear. Polymer viscosity decreases with increasing temperature and this effect is represented graphically by a downward shift in the viscosity curve. For the Power-Law function, this is equivalent to changing the consistency index (m), which becomes in the form:

$$m = m_0 * exp[-\beta(T - T_o)] \quad (2.24)$$

The parameter β represents the sensitivity of the polymer to temperature and it is determined from a set of shear viscosity vs shear rate data at different temperatures.

The power law index (n) is defined as the slope of the curve in this region and represents the sensitivity of the polymer to shear. Therefore, higher values of the power law index are likely to result from low shear sensitivity as shown in Figure 2.36 . As a result, higher melt temperatures may be required in the process, causing a major effect on energy consumption. It has been reported that shear sensitivity is of paramount importance for the designing of screw geometries (Eslami, 2014). The helix angle tends to increase with increasing power law index and therefore less shear sensitive materials require larger screw helix angles. Careful considerations are also made when selecting the screw channel in the metering section of the extruder. For example, highly viscous materials are known to need deeper channels than lower viscosity materials in order to improve extrusion performance.

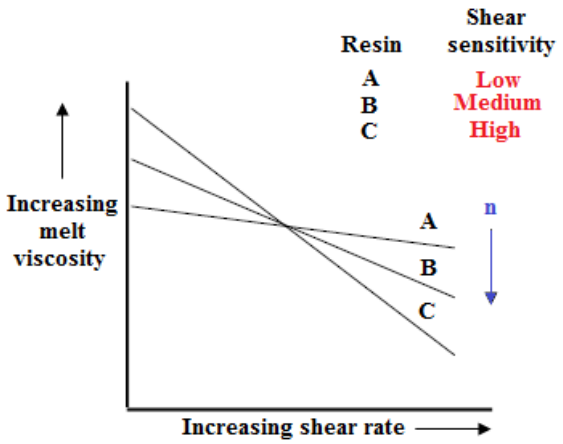

Figure 2.36 Shear sensitivity of polymer melts

Moreover, it has been reported that small increases in power law index can also cause significant increases in viscous heating (Rauwendaal & Ponzielli, 2003). The relationship between viscous heating and power law index is defined as:

$$\eta_h = \frac{m*(\pi D)^{n+2} N^{n+1}}{{h_d}^n C_p \dot{m}} \qquad (2.25)$$

where η_h is the viscous heating, m is the consistency index, D is the screw diameter, n is the power law index, h_d is the channel depth, C_p is the specific heat capacity and $\dot{m}$ is the mass flow rate.

2.11 Thermal properties of polymers

Differential scanning calorimetry (DSC) is a thermal analysis technique widely used to examine the thermal characteristics of polymers by measuring the difference in heat flow to the sample and a reference as a function of temperature during heating or cooling (Figure 2.37).

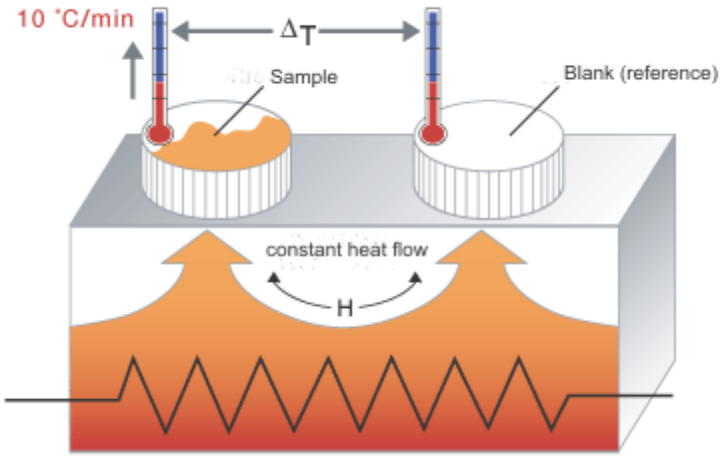

Figure 2.37 Schematic principle of DSC measurement (TU Braunschweig, 2015)

The heat flow difference is defined as:

$$\text{Heat flow difference} = \Delta\frac{dH}{dt} = \left(\frac{dH}{dt}\right)_{sample} - \left(\frac{dH}{dt}\right)_{reference} \quad (2.26)$$

During the heating of a sample, for example, DSC enables determination of thermal transitions as well as the temperatures at which they occur such as glass transition temperature, crystallisation temperature and melting as shown in Figure 2.38.

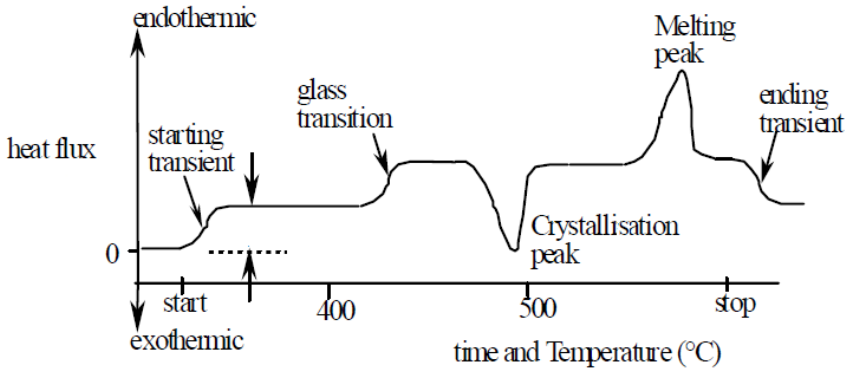

Figure 2.38 A schematic DSC curve showing types of thermal transitions (College, 2015)

Glass transition is the region at which the material changes from a rigid glassy to softer amorphous form and the effect in a DSC curve is recorded as a slight endothermic step change at the glass transition temperature.

Crystallisation is an exothermic transition where polymers become ordered, crystallised, and so their atoms/molecules re-arrange into a more stable state. In the melting process, polymers melt and consequently become disordered in the form of an amorphous liquid. It is an endothermic process at which the crystalline volume is destroyed at a specific temperature known as the melting temperature.

2.12 Extruder scale up

The first attempt to study the scale-up theory for single screw extrusion was initiated by (Carley & McKelvey, 1953) in order to predict the performance of large production size extruders on the basis of geometrically similar small extruders. Considering isothermal melt extruders, it was shown that both the output rate and power consumption increased by the cubic power of the diameter ratio of the screws. In addition, it was found that these scale-up factors were also applicable to plasticating extruders. However, this scale-up method led to undesirable extrusion performance at higher screw speeds, where output rates are more limited by the melting ability of the extruder screws.

Maddock, (1974) used several scale-up factors and examined other inherent problems such as barrel surface area and heat transfer coefficient. By the square root rule, this is scaling-up the channel depth in the metering section to the square root of the diameter ratio whilst the screw speed is scaled-down by the same factor, it was shown that lower output rates were measured at equivalent melt temperatures. Furthermore, viscous heat generation and cooling requirements were found to increase with increasing screw diameter irrespective of the scale-up rule.

This scale-up method by the square root rule led to higher melt temperatures, specific energy consumption and poorer homogeneity of the melt. On the basis of this method, Chung, (1984) analysed the major functions of a conventional extruder screw in order to accomplish a more satisfactory analysis of the scale-up theory. It was shown that the effect of scale-up clearly had an effect on extruder performance, leading to an imbalance in solids conveying, melting and pumping rate. He noticed that the melting capacity increased at a rate lower than the square of the diameter as screw diameter was increased whilst the solid conveying and pumping capacities exhibited a greater increase.

In a similar manner, Pearson, (1976) analysed the solid conveying, melting and melt conveying sections of the extruder screw to develop a thorough analysis of the scale-up theory. It was shown that all three functions balanced properly as long as the screw helix angle and the temperature in the extruder barrel remained constant. The theory allowed control over temperature, variation in temperature and pressure.

Fenner & Williams, (1971) performed dimensional analysis for scaling up the melt flow in the metering section of a conventional screw extruder. They found that thermal problems gained major importance in large screw extruders when the process involved the use of plastics with low thermal conductivity and high viscosity. This work was later extended by (Yi & Fenner, 1976) and the major drawback was that it gave higher specific energy consumptions as a result of excessive viscous heat generation.

The above studies were based on the assumption of a constant L/D ratio. Schenkel, (1978) kept L/H ratio constant and noticed that a reduction in L/D ratio allowed a more satisfactory scale-up theory. This procedure, however, was based on considerations related to the melt conveying process and therefore there was a strong imbalance between the melting and melt conveying rates, making the theory particularly suitable for melt fed extruders.

Potente & Fisher, (1977) surveyed scale-up rules for single screw extruders based on the analysis of the solids and melt conveying. For conventional extruders, they found similar rules to those proposed by Maddock. This method resulted in an imbalance rate between the melting and the solids and melt conveying with an increase of the specific energy consumption. This work was later extended by (Potente, 1991) and improved by including variable length and analysis of twin screw extruders.

Rauwendaal, (1987) proposed two new scale-up methods by addressing the most relevant conditions for scaling up production; a constant specific energy consumption and balanced melting and pumping rates. The first theory remained constant the specific surface area and gave satisfactory results although the melting rate increased insufficiently. This led to the formulation of a second theory in which the melting and pumping rates were kept constant. Rauwendaal, (1994) summarised these scale up factors as shown in Table 2.3.

Table 2.3 Common scale up factors for single screw extruders (Rauwendaal, 1994)

	Small Extruder	Large Extruder
Diameter	D_1	D_2
Channel width	W_1	$W_2 = W_1\,(D_2/D_1)$
Channel depth	H_1	$H_2 = H_1\,(D_2/D_1)^{0.5}$
Screw speed	N_1	$N_2 = N_1\,(D_2/D_1)^{0.5}$
Output rate	$\dot{V}_1$	$\dot{V}_2 = \dot{V}_1\,(D_2/D_1)^{2}$
Shear rate	$\dot{\gamma}_1$	$\dot{\gamma}_2 = \dot{\gamma}_1\,(D_2/D_1)^{0}$
Circumferential speed	V_{b1}	$V_{b2} = V_{b1}\,(D_2/D_1)^{0.5}$
Residence time	t_1	$t_2 = t_1\,(D_2/D_1)^{0.5}$
Plasticating capacity	$\dot{M}_{p1}$	$\dot{M}_{p2} = \dot{M}_{p1_1}\,(D_2/D_1)^{1.75}$
Solids conveying rate	$\dot{M}_{s1}$	$\dot{M}_{s2} = \dot{M}_{s1}\,(D_2/D_1)^{2}$
Screw power	$\bar{Z}_1$	$\bar{Z}_2 = \bar{Z}_1\,(D_2/D_1)^{2.5}$
Specific energy consumption	$\hat{Z}_1$	$\hat{Z}_2 = \hat{Z}_1(\,D_2/D_1)^{0.5}$

Due to the lack of generality of the existing scale-up rules, the theories may lead to contradictory results as a result of simplified extrusion process analysis. Recently, Covas & Gaspar-Cunha, (2009) performed a multi-criteria optimisation approach which was based on the interrelationships between computational modelling, routine quantification and multi-objective optimisation that allowed more efficient analysis than conventional scale-up methods.

2.13 Summary

This chapter presented an extensive literature review of relevant research carried out in the field of single screw extrusion. Background information relevant to extruder screw geometries was provided in section 2.5. It was found that the effectiveness of the melting process is strongly affected by the geometry of the screw. Differences in design between non-barrier and barrier screws were discussed to highlight the improved melting performance provided by the barrier flighted screw and its corresponding influence on melt homogeneity.

Temperature measurement methods were reviewed in section 2.6 to show that thermocouple grid sensors in conjunction with infra-red thermometry enabled examination of the thermal dynamics of the extrusion process due to the rapid dynamic response on both techniques.

In addition, these techniques were found to provide accurate temperature measurements, being highly sensitive to thermal fluctuations relating to the melting performance of the extruder screw. Thermal stability is concerned with the relationship between screw geometry and melting. In section 2.7, different melting models were described to understand the melting process mechanism that takes place along the screw. The rate of melting was found to be dependent upon polymer type, processing conditions such as barrel set temperature and extruder screw speed and this was very sensitive to polymer rheology and thermal properties.

In section 2.9, a balance of energy in single screw extrusion was presented with equations for the extrusion process energy consumption due to its relevance to the project aims. The pseudoplastic nature of the melt appeared to be a crucial factor for energy consumption highlighting the importance of polymer rheology, in particular melt shear viscosity. In addition, screw dimensions, process settings and thermal properties were key variables in the analysis of power consumption. Sections 2.10 and 2.11, therefore, aimed to examine the rheological and thermal characteristics of polymers and their role in screw design, rate of melting and energy consumption. Melt viscosity and thermal measurements such as melting point and enthalpy of melting were found to significantly affect process energy consumption, melting performance of the extruder screw and design. Finally, section 2.12 provided a review of several scale up factors and their effect of extrusion performance.

CHAPTER THREE

3 EXPERIMENTAL EQUIPMENT AND MATERIALS

3.1 Introduction

This chapter provides information of materials and details of the experimental equipment used to carry out the experimental work. In section 3.2 the specification of the materials is given, with their properties and applications. In section 3.3, the experimental equipment, operation conditions and monitoring techniques carried out using a large scale single screw extruder (63.5 mm diameter) are described in detail. In section 3.4, the experimental equipment used to study the effect of extruder scale on temperature and energy measurements is provided. The experimental equipment, operation conditions and monitoring techniques carried out using a small scale single screw extruder (38 mm diameter) are also described in detail. Finally, rheological and thermal techniques are covered in sections 3.5.

3.2 Materials

Eight different polymers were used throughout the studies, five grades of polyethylene (LDPE, LLDPE and three grades of HDPE), polystyrene, polypropylene and polyethylene terephthalate (data sheets can be found in Appendix A) . These resins were selected because they are among the most widely used engineering plastics in the polymer industry, as shown in section 2.3, Figure 2.4. These polymer types represented 62% of the total European plastics demand in 2011 (29.14 million tonnes), 21% of the total world production (PlasticsEurope, 2013).

3.2.1 Low density polyethylene (LDPE)

Low density polyethylene (LDPE) was supplied in the form of pellets by LyondellBasell Industries. It is a non-additive polyethylene (Lupolen 2420 H) for use in blown and cast film applications.

3.2.2 Linear low density polyethylene (LLDPE)

Linear low density polyethylene (LLDPE) was delivered in the form of pellets by Versalis.S.p.A. It is a butene copolymer (C4-LLDPE), with antioxidants suitable for cast or thin film extrusion applications.

3.2.3 High density polyethylene (HDPE)

Three different molecular weight grades of high density polyethylene were supplied by INEOS Polyolefins in the form of pellets. The first material was a high density copolymer (Rigidex HD5050EA) with a narrow molecular weight distribution for use in injection and compression moulding applications where high environmental stress cracking resistance is required. The second resin was a medium molecular weight homopolymer polyethylene (Rigidex HD6007S) designed for blow moulding and extrusion applications. The third material was a high molecular weight copolymer grade (Rigidex HM5411EA) supplied for medium and large blow moulding applications requiring high environmental stress cracking resistance and good rigidity.

The nominal molecular weight characteristics of the three polymers are presented in Table 3.1

Table 3.1 Molecular weight characteristics for three grades of HDPE

	$\bar{M}_w$	$\bar{M}_w$ / $\bar{M}_n$ **(MWD)**
HD5050	91727	4.1
HD6007	119000	5.8
HD5411	256000	15

3.2.4 Polystyrene (PS)

Polystyrene (PS) was delivered in the form of pellets by STYROLUTION. It is a general purpose polystyrene grade (PS 124N) for use in injection moulding applications and blending.

3.2.5 Polypropylene (PP)

Polypropylene (PP) was supplied in the form of pellets by LyondellBasell Industries. It is a nucleated homopolymer (Moplen HP640J) for extrusion and thermoforming applications.

3.2.6 Polyethylene terephthalate (PET)

Polyethylene terephthalate (PET) was supplied in the form of pellets by Tergal Fibre. This grade (T74F9 080) has an intrinsic viscosity of 0.8dl/g in a 50/50 mixture of phenol/o-dichlorobenzene with a PET concentration of $5gl^{-1}$. It is used for film extrusion applications.

More information of relevant properties of these polymers can be found in Appendix A. The density of these polymers is given in Table 3.2 due to its relevance to the project aims.

Table 3.2 Density of materials

	Density (kg/m^3)
LDPE	924
LLDPE	918
HD5050	950
HD6007	962
HD5411	952
PP	900
PS	1040
PET	1400

3.3 Experimental equipment using a large scale single screw extruder

3.3.1 Large scale single screw extruder

Experiments were carried out using a 63.5 mm diameter single screw extruder (Davis standard BC60) which operates with a flood feeding system as shown in Figure 3.1. Consequently, the screw channels in the feeding section are completely filled with polymer and the extruder throughput is determined by screw speed.

The temperature along the barrel is controlled with Davis Standard "Dual-Therm" temperature controllers and air cooling. Temperature controllers are placed along the extruder barrel arranged in four zones and two thermocouples in each zone are used in a cascade control system. A speed controller (MENTOR II) is used to control the motor speed through a DC tachometer generator.

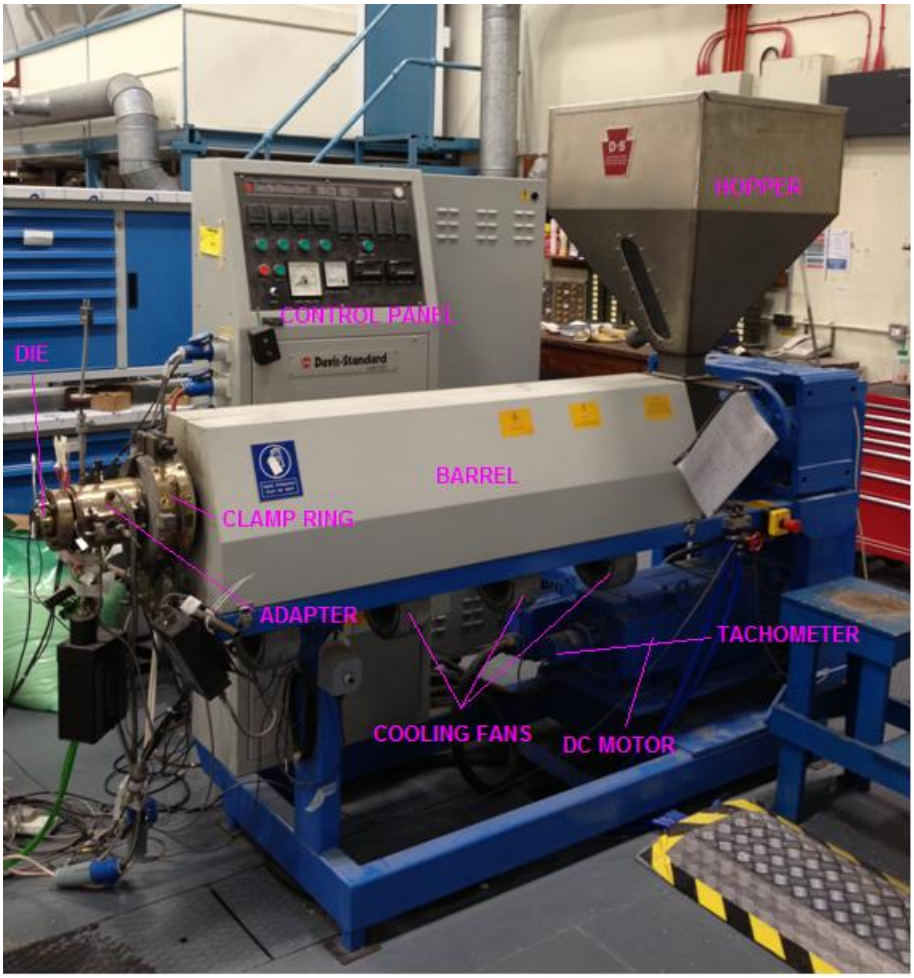

Figure 3.1 Large scale single screw extruder (63.5mm diameter)

3.3.2 Screw geometries used in the large scale single screw extruder

Three extruder screws, representative of those typically used in the polymer industry, were used throughout the experiments all with a length to diameter ratio of 24:1. Schematic representations of the screw designs are shown in Figure 3.2. These designs were selected to study the role of geometry on the melting performance in single screw extrusion. The free volume (FV) of each screw was defined as the free space used to process material in the extruder. These values were determined empirically using a volume displacement method (each screw was inserted into a pipe filled with water).

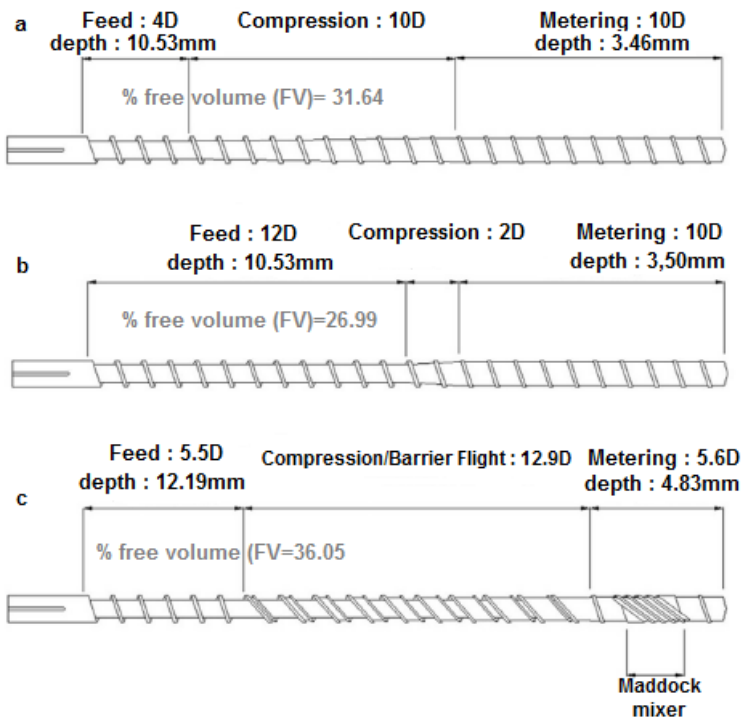

Figure 3.2 Extruder screw geometries used in the large scale single screw extruder a) Single flighted, tapered compression b) Single flighted, stepped compression c) Barrier flighted with spiral mixer (Kelly et al., 2006).

3.3.3 Operating conditions used in the large scale single screw extruder

Experiments were performed at a range of extruder screw speeds from 10 – 90 rpm in steps of 20 rpm, and sufficient time was allowed for conditions to stabilise at each screw speed before data were recorded. Three set temperature conditions were used for each material and are detailed in Table 3.3. Whenever possible the same set temperatures were used for each polymer and three extruder screw geometries. For example, HD5050, LDPE, LLDPE, PS and PP (only two set temperatures) were extruded under the same set temperatures. However, where this was not possible (for example because of excessive extruder torque or irregular solids conveying) set temperatures were adjusted to maintain a stable extrusion process (see HD6007 and HD5411). PET was extruded at higher set temperatures as shown in Table 3.3.

Table 3.3 Extruder set temperatures used in the large scale single screw extruder

HD5050, LDPE, LLDPE, PS					
All 3 screw geometries	**Zone 1**	**Zone 2**	**Zone 3**	**Zone 4**	**Die zones**
180°C	130	155	165	180	180°C
200°C	140	170	185	200	200°C
220°C	150	185	205	220	220°C
HD6007					
Tapered (TA)	**Zone 1**	**Zone 2**	**Zone 3**	**Zone 4**	**Die zones**
180°C	150	170	170	180	180°C
200°C	150	180	185	200	200°C
220°C	150	185	205	220	220°C
Stepped (ST)	**Zone 1**	**Zone 2**	**Zone 3**	**Zone 4**	**Die zones**
180°C	130	155	165	180	180°C
200°C	140	170	185	200	200°C
220°C	150	185	205	220	220°C
Barrier flighted (BA)	**Zone 1**	**Zone 2**	**Zone 3**	**Zone 4**	**Die zones**
180°C	140	165	165	180	180°C
200°C	140	170	185	200	200°C
220°C	150	185	205	220	220°C
HD5411					
Tapered (TA)	**Zone 1**	**Zone 2**	**Zone 3**	**Zone 4**	**Die zones**
180°C	100	130	165	180	180°C
200°C	100	130	185	200	200°C
220°C	100	130	205	220	220°C
Stepped (ST)	**Zone 1**	**Zone 2**	**Zone 3**	**Zone 4**	**Die zones**
180°C	85	130	165	180	180°C
200°C	85	130	185	200	200°C
220°C	100	130	205	220	220°C
Barrier flighted (BF)	**Zone 1**	**Zone 2**	**Zone 3**	**Zone 4**	**Die zones**
180°C	180	180	180	180	180°C
200°C	180	180	185	200	200°C
220°C	180	180	205	220	220°C

Table 3.3 Extruder set temperatures used in the large scale single screw extruder

PP					
Tapered (TA)	**Zone 1**	**Zone 2**	**Zone 3**	**Zone 4**	**Die zones**
200°C	140	170	185	200	200°C
220°C	150	185	205	220	220°C
240°C	150	185	220	240	240°C
Stepped (ST)	**Zone 1**	**Zone 2**	**Zone 3**	**Zone 4**	**Die zones**
200°C	140	170	185	200	200°C
220°C	150	185	205	220	220°C
240°C	150	185	220	240	240°C
Barrier flighted (BF)	**Zone 1**	**Zone 2**	**Zone 3**	**Zone 4**	**Die zones**
200°C	140	170	185	200	200°C
220°C	150	185	205	220	220°C
240°C	150	185	220	240	240°C
PET					
Tapered (TA)	**Zone 1**	**Zone 2**	**Zone 3**	**Zone 4**	**Die zones**
280°C	240	260	280	280	280°C
290°C	250	270	290	290	290°C
300°C	260	280	300	300	300°C
Stepped (ST)	**Zone 1**	**Zone 2**	**Zone 3**	**Zone 4**	**Die zones**
280°C	240	260	280	280	280°C
290°C	250	270	290	290	290°C
300°C	260	280	300	300	300°C
Barrier flighted (BF)	**Zone 1**	**Zone 2**	**Zone 3**	**Zone 4**	**Die zones**
280°C	240	260	280	280	280°C
290°C	250	270	290	290	290°C
300°C	260	280	300	300	300°C

3.3.4 Monitoring techniques used in the large scale single screw extruder

In-process monitoring techniques were used to assess the extrusion process using an instrumented die adaptor (internal diameter 38mm) downstream of the screw and prior to the entrance of a 6mm diameter rod die. Die temperature was controlled with band heaters clamped to the die clamp ring, adapter and die. All measurements were made at a frequency of 10Hz using software developed in-house. A schematic diagram of this measurement region is shown in Figure 3.3

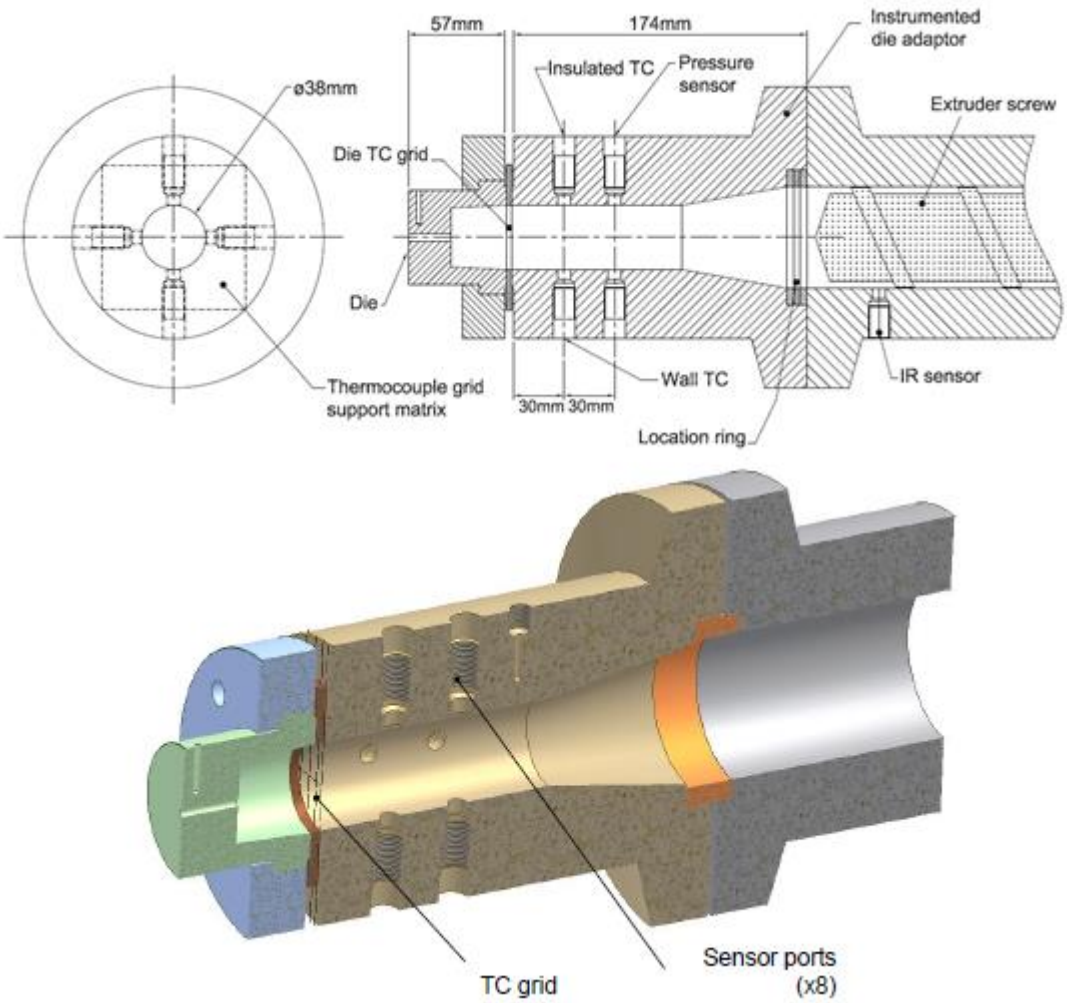

Figure 3.3 Instrumented extruder die showing location of thermocouple grid at die entrance

Thermal homogeneity was assessed using thermocouple grid sensors in conjunction with infra-red thermometers.

In the adaptor, a wall thermocouple (3 mm diameter J-Type) and an insulated J-Type thermocouple of 0.5 mm diameter protruding 1.0 mm into the melt were fitted. This enabled measurement of two melt temperatures values; one representing the temperature of the wall and another representing the temperature of the melt close to the wall. The thermocouple grid sensors used in this work have been described in detail previously (Brown et al., 2004) including calibration techniques and quantification of shear heating and conduction errors. These devices consist of a two dimensional array of interconnected exposed thermocouple junctions mounted in a supporting frame.

Two different wire types were used to construct thermocouple junctions; at each junction, an EMF is generated which can be correlated to the local temperature. To create the thermocouple junctions, wires were fused together using a controlled amount of current discharged from a capacitor. Thermocouple wire diameter was 0.3 mm. These thermocouple junctions can be then monitored in real time by a PC thermocouple card. The thermocouple grid was located at the entrance to a 6 mm diameter rod die, in the instrumented adaptor section (internal diameter 38mm) of the single screw extruder (Figure 3.3), which in conjunction with the thermocouples described above generated detailed information concerning melt temperature across the flow path.

Previously reported studies (Brown et al., 2004) using the same technique showed that temperature of the flowing melt was radially symmetrical when averaged over a significant period of time. The design of the thermocouple mesh then incorporated seven junctions located on a central axis across the flow channel in a non-symmetrical spacing. The thermocouple grid allowed 2D profiles of melt temperature flowing through the die to be measured in real time, enabling characterisation of the thermal dynamics of the extrusion process.

Temperature measurements were examined at each position over 1 minute, providing 14 data points about the central axis plus and averaged output from wall and insulated wall thermocouples. In total, 15 data points were used to construct radial melt temperatures to collect information relating to thermal homogeneity. The geometry of the thermocouple mesh sensor is shown in Figure 3.4 .

Melt temperature fluctuation over a period of 1 min was calculated by taking an average of the standard variation at each individual position (TSD), reflecting only fluctuation and not range of temperature (max value-min value) across the melt flow.

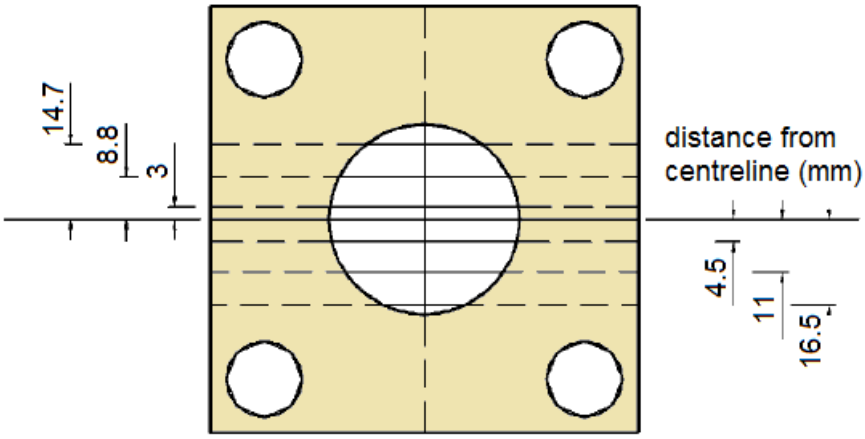

Figure 3.4 Thermocouple mesh

An infrared temperature sensor (Dynisco MTX 922) was flush mounted to the surface of the extruder barrel at a position corresponding to the metering section of the extruder screw. This was used to monitor the melt temperature across the width of the screw channel and generate a melt temperature profile across the channel during each rotation, between screw flights. The infrared sensor (0–5 V output) had a quoted response time of 10 ms and measured infrared energy between the wavelengths of 1.6 to 2.2 µm (Kelly et al., 2003). It was calibrated statically for each polymer at a range of set temperatures. Measured data from the IR sensor was collected at a frequency of 20 Hz

A melt pressure transducer (Dynisco PT422A) was fitted in the die adaptor in order to examine pressure variation and its relationship to melt temperature, providing information regarding fluctuations caused by melting instabilities. Real-time quantification of energy consumption was monitored using a 3-phase unbalanced loads energy meter (Hioki 3169) connected to the 3-phase power supply of the extruder Figure 3.5 This energy meter was used with HD5050, HD6007 and HD5411. This measured total energy consumption of the extrusion process, including consumption by the motor, heaters and cooling fans. Two Acuvim IIE three-phase power meters were also used with PP, PS, LDPE and LLDPE, separately measuring total energy consumption and that of the motor (Figure 3.5). Energy consumption required by the heaters and cooling fans was measured as the difference in energy between the total and the motor consumptions.

As a result, the relationships between set process conditions, thermal dynamics, melt pressure and energy consumption could be explored

Figure 3.5 a) Hioki 3169 b) Acuvim IIE

3.4 Experimental equipment using a small scale single screw extruder

3.4.1 Small scale single screw extruder

Measurements were carried out using a flood fed 38mm diameter single screw extruder (Davis Standard Betol BK 38), as shown in Figure 3.6. This was equipped with Dual-Therm barrel temperature control and air cooling. The temperature control is provided by individual heating and cooling zones along the barrel arranged in four zones. A speed controller (MENTOR II) is used to control the motor speed through a DC tachometer generator

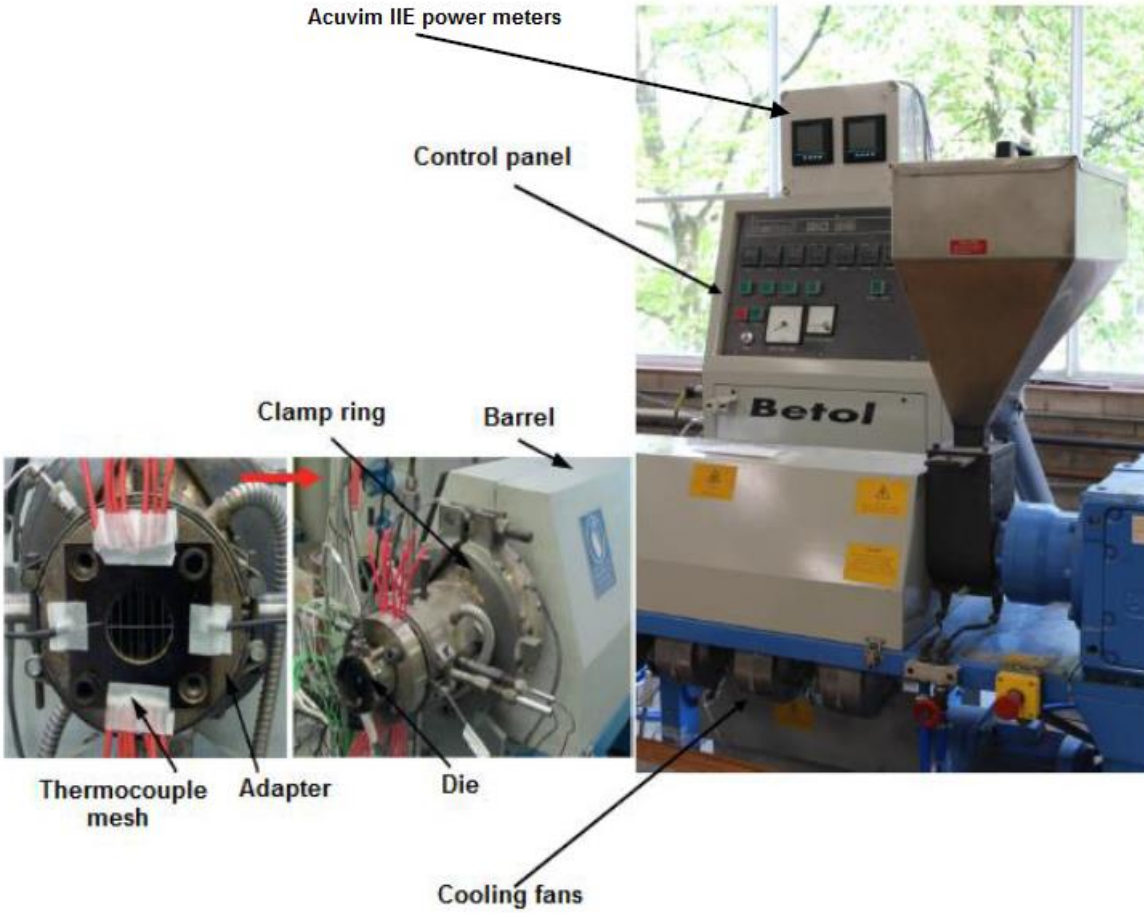

Figure 3.6 Small scale single screw extruder (38mm diameter)

3.4.2 Screw geometries used in the small scale single screw extruder

Two single flighted extruder screws (tapered and stepped compression) and one barrier flighted screw with a spiral mixer were used, having length to diameter ratios of 24:1 and compression ratios of 3:1 and 2:5:1 respectively (Figure 3.7). These polyolefin screw designs were identical to those used in the large extruder.

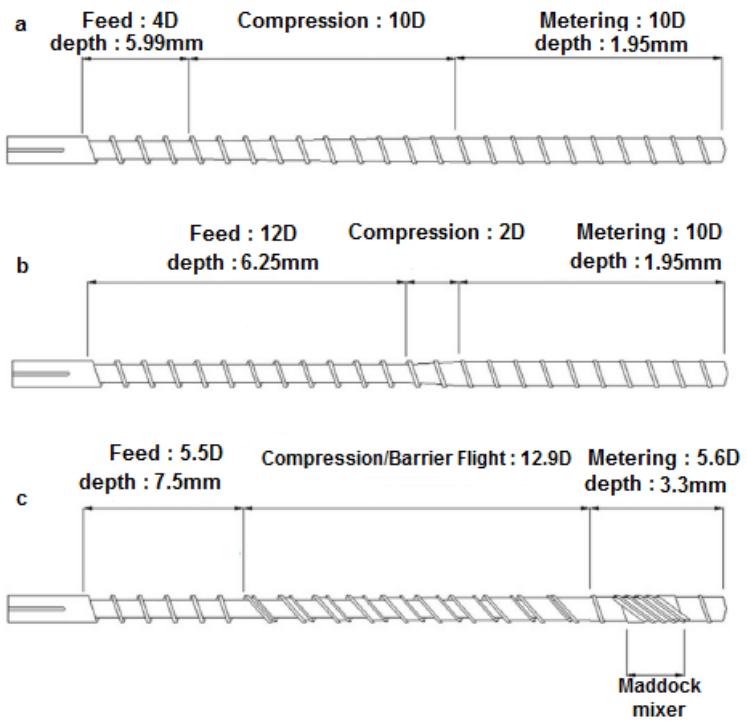

Figure 3.7 Extruder screw geometries used in the small scale single screw extruder a) Single flighted, tapered compression. b) Single flighted, stepped compression, c) Barrier flighted with spiral mixer.

3.4.3 Operating conditions used in the small scale single screw extruder

In this study, each screw was also run at a range of screw speeds from 10 – 90 rpm in steps of 20rpm, and sufficient time was allowed to achieve thermal stability at each screw speed. In order to provide a direct comparison to the extrusion data measured with the large extruder, same set temperatures and polymers (LDPE and HD5050) were used, as detailed as detailed in Table 3.4.

Table 3.4 Extruder set temperatures used in the small scale single screw extruder

HD5050 and LDPE					
All 3 screw geometries	**Zone 1**	**Zone 2**	**Zone 3**	**Zone 4**	**Die zones**
180°C	130	155	165	180	180°C
200°C	140	170	185	200	200°C
220°C	150	185	205	220	220°C

3.4.4 Monitoring techniques used in the small scale single screw extruder

Quantification of the thermal stability of the 38 mm extrusion process was assessed employing the same instrumented die adaptor (which was used in the large scale single screw extruder) with temperature techniques and pressure transducer. These have been previously described in section 3.3.4.

Additionally, two Acuvim IIE three-phase power meters were also used, separately measuring total energy consumption and that of the motor (Figure 3.5). Energy consumption required by the heaters and cooling fans was also measured as the difference in energy between the total and the motor consumptions.

3.5 Rheological and thermal characterisation

3.5.1 Capillary rheometry

The rheological behaviour for all materials was studied using capillary rheometry. The rheological experiments were conducted to compare the shear viscosity for each material at three set temperatures (identical to those used in the extruder die zones) and also to examine how sensitive each polymer is to temperature and shear rate. This will help to highlight the importance of the rheology and its role on the polymer processability in single screw extrusion. In addition, the measured rheological data was used to calculate bulk viscosity in the screw channel at the end of the extruder barrel, allowing investigation of the effect of melt viscosity on set process conditions, thermal dynamics, melt pressure and energy consumption. All off-line rheological measurements were made using a Rosand RH10 twin bore capillary rheometer over a shear rate range of 10 – 1000s^{-1} in 8 stages. The twin bore capillary rheometer is shown in Figure 3.8

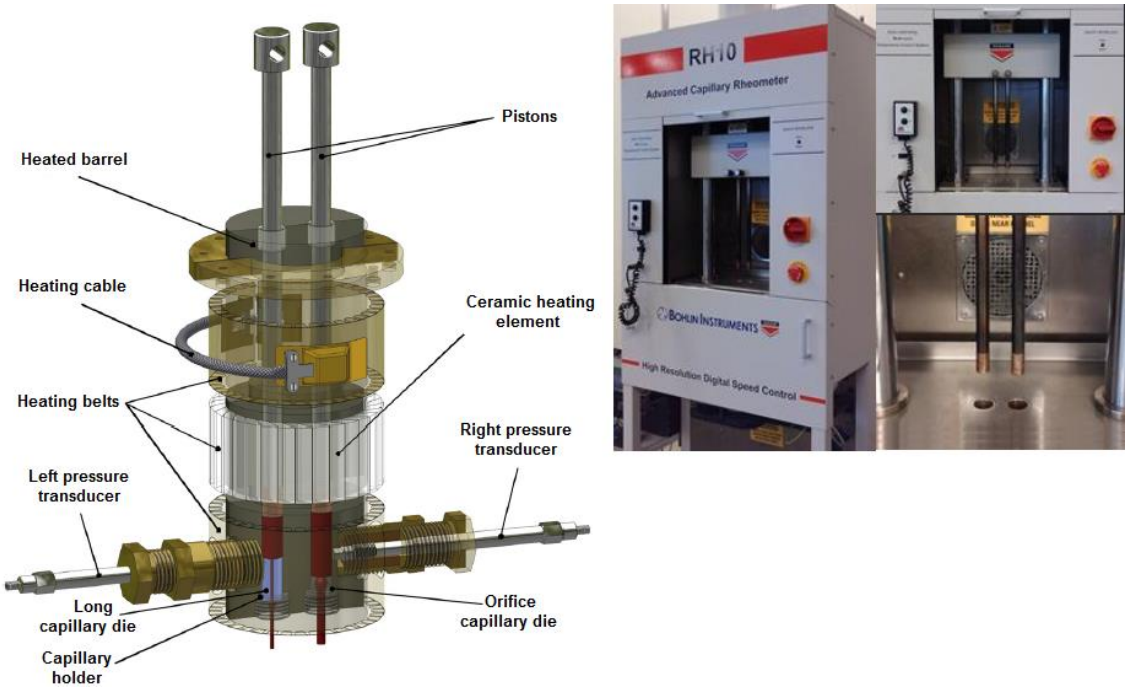

Figure 3.8 Twin bore capillary rheometer (Rosand RH10) (Zatloukal & Musil, 2009)

This commercial rheometer is equipped with two barrels and enables Bagley's correction to be performed automatically by measuring the pressure drop through a zero-length die. The software also includes the option of Weissenberg/Rabinowitsch correction. The capillary dies had 180° entrance angles and dimensions of 32 × 2mm diameter and 0 × 2mm diameter. Two repeated tests were performed for all materials at rheometer set temperatures of 180° C, 200°C and 220°C for each of the PE's and PS, 200°C, 220°C and 240°C for PP and 280°C, 290°C and 300°C for PET. For PET, pellets were dried prior to rheological testing using a drier. Polymer granules were fed into the barrel and sufficient time was allowed for the polymer to melt. The samples were then slightly compressed at first before the test was run. The results files were saved in a compatible format with Microsoft Excel enabling further analysis.

3.5.2 Differential Scanning Calorimetry

Thermal analysis of the materials was performed using a differential scanning calorimeter (DSC Q20, TA instruments). DSC experiments were used to determine the melting temperature, enthalpy of melting (fusion) and degree of crystallinity of the polymers used throughout the studies.

DSC analysis was performed on 5-10 mg samples by heating over the temperature range from ambient to 200°C at 10°C/min heating rate under nitrogen atmosphere, followed by controlled cooling at 10°C/min to ambient. The samples were sealed into a small aluminium pan and an empty sample pan was used as a reference. For PET, the temperature was raised up to 300°C at 10°C/min, followed by controlled cooling at 10°C/min and then heating up to 300°C at 10°C/min. During the heating of a sample, the peak of the curve corresponds to the melt peak temperature or melting point (T_m) and the area under the curve is the enthalpy of melting (ΔH_m). Both values were calculated from the DSC thermogram (heat flow vs. temperature) and a sample is shown in Figure 3.9 for HD5050. For PET, melting point and enthalpy of melting were calculated from the second heating stage.

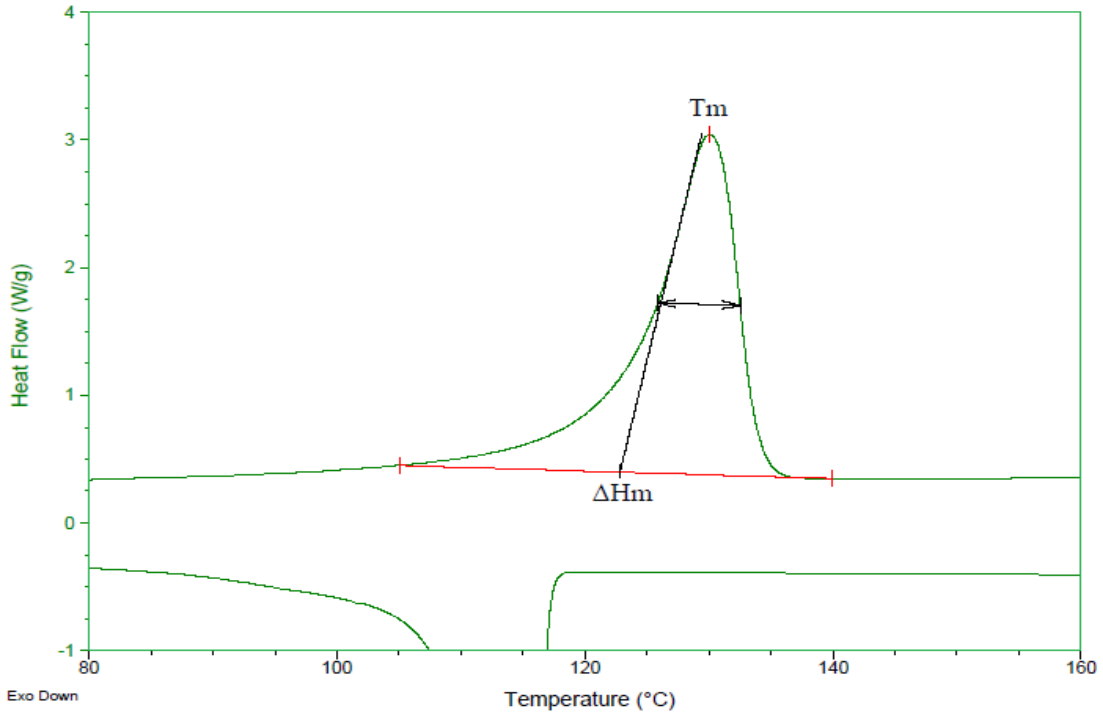

Figure 3.9 Melting temperature and enthalpy of melting from the DSC thermogram for HD5050

Degrees of crystallinity (X_c) were calculated by using the following equation:

$$X_c(\%) = \frac{\Delta H_m}{\Delta H_o} \times 100$$

where ΔH_m is the enthalpy of melting of the sample and ΔH_o is the theoretical enthalpy of melting for a 100% crystalline sample.

CHAPTER FOUR

4 RESULTS AND DISCUSSION

4.1 Rheological results

In this section the rheological behaviour of the polymers at three set temperatures over a shear strain rate relevant to the extrusion process (10 – 1000 s^{-1}) is presented and discussed.

Figure 4.1 and Figure 4.2 display shear viscosities for all polyethylenes at set temperatures of 180 °C, 200 °C and 220 °C. Overall, viscosities decreased with increasing temperature and exhibited shear-thinning behaviour, reflected by the lower values of shear viscosity at high shear rates.

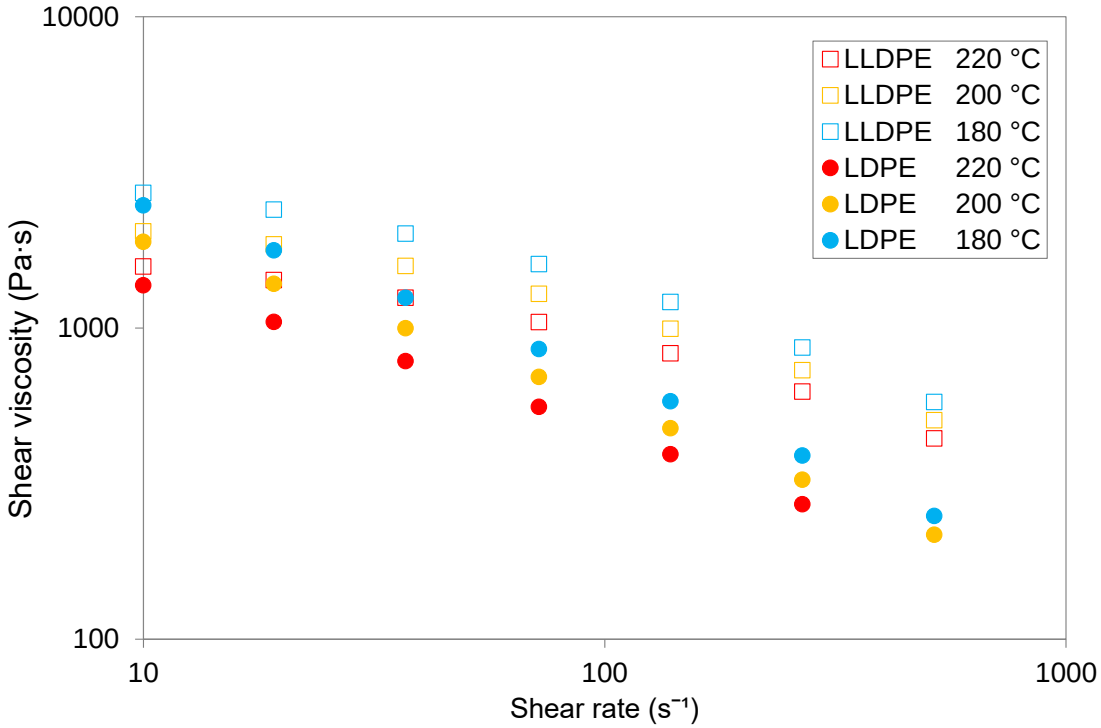

Figure 4.1 Shear viscosity vs shear rate measured using a twin bore capillary rheometer for LDPE and LLDPE

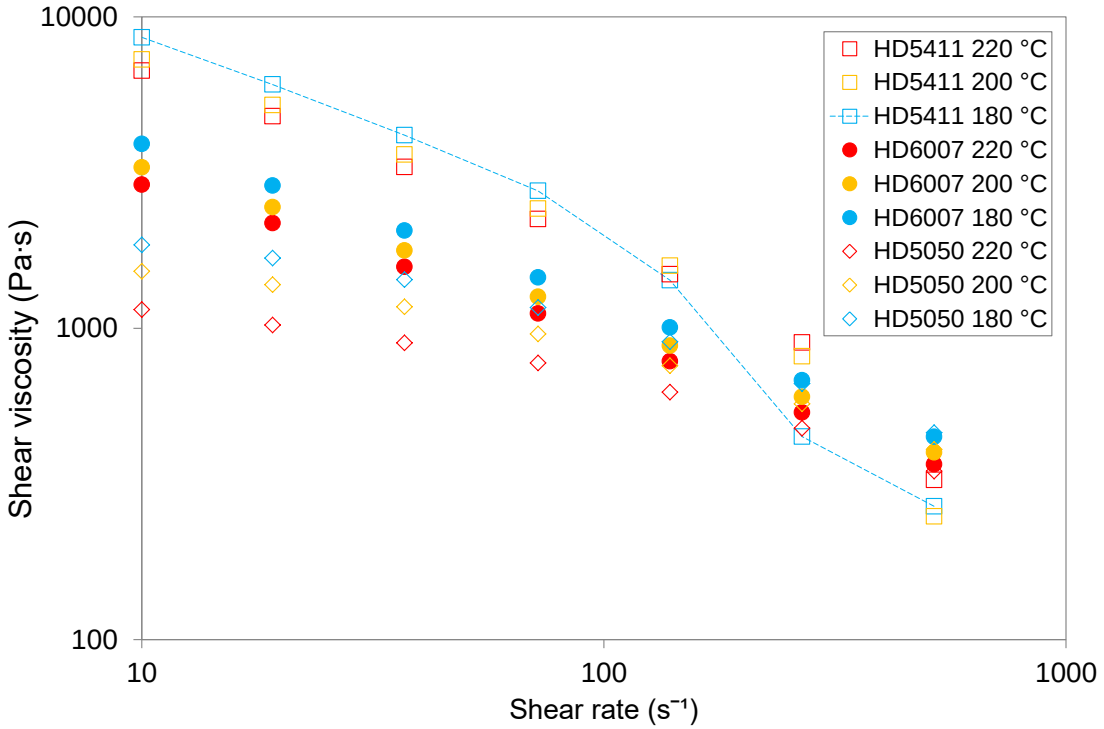

Figure 4.2 Shear viscosity vs shear rate measured using a twin bore capillary rheometer for three grades of HDPE

From the data shown in Figure 4.1, the differences in rheological behaviour between LLDPE and LDPE are confirmed. It has been reported that LLDPE is less likely to be affected by shear when compared to LDPE because of its narrower molecular weight distribution and shorter chain branching. Dealy & Wissbrun, (1999) observed that LLDPE exhibited then higher viscosities at higher shear rates, which is clearly shown in Figure 4.1.

Figure 4.2 shows measured shear viscosity for all grades of HDPE at the same conditions, enabling examination of the dependence of melt viscosity on molecular weight. Viscosity is shown to decrease with decreasing molecular weight as could be expected. The shear viscosity was clearly ordered as follows: HD5411 > HD6007 > HD5050. Moreover, it was noticed the effect of surface melt fracture for the highest molecular weight (HD5411) leading to the lowest values of shear viscosity over the shear range of 500 - 1000s^{-1}. This is commonly known as oscillating melt fracture flow region (Fyrillas et al., 1999), a processing instability characterised by pressure and flow rate oscillations that causes periodic and alternating rough and smooth regions on the surface of the extrudate (Delgadillo-Velazquez et al., 2008). This effect has been highlighted by adding a trend-line to the measured rheological data at 180°C.

The rheological behaviour of PS, PP and PET is presented in Figure 4.3. These measurements were made at different rheometer set temperatures (section 3.5.1) and, therefore, a direct comparison of their rheological properties may result in a very complex analysis. However, it was found that shear viscosity for all materials exhibited shear-thinning behaviour and this decreased with increasing set temperature.

Giles et al., (2005) reported that shear viscosity for PP was more sensitive with respect to shear than temperature whilst other polymers such as PET were more temperature sensitive. In contrast, the viscosity of PS was found to be sensitive to both shear and temperature. From Figure 4.3, according to (Giles et al., 2005), it can be seen that PS and PP exhibited greater shear-thinning behaviour than PET.

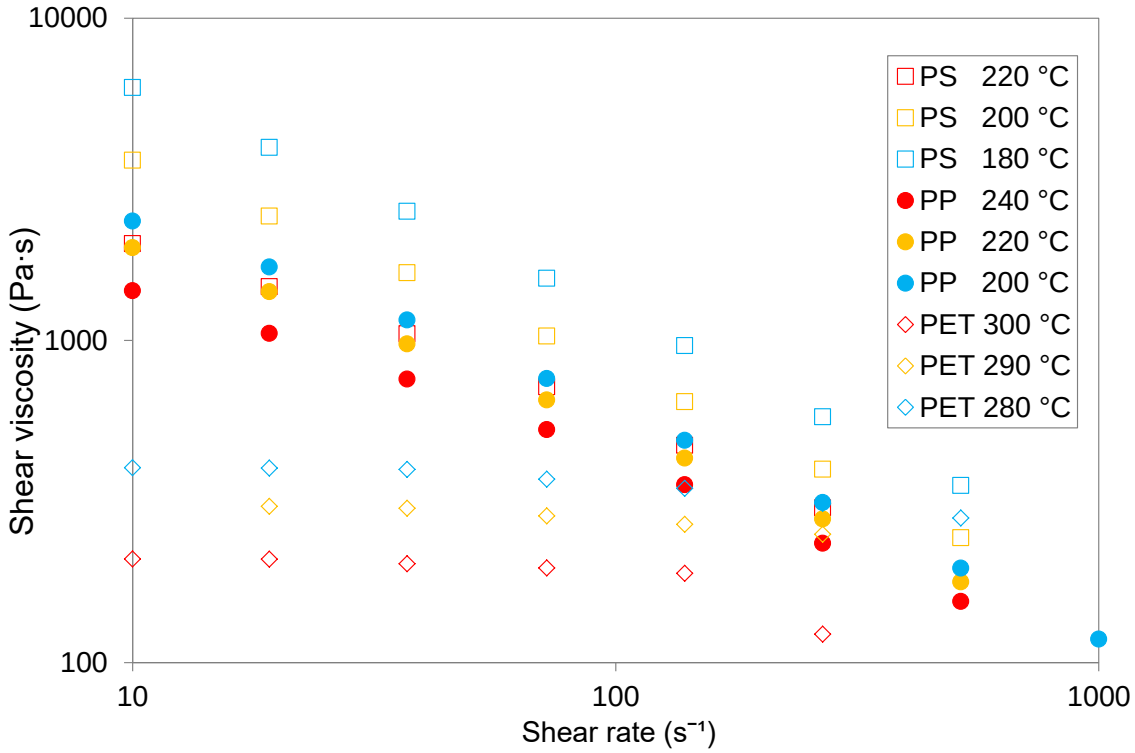

Figure 4.3 Shear viscosity vs shear rate measured using a twin bore capillary rheometer for PS, PP and PET

As mentioned in section 2.10.2 , when examining the shear viscosity of polymer melts being extruded by capillary rheometry, polymers exhibit a shear-thinning region in which viscosity decreases with shear rate. In order to quantify the change in viscosity with shear rate, the power law index is widely used. This is a measure which represents the sensitivity of the polymer to shear.

Values of power law index for each material and set temperature conditions are shown in Table 4.1. In general, power law index decreased with decreasing set temperature. These results highlighted the melt flow properties observed for LLDPE and LDPE. Compared to LDPE, LLDPE is shown to be less shear sensitive due the higher values of power law index observed (Table 4.1). This confirms that LLDPE had a higher viscosity over the shear rate range studied.

On the other hand, the lowest values of power law index were associated with the highest molecular weight HD5411 (Table 3.1), reflecting both the dependence of melt viscosity on molecular weight and the greatest shear thinning behaviour noticed in Figure 4.2. According to (Giles et al., 2005), PET was found to be more sensitive to change in temperature due the high values of power law index measured. Compared to PS and PP, the shear viscosity of PET was found to be relatively unaffected by shear, especially at medium shear rates.

Temperature dependence for each polymer was modelled using exponential temperature dependence, allowing quantification of temperature sensitivity (see section 2.10.2.2). Values of temperature sensitivity coefficient (β) for each polymer are also given in Table 4.1. Most notably, for the highest and medium viscosity grades of HDPE, the effect of set temperature had less effect on melt viscosity, especially for the highest viscosity grade of HDPE ($\beta = 0.0101°C^{-1}$). This is thought to result from the higher molecular weight distribution of these grades, as shown in section 3.2, Table 3.1.

Moreover, according to Giles et al., 2005, the effect of set temperature was found to have a major effect on measured viscosity data for PS and PET due the highest values of temperature sensitivity coefficient measured, corresponding to 0.0615 and $0.0624°C^{-1}$ respectively.

Table 4.1 Values of power law index and temperature sensitivity coefficient for all materials

LDPE	**220°C**	**200°C**	**180°C**	**LDPE**	
n	0.51	0.45	0.43	$\boldsymbol{\beta}(°\boldsymbol{C}^{-1})$	0.024
LLDPE	**220°C**	**200°C**	**180°C**	**LLDPE**	
n	0.7	0.65	0.61	$\boldsymbol{\beta}(°\boldsymbol{C}^{-1})$	0.0164
HD5050	**220°C**	**200°C**	**180°C**	**HD5050**	
n	0.7	0.67	0.65	$\boldsymbol{\beta}(°\boldsymbol{C}^{-1})$	0.0152
HD6007	**220°C**	**200°C**	**180°C**	**HD6007**	
n	0.47	0.47	0.45	$\boldsymbol{\beta}(°\boldsymbol{C}^{-1})$	0.0139
HD5411	**220°C**	**200°C**	**180°C**	**HD5411**	
n	0.3	0.2	0.1	$\boldsymbol{\beta}(°\boldsymbol{C}^{-1})$	0.0101
PS	**220°C**	**200°C**	**180°C**	**PS**	
n	0.43	0.31	0.28	$\boldsymbol{\beta}(°\boldsymbol{C}^{-1})$	0.0615
PP	**240°C**	**220°C**	**200°C**	**PP**	
n	0.44	0.39	0.36	$\boldsymbol{\beta}(°\boldsymbol{C}^{-1})$	0.0231
PET	**300°C**	**290°C**	**280°C**	**PET**	
n	0.96	0.94	0.92	$\boldsymbol{\beta}(°\boldsymbol{C}^{-1})$	0.0624

4.2 Thermal properties

The melt peak temperature (melting point), enthalpy of melting and degree of crystallinity, considering 293 J/g for a 100% crystalline polyethylene, 207J/g for a 100% crystalline polypropylene and 140 J/g for a 100% crystalline polyethylene terephthalate (Blaine, 2014), were calculated using DSC and summarised in Table 4.2.

Table 4.2 Thermal properties of polymers

	Melt peak temperature (°C)	Enthalpy (J/g)	Theoretical enthalpy (100%) (J/g)	Crystallinity (%)
LDPE	113.07	73.96	293	25.24
LLDPE	116.30	56.37	293	19.24
HD5050	130.82	139.03	293	47.45
HD6007	133.75	175.90	293	60.03
HD5411	131.32	133.90	293	45.70
PP	166.36	73.83	207	35.67
PET	248.64	77.00	140	55.00

The degree of branching affects polymer crystallinity (Crystallinity in polymers, 2014). In polymers that have linear chains with little branching such as HDPE, molecules can pack closely together causing polymers to be more ordered, leading to a higher degree of crystallinity. From the data shown in Table 4.2, all HDPE´s exhibited higher crystallinities than branched polymers such as LDPE (long-chain few branched) and LLDPE (short-chain branched, as shown in section 2.2, Figure 2.1). On the other hand, it has been reported that highly short-branched polymers are less crystalline because branches interfere with the close packing of molecules, causing the polymers to be less ordered. This explains the lowest crystallinity exhibited by LLDPE, suggesting that this polymer contains a significant degree of short chain branching.

In addition, Hoffman & McKinley (1985) noticed that higher degrees of crystallinity were associated with moderate molecular weight, and higher densities of HDPE resulted from the higher crystalline fraction. The density of polyethylenes was found to be ordered as: HD6007 > HD5411> HD5050 > LDPE > LLDPE (see section 3.2, Table 3.2) According to them, from the data shown in Table 4.2, it is revealed that the degree of crystallinity is clearly ordered as follows: HD6007 > HD5411> HD5050 > LDPE > LLDPE.

From Table 4.2, thermal properties of polypropylene homopolymer are confirmed (Farmer, 2013). This polymer is shown to exhibit a degree of crystallinity lower than HDPE with a higher heat resistance. Compared to polypropylene copolymer, which has a lower melting point (152°C) due to the incorporation of ethylene, this polymer exhibited a melting point which ranged between (160-170°C), as could be expected. According to (Al-Fouzan, 2011), PET was found to be a semi-crystalline polymer showing double melting endotherm behaviour thought to result from the presence of more than one polymorphism; changes in morphology and/or the effect of molecular weight distribution (Kong & Hay, 2003). This is shown in Appendix B, Figure B3.

4.3 Extrusion measurements on the large scale extruder

4.3.1 Introduction

Extrusion data are presented to show the effects of screw rotation speed, extruder screw geometry and set extrusion temperatures on melt quality, die pressure and measured specific energy consumption for the extrusion process, motor and heaters/cooling fans. Here, melt quality is measured in terms of temperature and temperature homogeneity which is defined as the average of the standard deviation at each individual thermocouple mesh junction across the flow path. Moreover, the effect of polymer rheology on the extrusion performance has been examined using different polymer types, such as LDPE, LLDPE, three grades of HDPE, PS, PP and PET.

4.3.2 LDPE

In order to examine the effect of polyethylene rheology and set processing conditions on the thermal efficiency of the process, extrusion measurements from five grades of polyethylene are presented in this section. A comparison of shear viscosity for each polyethylene was shown in section 4.1, Figure 4.1 and Figure 4.2 and data clearly showed that LDPE exhibited the lowest viscosity among these polymers. In this chapter, LDPE is therefore used to provide reference extrusion data enabling further examination and comparison of the effect of melt viscosity on the thermal measurements and process energy demand.

LDPE results

The performance of each of the three extruder screws in terms of throughput for LDPE is compared in Figure 4.4 at each set temperature and screw rotation speed. It was noticed that for all three extruder screws there was a linear relationship between screw speed and throughput. The effect of set temperature was found to have a negligible effect on throughput measurements. However, the effect of screw geometry had a major effect; the barrier flighted screw with a spiral mixer produced higher throughputs than the two single flighted screws at the same conditions. This is thought to result from the improved melting ability of the barrier section which tends to provide higher mass productions as a result of a greater free volume as compared to non-barrier screws, as shown in section 3.3.2, Figure 3.2.

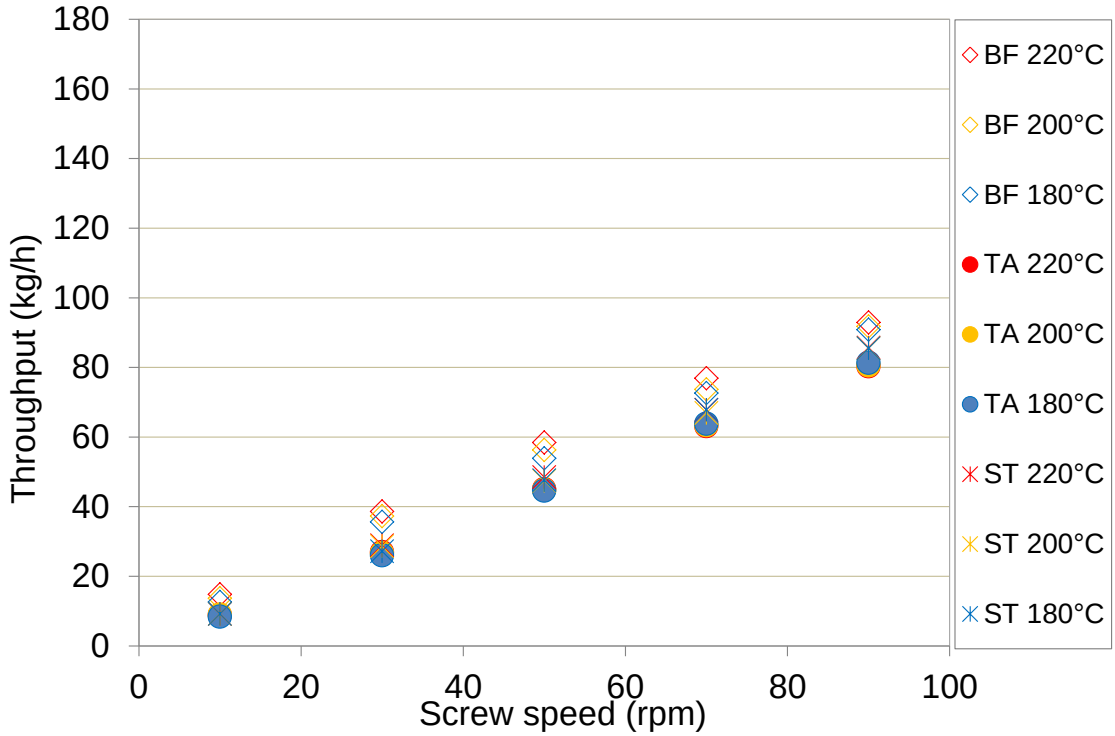

Figure 4.4 Extruder throughput for LDPE vs screw speed (BF: Barrier Flighted Screw; TA: Tapered Compression Screw; ST: Stepped Compression Screw)

Measured radial melt temperatures profiles (averaged over 1 minute) at the entrance to the extruder die for LDPE at 200°C are displayed in Figure 4.5. At 10 rpm, temperature profiles generated by each screw were very similar, with a profile which was flat in shape across the flow channel and dropping towards the die walls. At higher screw speeds, melt temperature profiles were shown to be more dependent upon extruder screw geometry. At 90 rpm both single flighted screws exhibited dips in temperature near to the die walls. This is likely to result from the inherent limitations of non-barrier screws in achieving melt quality performances, leading to the solid bed of polymer to become fully molten close to the end of the extruder screw (Kelly et al., 2006). For the barrier flighted screw, the effect of the screw rotation speed had less effect on radial melt temperatures and these were more consistent in the die section, with no areas of low temperature being observed. This highlights the improved melting ability provided by this geometry leading to consistency in melt temperature at the extruder die.

The effect of extruder set temperature on radial melt temperatures for each screw geometry is shown in more detail in Figure 4.6. The effect of set temperature caused a shift in the profile as could be expected. At 10 rpm, melt temperature profiles were similar in shape irrespective of extruder set temperature and screw geometry. At a set temperature of 220°C, radial melt temperatures are shown to be more sensitive to screw speed as compared to those measured at 200 and 180°C, reflecting a greater variation of temperature across the flow channel which decreased with increasing screw speed. For example, the bulk of temperature in the centre of the flow for both non-barrier screws ranged from 240°C at 10 rpm to 230°C at 90 rpm, as shown in Figure 4.6.

At a set temperature profile of 180°C, however, melt temperature profiles increased with increasing screw speed across the total flow volume. The effect of screw speed on radial melt temperatures was more pronounced for the barrier flighted screw, especially in the centre of the flow where temperatures are shown to reach maximum values (Figure 4.6). In general, radial melt temperatures were more consistent as extruder set temperature decreased. This reflects the rheological behaviour of LDPE and its lower sensitivity to shear exhibited at 180 °C (section 4.1, Table 4.1), causing an increase in melt temperature by viscous energy dissipation via shearing.

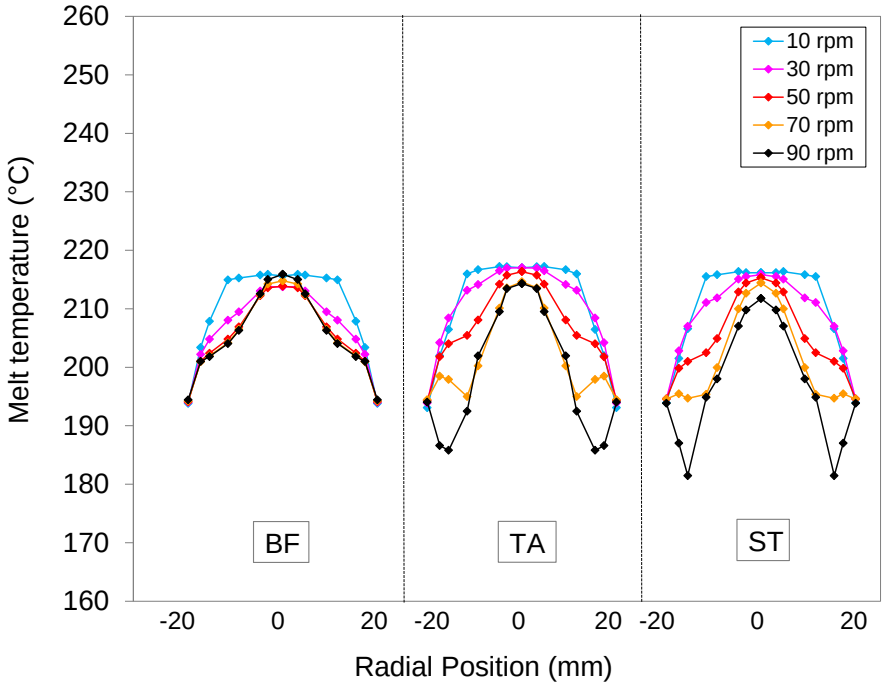

Figure 4.5 Effect of screw geometry on radial melt temperatures measured for LDPE at 200°C (BF: Barrier Flighted Screw; TA: Tapered Compression Screw; ST: Stepped Compression Screw)

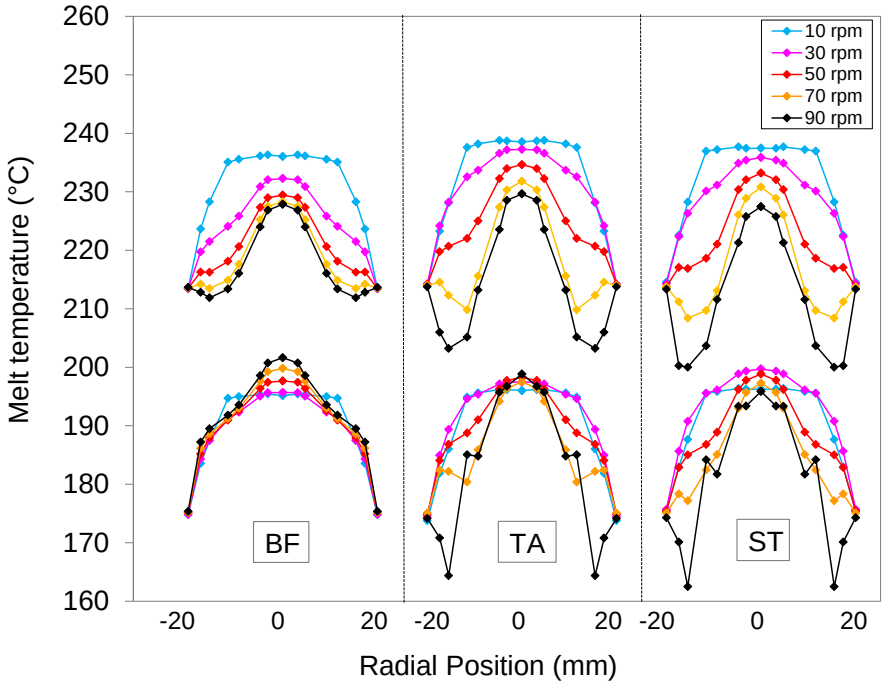

Figure 4.6 Effect of set temperature and screw geometry on radial melt temperatures measured for LDPE at 180°C and 220°C (BF: Barrier Flighted Screw; TA: Tapered Compression Screw; ST: Stepped Compression Screw)

Bulk values of temperature (averaged over a period of 1 min) are plotted against throughput in Figure 4.7 to highlight the melting capability provided by these screw geometries and its effect on measured temperature. For both single flighted screws, it was observed that melt temperatures tended to initially increase with increasing throughput but then decreased above a critical point (corresponding to extruder throughput at screw speed of 30 rpm), especially at the lowest set temperature. This reflects the inefficient melting ability of these screws when there is insufficient time for the volume of polymer within the screw channel to be melted homogeneously causing a decrease in melt temperature. For the barrier flighted screw the effect of decreasing temperature was less pronounced. At 200°C, for example, the variation of temperature was less than 5°C across the range of screw speeds compared to 10°C measured for both single flighted screws. At 180°C, however, temperatures slightly increased with increasing throughput, highlighting the improved melting action of the barrier screw.

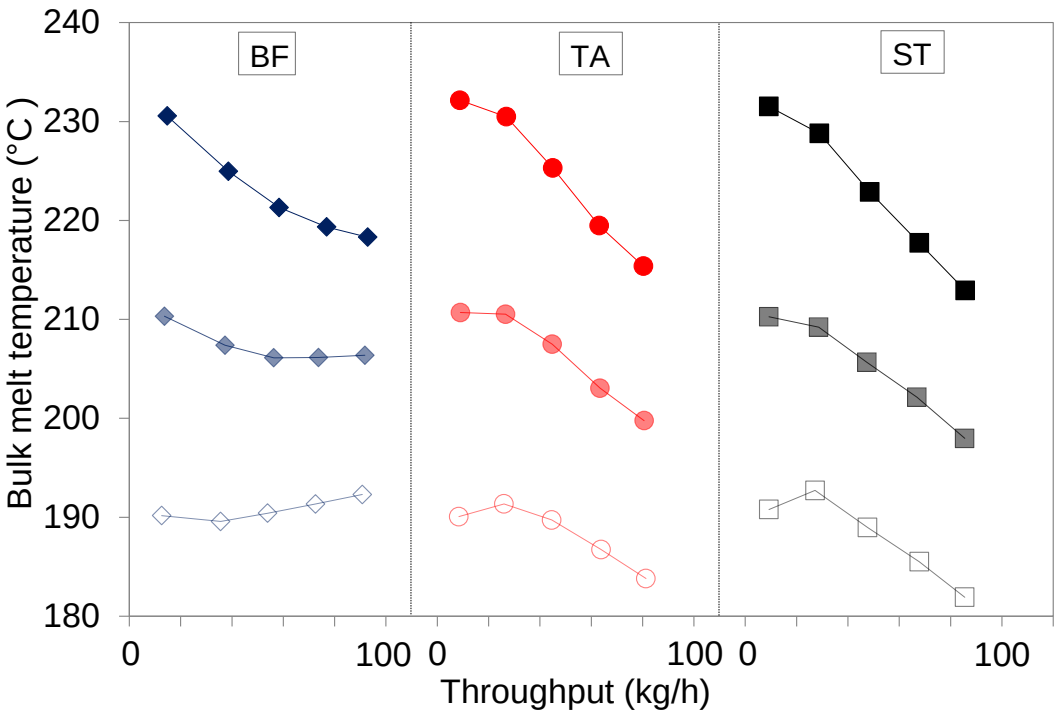

Figure 4.7 Bulk melt temperature measurements vs throughput for LDPE (dark colours represent 220°C, medium 200°C and light 180°C) and (BF: Barrier Flighted Screw; TA: Tapered Compression Screw; ST: Stepped Compression Screw)

Stability of melt temperature is also an important feature which affects melt and product quality. Figure 4.8 shows a corresponding plot of melt temperature fluctuation at the same conditions as shown in Figure 4.7. The data clearly indicates a critical screw speed of 30 rpm, at which temperature fluctuations for both single flighted screws rapidly increased in magnitude with increasing screw speed. This is in agreement with the data shown in Figure 4.7, highlighting the poorer melting performance achieved with both single flighted screws. Data suggests that a breakdown in the effectiveness of the melting process is associated with a corresponding decrease in melt homogeneity. By contrast, lower levels of fluctuation were measured for the barrier flighted screw, reflecting the higher melting capability provided by this geometry.

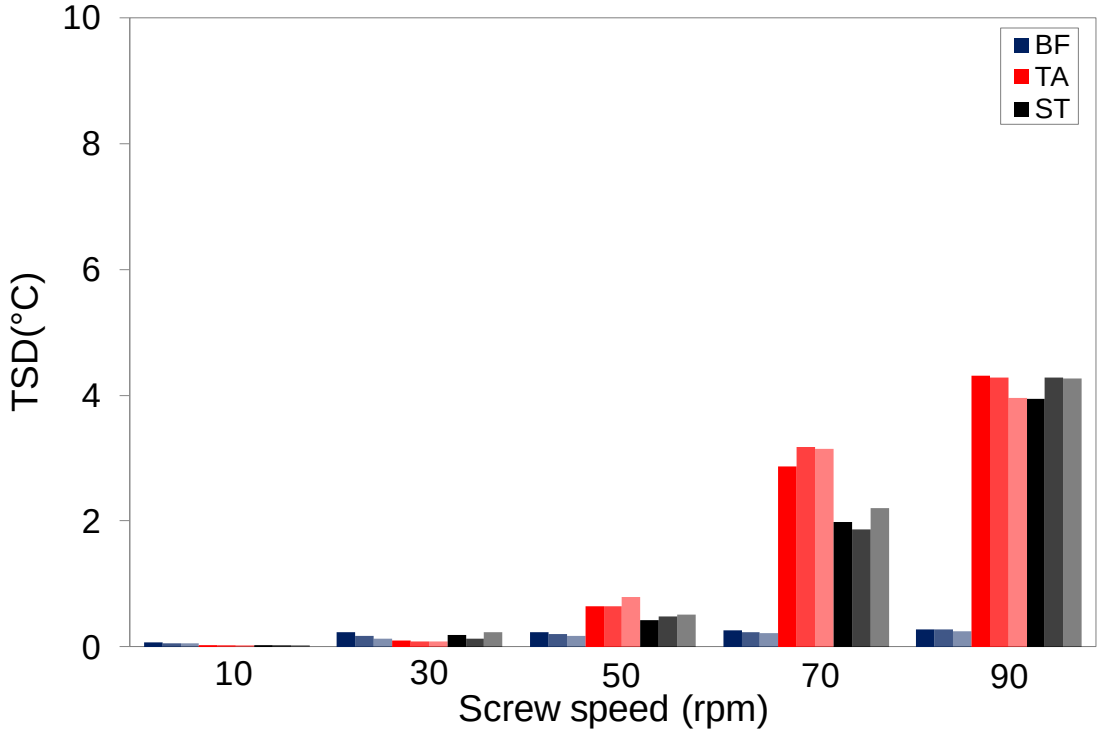

Figure 4.8 Variation of melt temperature vs screw speed for LDPE (dark colours represent 220°C, medium 200°C and light 180°C), (BF: Barrier Flighted Screw; TA: Tapered Compression Screw; ST: Stepped Compression Screw) and (TSD: Variation of melt temperature over a period of 1 min calculated by taking an average of the standard variation at each individual position)

Measured die melt pressure is displayed in Figure 4.9. In general, die pressures were found to increase with extruder screw speed. In addition, these increased as set temperature decreased, due to the fact that polymer melt viscosity increased with decreasing temperature (section 4.1, Figure 4.1). At higher screw speeds (70 and 90 rpm) die pressures were less dependent on extruder screw geometry. However, at these screw speeds, the barrier flighted screw produced higher throughputs than the two single flighted screws, as shown in Figure 4.4. This highlights the lower processing capability (measured in terms of throughput) provided by these geometries, which corresponded to the higher levels of temperature variation seen in Figure 4.8.

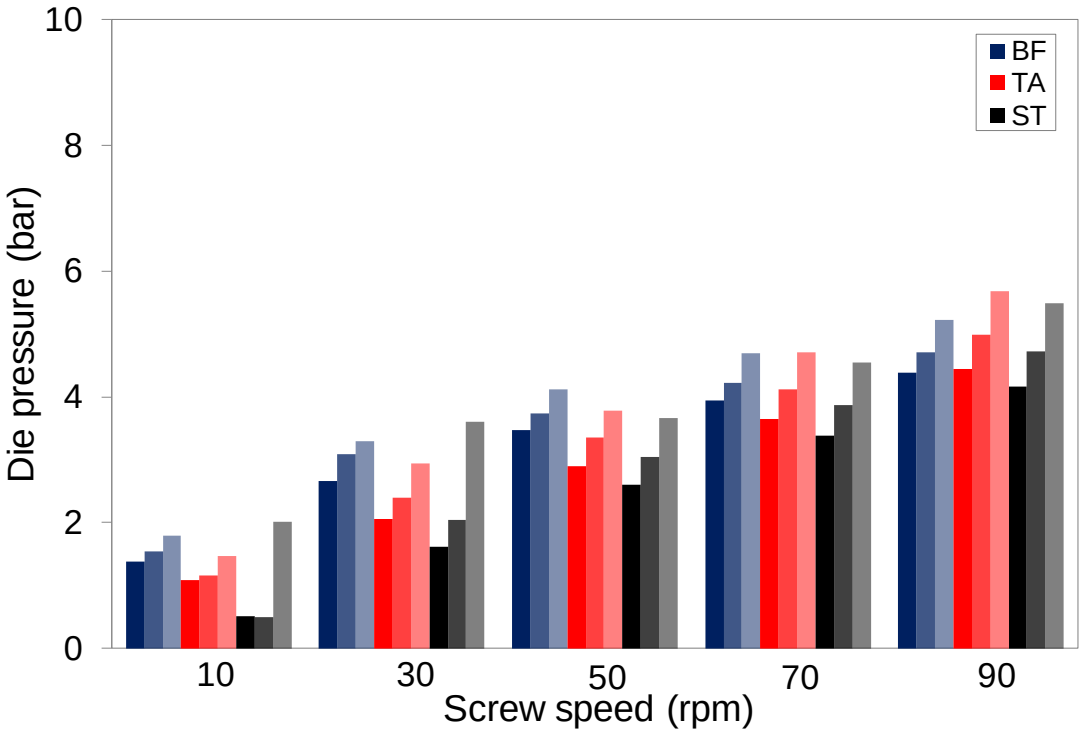

Figure 4.9 Die melt pressure vs screw speed for LDPE (dark colours represent 220°C, medium 200°C and light 180°C) and (BF: Barrier Flighted Screw; TA: Tapered Compression Screw; ST: Stepped Compression Screw)

Energy consumption is crucial in measuring the efficiency of the extrusion process. Figure 4.10 - Figure 4.12 display specific energy consumption (J/g) for the extrusion process, motor and barrel/die heaters plus cooling fans. A large variation in total energy consumption was observed, between 800 and 2550 J/g, dependent upon screw geometry, set temperature and screw speed as shown in Figure 4.10. Overall, energy consumption was decreased by both increasing screw speed and decreasing extruder set temperature.

The highest values of energy consumption were measured at the lowest screw speed of 10 rpm and at this screw speed these energy values were highly affected by screw geometry. Clearly, specific energy consumption was lower for the barrier flighted screw than the two single flighted screws. At screw speeds above 10 rpm, however, the effect of screw geometry had less effect on measured energy.

The demand of specific energy required from the motor is shown in Figure 4.11. Here, a smaller variation in energy consumption was found over the range of extruder screw speeds. In contrast to the total energy consumption, the demand of motor energy increased with increasing screw speed and the effects of screw geometry and set temperature had less impact on energy consumption. In general, the motor demand of specific energy increased from 225 to 655 J/g. In addition, the lowest levels of motor energy consumption were measured at the highest set temperatures for all conditions which suggest that higher set temperatures resulted in the polymer melt having lower viscosity and therefore resulting lower torque requirements.

Specific energy consumption from barrel/die heaters plus cooling fans is presented in Figure 4.12. The relationship between energy consumption and extruder screw speed exhibited similar trends to those measured for the total energy consumption. It is shown that heaters in conjunction with cooling fans consumed less energy when the extruder was operated at higher screw speeds. This is in agreement with recent experimental studies carried out by (Kantor, 2010).

Moreover, a clear dependence of energy consumption on extruder set temperature was found. Measured energy decreased with decreasing set temperature, irrespective of screw geometry. At low screw speed (Figure 4.12), it was noticed that the contribution of energy from heaters/cooling fans to the total energy consumption was found to be much larger than the contribution of the motor (Figure 4.11), which could explain the relationship between total energy consumption and screw speed seen in Figure 4.10.

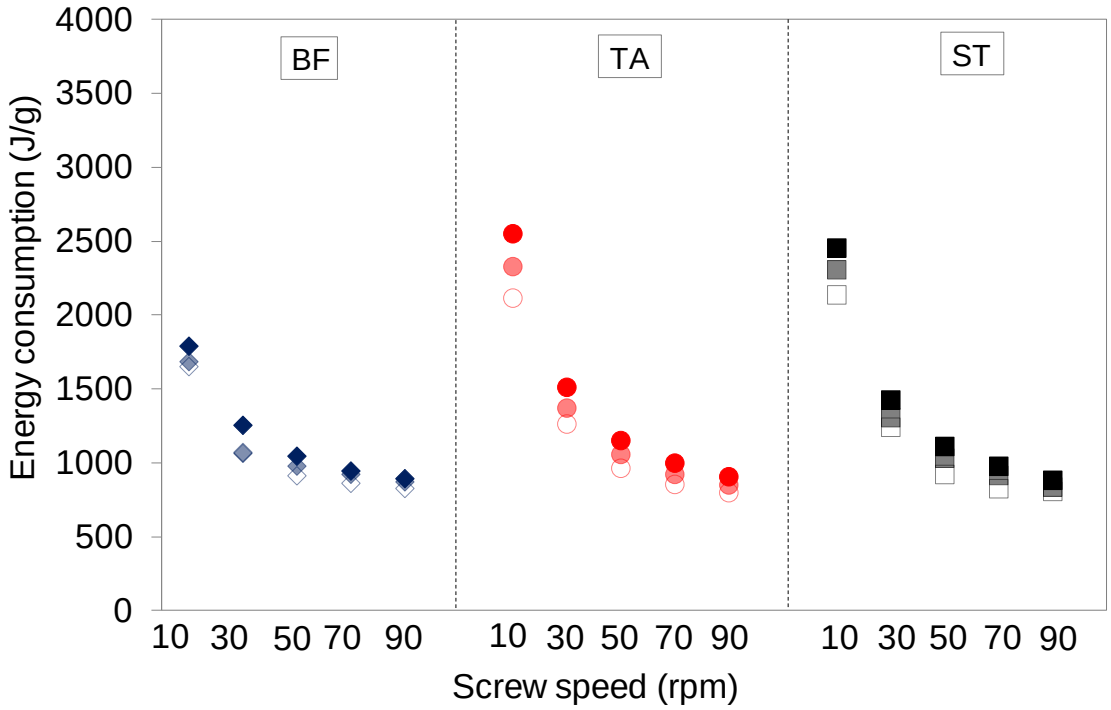

Figure 4.10 Total specific energy consumption vs screw speed for LDPE (dark colours represent 220°C, medium 200°C and light 180°C) and (BF: Barrier Flighted Screw; TA: Tapered Compression Screw; ST: Stepped Compression Screw)

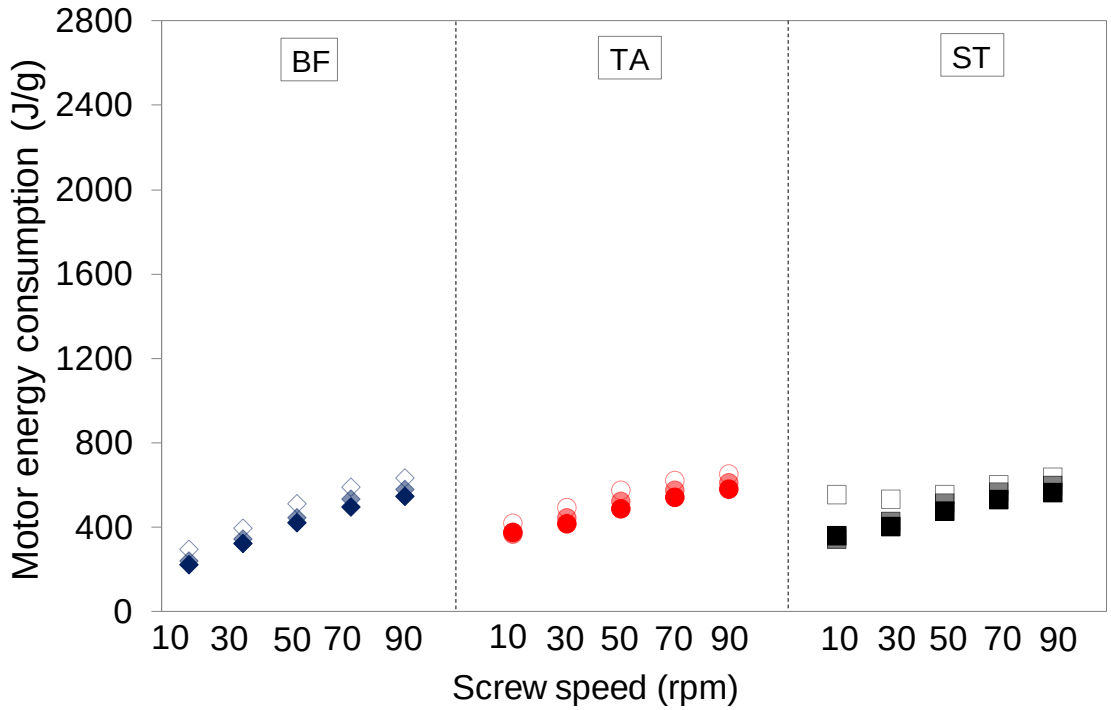

Figure 4.11 Specific energy consumption for the motor vs screw speed and LDPE (dark colours represent 220°C, medium 200°C and light 180°C) and (BF: Barrier Flighted Screw; TA: Tapered Compression Screw; ST: Stepped Compression Screw)

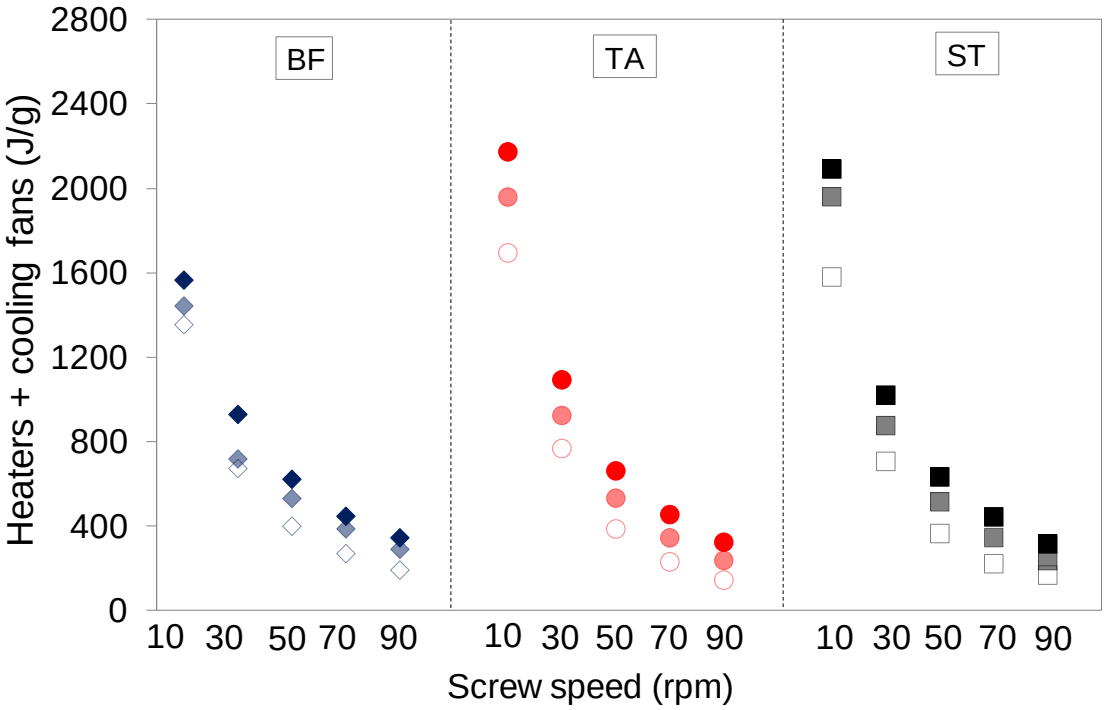

Figure 4.12 Specific energy consumption for the heaters/cooling fans vs screw speed and LDPE (dark colours represent 220°C, medium 200°C and light 180°C) and (BF: Barrier Flighted Screw; TA: Tapered Compression Screw; ST: Stepped Compression Screw)

4.3.3 LLDPE

This section describes the extrusion measurements of a linear low density polyethylene (LLDPE). The introduction of this polymer into the experimental program enabled examination of the dependence of melt flow properties on molecular structure. LDPE contains long chain branching whilst LLDPE has extensive shorter chain branching. This difference in branching has been reported to have a strong effect on melt rheology and polymer processability (Dealy & Wissbrun, 1999). Therefore, a comparison between LLDPE and LDPE was made throughout this section to highlight the impact of chain branching on extrusion performance and provide a quantification of its effect on productivity, thermal homogeneity of the melt and specific energy consumption.

LLDPE results

Figure 4.13 shows measured extruder throughputs from each extruder screw for LLDPE at each set temperature and screw rotation speed. The general trend indicated that extruder throughputs linearly increased with increasing screw speed and remained higher for the barrier flighted screw. Similarly, as argued earlier in section 4.3.2, Figure 4.4, this could also be explained by the higher free volume measured for the barrier geometry. From Figure 4.13, it is shown that mass throughputs were of similar magnitude for the two single flighted screws whilst for the barrier these were more affected by set temperature. At 180°C, for example, the barrier flighted screw produced the lowest throughputs over the screw speed range, especially at 70 and 90 rpm. Compared to LDPE, at identical conditions, throughputs were higher for LLDPE. This is explained by the differences in rheological behaviour observed in section 4.1, which are discussed in more detail throughout this section.

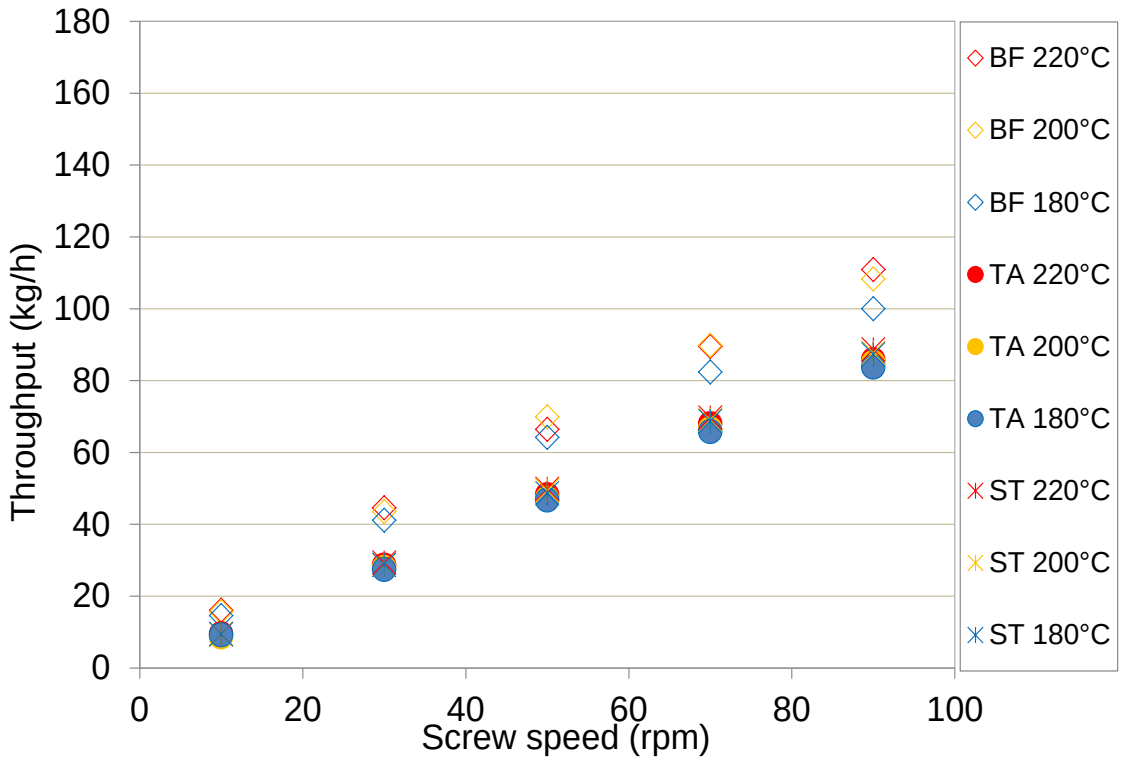

Figure 4.13 Extruder throughput for LLDPE vs screw speed (BF: Barrier Flighted Screw; TA: Tapered Compression Screw; ST: Stepped Compression Screw)

Figure 4.14 shows radial melt temperature profiles for LLDPE generated by each screw at 200°C. Data revealed that melt temperatures were strongly affected by screw speed and these became more pointed in shape at higher speeds, reaching maximum values in the centre of the flow. For example, temperature differences of up to 20 and 30°C were measured in the centre for the barrier and the two single flighted screws respectively when the screw speed was increased from 10 to 90 rpm. Compared to melt temperature measurements of LDPE at identical conditions (Figure 4.5), dips in melt temperature were not noticed near to the die wall. Furthermore, the effect of screw geometry had a minor effect on radial melt temperatures and these were found to gradually increase with increasing screw speed, particularly for the non-barrier screws.

A detailed examination of the effect of set extrusion temperature on measured melt temperatures is presented in Figure 4.15. Results showed that radial melt temperatures were more affected by screw speed at 180°C, highlighting the effect of viscous shear on temperature measurements. For both single flighted screws, melt temperatures in the centre of the flow were found to range from 198°C at 10rpm to 233°C at 90rpm (Figure 4.15).

These results confirm the importance of polymer rheology and its effect on thermal measurements for single screw extrusion. LLDPE contains short chain branching and has been reported to be less sensitive to shear than LDPE (Dealy & Wissbrun, 1999). According to them, LLDPE was found to have a high degree of short chain branching (see section 4.2) and its viscosity remained higher than LDPE at higher shear strain rates, as shown in Figure 4.1. This caused higher melt temperatures due the higher levels of viscous shear heat generated during the extrusion process (Figure 4.14 and Figure 4.15).

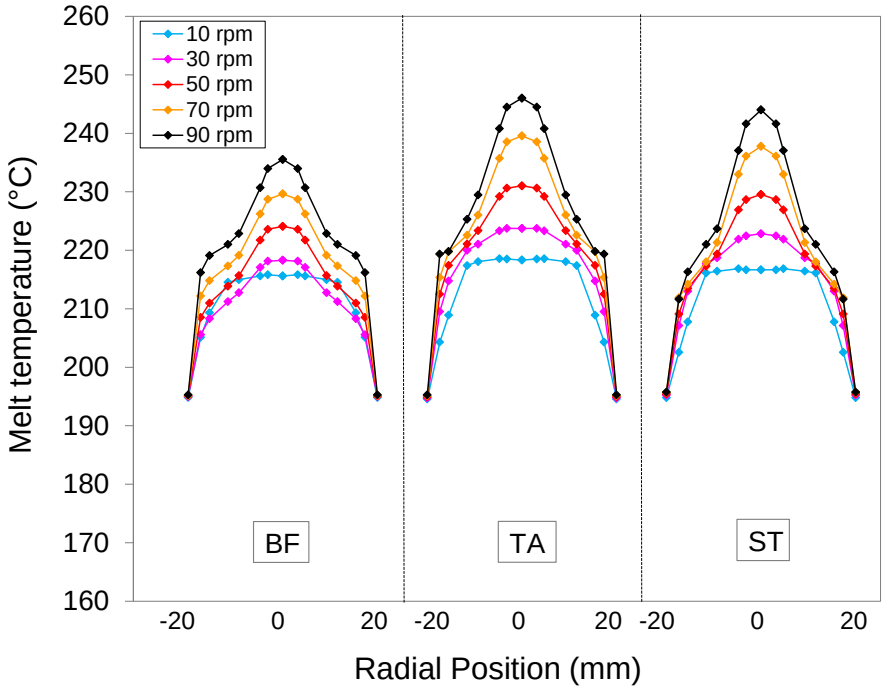

Figure 4.14 Effect of screw geometry on radial melt temperatures measured for LLDPE at 200°C (BF: Barrier Flighted Screw; TA: Tapered Compression Screw; ST: Stepped Compression Screw)

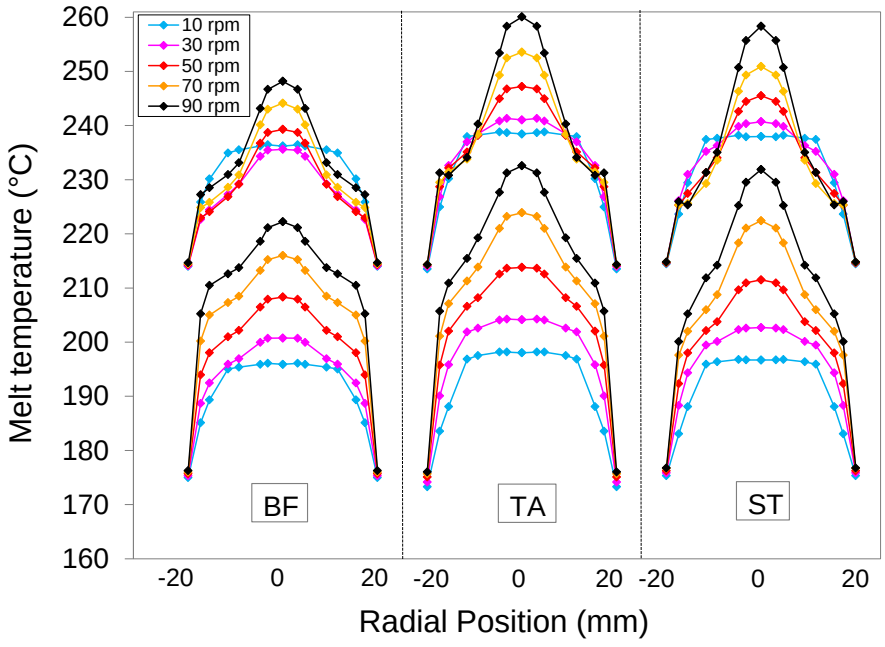

Figure 4.15 Effect of set temperature and screw geometry on radial melt temperatures measured for LLDPE at 180 and 220°C (BF: Barrier Flighted Screw; TA: Tapered Compression Screw; ST: Stepped Compression Screw)

The absence of dips in melt temperature near to the die wall is shown in Figure 4.16, reflecting the improved melting performance provided by these screw geometries when the extruder was run with LLDPE. In general, bulk melt temperatures increased with increasing screw speed, particularly at 180°C, highlighting the viscous effects generated at lower set temperatures, as discussed above. Clearly, the critical screw speed at which fluctuations were caused by melting instabilities was not noticed (Figure 4.8), reflecting the higher melt temperature homogeneity of LLDPE compared to LDPE (Figure 4.7)

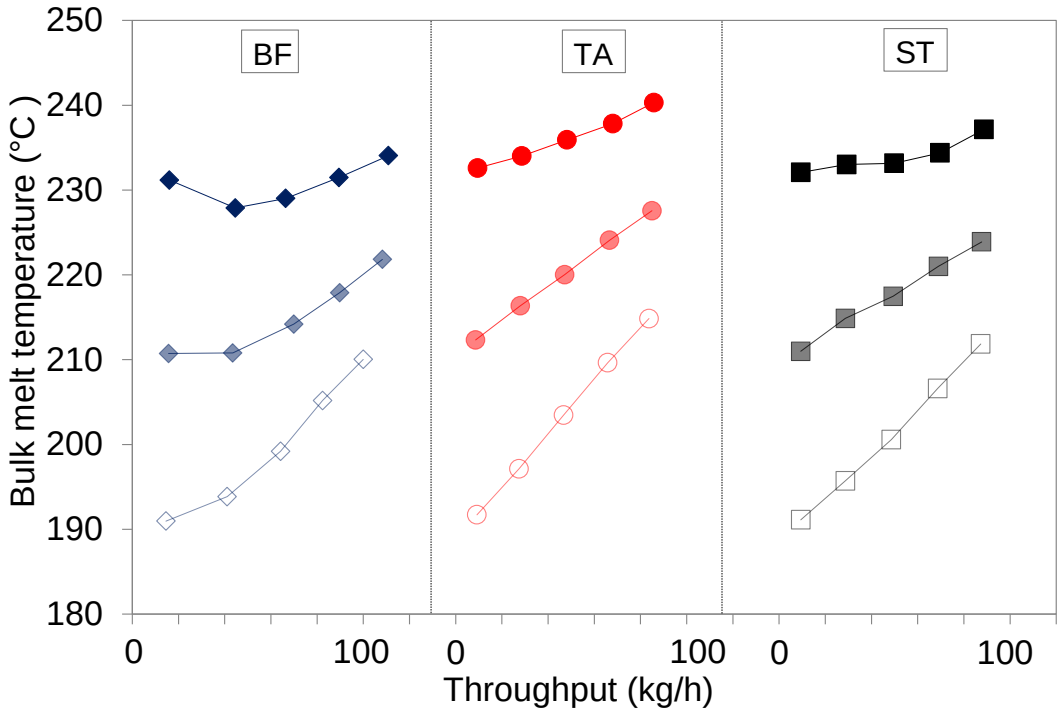

Figure 4.16 Bulk melt temperature measurements vs throughput for LLDPE (dark colours represent 220°C, medium 200°C and light 180°C) and (BF: Barrier Flighted Screw; TA: Tapered Compression Screw; ST: Stepped Compression Screw)

Figure 4.17 shows variations of melt temperature for LLDPE to reveal that levels of temperature fluctuation across the die flow were lower than those for LDPE. Extruder screw geometry was found to have a major effect on the thermal homogeneity at higher throughputs. However, differences in melt homogeneity observed between the barrier and the non-barrier screws were lower for LLDPE (Figure 4.17), highlighting the poorer thermal homogeneity observed for LDPE and its higher dependence on screw geometry (Figure 4.8).

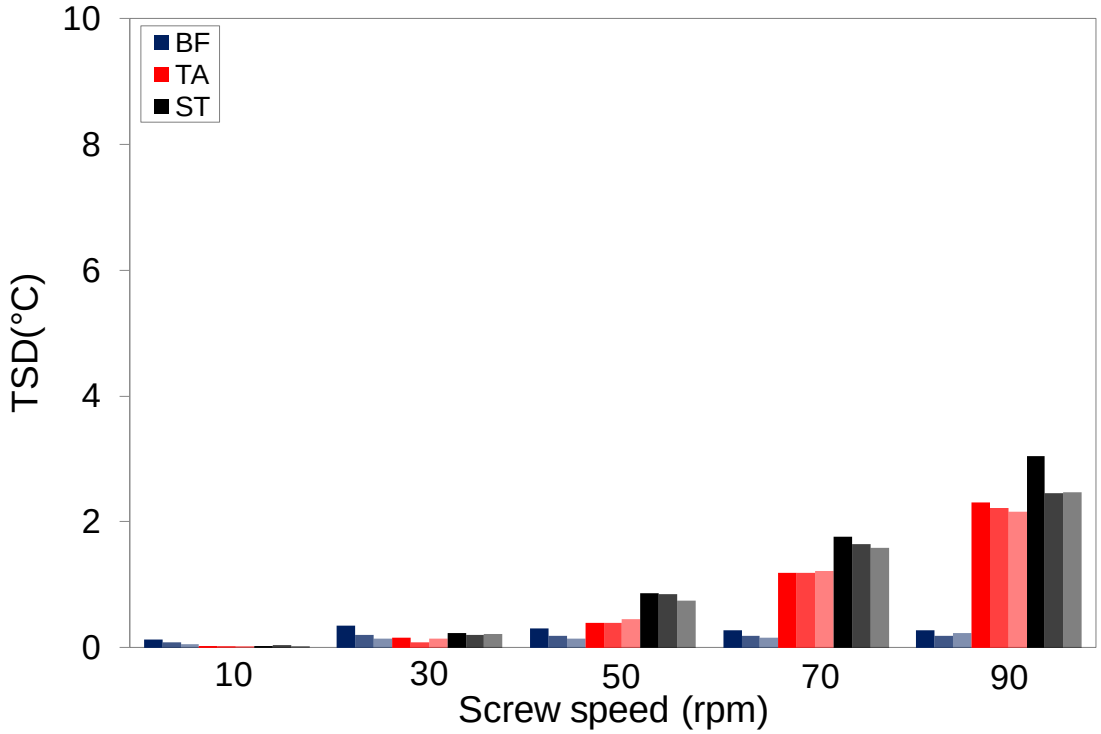

Figure 4.17 Variation of melt temperature vs screw speed for LLDPE (dark colours represent 220°C, medium 200°C and light 180°C), (BF: Barrier Flighted Screw; TA: Tapered Compression Screw; ST: Stepped Compression Screw) and (TSD: Variation of melt temperature over a period of 1 min calculated by taking an average of the standard variation at each individual position)

Melt pressure measurements in the die for LLDPE are displayed in Figure 4.18. Results showed that melt pressure increased following a linear dependence across the range of screw speeds. In addition, the highest extruder set temperature of 220 °C was found to cause the lowest melt pressures due to the clear dependence of melt viscosity on temperature. The barrier flighted screw is shown to generate higher pressures than the two single flighted screws which could explain the higher throughputs observed in Figure 4.13. From Figure 4.18, it was observed that much higher pressures were measured with LLDPE compared to LDPE, which were likely to result from the lower shear sensitivity exhibited of the former (Figure 4.1). The improved melting performance achieved with LLDPE also explains the higher throughputs measured for LLDPE compared to LDPE.

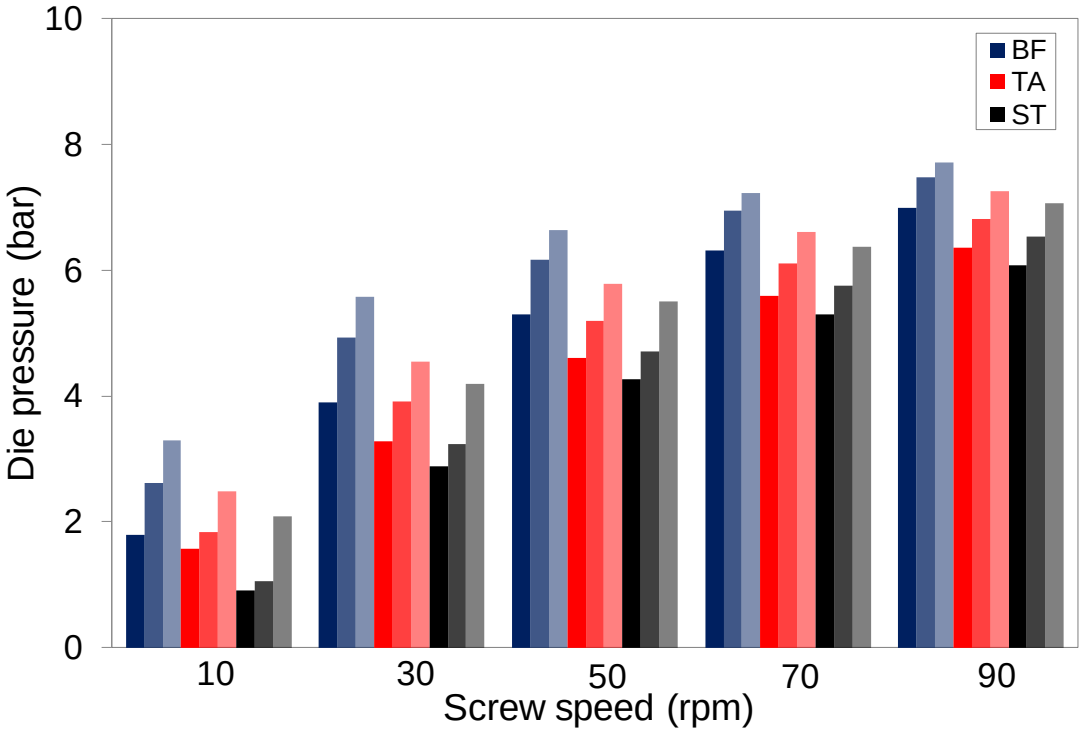

Figure 4.18 Die melt pressure vs screw speed for LLDPE (dark colours represent 220°C, medium 200°C and light 180°C) and (BF: Barrier Flighted Screw; TA: Tapered Compression Screw; ST: Stepped Compression Screw)

Measured energy consumption for LLDPE is shown in Figure 4.19. Extruder set temperature and screw geometry appeared to have a major effect on total energy consumption at 10 rpm. For example, the demand of energy for the barrier flighted screw ranged from~1500 to 1700J/g compared to~2000-2500J/g for both single flighted screws. At higher screw speeds, specific energy consumption gradually decreased and tended to be similar, irrespective of set temperature and screw geometry, especially for the non-barrier screws.

Motor energy consumption, however, increased over the full range of screw speeds (Figure 4.20). A clear dependence of energy consumption on melt viscosity was observed, increasing with decreasing set temperature due the temperature dependent viscosity of the polymer. The demand of energy required for the barrier flighted screw was much lower; energy consumption at 90 rpm was lower than the values required at 50rpm for the two single-flighted screws.

Energy contribution from heaters/cooling fans to the extrusion process is displayed in Figure 4.21. The relationship between energy consumption and extruder screw speed was similar to that for the total energy consumption; specific energy consumption decreased as screw speed increased. However, large energy variations of up to 1890J/g were measured across the range of screw speeds which implied that energy consumption dropped to very low values (~66J/g), highlighting that the major contribution to the total energy consumption was provided by the motor at higher throughputs. This can be explained by the rheological behaviour of LLDPE, leading to higher energy consumption from the motor as a result of its lower sensitivity to shear. Compared to LDPE, it was confirmed that the major difference in energy was observed from the motor, especially at higher screw speeds (Figure 4.11 and Figure 4.20). These results showed that polymer rheology is one of the key variables when examining energy consumption for a single screw extrusion process.

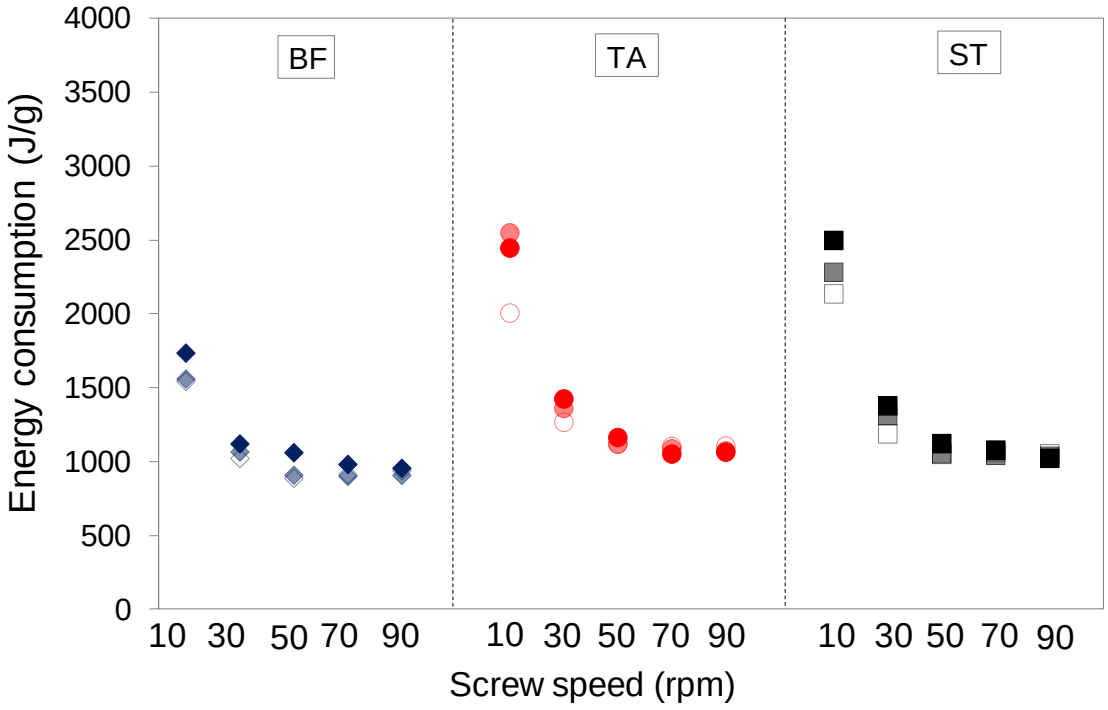

Figure 4.19 Total specific energy consumption vs screw speed for LLDPE (dark colours represent 220°C, medium 200°C and light 180°C) and (BF: Barrier Flighted Screw; TA: Tapered Compression Screw; ST: Stepped Compression Screw)

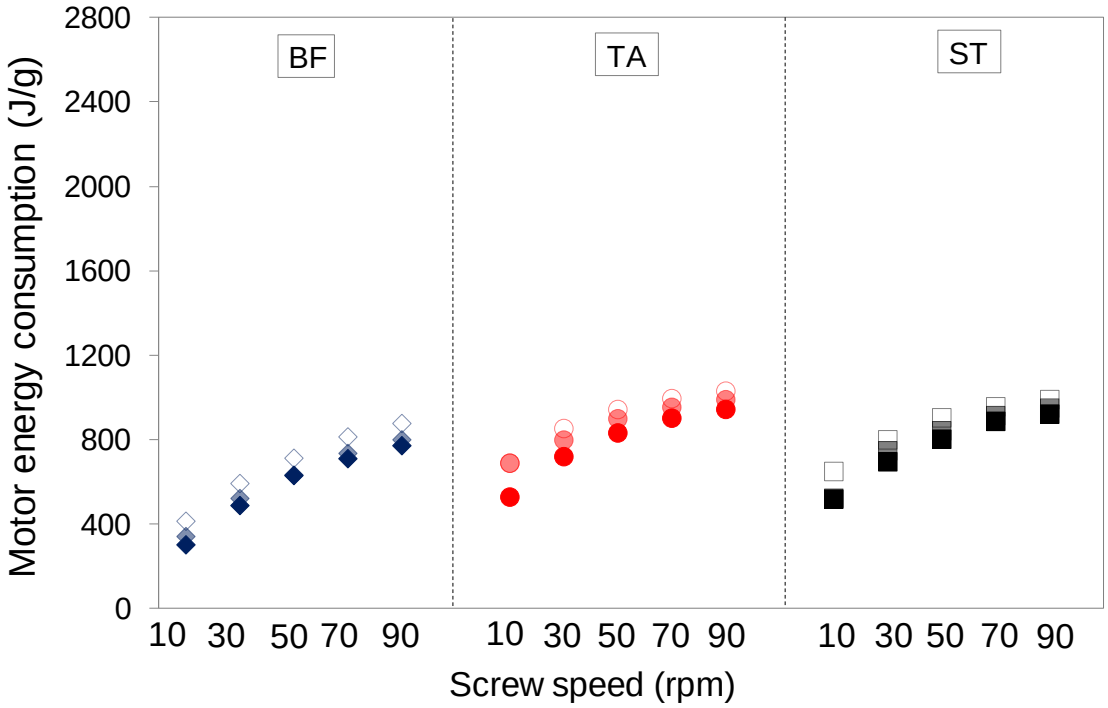

Figure 4.20 Specific energy consumption for the motor vs screw speed and LLDPE (dark colours represent 220°C, medium 200°C and light 180°C) and (BF: Barrier Flighted Screw; TA: Tapered Compression Screw; ST: Stepped Compression Screw)

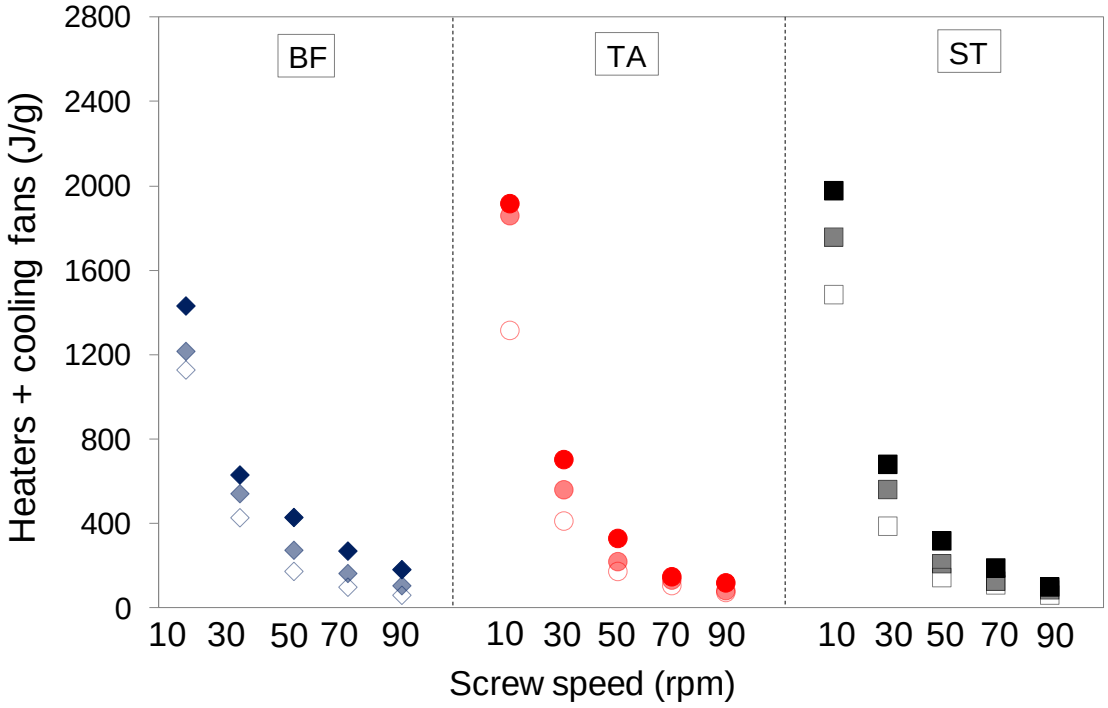

Figure 4.21 Specific energy consumption for the heaters/cooling fans vs screw speed and LLDPE (dark colours represent 220°C, medium 200°C and light 180°C) and (BF: Barrier Flighted Screw; TA: Tapered Compression Screw; ST: Stepped Compression Screw)

4.3.4 HDPE

Extrusion data from LDPE and LLDPE have shown the complex nature of extrusion thermal dynamics and have provided evidence that polymer rheology can significantly influence measured melt temperatures and energy consumption. In this section, three different molecular weight grades of HDPE were used to study the dependence of melt viscosity on molecular weight and its effect on the extrusion performance. Here, melt temperature and energy consumption measurements are plotted against melt viscosity to facilitate an examination of the important role that melt viscosity plays when examining polymer processability in single screw extrusion. In addition, extrusion thermal dynamics were examined over a shorter period of time providing information relating to short-term temperature changes across the melt flow path and their dependence on the melt viscosity.

HDPE results

Figure 4.22 - Figure 4.24 display extruder performance in terms of throughput for all grades of HDPE by examining the effects of screw speed, extruder set temperature and screw geometry. This highlights the dependence of productivity on melt viscosity; throughputs were higher for HD5050 compared to HD5411, reflecting the lower molecular weight of the former and its effect on shear viscosity, as previously shown in section 4.1, Figure 4.2.

Set temperature appeared to have a major effect on throughput for the barrier flighted screw processing HD5050 as seen in Figure 4.22. At the same set temperature profile of 220°C, the barrier flighted screw produced higher throughputs than the two single flighted screws. As discussed above, these results could be explained by the free volume of the barrier flighted screw which is significantly greater than the free volume of single flighted screws.

At 180°C, however, a non-linear behaviour and a lower throughput was observed. Throughput is heavily dependent upon the polymer's thermal and frictional properties and due to their design, barrier flighted screws require more work input to melt the polymer as it is forced to flow over extra flights in the barrier and mixer sections of the screw. The extra work required at lower temperature appears here to inhibit the total throughput, especially at higher speeds where achieving melting is more challenging. This could also explain the lower throughputs observed for the highest viscosity grade HD5411 (Figure 4.24) despite the careful selection of the barrel set temperature profiles (section 3.3.3, Table 3.3).

Extruder throughput for the medium grade HD6007 was found to be relatively unaffected by screw geometry and set temperatures as shown in Figure 4.23, which could be explained by optimized selection of barrel set temperature profiles (section 3.3.3, Table 3.3).

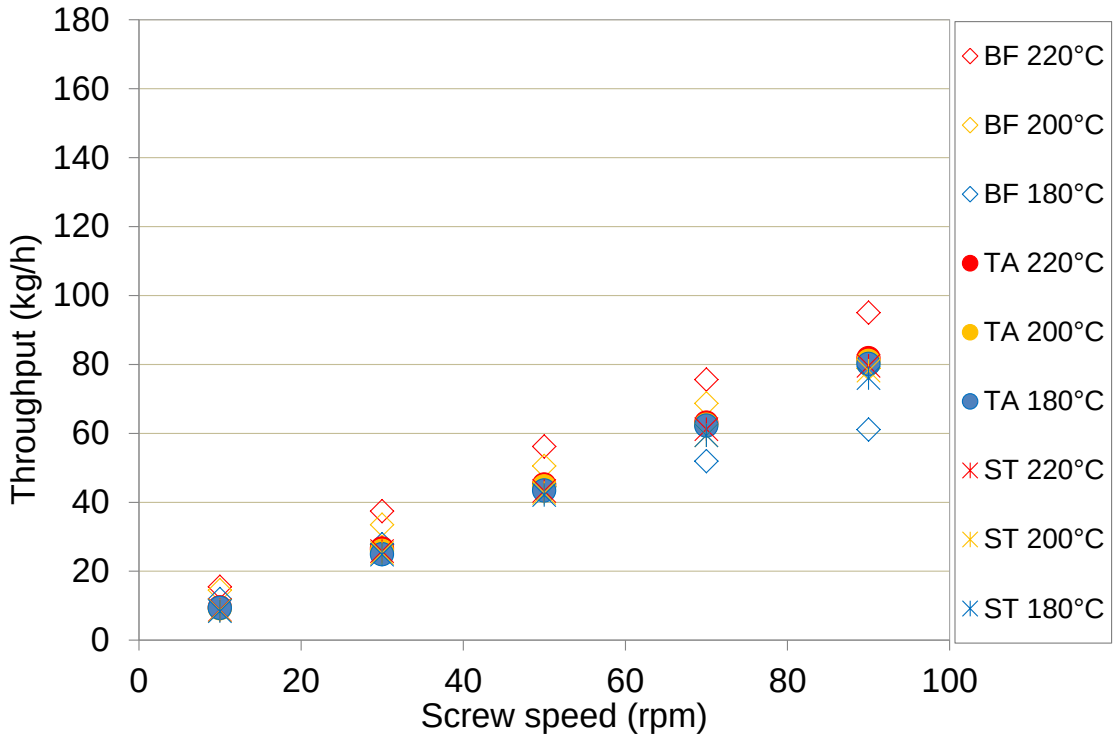

Figure 4.22 Extruder throughput vs screw speed for HD5050 (BF: Barrier Flighted Screw; TA: Tapered Compression Screw; ST: Stepped Compression Screw)

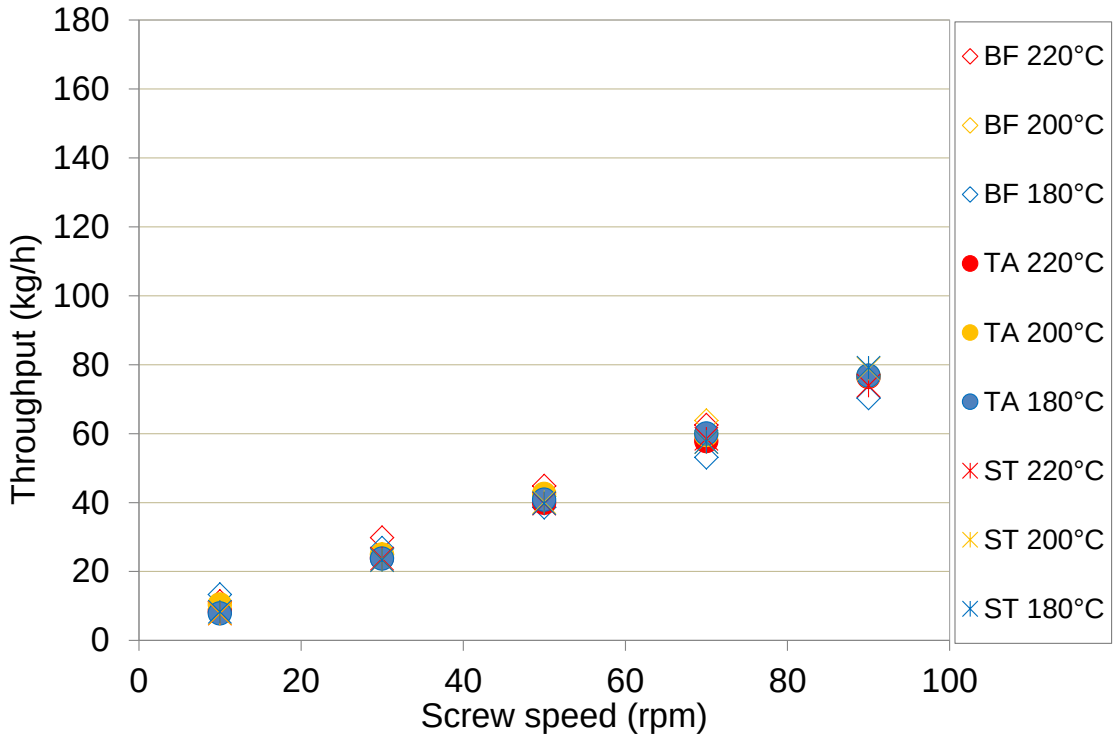

Figure 4.23 Extruder throughput vs screw speed for HD6007 (BF: Barrier Flighted Screw; TA: Tapered Compression Screw; ST: Stepped Compression Screw)

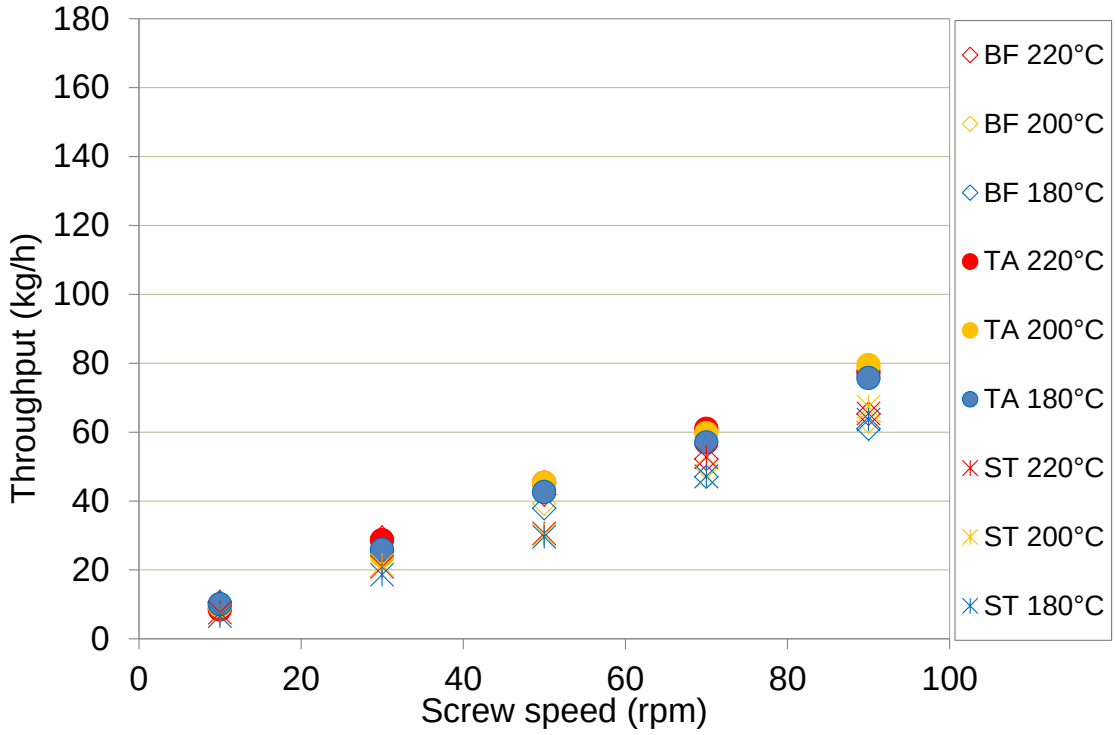

Figure 4.24 Extruder throughput vs screw speed for HD5411EA (BF: Barrier Flighted Screw; TA: Tapered Compression Screw; ST: Stepped Compression Screw)

Melt temperature was less consistent as screw speed increased, especially for single flighted screws; therefore the effect of molecular weight on thermal dynamics is compared directly at 90 rpm for all grades of HDPE at 200°C using three different screws over a 5 second period and shown in Figure 4.25 - Figure 4.27. It can be observed for single flighted screws that the range of temperature variation at each junction significantly increased with increasing HDPE viscosity. The largest ranges of fluctuations were measured for the highest viscosity grade (HD5411). A temperature difference of up to 65°C was recorded at 8.8 mm from the centre of the flow for the tapered compression screw during the measurement period (Figure 4.27).

However, melt temperature variations were smaller with the barrier flighted screw for all grades of HDPE at the same conditions, as seen in Figure 4.25 - Figure 4.27 . It was noticed that for HD5411 and the barrier flighted screw (Figure 4.27), the melt temperature increased across the flow volume having a peak temperature in the centre of around 240°C which could be explained by the highest barrel set temperature profiles being required for HD5411 (section 3.3.3, Table 3.3) in addition to increased viscous energy dissipation via shearing.

These results highlight the dependence of molecular weight on melt viscosity and its effect on the thermal dynamics of the extrusion process; the high viscosity of this grade of HDPE leading to a high dependence of homogeneity on screw geometry.

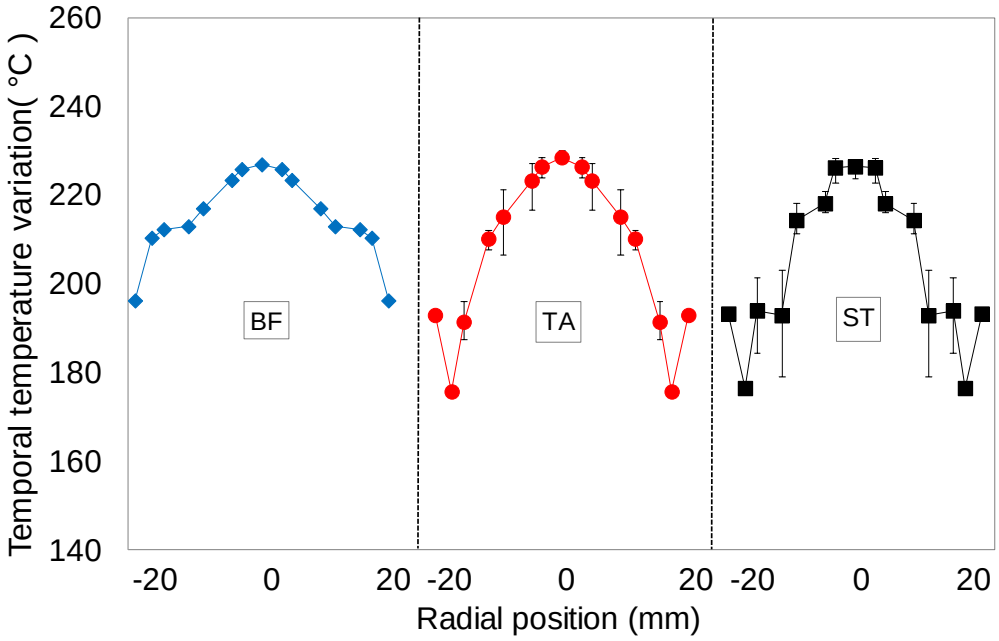

Figure 4.25 Range of temperature variation (max value-min value) at each thermocouple mesh junction for HD5050 at 200°C, measured over 5 seconds at 90rpm (BF: Barrier Flighted Screw; TA: Tapered Compression Screw; ST: Stepped Compression Screw)

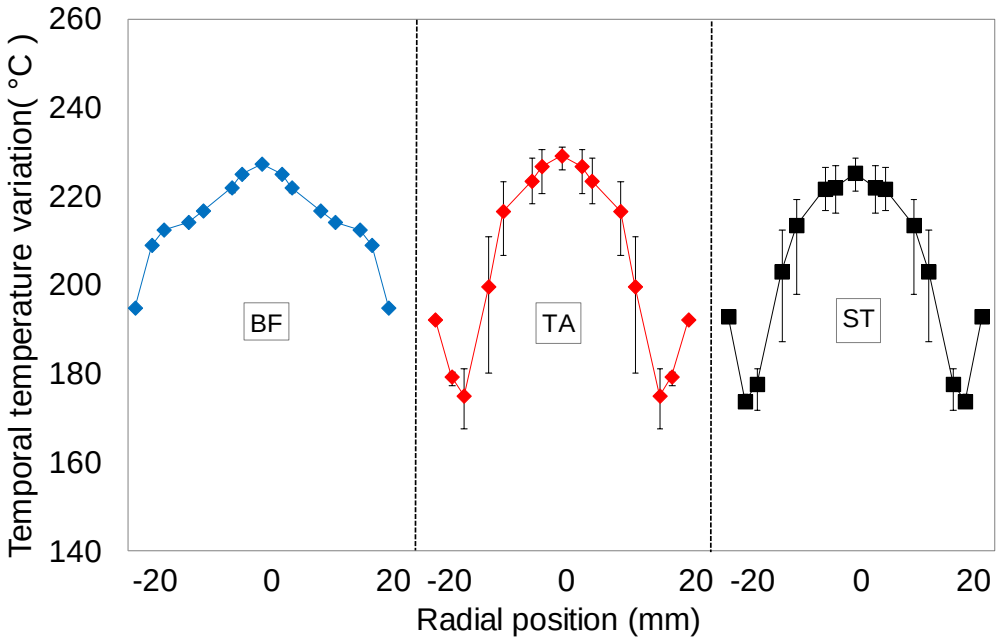

Figure 4.26 Range of temperature variation (max value-min value) at each thermocouple mesh junction for HD6007 at 200°C, measured over 5 seconds at 90rpm (BF: Barrier Flighted Screw; TA: Tapered Compression Screw; ST: Stepped Compression Screw)

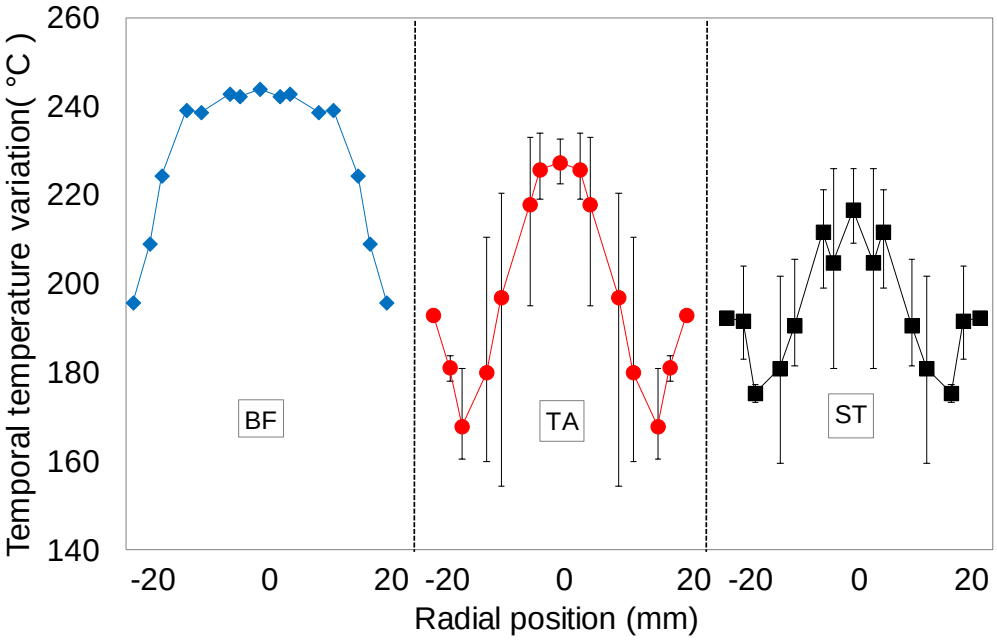

Figure 4.27 Range of temperature variation (max value-min value) at each thermocouple mesh junction for HD5411 at 200°C, measured over 5 seconds at 90rpm (BF: Barrier Flighted Screw; TA: Tapered Compression Screw; ST: Stepped Compression Screw)

To examine the effect of shear viscosity on measured melt temperatures and energy consumption, a Carreau-Yasuda model (Carreau, 1968,Yasuda, 1979) was fitted to the measured rheological data for each material and set temperature (section 4.1, Figure 4.2), as shown in Figure 4.28. A good agreement between the model and experimental data was found. Temperature dependence for each polymer was also modelled using exponential temperature dependence at a reference temperature (T_r) of 180°C.

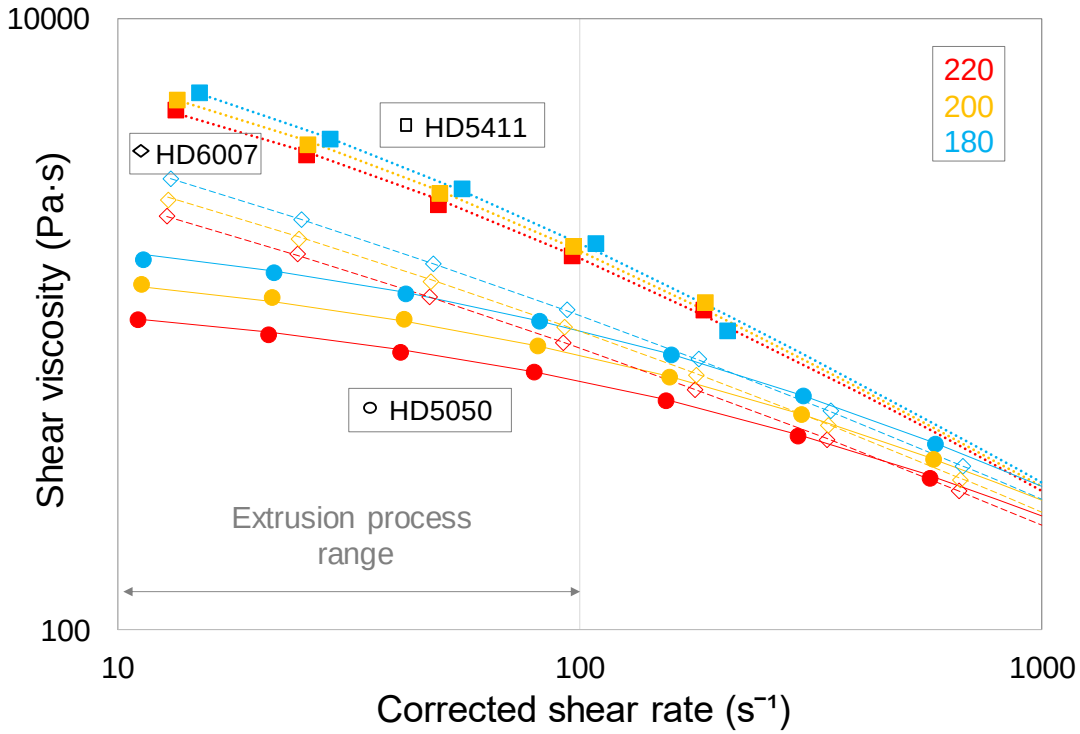

Figure 4.28 Shear viscosity measured using a twin bore capillary rheometer for the three HDPEs (lines indicate fit of Carreau-Yasuda model)

The exponential temperature dependence and Carreau-Yasuda model are given by:

$$f(T) = e^{-\beta(T-T_r)} \tag{4-1}$$

$$\eta\,(\dot{\gamma},T) = \frac{\eta_o\, f(T)}{[1+(r\dot{\gamma}f(T))^a]^{\frac{1-n}{a}}} \tag{4-2}$$

where β is the coefficient of temperature sensitivity, η_0 is the zero-shear viscosity, r is the viscous relaxation time, n is the power law index and a is the width of the transition between the zero-shear viscosity region and the power law region

This modelled data was then used to calculate bulk viscosity inside the metering section of the extruder screw, for each polymer, set temperature, screw geometry and screw rotation speed. Shear rate ($\dot{\gamma}$) in the screw channel at the end of the metering section was calculated from (Giles et al., 2005):

$$\dot{\gamma} = \frac{\pi \times D \times N}{60 \times h_d} \qquad (4\text{-}3)$$

where D is the screw diameter, N is the screw speed and h_d is the channel depth.

Measured temperatures from the thermocouple mesh junctions, averaged over a period of 1 minute (Kelly et al., 2006) coupled with the above equation and modelled rheological data were used to predict melt viscosity at the end of the extruder screw at each experimental condition. An example is shown in Table 4.3.

Table 4.3 Example of melt viscosity calculation at the end of extruder screw

HD5050 TAPERED 200°C	**h_d(mm)**	**$\dot{\gamma}$ (s^{-1})**	**Mesh (°C)**	***f(T)***	**η (Pa.s)**
rpm					
10	3.46	9.54	231.00	0.479	917.01
30	3.46	28.62	231.89	0.473	776.10
50	3.46	47.70	228.84	0.494	725.50
70	3.46	66.78	226.26	0.513	688.01
90	3.46	85.87	223.82	0.531	658.85

These calculations in conjunction with temperatures measured using the thermocouple mesh and real-time quantification of energy consumption enabled the exploration of the effect of melt viscosity on the thermal dynamics of the extrusion process and energy demand.

The magnitude and levels of fluctuation in measured melt temperature are plotted against melt viscosity in Figure 4.29 and Figure 4.30 at a set extruder die temperature of 200°C. Figure 4.29 shows that melt viscosity had a pronounced effect on measured temperature, which increased with increasing melt viscosity. This can be explained by the higher levels of viscous shear generated during extrusion of the higher viscosity polymer. For both single flighted screws the measured temperature initially increased with increasing screw rotation speed (as could be expected to due viscous shear heating) but then decreased above a critical screw speed, typically 30 or 50 rpm. This again reflects a point at which the melting mechanism began to break down when there was insufficient time for the volume of polymer within the screw channel to be melted homogenously. For the barrier flighted screw this critical point was not reached and measured melt temperature continued to rise with increasing screw speed, reflecting the improved melting action of the barrier screw.

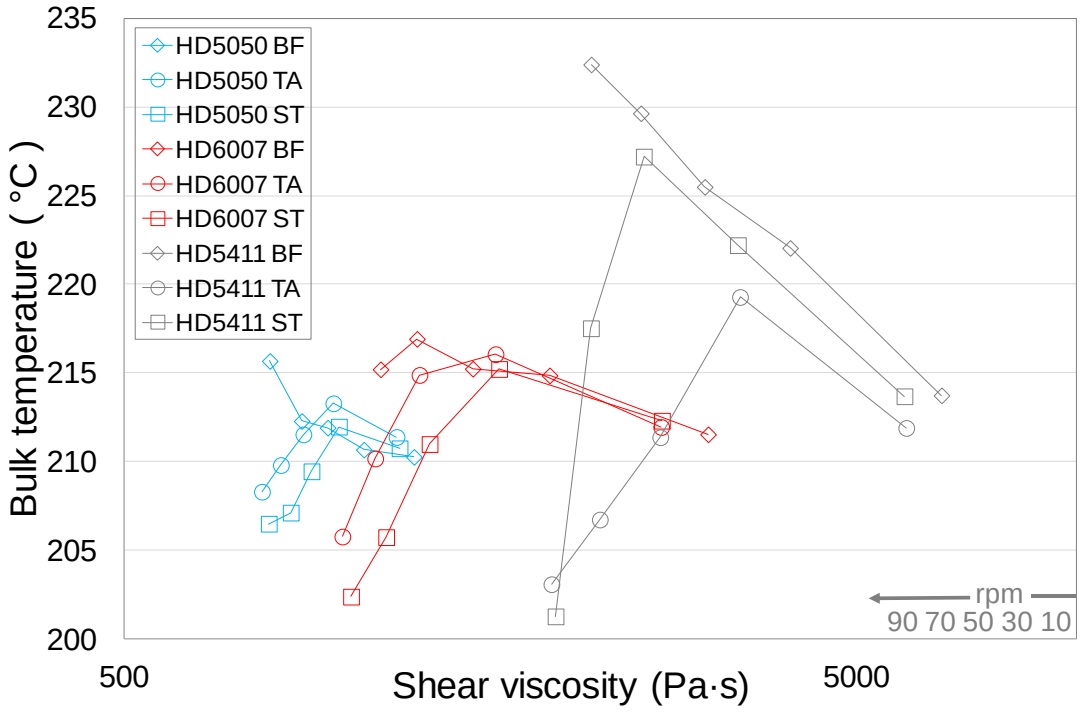

Figure 4.29 Bulk melt temperature measurements vs shear viscosity for the three HDPEs at an extruder die set temperature of 200°C from 10 to 90 rpm (data is read from right to left) (BF: Barrier Flighted Screw; TA: Tapered Compression Screw; ST: Stepped Compression Screw)

Figure 4.30 shows a corresponding plot of melt temperature fluctuation over a period of 1 min, versus melt viscosity, at the same set conditions as shown in Figure 4.29. The viscosity of the different HDPE grades had a less significant effect on temperature variation (quantified by standard deviation), which ranged from 0.01 to 8.3°C. The lowest viscosity grade of HDPE exhibited fluctuations between 0.01 and 3.7°C compared to 0.01–8.3°C for the highest viscosity grade. The most significant observation related to a large increase in the levels of fluctuation above the critical screw speed described earlier, for single flighted screws. This suggests that a break down in the effectiveness of the melting process is associated with a corresponding decrease in melt homogeneity.

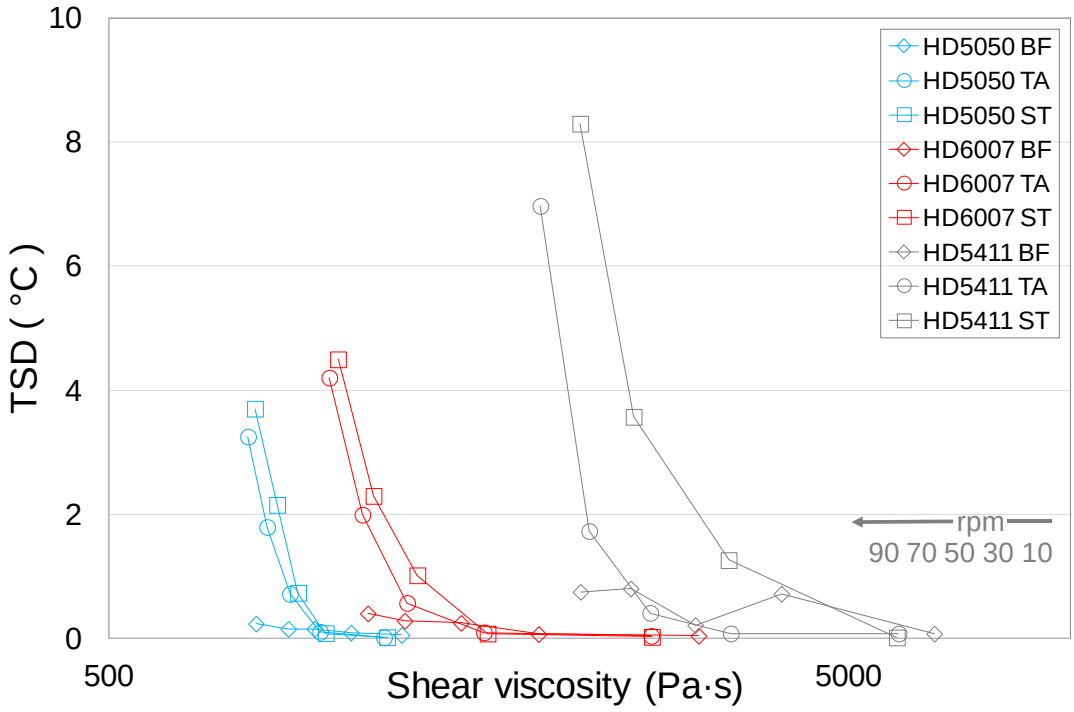

Figure 4.30 Standard deviation of temperature measurements for the three HDPEs at a set temperature of 200°C from 10 to 90 rpm (data is read from right to left) (BF: Barrier Flighted Screw; TA: Tapered Compression Screw; ST: Stepped Compression Screw) and (TSD: Variation of melt temperature over a period of 1 min calculated by taking an average of the standard variation at each individual position)

Measured die pressure is displayed in Figure 4.31 at the highest set screw speeds of 70 and 90 rpm. Die pressures increased as set temperatures decreased and were lower for the barrier flighted screw for all grades of HDPE. High die pressures were observed for HD5411 which were strongly dependent upon screw geometry and set extruder temperatures. Despite the higher pressures measured for HD5411, lower throughputs were produced, as shown earlier in Figure 4.24. This reflected the poorer processing capability (measured in terms of throughput) of these screw geometries for high molecular weight HDPE, which corresponded to the higher levels of temperature fluctuation shown in Figure 4.30.

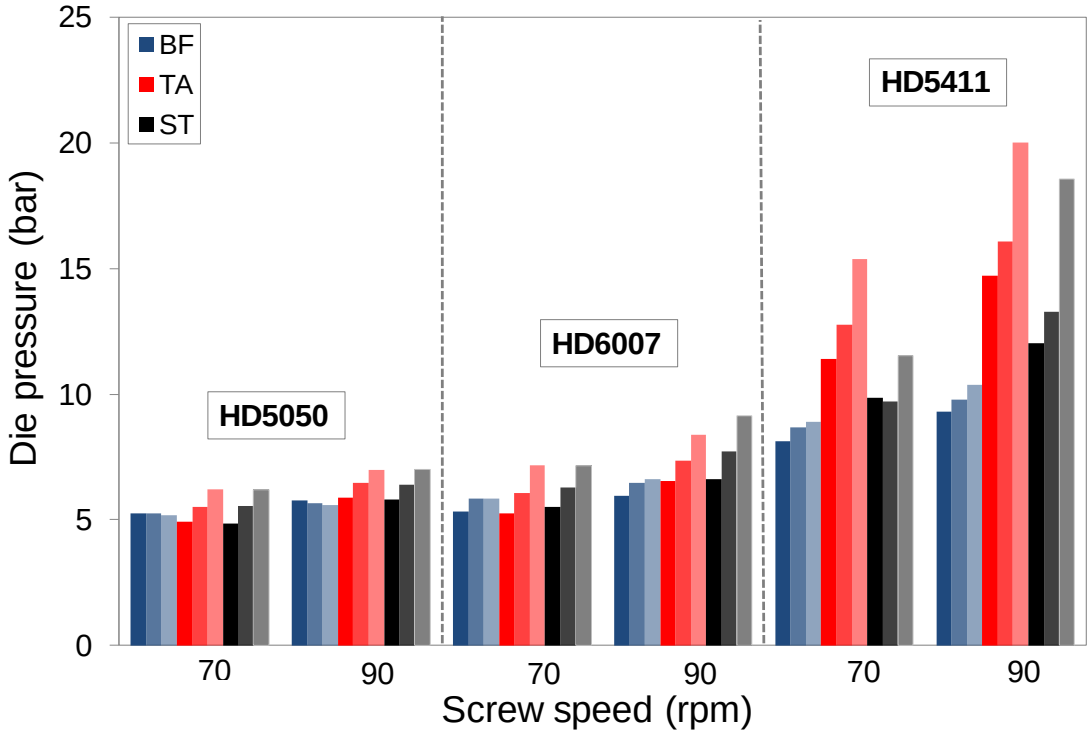

Figure 4.31 Die pressure vs screw speed for all grades of HDPE (dark colours represent 220°C, medium200°C and light 180°C) and (BF: Barrier Flighted Screw; TA: Tapered Compression Screw; ST: Stepped Compression Screw)

The effect of shear viscosity on extrusion process energy demand is shown in Figure 4.32. Shear viscosity is plotted on the x-axis and reduces as screw speed increases from 10 rpm to 90 rpm. A large variation in specific energy consumption was observed, between 800 and 3700 J/g, dependent upon polymer grade, screw geometry, set temperature and screw speed. Figure 4.32 shows a clear dependence of energy consumption on melt viscosity, across all three HDPE grades and set temperatures. In general, energy consumption increased with increasing melt viscosity due to the dependence of viscous shear heating on melt viscosity. Specific energy consumption was generally found to be lower for the barrier flighted screw corresponding to the improved melting performance of this screw previously discussed. Highest energy consumption was observed for all grades of HDPE at the lowest screw rotation speed of 10 rpm. At screw speeds above 10 rpm, however, the measured specific energy consumption for all HDPEs and set conditions followed a relatively linear dependence upon melt viscosity, irrespective of set temperature and screw geometry.

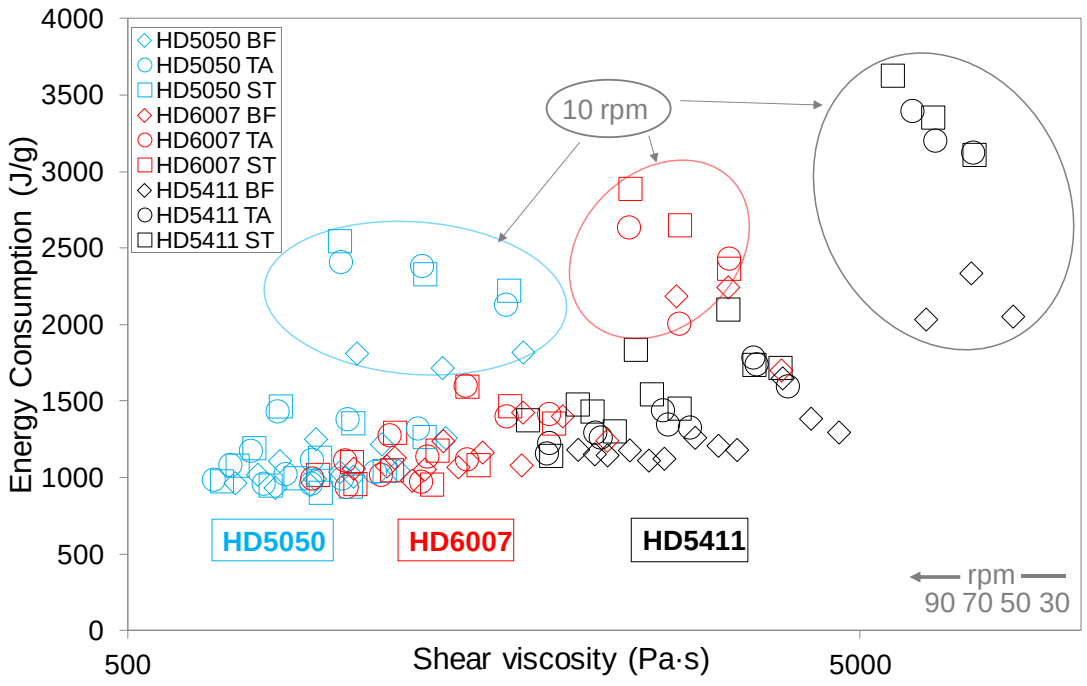

Figure 4.32 Effect of shear viscosity on process energy demand, representing three grades of HDPE for three screw geometries and set temperatures from 10 to 90 rpm (read data from right to left) (BF: Barrier Flighted Screw; TA: Tapered Compression Screw; ST: Stepped Compression Screw)

4.3.5 PP

The melting point of polypropylene (PP) was found to be higher than the polyethylenes as shown in section 4.2, Table 4.2. Therefore, barrel set temperature profiles were slightly increased up to 240°C. However, at 200°C and 220°C set temperature conditions were identical to those used for the polyethylenes. In this section, extrusion data for PP are then used to provide a direct comparison of the processing capability of these screw geometries, highlighting the dependence of the melting behaviour on screw speed or residence time and its effect on the thermal homogeneity of the melt and consequent process energy consumption.

PP results

The relationship between extruder throughput and screw speed for PP was found to be non-linear when examining the effect of screw geometry and extruder set temperature, as shown in Figure 4.33. Results indicated that screw geometry significantly affected throughput measurements, particularly at higher screw speeds. Much lower throughputs were produced for the barrier flighted screw than the two single flighted screws; for example, a difference of up to 36 kg/h was measured at 200°C and 90 rpm, reflecting the poorer processing capability of the barrier screw for this particular polymer. PP has a higher melting point (T_m =166.36°C) causing the polymer to be insufficiently molten to flow at identical barrel set temperatures. Compared to polyethylenes, this led to the lowest mass throughputs measured at all conditions, as seen in Figure 4.33, especially for the barrier flighted screw where achieving melt flow is more challenging.

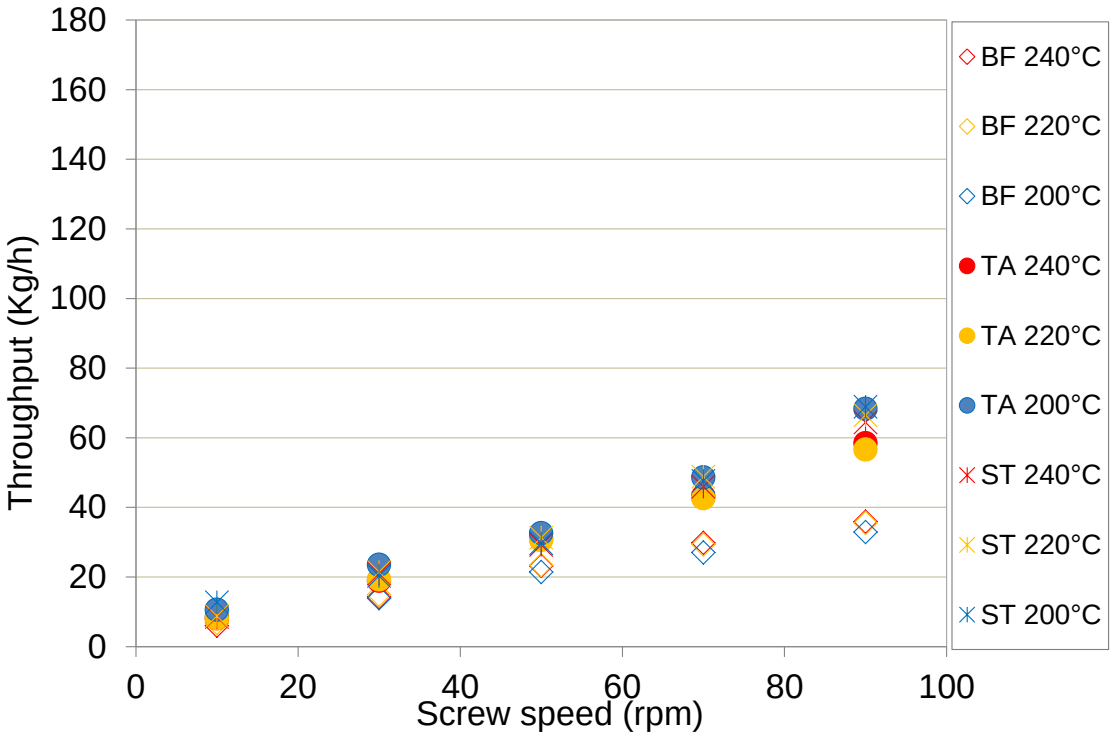

Figure 4.33 Extruder throughput vs screw speed for PP (BF: Barrier Flighted Screw; TA: Tapered Compression Screw; ST: Stepped Compression Screw)

The selection of non-optimal process settings can lead to poorer thermal homogeneity, particularly in conventional screw designs when the melting rate is not large enough and therefore fragments of solid polymer can be discharged from the extruder deteriorating the quality of the extruded polymer (Kelly et al., 2006). As seen in Figure 4.34 at 220°C, it was clearly shown that non-barrier screws achieved much poorer temperature homogeneity across the melt channel compared to the barrier flighted screw; dips in temperature of up to 23.5°C were measured near to the wall for the tapered compression screw at 90 rpm. For the stepped compression screw, however, melt temperature was not recorded at the same conditions because the thermocouple mesh was damaged due solid polymer exiting the die. Measured temperatures for the barrier flighted screw also decreased with increasing screw speed but these were more consistent across the flow path.

At 240°C it was observed that the relationship between melt temperature and screw speed was similar to 220°C for all three screw geometries (Figure 4.35). The lowest viscosity of PP occurred at this temperature (section 4.1, Figure 4.3) and allowed quantification of radial melt temperatures at the highest screw speeds. At 90 rpm and close to the die walls, temperature drops of up to 31 and 43.5°C were measured for tapered and stepped compression screws, respectively.

Radial melt temperatures generated by the barrier flighted screw were found to be more sensitive to screw speed than those at 220°C; temperatures were less consistent and tended to decrease as screw speed increased. At 200°C, however, melt temperature profiles increased or decreased as screw speed increased depending upon screw geometry (Figure 4.35). Improved melting performance was observed when polypropylene was extruded with the barrier flighted screw, which caused a slight increase in melt temperature at each screw speed. On the contrary, lower melt temperatures were measured for the two non-barrier screws at higher screw speeds due to their limited rate of melting. As a consequence, at 200°C and 90rpm melt temperatures were not recorded for the same reasons as discussed above.

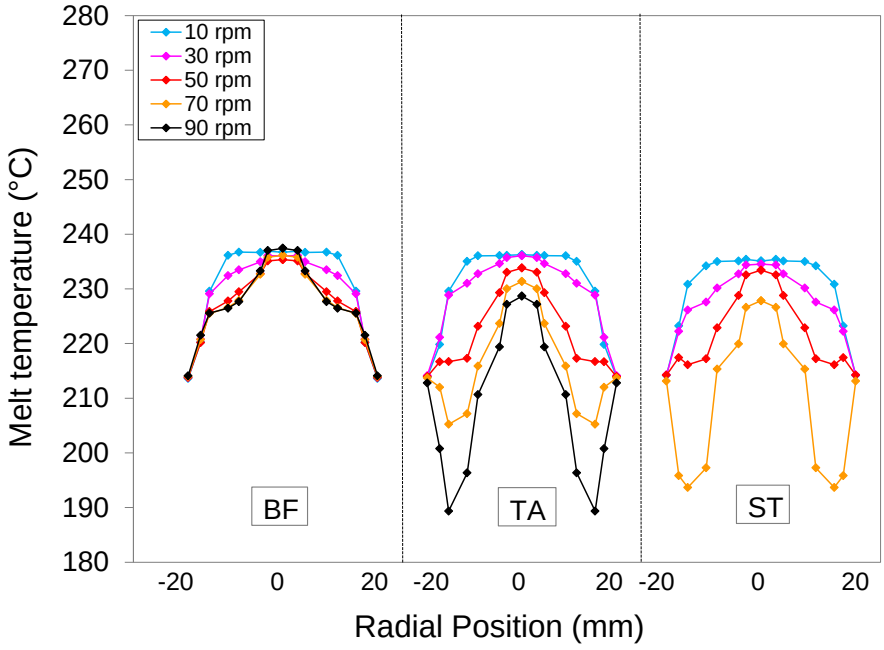

Figure 4.34 Effect of screw geometry on radial melt temperatures measured for PP at 220°C (BF: Barrier Flighted Screw; TA: Tapered Compression Screw; ST: Stepped Compression Screw)

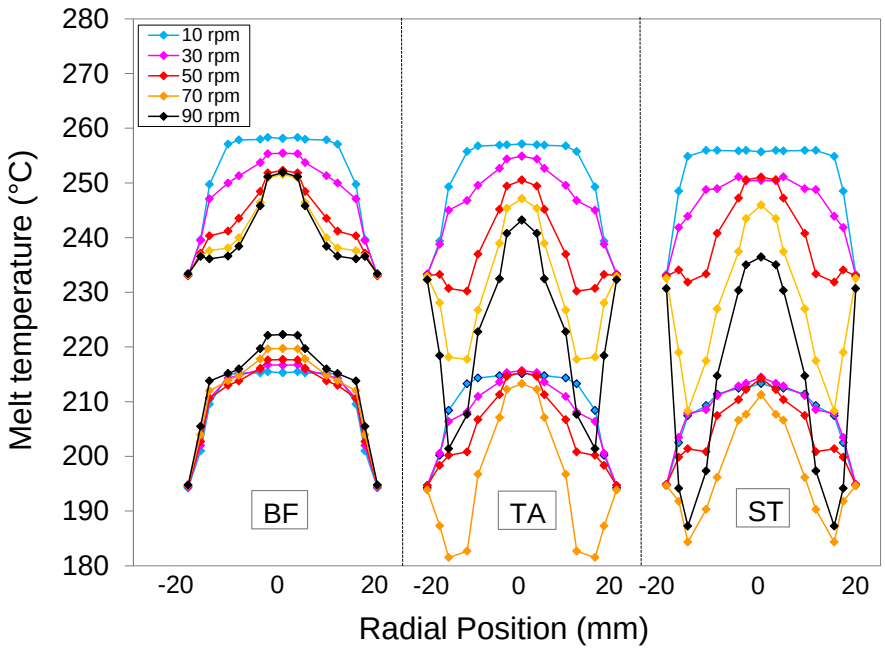

Figure 4.35 Effect of set temperature and screw geometry on radial melt temperatures measured for PP at 200 and 240°C (BF: Barrier Flighted Screw; TA: Tapered Compression Screw; ST: Stepped Compression Screw)

The inappropriate selection of the barrel set temperatures and its effect on measured temperature was clearly reflected in Figure 4.36. In general, melt temperature was found to be lower with increasing screw speed due the inefficient melting ability of these screws at higher throughputs to homogeneously melt the volume of polymer within the screw channel, particularly for both non-barrier screws as discussed previously. Here, at 240°C a difference of up to 37°C was observed for the stepped compression screw across the range of screw speeds.

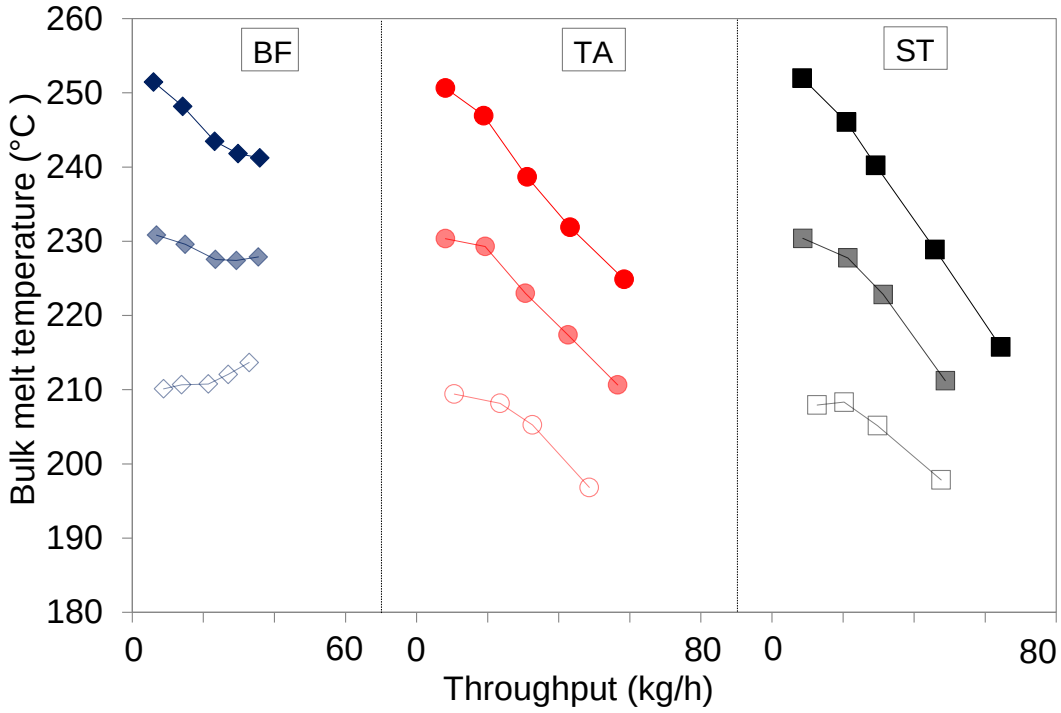

Figure 4.36 Bulk melt temperature measurements vs throughput for PP (dark colours represent 240°C, medium 220°C and light 200°C) and (BF: Barrier Flighted Screw; TA: Tapered Compression Screw; ST: Stepped Compression Screw)

Measurements of temperature variation for PP are displayed in Figure 4.37, confirming the poorer thermal homogeneity of the melt achieved with the two single flighted screws at higher throughputs. At screw speeds above 50 rpm, melt quality was significantly affected by set temperature. At 200°C, temperature data were recorded at 70 rpm to highlight that levels of variation are shown to be higher for this lower set temperature, especially for the stepped compression screw, corresponding to the drops of temperature near the wall seen in Figure 4.43. These variations, however, were smaller for the barrier flighted screw and relatively unaffected by set temperature.

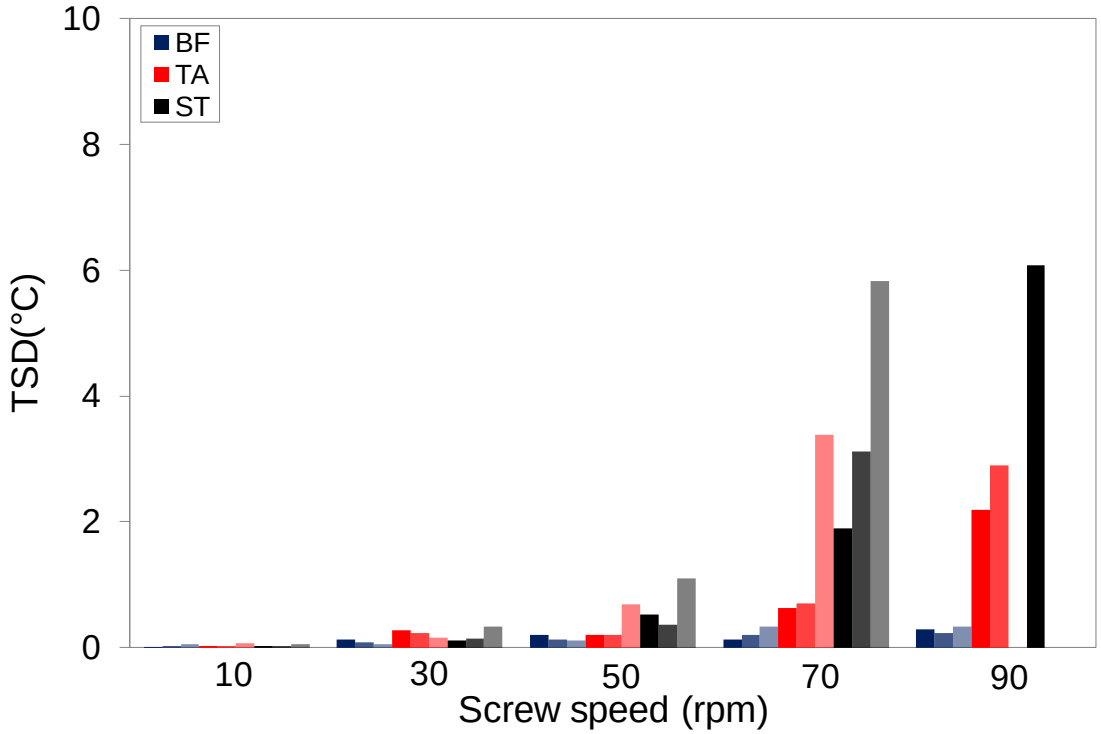

Figure 4.37 Variation of melt temperature vs screw speed for PP (dark colours represent 240°C, medium 220°C and light 200°C), (BF: Barrier Flighted Screw; TA: Tapered Compression Screw; ST: Stepped Compression Screw) and (TSD: Variation of melt temperature over a period of 1 min calculated by taking an average of the standard variation at each individual position)

Measured die pressure generated by each screw and extruder set temperature is compared in Figure 4.38. As screw speed was increased the pressure difference observed between the two single flighted and the barrier flighted screw gradually increased in conjunction with the effect of set temperature on pressure measurements. Pressure measurements for the barrier flighted screw were much lower than the two single flighted screws and less affected by set temperature, reflecting the mass throughputs observed in Figure 4.33. Despite the fact that set temperature had a major effect on measured pressure for the stepped compression screw, throughputs were similar to those generated by the tapered compression screw. This reflects the poorer processing capability of this screw which could also explain the lower temperature homogeneity shown in Figure 4.34 and Figure 4.35.

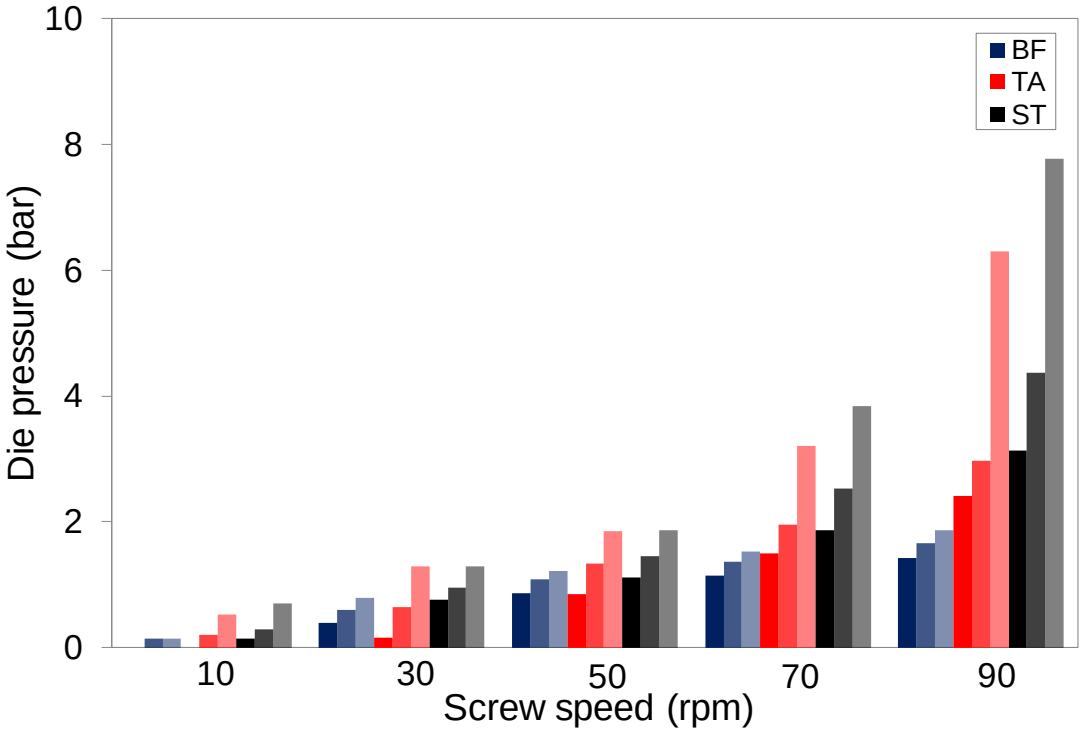

Figure 4.38 Die melt pressure vs screw speed for PP (dark colours represent 240°C, medium 220°C and light 200°C) and (BF: Barrier Flighted Screw; TA: Tapered Compression Screw; ST: Stepped Compression Screw)

Energy consumption measurements for polypropylene are shown in Figure 4.39. Clearly, at identical conditions, the demand of energy highly exceeded the energy required to process the PE's, particularly for the barrier flighted screw. For example, total energy consumption for PP using the barrier screw at 200°C ranged from 2980 J/g at 10 rpm to 1460J/g at 90 rpm compared to 1790-895 J/g for LDPE, 1740-940 J/g for LLDPE and 1820-940 J/g for HD5050. Overall, results indicated that selection of unsuitable extruder screw geometry for PP and set extrusion temperature led to a poorer processing capability causing an increase in the demand of specific energy consumption required by the motor, heaters/cooling fans and consequently total energy consumption of the extrusion process (Figure 4.39 - Figure 4.41).

In addition, data highlighted that motor energy allowed more sensitive examination of the effect of processing conditions on melt viscosity and its effect on energy measurements (Figure 4.40).

Measured energy from the motor revealed more complex relationships between energy and screw speed and their dependence on screw geometry and extruder set temperature. The lowest viscosity measured for PP at 240°C (see section 4.1, Figure 4.3) was found to cause a significant increase in energy measurements, irrespective of screw geometry over the range of screw speeds.

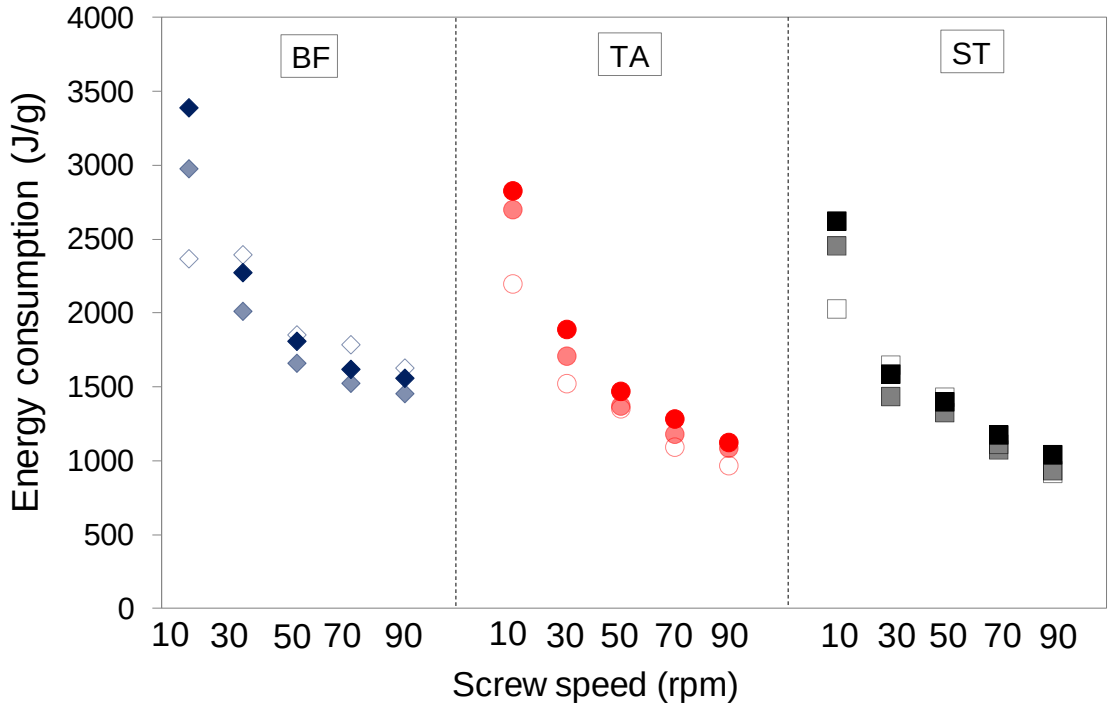

Figure 4.39 Total specific energy consumption vs screw speed for PP (dark colours represent 240°C, medium 220°C and light 200°C) and (BF: Barrier Flighted Screw; TA: Tapered Compression Screw; ST: Stepped Compression Screw)

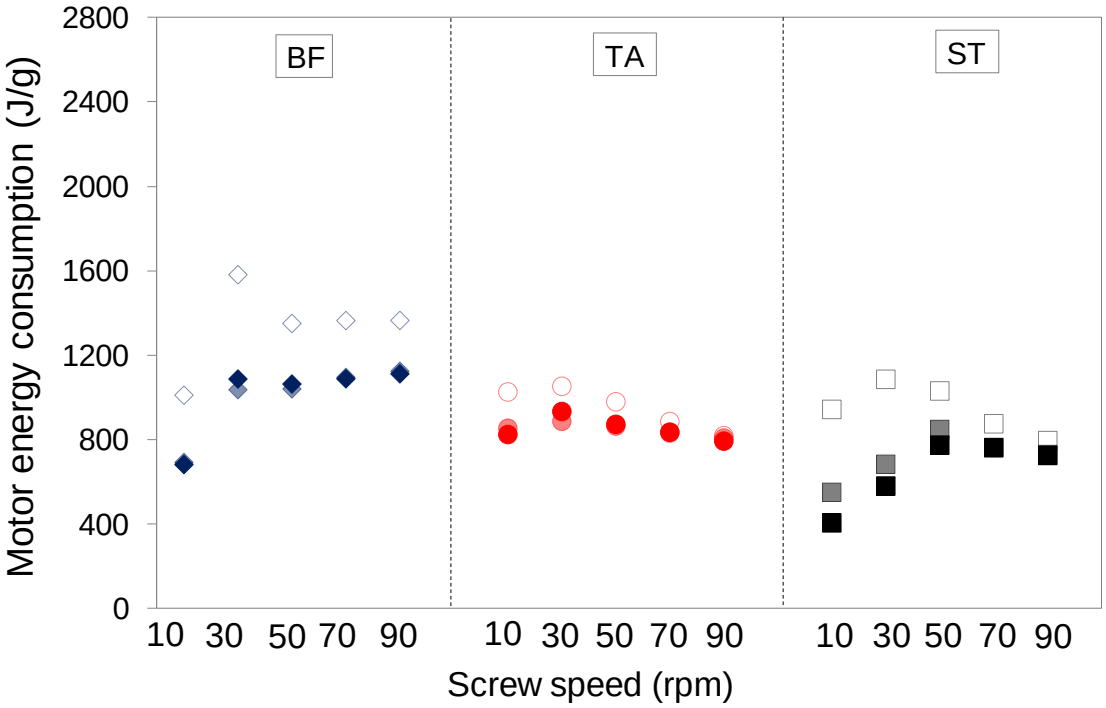

Figure 4.40 Specific energy consumption for the motor vs screw speed and PP (dark colours represent 240°C, medium 220°C and light 200°C) and (BF: Barrier Flighted Screw; TA: Tapered Compression Screw; ST: Stepped Compression Screw)

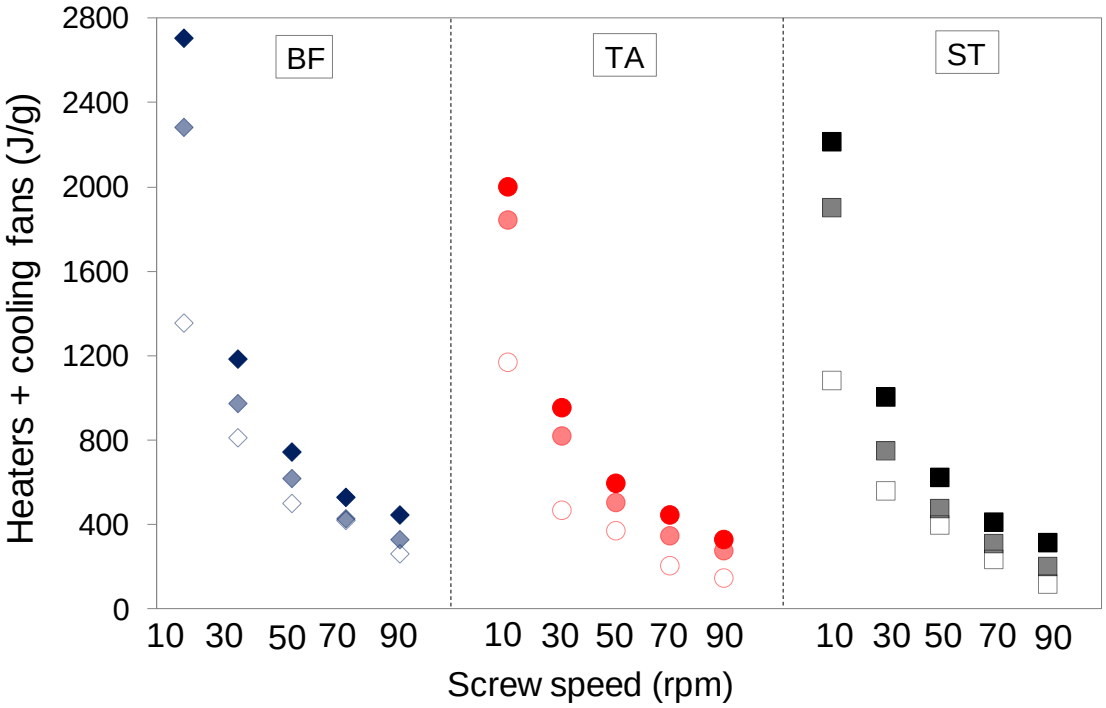

Figure 4.41 Specific energy consumption for the heaters/cooling fans vs screw speed and PP (dark colours represent 240°C, medium 220°C and light 200°C) and (BF: Barrier Flighted Screw; TA: Tapered Compression Screw; ST: Stepped Compression Screw)

4.3.6 PS

As discussed in section 2.7.3, amorphous thermoplastics do not have a melting point at which the polymer begins to flow as with semi-crystalline polymers. It was found that under extrusion conditions these polymers flow at $T \geq T_{cf}$. T_{cf} was defined as the "critical flow temperature" and it represents the temperature at and above these polymers are considered to be a "liquid" (Han et al., 1996). This section, therefore, aims to examine the differences in measured temperature and energy consumption that an amorphous polymer such as polystyrene (PS) may exhibit when compared to semi-crystalline thermoplastics, reflecting the effect that its irregular structure can have on extrusion melting performance.

PS results

Extruder throughput measured for PS is presented in Figure 4.42. Throughputs increased linearly with screw speed whilst screw geometry and set temperature were found to have little effect. However, at lower screw speeds, the barrier flighted screw produced slightly higher throughputs than the two single flighted screws. At identical conditions, throughputs were higher for PS compared to PP and polyethylenes such as LDPE, LLDPE and HD5050, especially for both single flighted screws. At 90 rpm, for example, a throughput of ~100 kg/h was achieved with PS compared to ~ 80 kg/h for HD5050 and LDPE and 85 kg/h for LLDPE. This is thought to result from the higher density of this polymer compared to polyethylenes, as shown in section 3.2, Table 3.2.

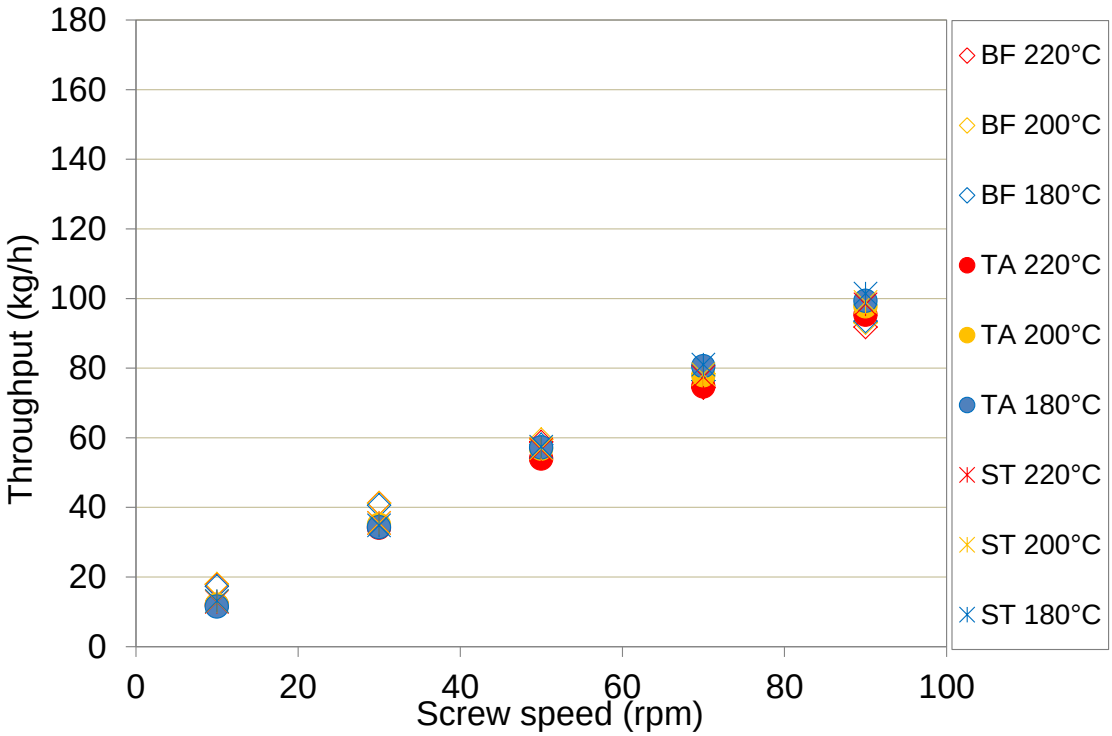

Figure 4.42 Extruder throughput vs screw speed for PS (BF: Barrier Flighted Screw; TA: Tapered Compression Screw; ST: Stepped Compression Screw)

Melt temperature data for polystyrene for each screw geometry is displayed in Figure 4.43 at 200°C. For both single flighted screws melt temperature profiles were notably pointed in shape as screw speed increased, reaching maximum values at the centre of the flow whereas lower melt temperatures were measured towards the walls. For the barrier flighted screw, however, radial melt temperatures were flat in shape across the die section at each screw speed, reflecting the improved melting performance achieved with this geometry.

The effect of set temperature and its influence on measured temperature profiles is shown in Figure 4.44. At 220°C, melt temperature profiles for non-barrier screws were found to be less pointed in shape with lower temperature drops near to the wall. Measured temperatures for the barrier flighted screw, however, were found to be relatively unaffected by screw speed.

The effect of screw speed was more pronounced at 180°C for all three extruder screws; melt temperatures increased with increasing screw speed and these were more consistent across the total flow volume, particularly for the barrier flighted screw. The viscosity of PS was reported to be sensitive to both shear and temperature (section 4.1, Figure 4.3) which could explain that melt temperature profiles were highly dependent upon set temperature, varying significantly with screw speed (Figure 4.44).

From Figure 4.45 it was noticed that for both single flighted screws there was a clear difference in melting performance at each set temperature. At 180°C, for example, melt temperatures increased as screw speed increased whilst at 220°C measured temperatures tended to decrease. For the barrier flighted screw, however, melt temperature rose with increasing screw speed but this tendency was less pronounced at higher set temperatures.

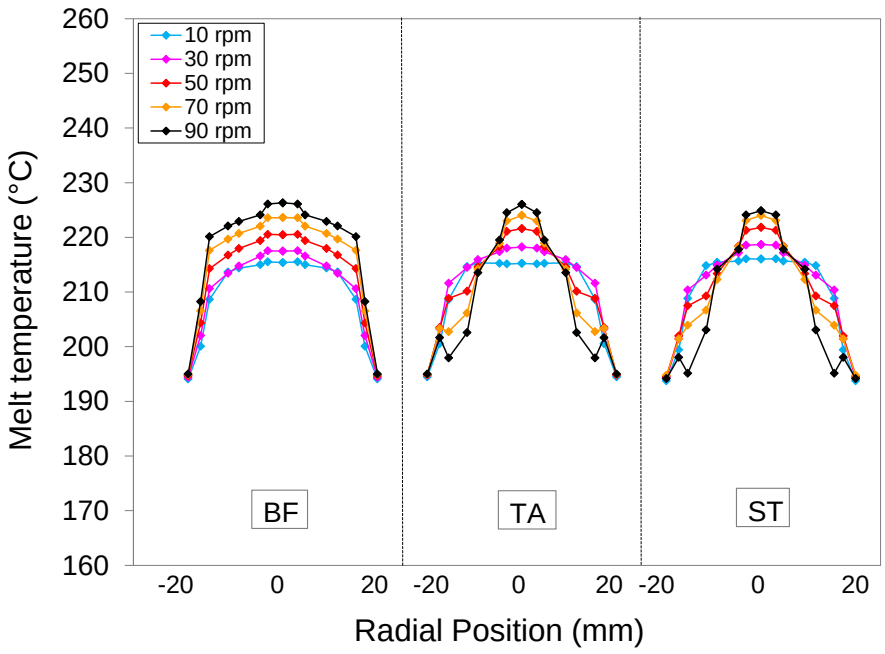

Figure 4.43 Effect of screw geometry on radial melt temperatures measured for PS at 200°C (BF: Barrier Flighted Screw; TA: Tapered Compression Screw; ST: Stepped Compression Screw)

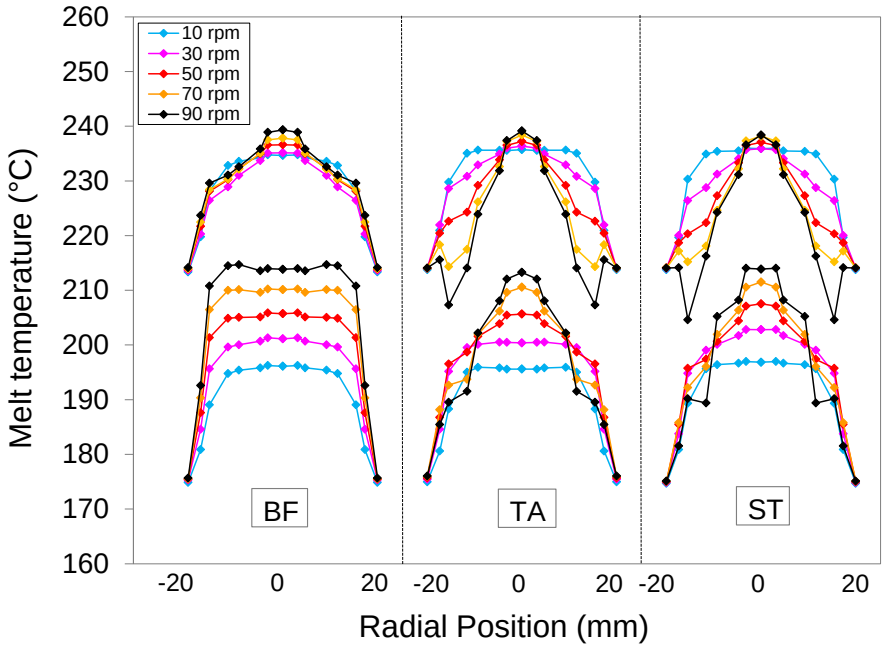

Figure 4.44 Effect of set temperature and screw geometry on radial melt temperatures measured for PS at 180 and 220°C (BF: Barrier Flighted Screw; TA: Tapered Compression Screw; ST: Stepped Compression Screw)

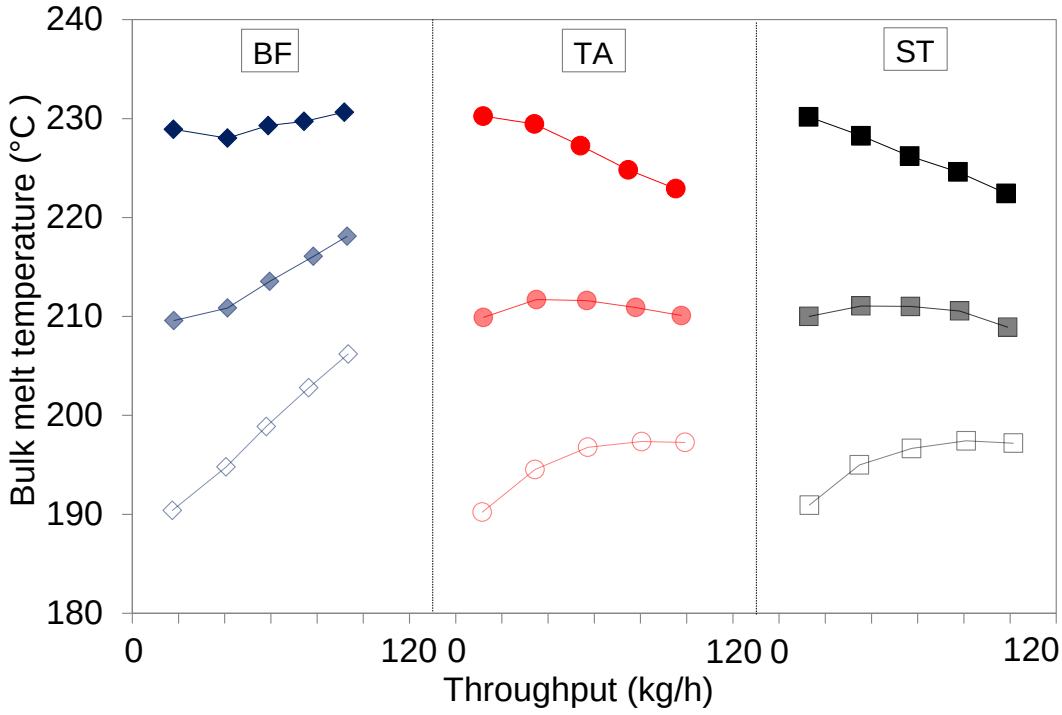

Figure 4.45 Bulk melt temperature measurements vs throughput for PS (dark colours represent 220°C, medium 200°C and light 180°C) and (BF: Barrier Flighted Screw; TA: Tapered Compression Screw; ST: Stepped Compression Screw)

The consistency in radial melt temperatures achieved with the barrier flighted screw across the die flow path is clearly shown in Figure 4.46, reflecting much lower levels of temperature variation over the range of screw speeds. Temperature fluctuations, however, for non-barrier screws gradually rose with increasing screw speed and these were strongly influenced by set temperature. At 180°C, for example, both single flighted screws exhibited the poorest temperature homogeneity, especially at 90 rpm.

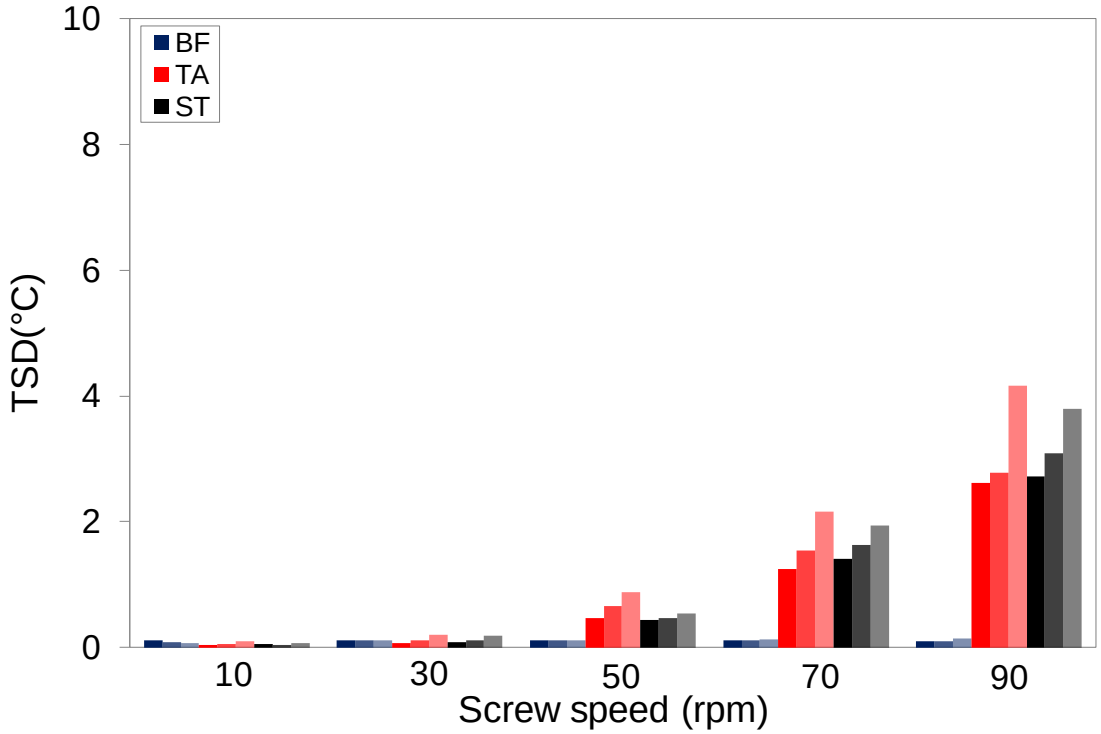

Figure 4.46 Variation of melt temperature vs screw speed for PS (dark colours represent 220°C, medium 200°C and light 180°C), (BF: Barrier Flighted Screw; TA: Tapered Compression Screw; ST: Stepped Compression Screw) and (TSD: Variation of melt temperature over a period of 1 min calculated by taking an average of the standard variation at each individual position)

Die pressure data for polystyrene is displayed in Figure 4.47. Compared to LDPE, LLDPE and HD5050 at identical conditions, a strong effect of set temperature and screw speed was observed on pressure measurements. This is likely to result from the viscous behaviour of PS and its dependence on temperature and shear described above. For example, at 90 rpm, a change of set temperature from 220 to 180 °C caused a pressure difference of up to ~3.5 bars for the two single flighted screws. However, at 10 rpm levels of die pressure generated at 220°C for tapered and stepped compression screws and 200 °C for the stepped compression were extremely low.

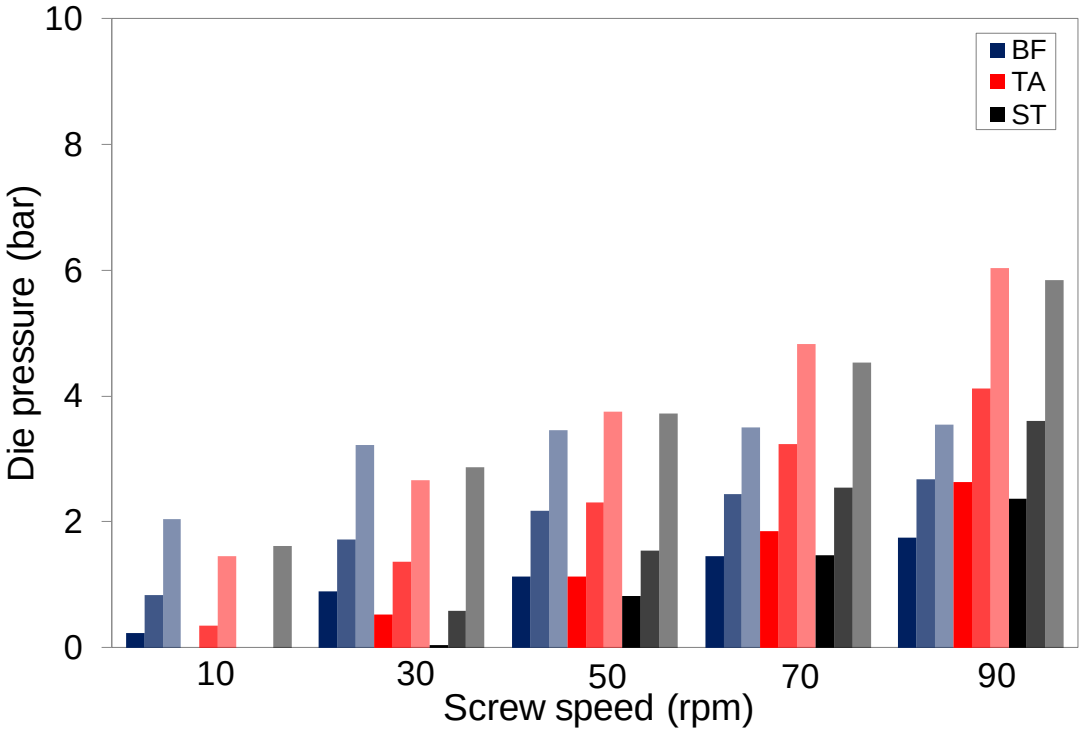

Figure 4.47 Die melt pressure vs screw speed for PS (dark colours represent 220°C, medium 200°C and light 180°C) and (BF: Barrier Flighted Screw; TA: Tapered Compression Screw; ST: Stepped Compression Screw)

Real-time quantification of extruder energy consumption for PS is shown in Figure 4.48. At identical set process conditions, PS required less specific energy to process compared to LDPE, LLDPE, HD5050 and PP, especially at lower throughputs. From Figure 4.50 it was found that specific energy consumption from heaters/cooling fans was the lowest among these polymers, particularly at 10 rpm. At 10 rpm, energy values for PS ranged from 600 to 1200 J/g compared to 1350-2175J/g for LDPE, 1130 - 1980J/g for LLDPE and 1350- 2285J/g for PP. This relatively small contribution to the extrusion process energy demand could be used to explain the low energy values shown in Figure 4.48. Figure 4.49 shows the demand of specific energy consumption required by the motor. A high dependence of energy consumption on extruder screw geometry was observed which, in turn, was strongly affected by extruder set temperature.

At 180 and 200°C, motor energy consumption for the two single flighted screws gradually decreased with increasing screw speed whereas at 220°C it progressively increased. Compared to non-barrier screws, the energy consumption for the barrier flighted screw increased over the full range of speeds at all set temperatures.

On the other hand, it has been found that pressure build-up along the screw can influence the extruder power requirements (McKelvey, 1983). Pressure and viscosity measurements for PS have shown to be strongly affected by set temperature which could explain the large difference in motor specific energy consumption measured between extruder set temperatures of 180 and 220°C, as shown in Figure 4.49.

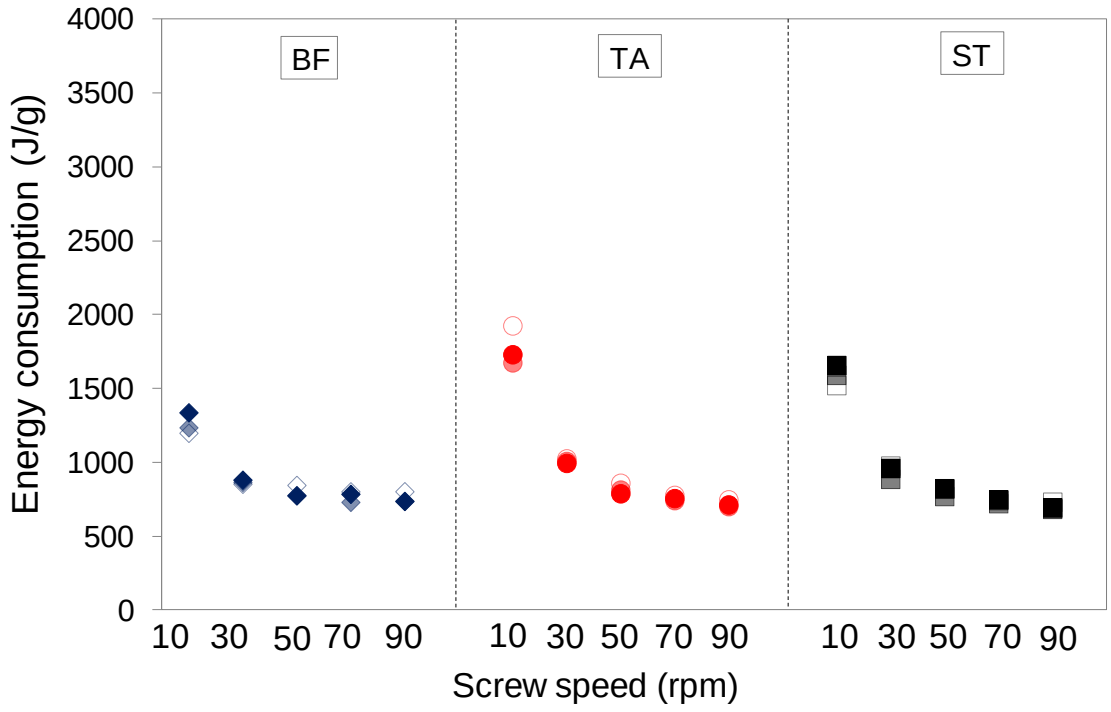

Figure 4.48 Total specific energy consumption vs screw speed for PS (dark colours represent 220°C, medium 200°C and light 180°C) and (BF: Barrier Flighted Screw; TA: Tapered Compression Screw; ST: Stepped Compression Screw)

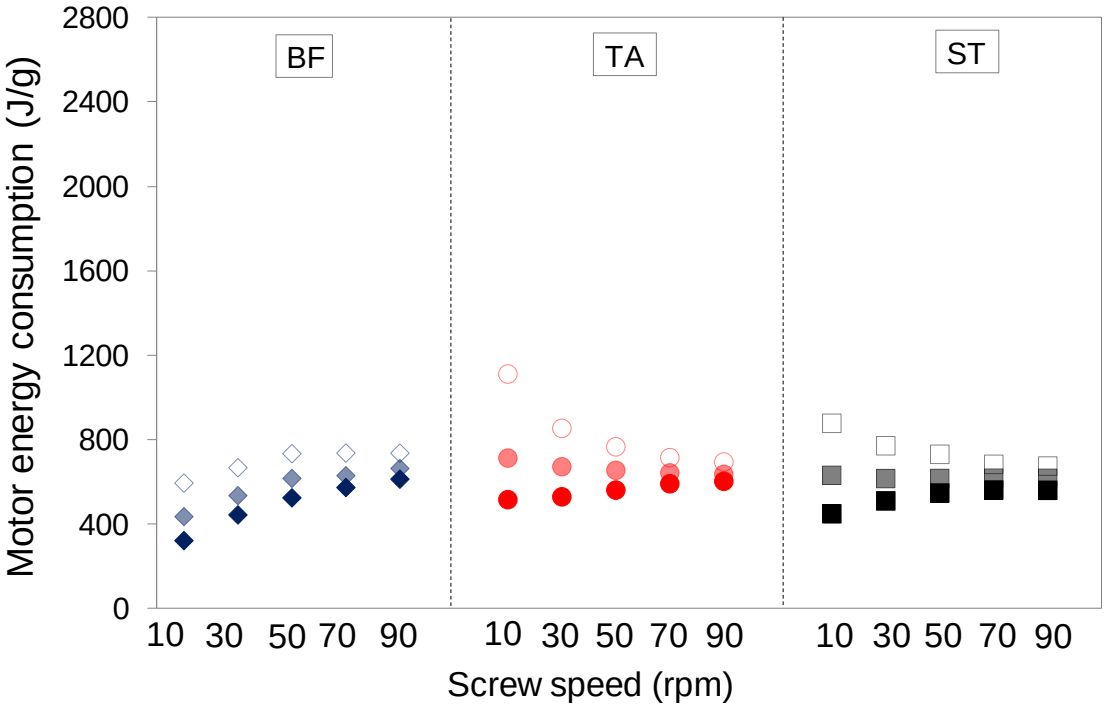

Figure 4.49 Specific energy consumption for the motor vs screw speed and PS (dark colours represent 220°C, medium 200°C and light 180°C) and (BF: Barrier Flighted Screw; TA: Tapered Compression Screw; ST: Stepped Compression Screw)

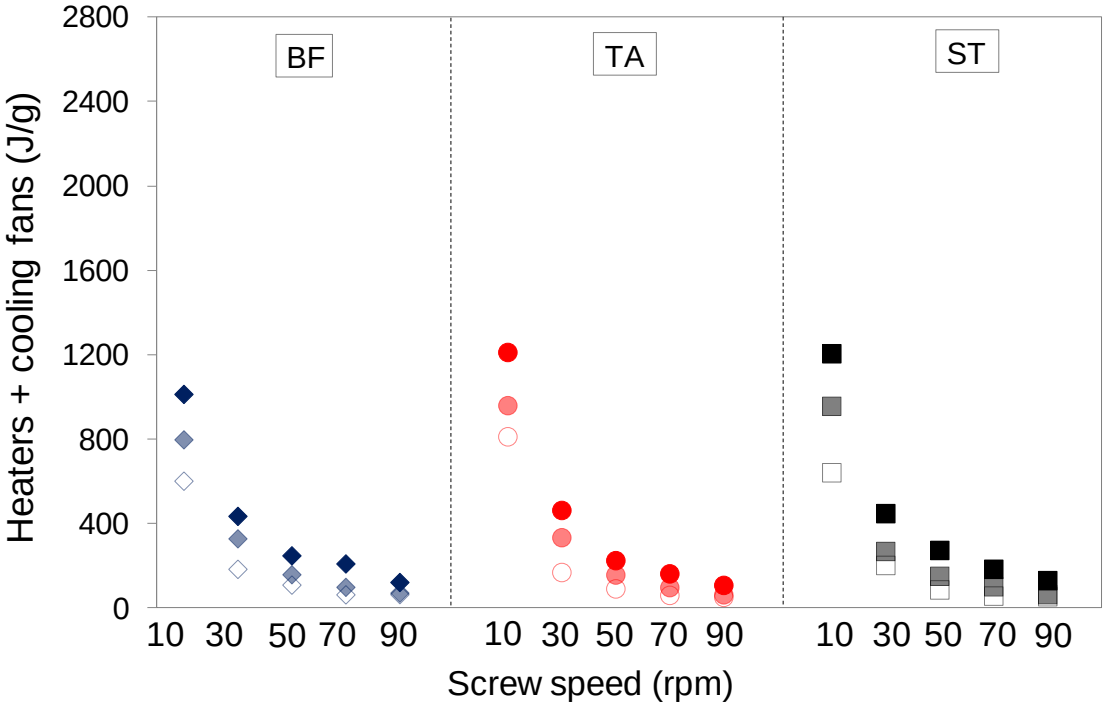

Figure 4.50 Specific energy consumption for the heaters/cooling fans vs screw speed and PS (dark colours represent 220°C, medium 200°C and light 180°C) and (BF: Barrier Flighted Screw; TA: Tapered Compression Screw; ST: Stepped Compression Screw)

4.3.7 PET

The aims of this section were to characterise the extrusion thermal behaviour for a polyethylene terephthalate resin (PET) and quantify the specific energy consumed within the process. Due to its hygroscopic nature and high sensitivity to moisture, PET requires drying prior of extrusion (Michaeli & Schmitz, 2004, Salminen, 2013). It has been found that oxidative and hydrolytic degradations can occur when processed in presence of moisture, deteriorating the melt quality performance (Hatzikiriakos et al., 1997, Verma et al., 1990). Here, extrusion data were generated after PET pellets were dried at 160 °C for at least four hours, accomplished with a drier and rapidly fed into the extruder to reduce the exposure to oxygen and moisture. In addition, higher set temperature profiles of 280, 290 and 300°C were required due to its melting point (T_m = 248.64°C) which was found to be the highest among the polymers used throughout the experimental program, as shown in section 4.2, Table 4.2).

PET results

The processing capability of the three extruder screws for PET is displayed in Figure 4.51. Throughput increased linearly with screw speed. Over the range of screw speeds, extruder throughputs for the barrier flighted screw remained higher than those produced with the two single flighted screws and these were more affected by extruder set temperature. For example, at 90 rpm a throughput difference of 11 kg/h was observed between set temperatures of 280 and 300°C. Despite the different barrel set temperatures used, the viscosity of PET was found to be the lowest (section 4.1, Figure 4.3). This could explain the highest extrusion outputs produced with PET as shown in Figure 4.51; throughputs for PET at 90 rpm ranged from ~ 120-160 kg/h compared to ~ 60-80 kg/h for HD5411, ~ 70-80 kg/h for HD6007, ~ 60-100 kg/h for HD5050, ~ 80-90 kg/h for LDPE, ~ 80-110 kg/h for LLDPE, ~ 90-100 kg/h for PS and ~ 30-70 kg/h for PP. Similarly to PS throughputs, PET was found to have the highest density among the polymers used throughout the studies (see section 3.2, Table 3.2).

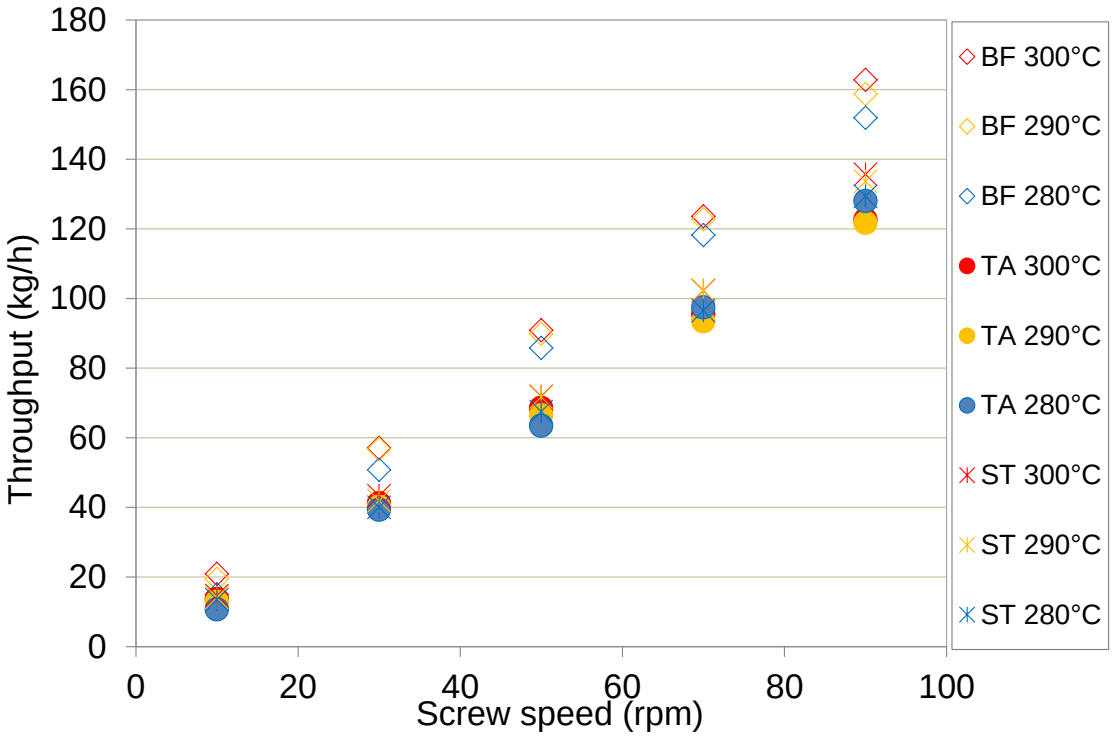

Figure 4.51 Extruder throughput vs screw speed for PET (BF: Barrier Flighted Screw; TA: Tapered Compression Screw; ST: Stepped Compression Screw)

Radial melt temperatures for PET at the medium set temperature of 290°C are displayed in Figure 4.52. Compared to those measured for the polymers described above, the effect of screw geometry on temperature measurements was different here for each screw, especially between the two single flighted screws. The major difference was observed in the centre of the flow where melt temperatures were more pointed in shape with the tapered compression screw (Figure 4.52). The relationship between melt temperature and screw speed for the barrier flighted screw was found to be similar to that for the tapered compression screw but radial melt temperatures were more consistent across the flowing melt and slightly lower in the centre of the channel. The effect of extruder set temperature had little effect on melt temperature profiles as shown in Figure 4.53. A change of 20°C in the barrel set temperature profile did not cause significant differences in radial melt temperatures, as clearly shown with the tapered compression screw. According to (Giles et al., 2005), results suggest that PET was relatively unaffected by shear, causing the temperature to be less affected by viscous shear heating at the lowest set temperature.

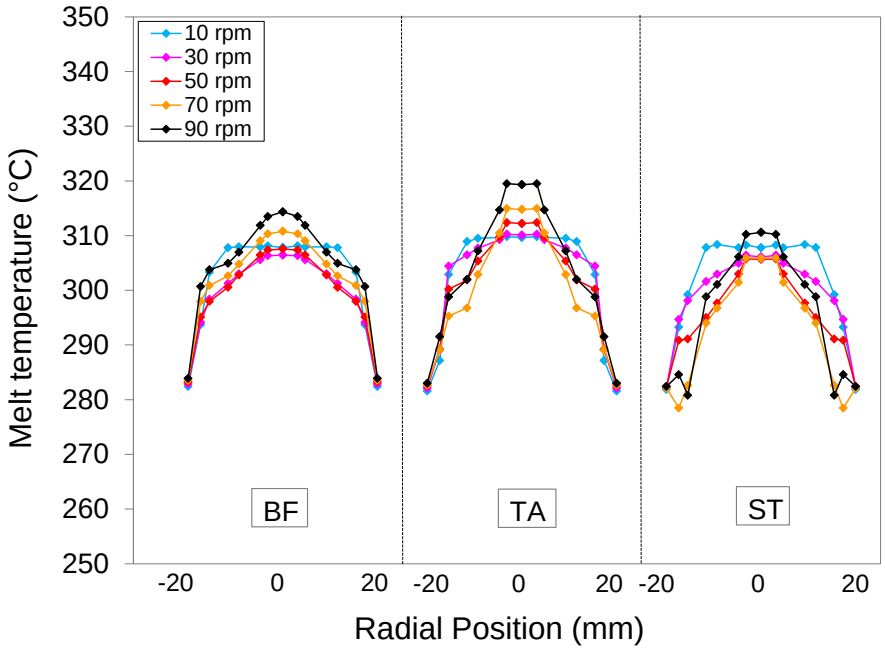

Figure 4.52 Effect of screw geometry on radial melt temperatures measured for PET at 290°C (BF: Barrier Flighted Screw; TA: Tapered Compression Screw; ST: Stepped Compression Screw)

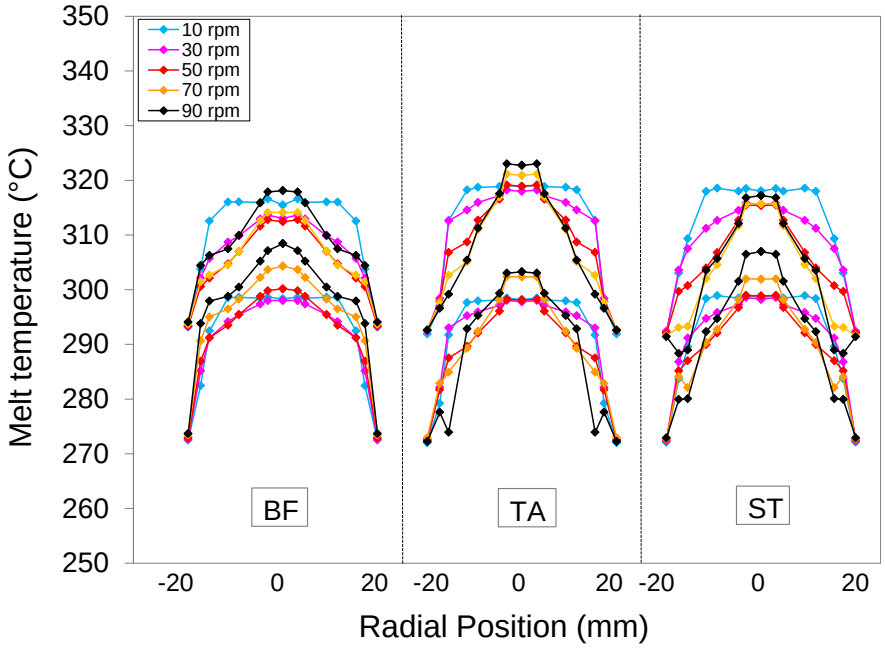

Figure 4.53 Effect of set temperature and screw geometry on radial melt temperatures measured for PET at 280 and 300°C (BF: Barrier Flighted Screw; TA: Tapered Compression Screw; ST: Stepped Compression Screw)

From Figure 4.54 it was shown that there was little effect of viscous shear generated during extrusion of PET at the lowest set temperature. The melting performance for the stepped compression screw was found to be poorer than the tapered compression screw at higher set temperatures, leading to lower temperatures at higher mass throughput. For the barrier flighted screw, however, the relationship between melt temperature and extruder throughput was similar at each set temperature, suggesting that this geometry achieved a more consistent melting performance. Melt temperature initially decreased with increasing throughput but then tended to increase above extruder throughputs corresponding to 30 or 50 rpm.

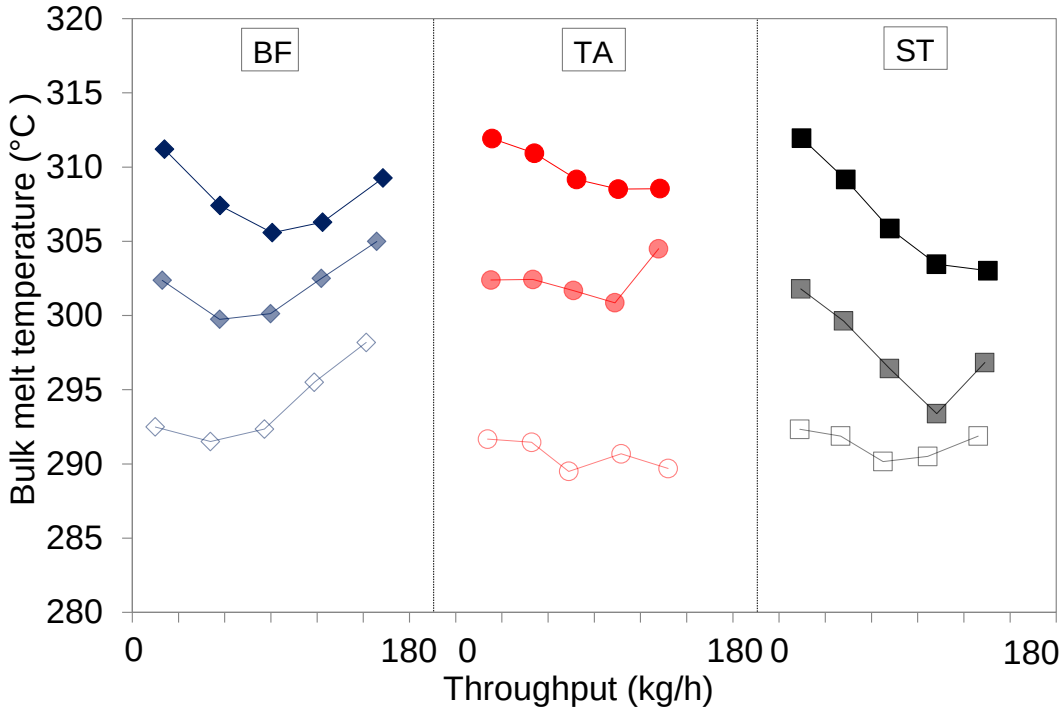

Figure 4.54 Bulk melt temperature measurements vs throughput for PET (dark colours represent 300°C, medium 290°C and light 280°C) and (BF: Barrier Flighted Screw; TA: Tapered Compression Screw; ST: Stepped Compression Screw)

The variation of temperature measured for PET and its relationship with screw geometry and set process conditions is displayed in Figure 4.55. Results revealed the improved melting action of the barrier screw leading to better temperature homogeneity. In general, levels of temperature variation for the stepped compression screw tended to be higher than the tapered geometry with increasing screw speed and set temperature, corresponding with the temperature dips near to the wall observed in Figure 4.52 and Figure 4.53.

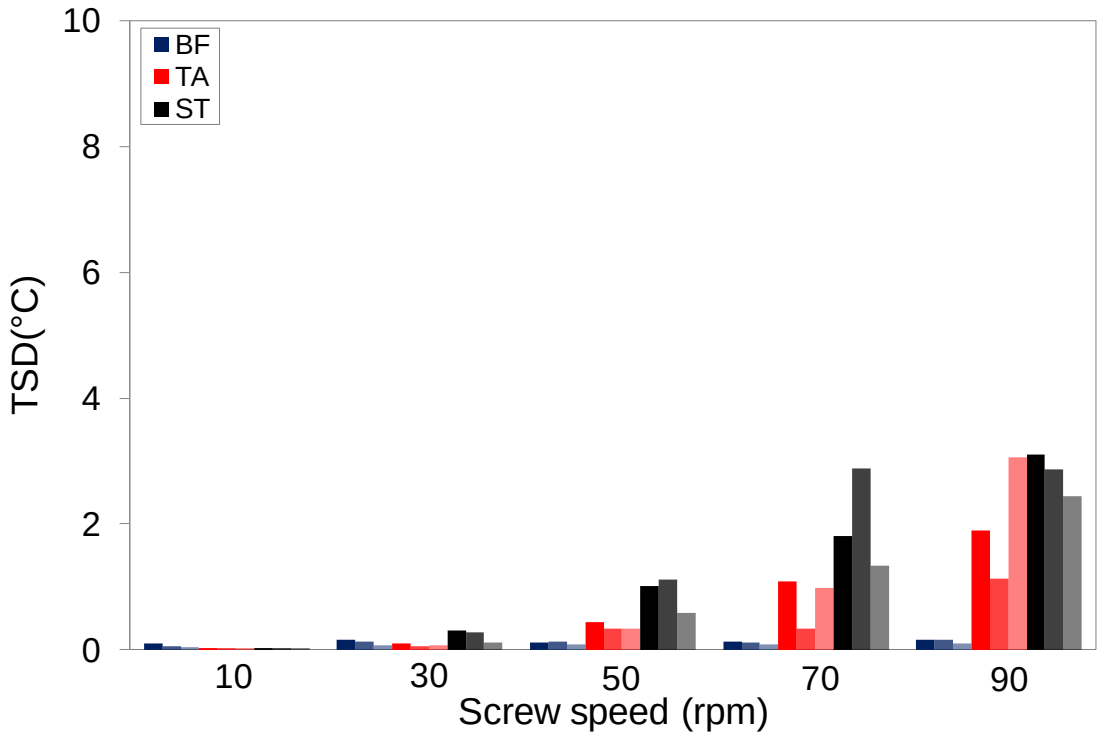

Figure 4.55 Variation of melt temperature vs screw speed for PET (dark colours represent 300°C, medium 290°C and light 280°C), (BF: Barrier Flighted Screw; TA: Tapered Compression Screw; ST: Stepped Compression Screw) and (TSD: Variation of melt temperature over a period of 1 min calculated by taking an average of the standard variation at each individual position)

From the pressure measurements shown in Figure 4.56 the higher processing capability of the barrier flighted screw was also observed. Despite the pressure difference between the barrier and the two single-flighted screws gradually decreasing as screw speed increased, throughput measurements remained much higher across the range of speeds (Figure 4.51).

This confirms the higher processability achieved with the barrier flighted screw when the effectiveness of the melting process is high, corresponding to the difference observed between throughput measured for LLDPE and LDPE. At 10 rpm levels of pressure were extremely low at all conditions.

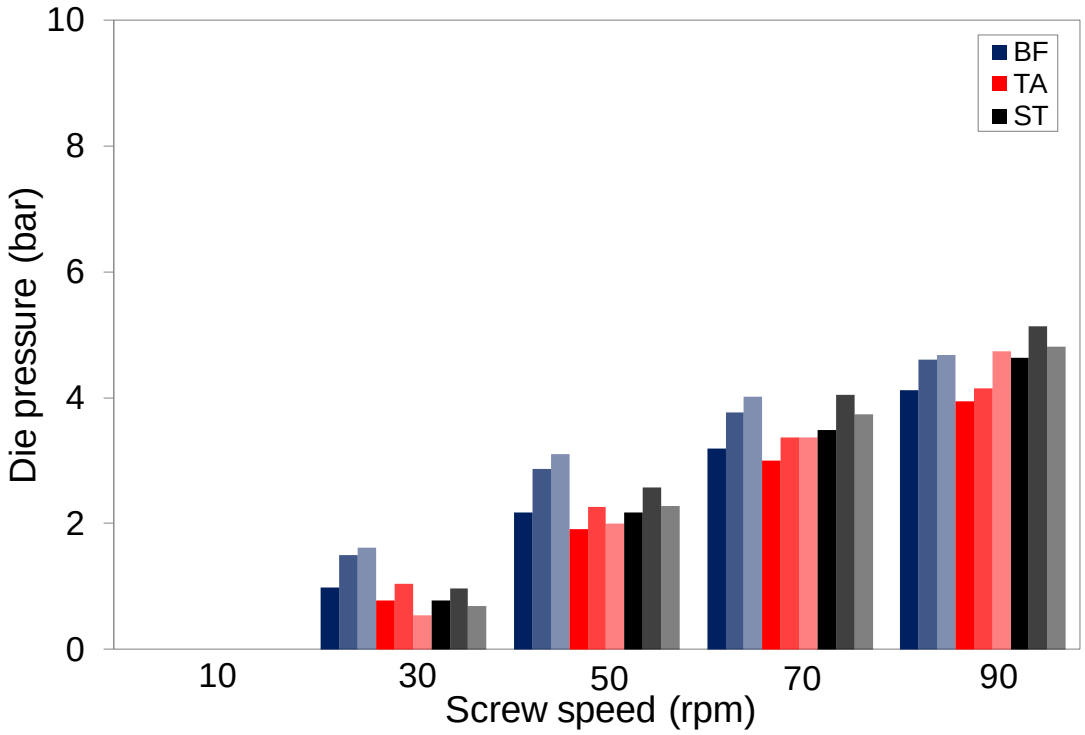

Figure 4.56 Die melt pressure vs screw speed for PET (dark colours represent 300°C, medium 290°C and light 280°C) and (BF: Barrier Flighted Screw; TA: Tapered Compression Screw; ST: Stepped Compression Screw)

Measured energy values for PET are displayed in Figure 4.57. As previously discussed, the relationship between energy consumption and screw speed and its dependence upon screw geometry and set temperature was found to be similar to PE's, PS and PP. However, from the throughput data shown in Figure 4.51, PET would be expected to require much lower specific energy to process. Due to the higher extruder set temperatures used, these two competing effects appeared here to be mutually cancelling to a large extent and as a result, energy measurements were similar to those required for PS, particularly at higher throughputs. Despite the lower values of specific energy consumption required, the additional installation costs and extra amount of energy required for drying have been reported to incur an increased demand of energy (Michaeli & Schmitz, 2004) .

From Figure 4.58 and Figure 4.59 it was observed that motor and heaters/cooling fans energies did not increase gradually as screw speed increased. For example, from Figure 4.58 it was observed that motor energy for the tapered compression screw at set temperature profiles of 280 and 290°C, showed a sharp peak and dip in energy at screw speeds of 50 and 70 rpm, respectively. Results have shown that motor energy measured in kilowatts tended to increase with extruder screw speed and rapidly reached equilibrium at each speed. (This is shown in Appendix D, Figure D1).

However, Figure D1 showed that motor energy did not remain constant at 290°C and 70 rpm and 280°C and 50 rpm. PET was found to be a temperature-sensitive polymer that exhibits rheological behaviour predominantly affected by temperature (see section 4.1, Table 4.1). Consequently, variations of temperature during drying and feeding (the polymer feedstock was manually fed into the extruder) led to changes in viscosity which subsequently influenced energy measurements from the motor at these conditions.

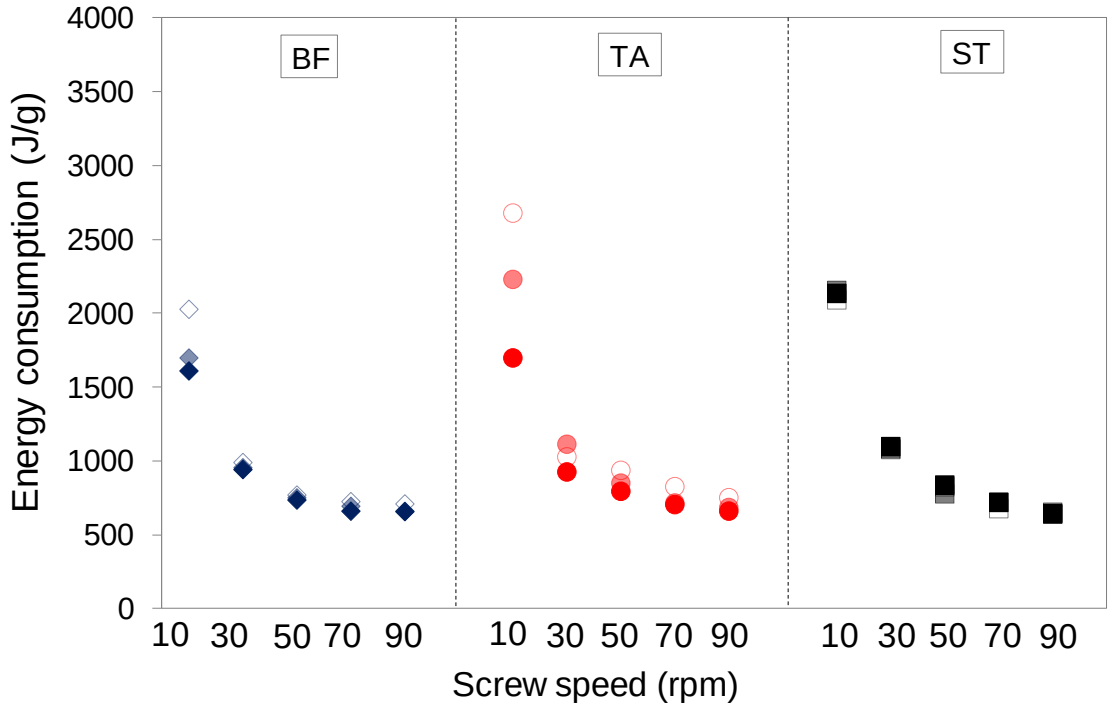

Figure 4.57 Total specific energy consumption vs screw speed for PET (dark colours represent 300°C, medium 290°C and light 280°C) and (BF: Barrier Flighted Screw; TA: Tapered Compression Screw; ST: Stepped Compression Screw)

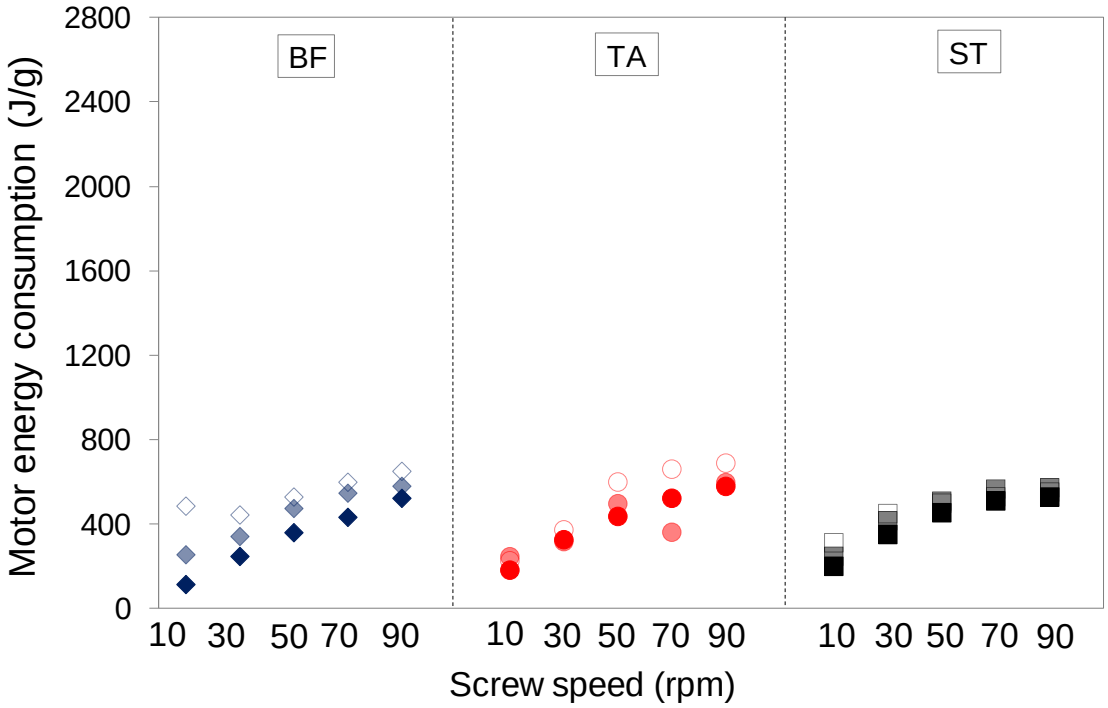

Figure 4.58 Specific energy consumption for the motor vs screw speed and PET (dark colours represent 300°C, medium 290°C and light 280°C) and (BF: Barrier Flighted Screw; TA: Tapered Compression Screw; ST: Stepped Compression Screw)

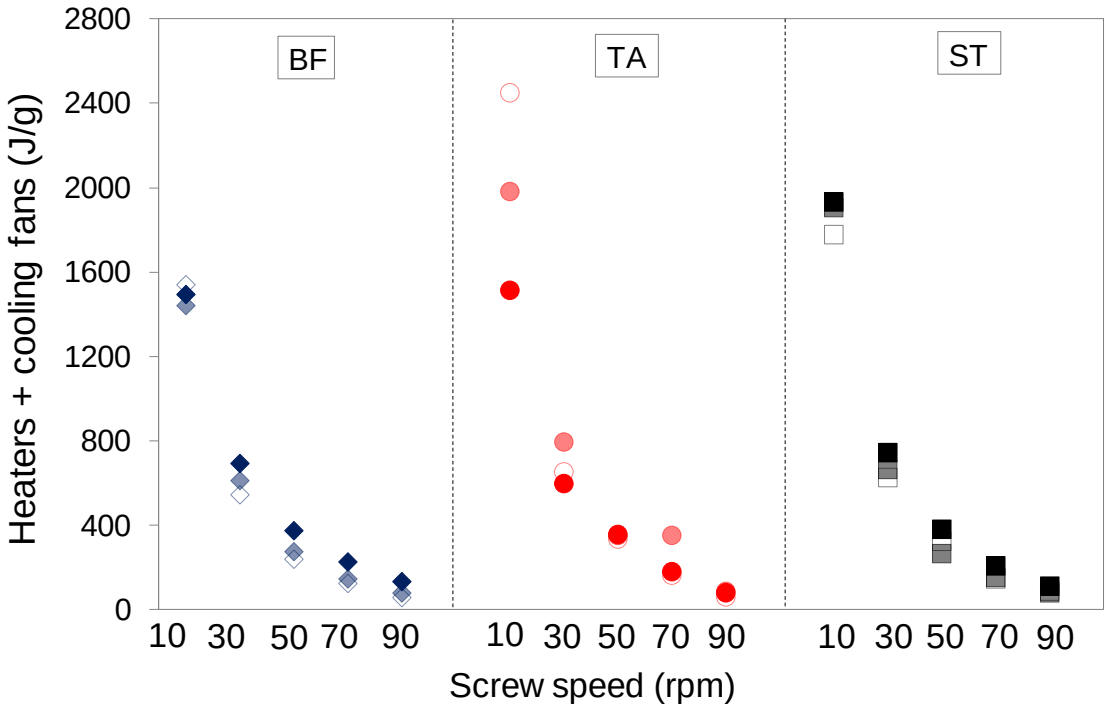

Figure 4.59 Specific energy consumption for the heaters/cooling fans vs screw speed and PET (dark colours represent 300°C, medium 290°C and light 280°C) and (BF: Barrier Flighted Screw; TA: Tapered Compression Screw; ST: Stepped Compression Screw)

4.3.8 Summary

Overall, extrusion measurements given throughout this section have shown the effect of set processing conditions and extruder screw geometry on extrusion performance. This was clearly evidenced in section 4.3.5, where it was shown that selection of unsuitable extruder screw geometry and set extrusion temperature led to a poorer processing capability of PP causing an increase in the demand of specific energy consumption.

Moreover, results have helped to quantify the effect of polymer rheology on extrusion thermal dynamics and energy consumption. In sections 4.3.2 - 4.3.4, the influence of side branching and molecular weight on melt viscosity and the important role that this plays when examining polyethylene processability in single screw extrusion and process energy demand was clearly confirmed. Furthermore, in section 4.3.7 PET was shown to exhibit a rheological behaviour strongly affected by temperature which subsequently influenced energy measurements.

Finally, the effect of thermal properties on extrusion process energy demand was clearly confirmed in section 4.3.6, highlighting the differences in energy consumption between amorphous and semi-crystalline thermoplastics.

CHAPTER FIVE

5 EXTRUDER SCALE

5.1 Introduction

Extruder scale has a significant influence on thermal characteristics of the extruder due to changes in surface area of the screw, barrel and heaters. This chapter examines the effect of extruder scale up by comparing the thermal and energy characteristics of a 38 mm diameter single screw extruder to that of a similar extruder with 63.5 mm screw diameter. Experiments, employing identical screw geometries, extruder set temperatures and range of screw speeds, were carried out on a 38mm diameter single screw extruder (Davis standard Betol BK38) processing LDPE and HDPE to quantify the effect of extruder scale on the measured throughputs, temperatures, pressure and energy consumption for the total process, motor and heaters/cooling fans.

5.2 LDPE

Extruder throughput of each of the three extruder screws for LDPE at each set temperature and screw rotation speed is compared in Figure 5.1. Mass throughputs were found to linearly increase with increasing screw speed at all conditions. Throughputs from the barrier flighted screw were higher than those provided by both single flighted screws across the range of screw speeds and these were more influenced by set temperature, especially at higher screw speeds. For all three screw geometries, throughput gradually decreased as set temperature decreased. Compared to mass throughput measured in a 63mm diameter single screw extruder (Figure 5.2) the relationship between throughput and screw speed and its dependence on screw geometry was found to be similar. However, the difference in throughput measured between the barrier and the two single flighted screws was lower and the effect of set temperature on measurements was not clearly ordered as 220°C > 200°C > 180°C.

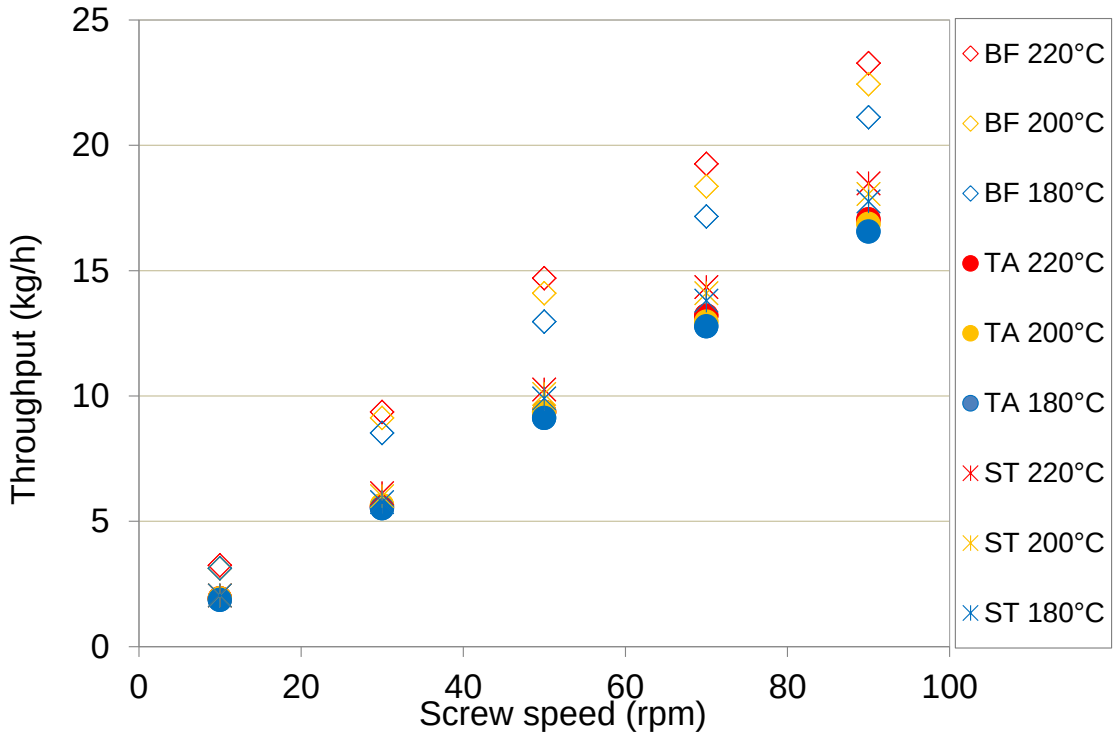

Figure 5.1 Extruder throughput vs screw speed for LDPE measured in 38 mm diameter single screw extruder (BF: Barrier Flighted Screw; TA: Tapered Compression Screw; ST: Stepped Compression Screw)

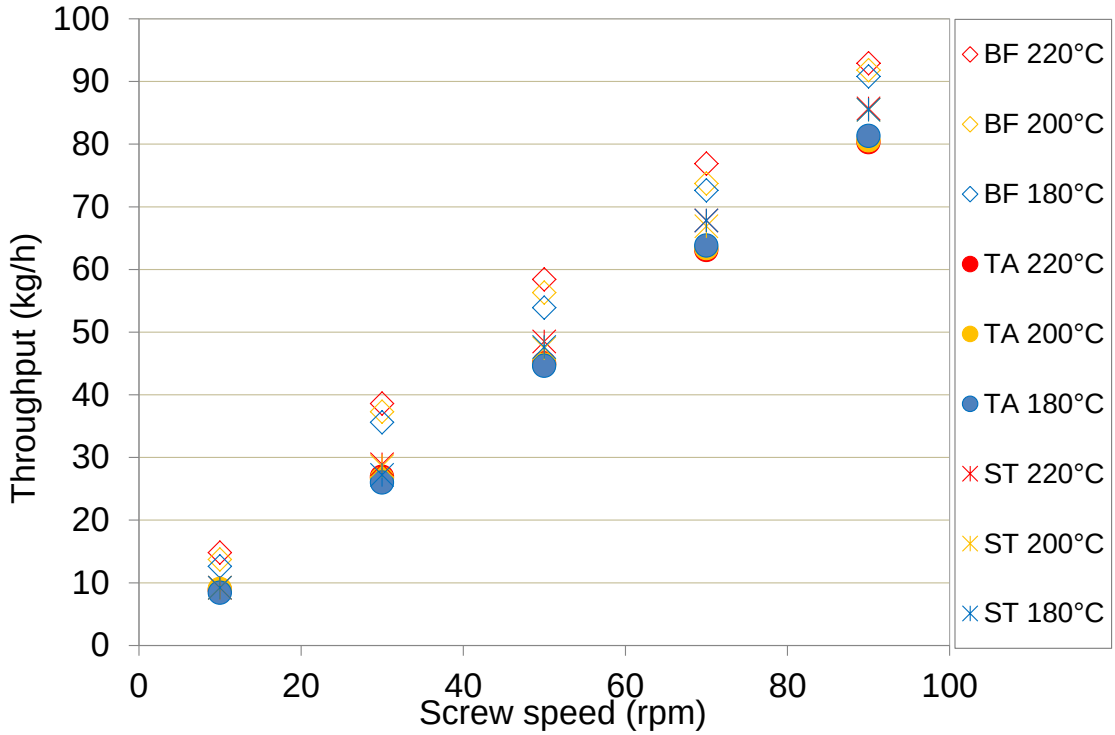

Figure 5.2 Extruder throughput vs screw speed for LDPE measured in 63 mm diameter single screw extruder (BF: Barrier Flighted Screw; TA: Tapered Compression Screw; ST: Stepped Compression Screw)

Measured radial melt temperature profiles prior to the die of a 38 mm diameter single screw extruder are presented in Figure 5.3 for LDPE using three extruder screw geometries at 200°C. Clearly, when compared to those measured in a 63 mm diameter single screw extruder (Figure 5.4), the effect of screw geometry and screw speed had significantly less effect on temperature measurements and hence relatively similar temperature profiles were measured for all screw geometries. For both single flighted screws, temperatures in the centre of the flow tended to increase with increasing screw speed reaching maximum values at 90 rpm, whereas lower temperature regions were measured towards the die walls. The major difference with the barrier flighted screw was found in the centre of the flow (Figure 5.3) where temperatures were less affected by screw speed, showing lower peaks of temperature at higher throughputs.

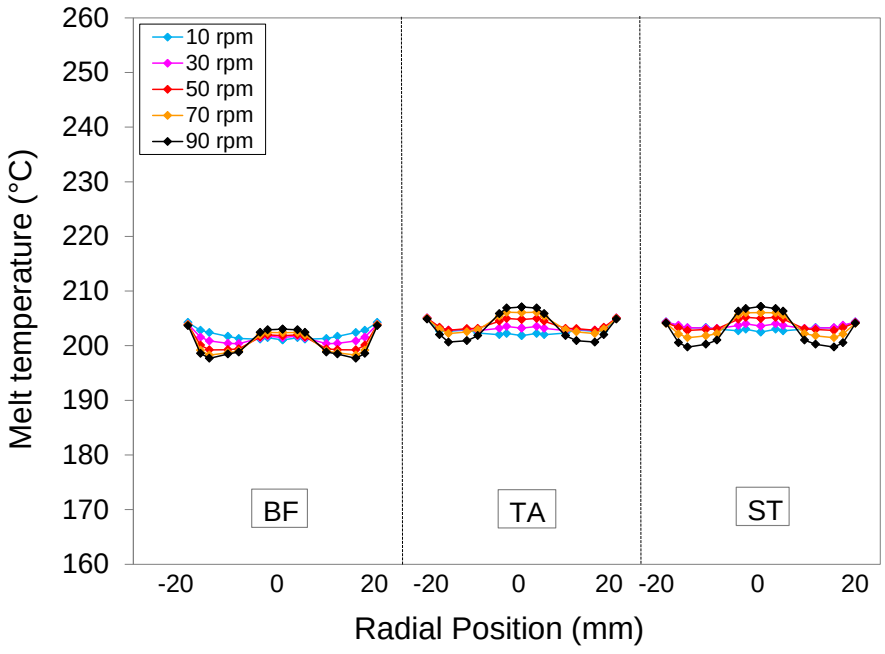

Figure 5.3 Effect of screw geometry on radial melt temperatures measured for LDPE at 200°C using 38 mm diameter single screw extruder (BF: Barrier Flighted Screw; TA: Tapered Compression Screw; ST: Stepped Compression Screw)

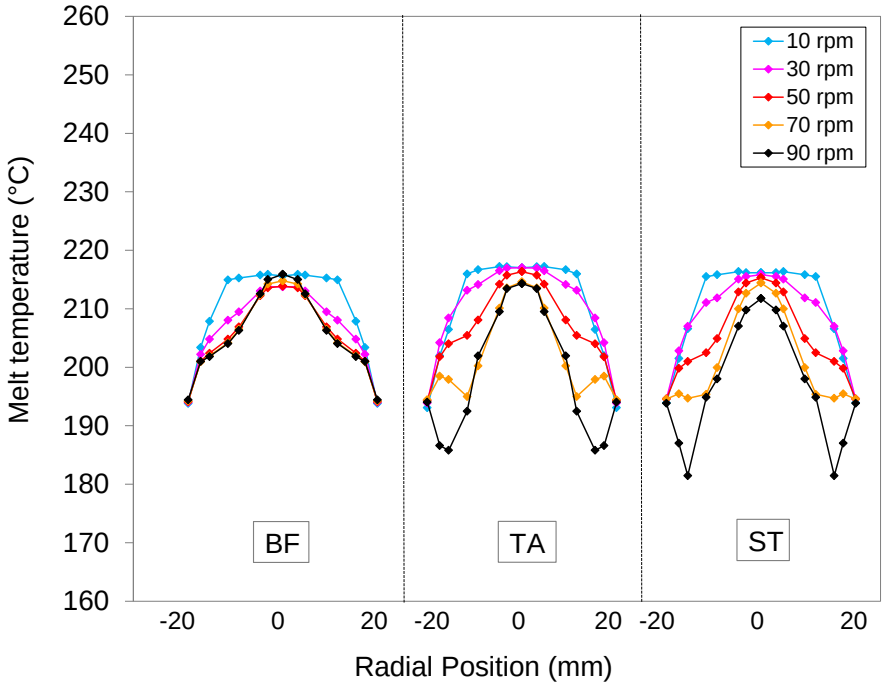

Figure 5.4 Effect of screw geometry on radial melt temperatures measured for LDPE at 200°C using 63 mm diameter single screw extruder (BF: Barrier Flighted Screw; TA: Tapered Compression Screw; ST: Stepped Compression Screw)

The effect of set temperature on radial melt temperatures was examined in more detail in Figure 5.5. At 220°C the dependence of temperature on screw geometry and screw speed was similar to that at 180°C but temperature profiles were more affected by screw speed which led to larger temperature drops towards the die walls. At 180°C, however, measurements were more sensitive to viscous shear heating which caused an increase in melt temperature across the flow channel.

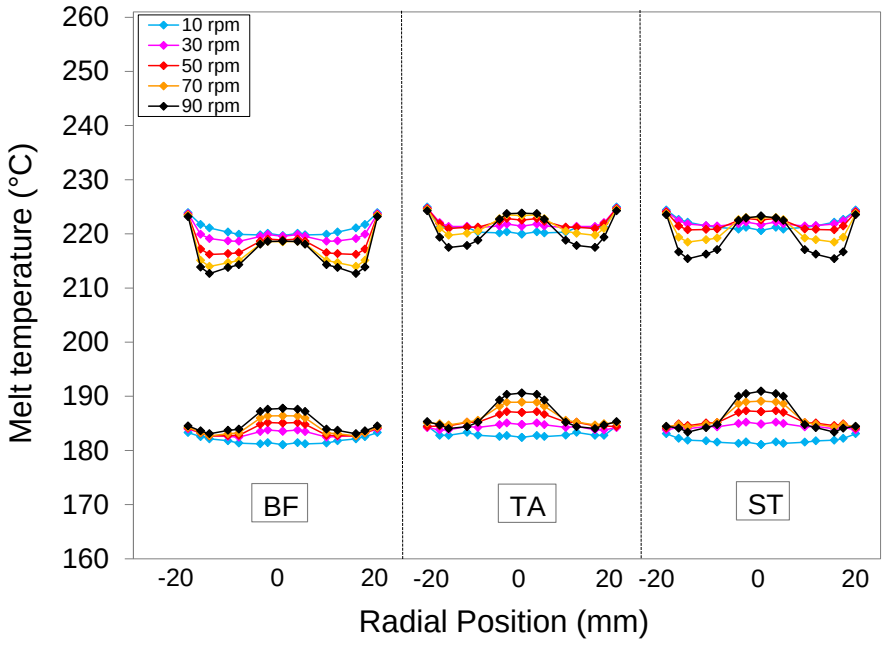

Figure 5.5 Effect of set temperature and screw geometry on radial melt temperatures measured for LDPE using 38 mm diameter single screw extruder (BF: Barrier Flighted Screw; TA: Tapered Compression Screw; ST: Stepped Compression Screw)

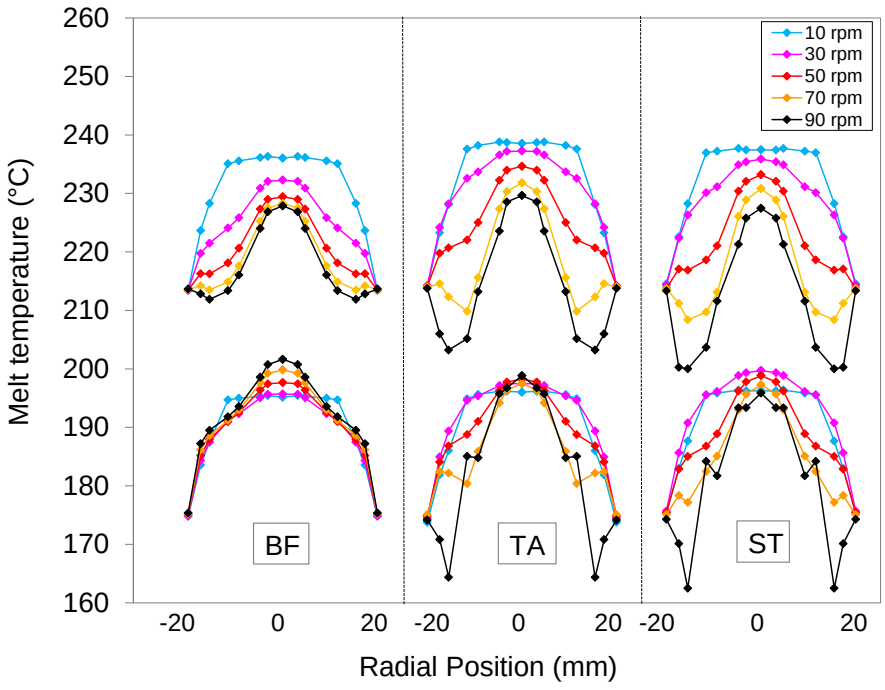

Figure 5.6 Effect of set temperature and screw geometry on radial melt temperatures measured for LDPE using 63 mm diameter single screw extruder (BF: Barrier Flighted Screw; TA: Tapered Compression Screw; ST: Stepped Compression Screw)

To provide a comparison between both melting performances for LDPE, the bulk melt temperature measured in the 38 mm diameter single screw extruder was compared directly to corresponding measurements from the 63mm diameter extrusion process (Figure 5.7). Most notably, it was not observed here the inefficient melting ability provided by both single flighted screws causing a decrease in melt temperature in the large scale extrusion process and the corresponding improved melting action of the barrier screw. On the contrary, melting performance at each set temperature tended to be relatively similar irrespective of screw geometry, suggesting that there was not a strong dependence of melt homogeneity on screw geometry in the small scale extrusion process.

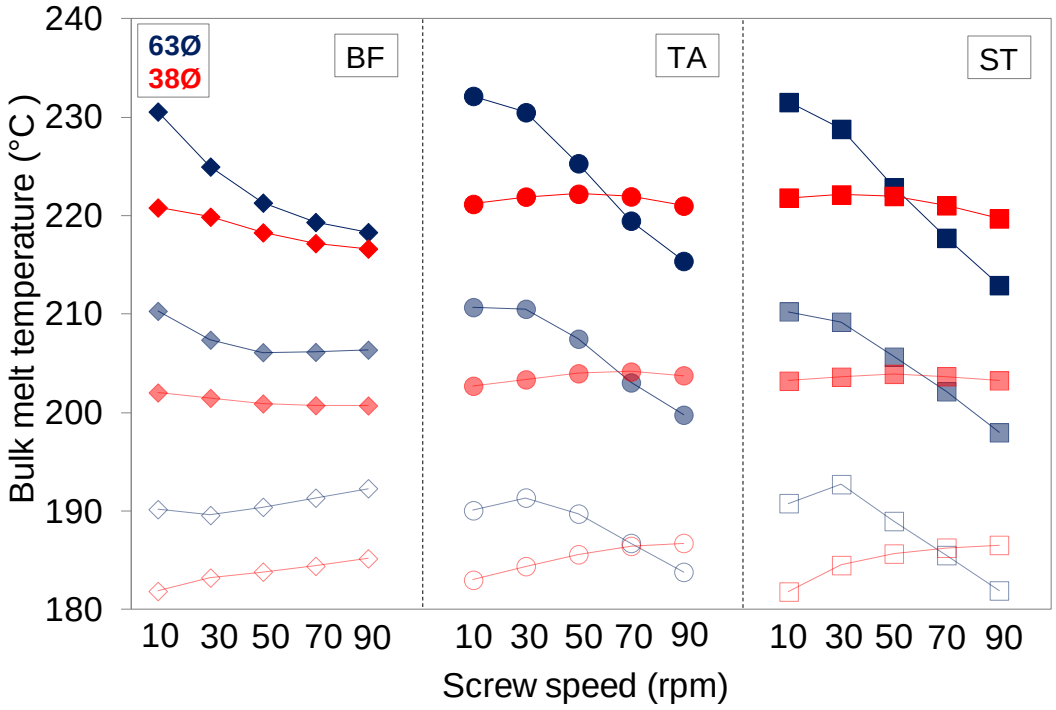

Figure 5.7 Effect of scale up on bulk melt temperature measurements vs screw speed for LDPE (dark colours represent 220°C, medium 200°C and light 180°C) and (BF: Barrier Flighted Screw; TA: Tapered Compression Screw; ST: Stepped Compression Screw)

The improved thermal homogeneity achieved with the 38 mm diameter extrusion process was clearly revealed in Figure 5.8. Despite the higher temperature variation measured at higher throughputs which was significantly dependent upon screw geometry, data indicated that the range of variation was less than 0.4°C at all conditions, almost negligible in comparison to those variations measured in the large extruder at identical conditions (Figure 5.9). This indicates that bulk temperatures were more consistent and less dependent upon screw geometry, as shown in Figure 5.7.

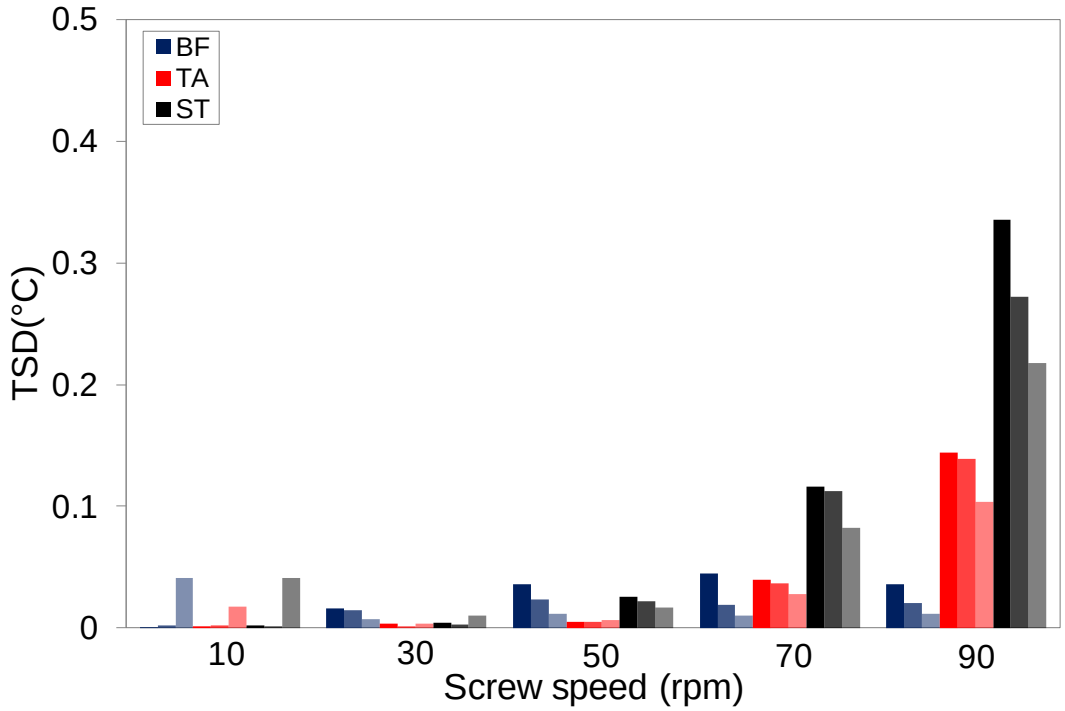

Figure 5.8 Variation of melt temperature vs screw speed for LDPE measured in 38 mm diameter single screw extruder (dark colours represent 220°C, medium 200°C and light 180°C), (BF: Barrier Flighted Screw; TA: Tapered Compression Screw; ST: Stepped Compression Screw) and (TSD: Variation of melt temperature over a period of 1 min calculated by taking an average of the standard variation at each individual position)

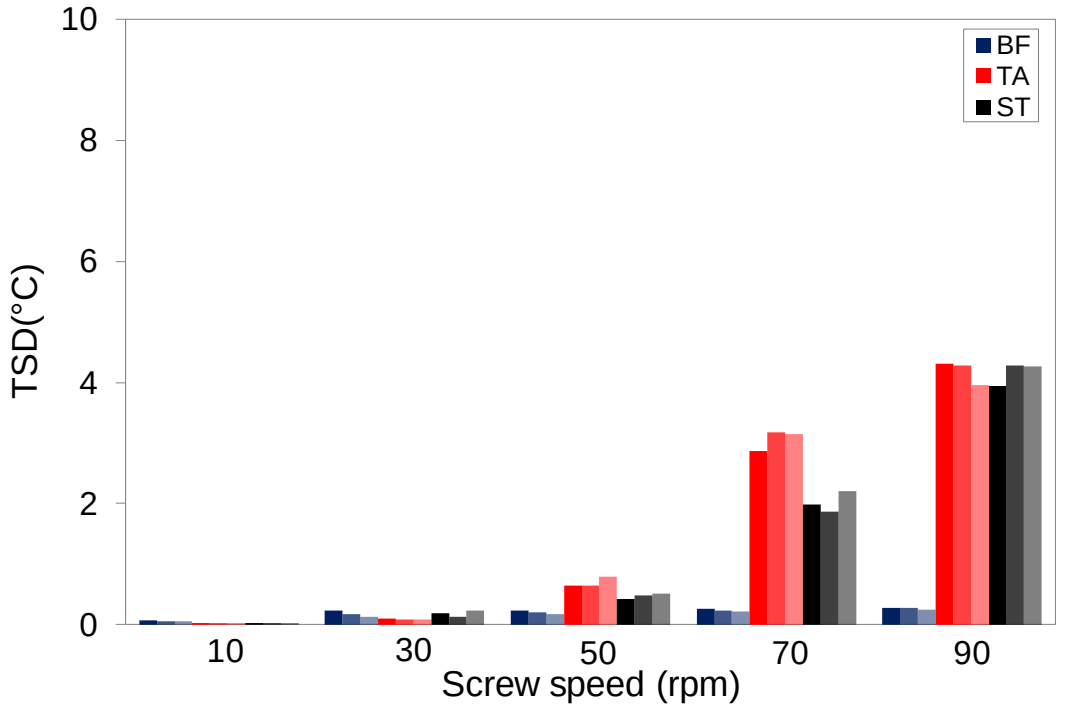

Figure 5.9 Variation of melt temperature vs screw speed for LDPE measured in 63 mm diameter single screw extruder (dark colours represent 220°C, medium 200°C and light 180°C), (BF: Barrier Flighted Screw; TA: Tapered Compression Screw; ST: Stepped Compression Screw) and (TSD: Variation of melt temperature over a period of 1 min calculated by taking an average of the standard variation at each individual position)

Die pressure data for LDPE is displayed in Figure 5.10. In general, pressure measurements were found to increase following a linear dependence across the range of screw speeds. In addition, die pressure increased with decreasing set temperature due to the dependence of melt viscosity on temperature and remained higher for the barrier flighted screw. Differences of pressure between the barrier and the two single flighted screws were found to be of similar magnitude in both extrusion processes (Figure 5.10 and Figure 5.11). However, as discussed above, the difference in throughput was larger in the 38mm extrusion process (Figure 5.1 and Figure 5.2), which reflects the better thermal homogeneity of this process (Figure 5.8) leading to a higher processing capability of the barrier flighted screw.

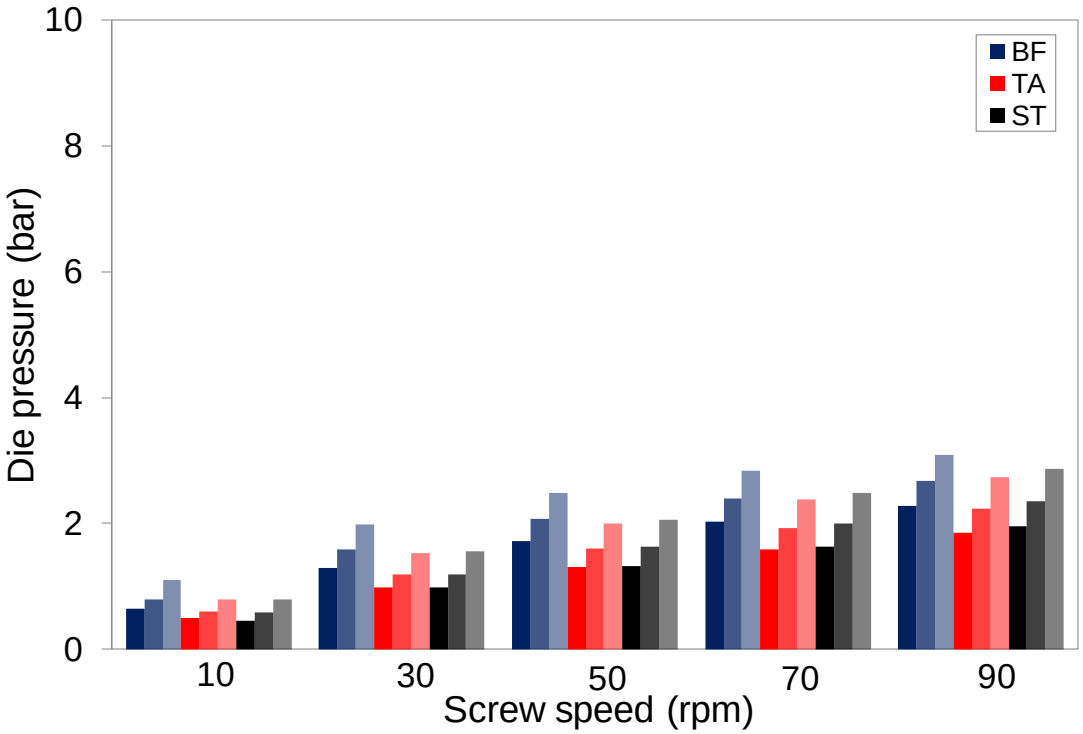

Figure 5.10 Die melt pressure vs screw speed for LDPE measured in 38 mm diameter single screw extruder (dark colours represent 220°C, medium 200°C and light 180°C) and (BF: Barrier Flighted Screw; TA: Tapered Compression Screw; ST: Stepped Compression Screw)

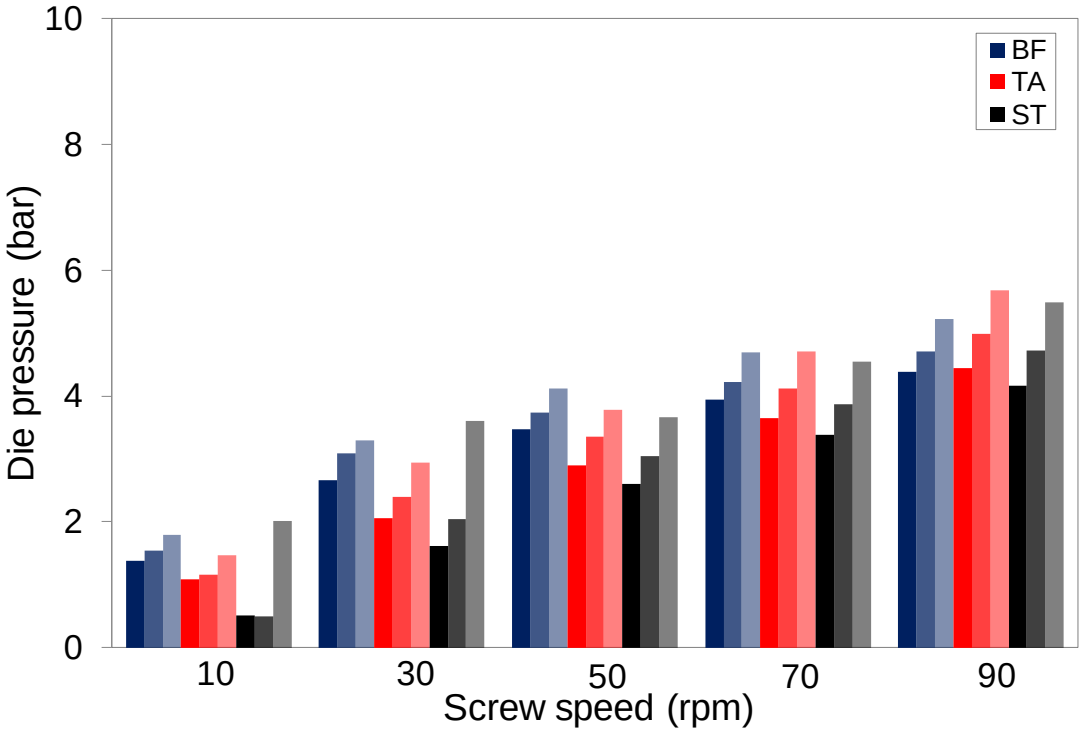

Figure 5.11 Die melt pressure vs screw speed for LDPE measured in 63 mm diameter single screw extruder (dark colours represent 220°C, medium 200°C and light 180°C) and (BF: Barrier Flighted Screw; TA: Tapered Compression Screw; ST: Stepped Compression Screw)

Measured specific energy consumption for LDPE using both single screw extruders at the same set conditions and screw geometry is displayed in Figure 5.12. Clearly, similar trends of energy consumption were observed for both machines which were shifted depending upon the size of the extruder. The demand of energy consumption for the 38 mm diameter extrusion process was much higher over the full range of screw speeds, especially at 10 rpm. The greatest difference in energy consumption measured between the barrier and the two single flighted screws was observed at 10rpm. For example, the demand of energy for the barrier flighted screw ranged from 3050 to 3500 J/g compared to 4300-5050 J/g for the stepped compression screw and 4500-5150 J/g for the tapered compression screw. At higher throughputs specific energy consumption for both single flighted screws tended to be similar and slightly higher than that measured for the barrier screw.

The energy required from the motor for LDPE in both extrusion processes is shown in Figure 5.13 to reflect that the relationship between specific energy consumption and screw speed was different in both processes. In the 38 mm diameter single screw extruder the measured specific energy consumption initially decreased with increasing screw speed but then increased or remained constant above a critical screw speed, typically 30 or 50 rpm. The highest energy consumption was observed at the lowest screw rotation speed of 10 rpm. Above 10 rpm the demand of energy required from the motor in the small machine tended to be similar to that measured in the large extruder although this remained slightly higher for both single flighted screws.

The energy contribution from the heaters/cooling fans to both extrusion processes for LDPE is displayed in Figure 5.14. Similar trends to those measured for the total energy consumption were observed (Figure 5.12), which were also strongly shifted depending upon extruder size. Overall, the specific energy required from the heaters/cooling fans in the small extruder was found to be higher than that measured in the large extruder. For the barrier flighted screw the effect of set temperature had less effect on energy measurements which could explain the similar values of total energy consumption observed in Figure 5.12. In general, energy values for both extrusion processes decreased gradually with decreasing set temperature irrespective of screw geometry over the full range of screw speeds.

The highest energy consumption for the heaters/cooling fans was measured at 10 rpm for the three extruder screw geometries which in conjunction with the major contributions from the motor also measured at this particular screw speed (Figure 5.13), could explain the large difference in total energy consumption measured between both extrusion processes, as shown in Figure 5.12.

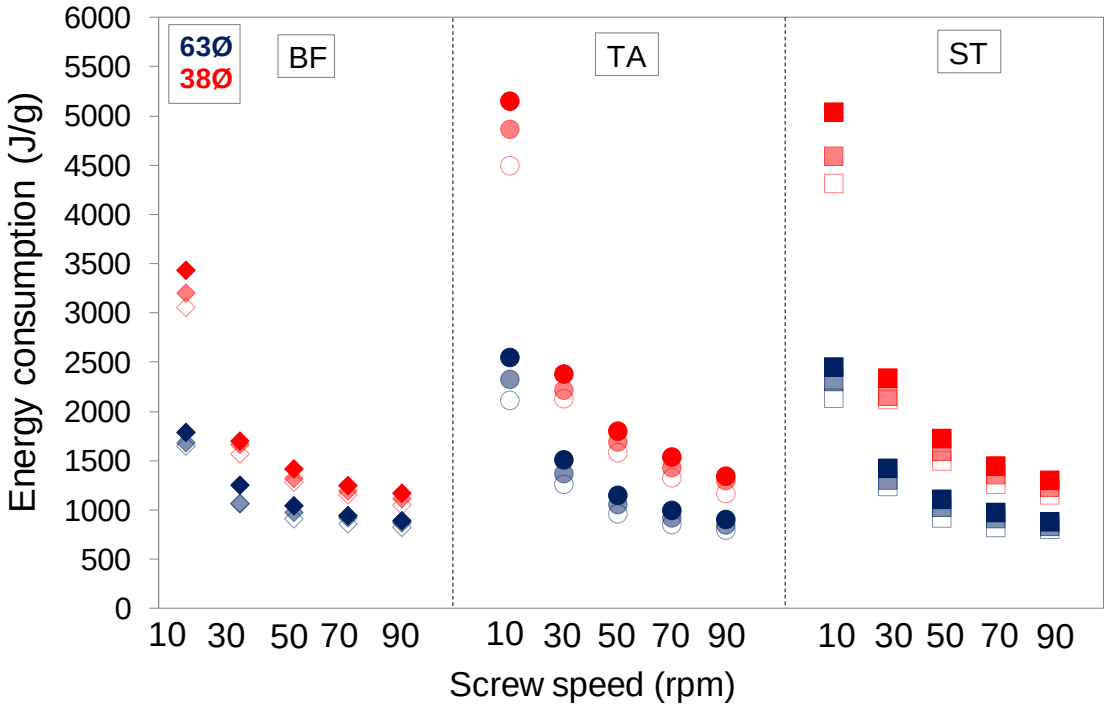

Figure 5.12 Effect of scale up on total specific energy consumption vs screw speed for LDPE (dark colours represent 220°C, medium 200°C and light 180°C) and (BF: Barrier Flighted Screw; TA: Tapered Compression Screw; ST: Stepped Compression Screw)

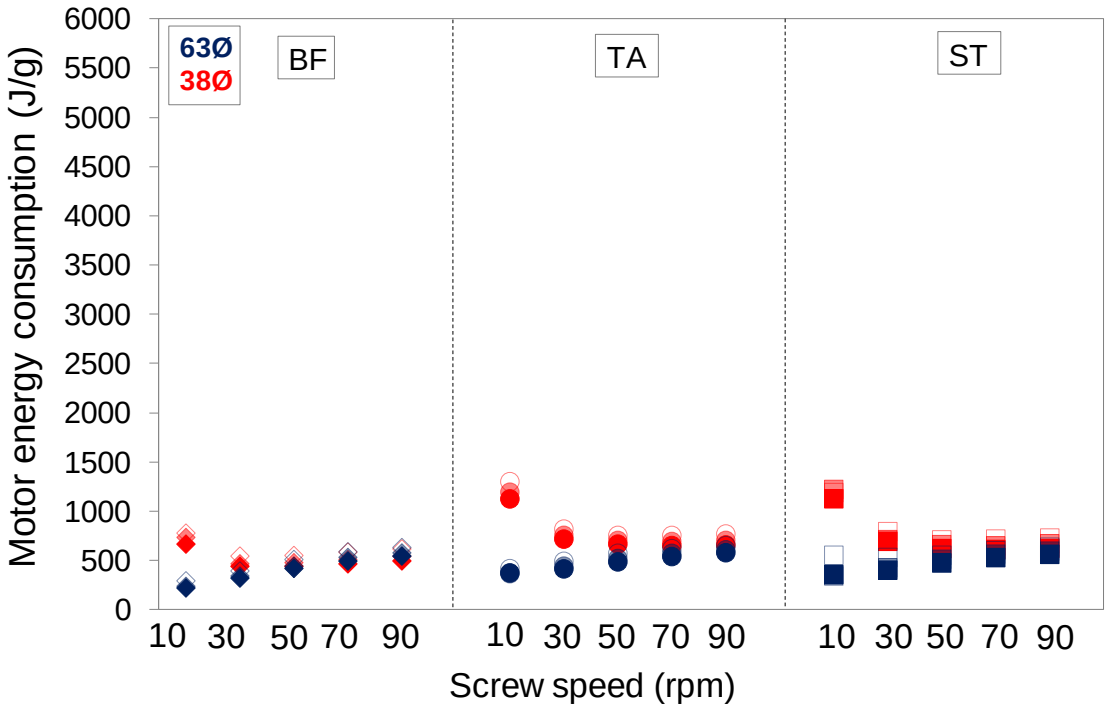

Figure 5.13 Effect of scale up on specific energy consumption for motor vs screw speed and LDPE (dark colours represent 220°C, medium 200°C and light 180°C) and (BF: Barrier Flighted Screw; TA: Tapered Compression Screw; ST: Stepped Compression Screw)

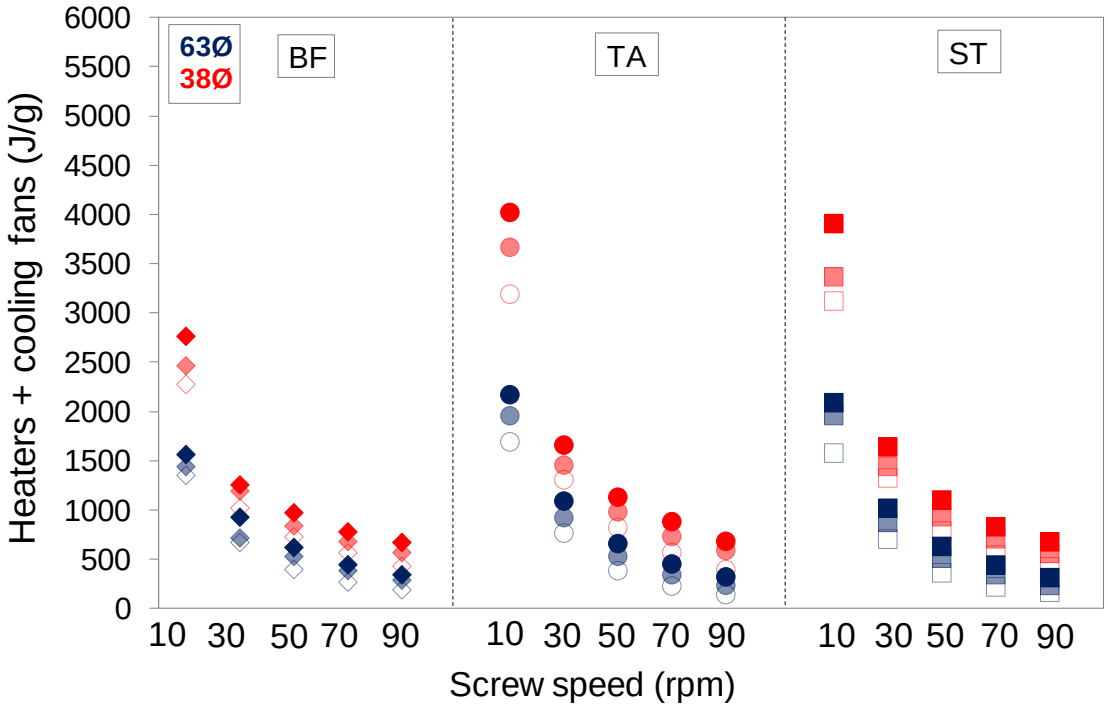

Figure 5.14 Effect of scale up on specific energy consumption for heaters/cooling fans vs screw speed and LDPE (dark colours represent 220°C, medium 200°C and light 180°C) and (BF: Barrier Flighted Screw; TA: Tapered Compression Screw; ST: Stepped Compression Screw)

5.3 HDPE

The performance of each of the three extruder screws in terms of throughput for HDPE (HD5050) is compared in Figure 5.15 at each set temperature and screw rotation speed. It was also found that set temperature appeared to have a major effect on throughput for the barrier flighted screw compared to those measured in the large extruder (Figure 5.16). As discussed earlier in section 4.3.4, this screw geometry provided higher throughputs at the highest set temperature as a result of both a greater free volume and a lower viscosity of the polymer at this temperature.

In addition, it was shown that the lower set temperature profile of 180°C inhibited the throughput measurements, especially at higher screw speeds where achieving melting is more challenging (Figure 5.15). For both single flighted screws throughput measurements in the small extruder were more affected by screw geometry and set temperature, as shown in Figure 5.15.

Throughputs were also found to be lower for HD5050 than LDPE at identical extrusion conditions (Figure 5.1), highlighting the higher shear thinning behaviour exhibited by the latter (section 4.1, Table 4.1).

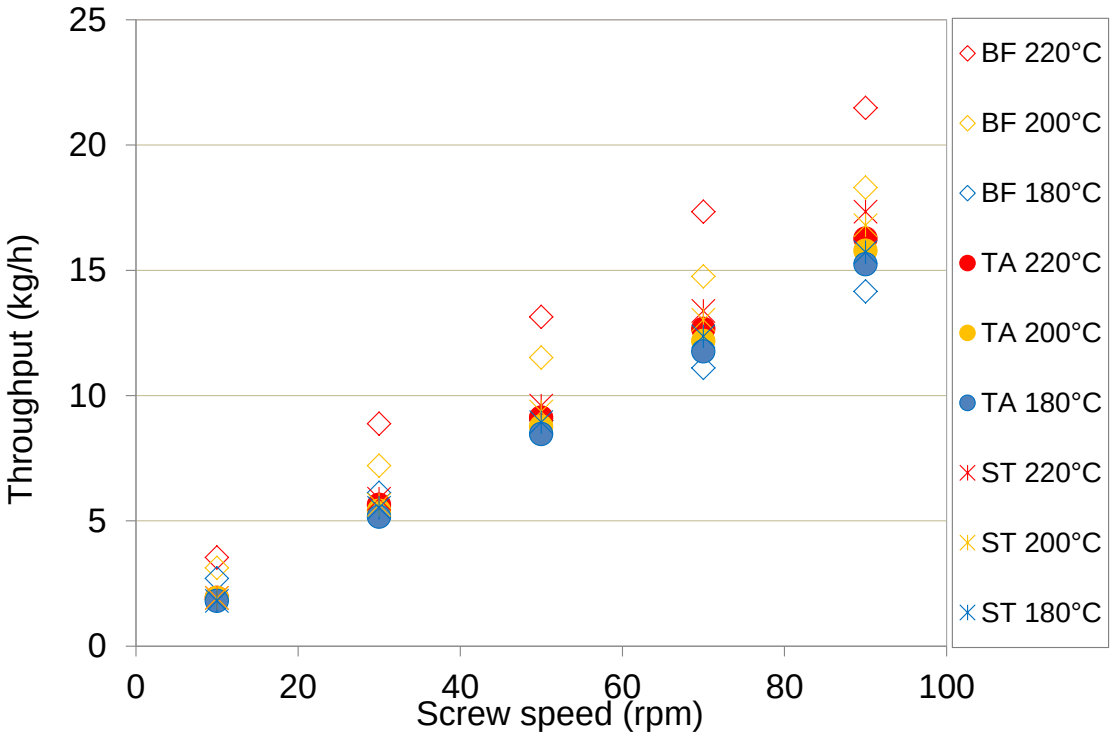

Figure 5.15 Extruder throughput vs screw speed for HD5050 measured in 38 mm diameter single screw extruder (BF: Barrier Flighted Screw; TA: Tapered Compression Screw; ST: Stepped Compression Screw)

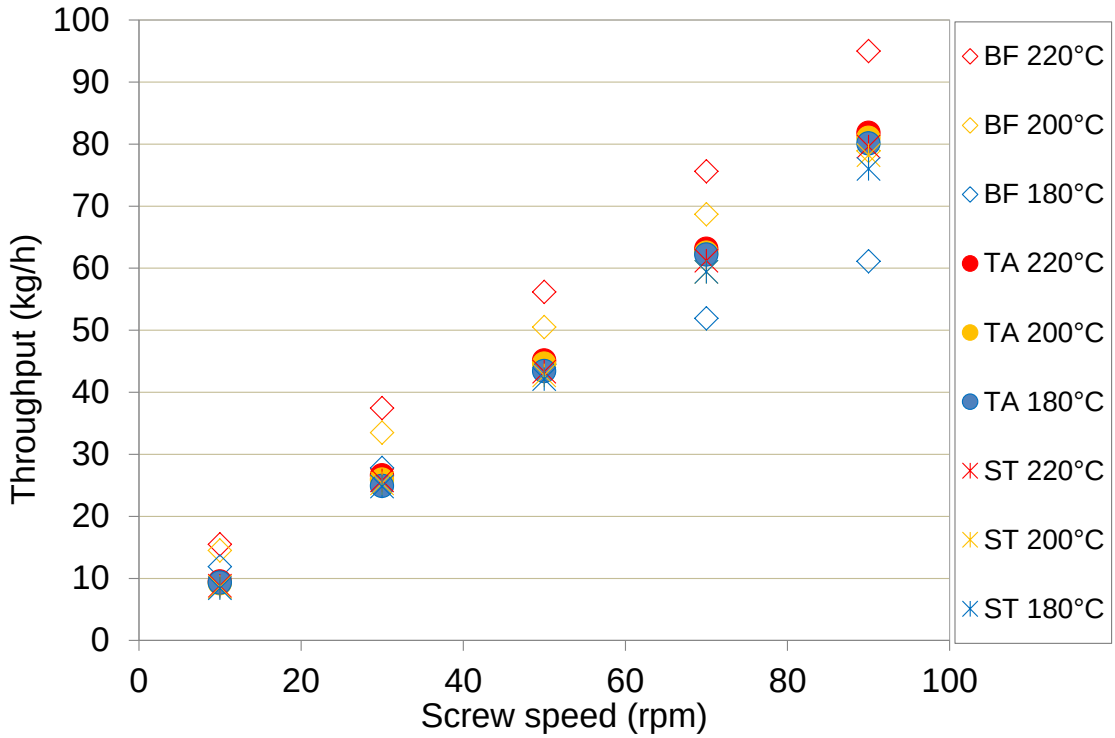

Figure 5.16 Extruder throughput vs screw speed for HD5050 measured in 63 mm diameter single screw extruder (BF: Barrier Flighted Screw; TA: Tapered Compression Screw; ST: Stepped Compression Screw)

Figure 5.17 shows radial melt temperature profiles measured in the 38mm diameter extrusion process for HD5050 at 200°C. Results highlighted that melt temperatures were relatively unaffected by screw geometry and these increased with increasing screw speed, reaching maximum values in the centre of the flow. Clearly, both single flighted screws did not exhibit dips in melt temperature close to the die walls as those measured in (Figure 5.18). In addition, melt temperatures for HD5050 were found to be more consistent across the total flow volume compared to those measured with LDPE (Figure 5.8) and thought to result from its lower sensitivity to shear (section 4.1,Table 4.1).

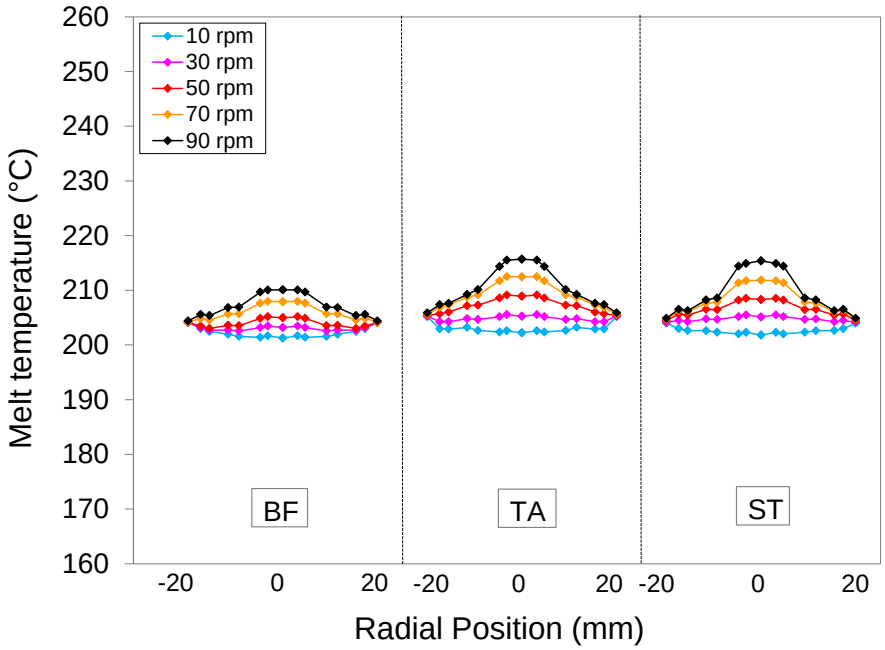

Figure 5.17 Effect of screw geometry on radial melt temperatures measured for HD5050 at 200°C using 38 mm diameter single screw extruder (BF: Barrier Flighted Screw; TA: Tapered Compression Screw; ST: Stepped Compression Screw)

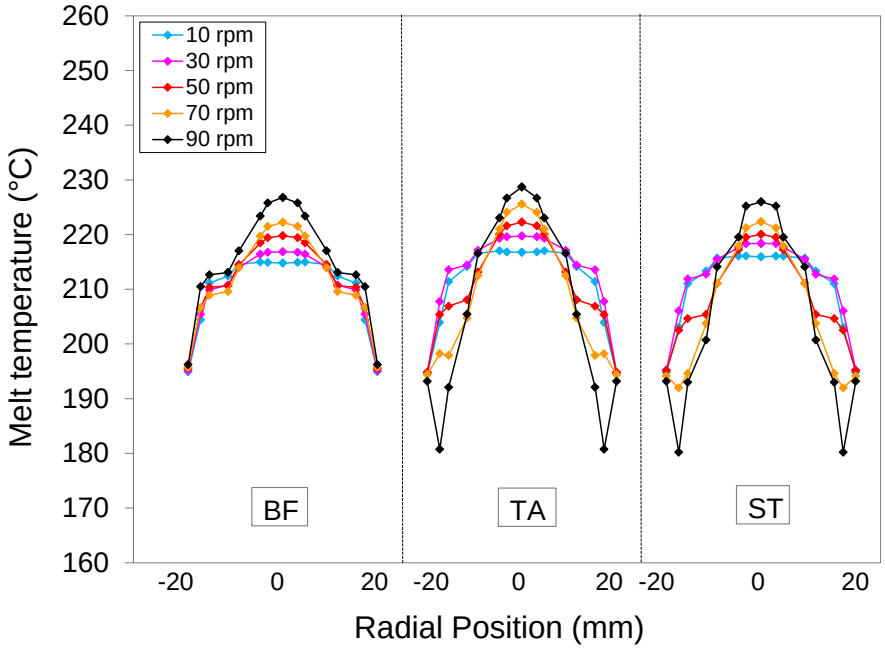

Figure 5.18 Effect of screw geometry on radial melt temperatures measured for HD5050 at 200°C using 63 mm diameter single screw extruder (BF: Barrier Flighted Screw; TA: Tapered Compression Screw; ST: Stepped Compression Screw)

The lower sensitivity to shear exhibited for HD5050 was reflected in Figure 5.19 at 180 °C. Melt temperature profiles were higher across the flow volume than LDPE at identical conditions (Figure 5.5) due to increased viscous dissipation via shearing. Here, the effect of screw geometry at 220°C had a major effect on temperature measurements (Figure 5.19). Radial melt temperature profiles for the barrier flighted screw were less sensitive to screw speed than the two single flighted screws, showing lower peaks of temperature in the centre of the flow.

Moreover, at 220 and 180°C single flighted screws (Figure 5.19) did not exhibit the pronounced areas of low temperature measured towards the die walls using the 63 mm diameter single screw extruder (Figure 5.20).

.

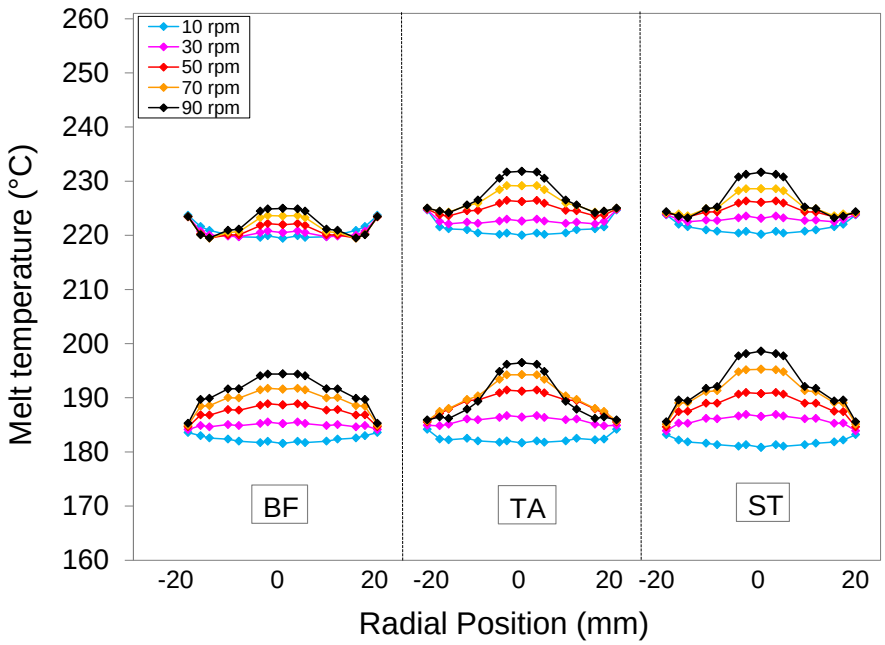

Figure 5.19 Effect of set temperature and screw geometry on radial melt temperatures measured for HD5050 using 38 mm diameter single screw extruder (BF: Barrier Flighted Screw; TA: Tapered Compression Screw; ST: Stepped Compression Screw)

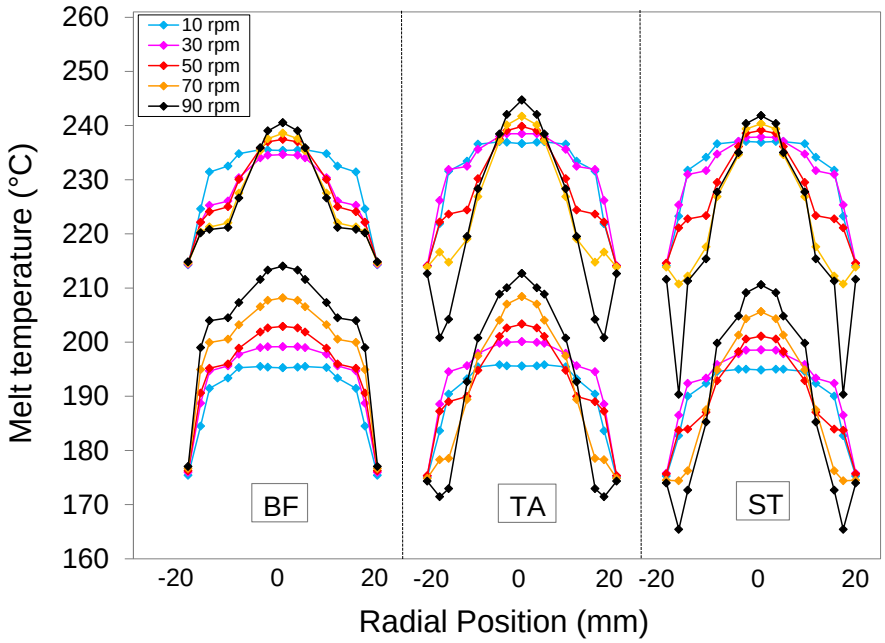

Figure 5.20 Effect of set temperature and screw geometry on radial melt temperatures measured for HD5050 using 63 mm diameter single screw extruder (BF: Barrier Flighted Screw; TA: Tapered Compression Screw; ST: Stepped Compression Screw)

The improved melting performance (consistency) achieved with the 38mm diameter extrusion process and its effect on melt temperature measurements for HD5050 is shown in Figure 5.21. At all conditions, bulk temperatures tended to increase with increasing screw speed, especially at the lowest set temperature of 180°C, highlighting the higher levels of viscous shear generated during extrusion of HD5050 compared to LDPE (Figure 5.7). Here, the enhanced performance achieved with both single flighted screws in the small extruder is clear, as they do not show a critical screw speed at which the melting mechanism began to break down deteriorating the quality of the melt. On the contrary, melt temperatures continued to rise with increasing screw speed, exhibiting similar trends to those measured with the barrier flighted screw. These results suggest that melting performance was less dependent upon screw geometry, as shown in Figure 5.21 at each set temperature.

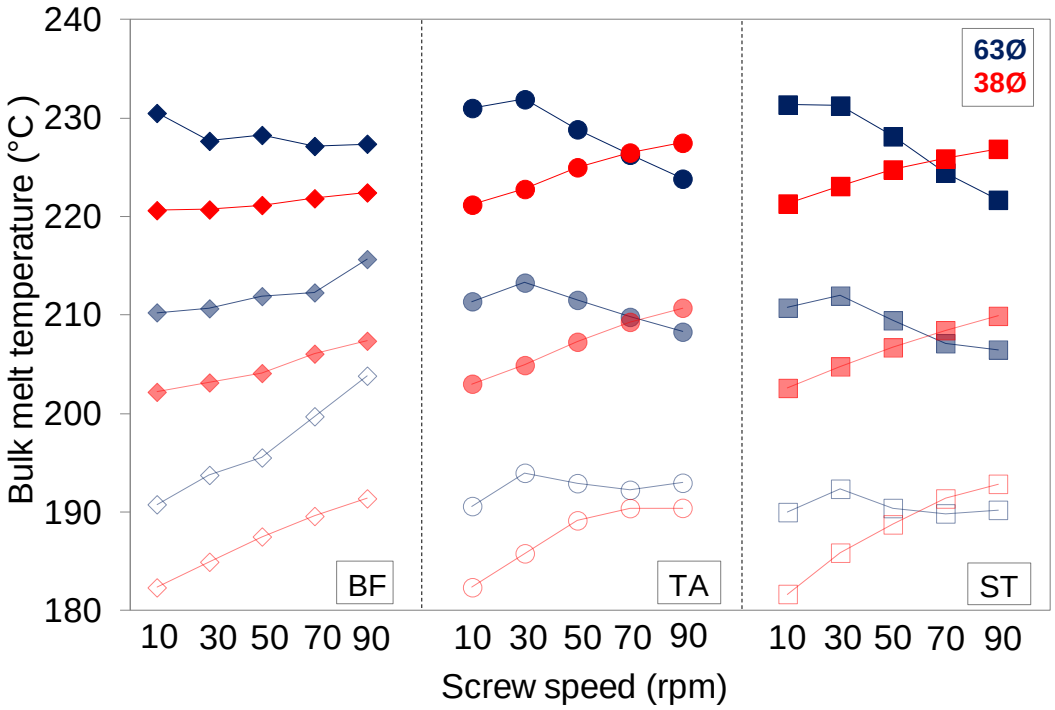

Figure 5.21 Effect of scale up on bulk melt temperature measurements vs screw speed for HD5050 (dark colours represent 220°C, medium 200°C and light 180°C) and (BF: Barrier Flighted Screw; TA: Tapered Compression Screw; ST: Stepped Compression Screw)

The improved temperature homogeneity across the melt channel for HD5050 using the small extruder is shown in Figure 5.22. Clearly, levels of temperature fluctuation were practically negligible compared to those measured in the large extruder (Figure 5.23). However, this variation of temperature was found to be similar to that for LDPE at identical conditions (Figure 5.8), which was less than 0.4°C at all conditions. This could be used to explain the pressure measurements observed in Figure 5.24.

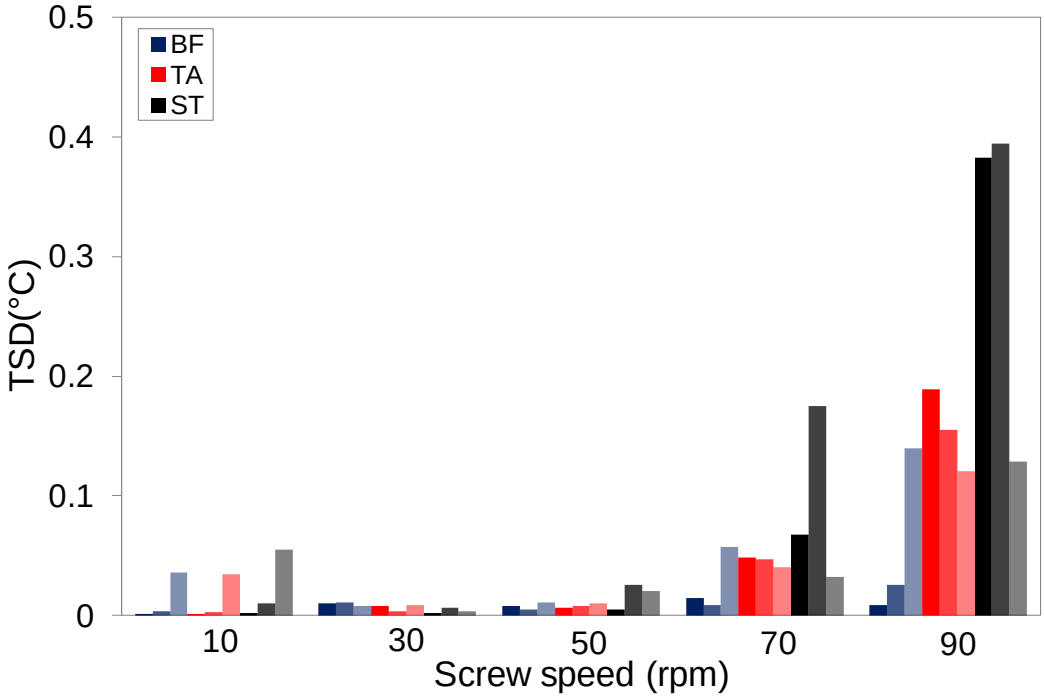

Figure 5.22 Variation of melt temperature vs screw speed for HD5050 measured in 38 mm diameter single screw extruder (dark colours represent 220°C, medium 200°C and light 180°C), (BF: Barrier Flighted Screw; TA: Tapered Compression Screw; ST: Stepped Compression Screw) and (TSD: Variation of melt temperature over a period of 1 min calculated by taking an average of the standard variation at each individual position)

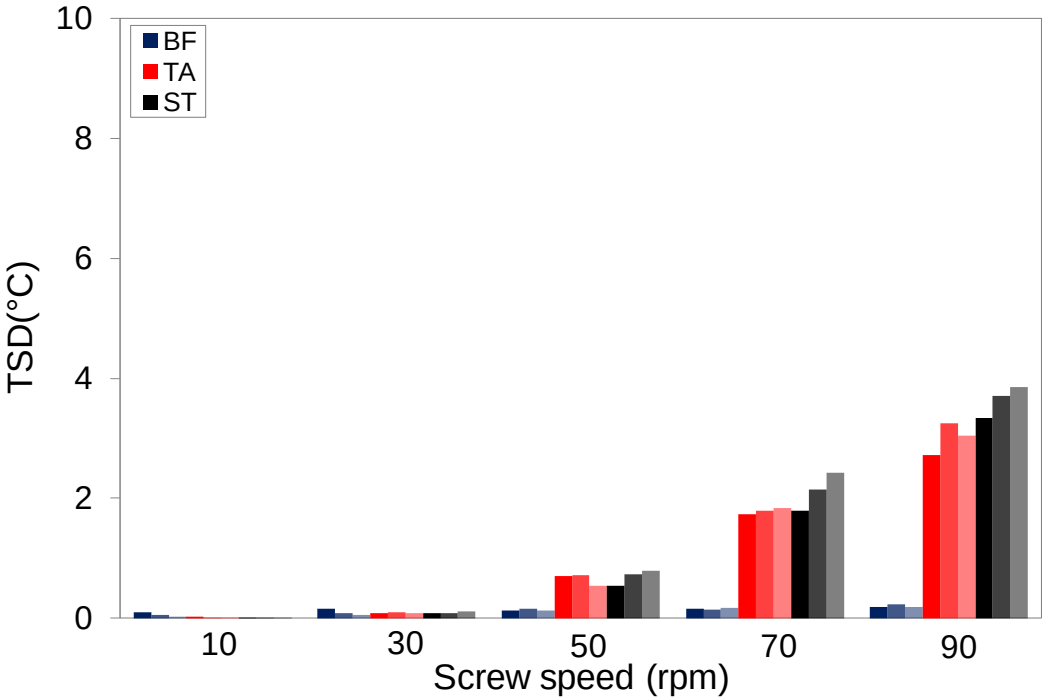

Figure 5.23 Variation of melt temperature vs screw speed for HD5050EA measured in 63 mm diameter single screw extruder (dark colours represent 220°C, medium 200°C and light 180°C), (BF: Barrier Flighted Screw; TA: Tapered Compression Screw; ST: Stepped Compression Screw) and (TSD: Variation of melt temperature over a period of 1 min calculated by taking an average of the standard variation at each individual position)

Measured die melt pressure for HD5050 is displayed in (Figure 5.24). In general, die pressures were found to increase with extruder screw speed and due to the fact that polymer melt viscosity decreased with decreasing set temperature (see section 4.1, Figure 4.2) these were higher at lower set temperatures. In contrast to pressure measurements in the large scale extruder (Figure 5.25), die pressures for the barrier flighted screw increased with decreasing set temperature and were similar to those measured with the two single flighted screws at higher screw speeds (70 and 90 rpm). This explains why throughput measurements at 180°C in the small extruder were less dependent upon extruder screw geometry, as shown in Figure 5.16.

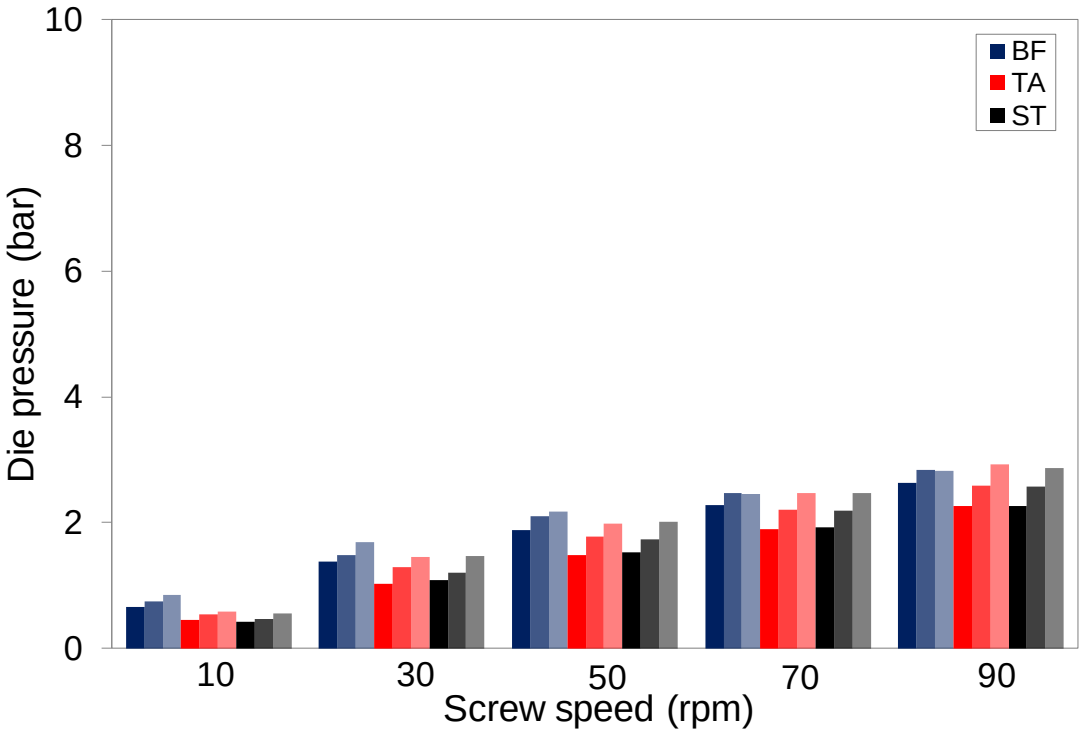

Figure 5.24 Die melt pressure vs screw speed for HD5050 measured in 38 mm diameter single screw extruder (dark colours represent 220°C, medium 200°C and light 180°C) and (BF: Barrier Flighted Screw; TA: Tapered Compression Screw; ST: Stepped Compression Screw)

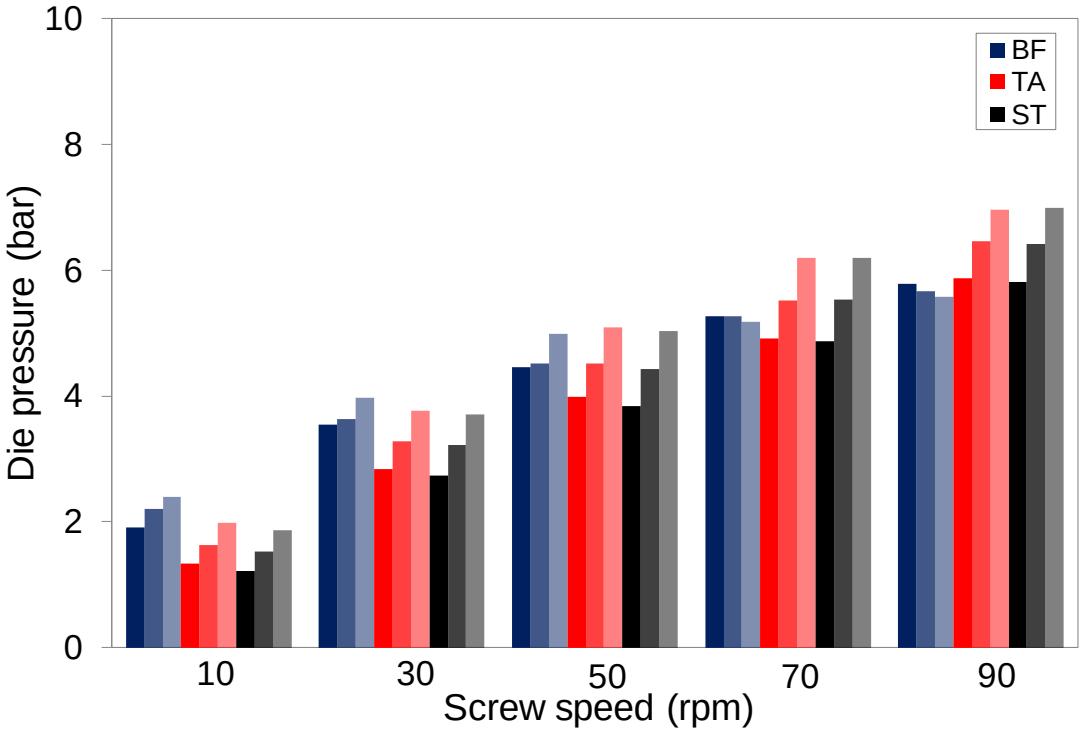

Figure 5.25 Die melt pressure vs screw speed for HD5050 measured in 63 mm diameter single screw extruder (dark colours represent 220°C, medium 200°C and light 180°C) and (BF: Barrier Flighted Screw; TA: Tapered Compression Screw; ST: Stepped Compression Screw)

A comparison of specific energy consumption for each single screw extruder using HD5050 is shown in Figure 5.26 to highlight the effect of scale up on energy measurements. As argued with LDPE in Figure 5.12, the demand of energy consumption for the 38 mm diameter extrusion process was much higher at all conditions and the relationship between energy consumption and screw speed exhibited similar trends for both machines. Clearly, at 10 rpm the major differences in energy consumption were measured between extrusion processes and the barrier flighted screw and the two non-barrier screws.

Above 10 rpm, specific energy consumption was found to be less affected by screw geometry and set temperature, especially in the large extruder. In the 38 mm diameter extrusion process the specific energy required for both single flighted screws remained slightly higher than the barrier flighted screw over the full range of screw speeds.

The effect of melt viscosity on the process energy demand is noted when comparing Figure 5.12 and Figure 5.26. Energy consumption measured in the small extruder for HD5050 was higher than LDPE at all conditions. This reflects the higher motor energy consumption measured for HD5050 as compared to LDPE (see Figure 5.13 and Figure 5.27).

From Figure 5.27 it was also observed that for HD5050 the relationship between motor energy consumption and screw speed was similar to LDPE (Figure 5.13), initially decreasing with increasing screw speed but then slightly increasing or remaining constant above a critical screw speed, typically 30 or 50 rpm. Here, motor energy values for HD5050 were not compared directly to corresponding measurements from the large extruder since motor energy consumption was not recorded in the 63 mm diameter extrusion process. Similarly, a comparison of energy consumption from the heaters/cooling fans for HD5050 between both extrusion processes is not shown in Figure 5.28. However, compared to LDPE as shown in Figure 5.14, data revealed that the effect of set temperature also had less effect on energy measurements for the barrier flighted screw and the greatest effects of screw geometry and set temperature on the energy consumption were measured at the lowest screw speed of 10 rpm, as shown in Figure 5.28.

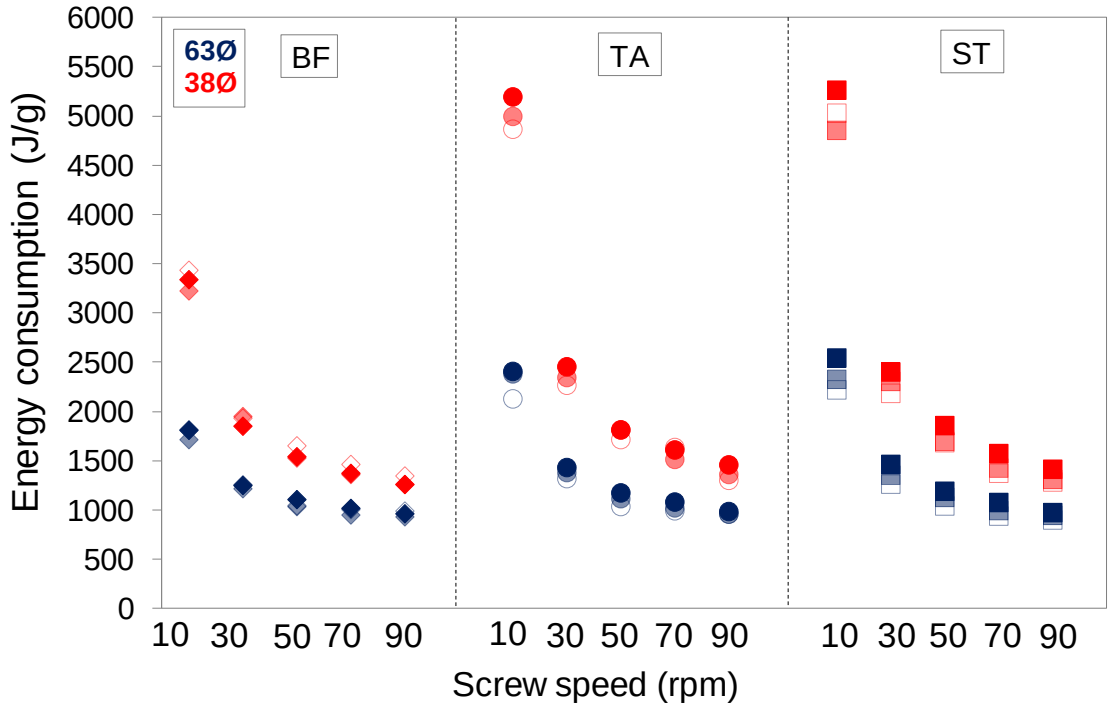

Figure 5.26 Effect of scale up on total specific energy consumption vs screw speed for HD5050 (dark colours represent 220°C, medium 200°C and light 180°C) and (BF: Barrier Flighted Screw; TA: Tapered Compression Screw; ST: Stepped Compression Screw)

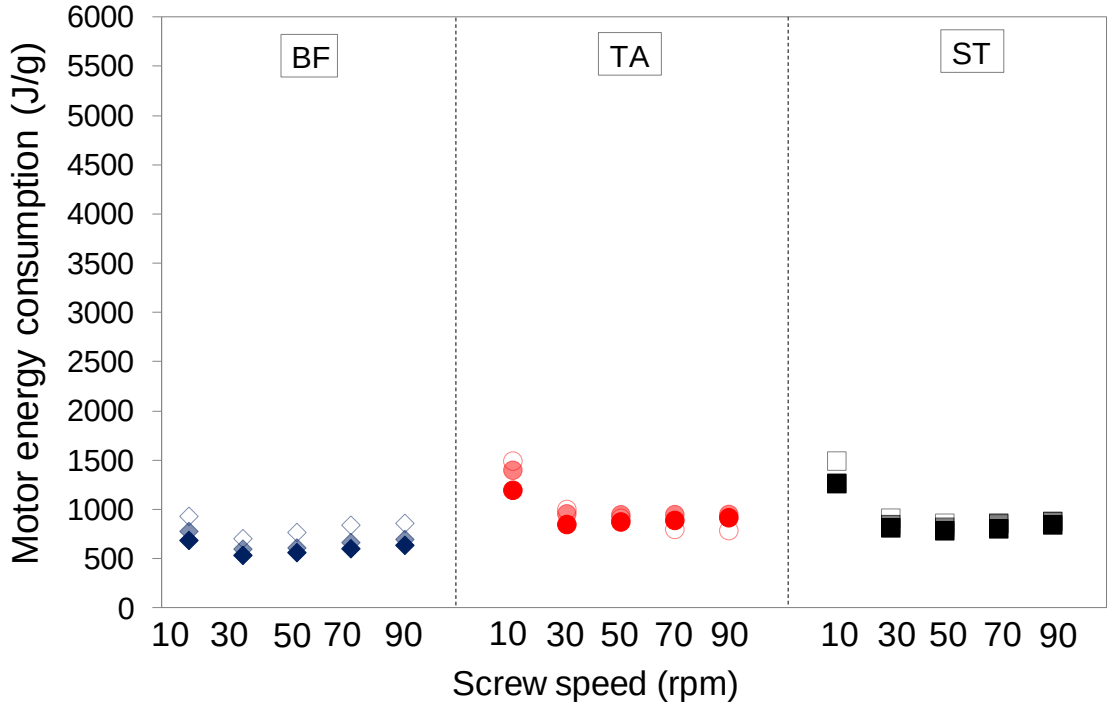

Figure 5.27 Specific energy consumption for motor vs screw speed measured on the small extruder for HD5050 (dark colours represent 220°C, medium 200°C and light 180°C) and (BF: Barrier Flighted Screw; TA: Tapered Compression Screw; ST: Stepped Compression Screw)

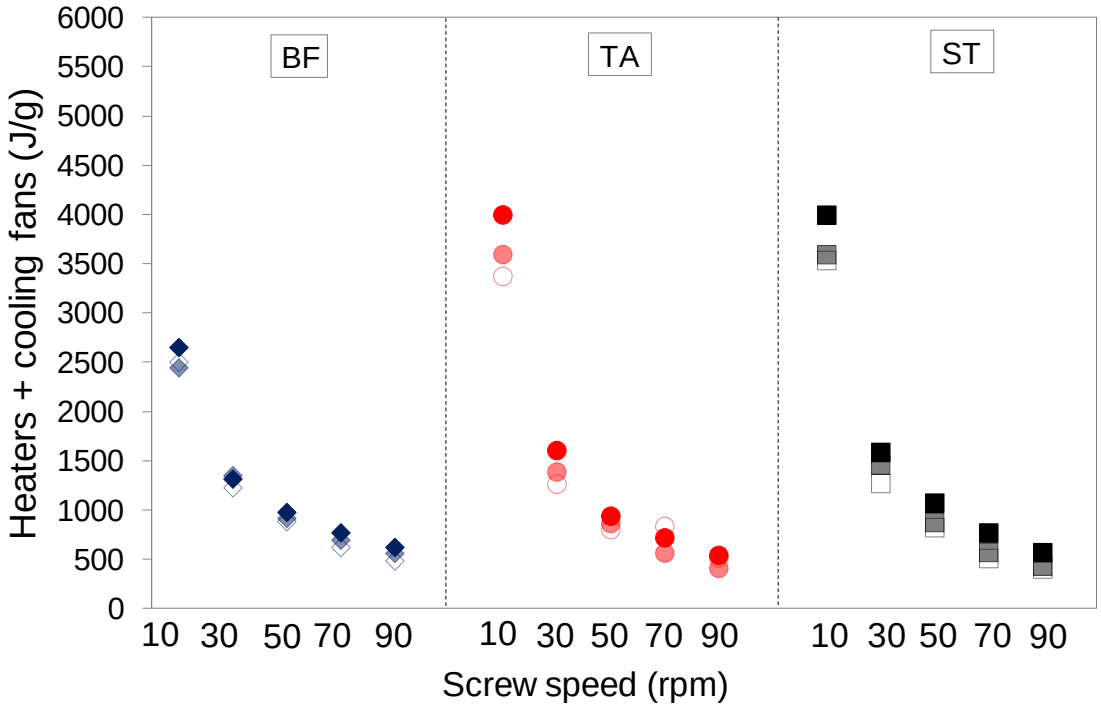

Figure 5.28 Specific energy consumption for heaters/cooling fans vs screw speed measured on the small extruder for HD5050 (dark colours represent 220°C, medium 200°C and light 180°C) and (BF: Barrier Flighted Screw; TA: Tapered Compression Screw; ST: Stepped Compression Screw)

5.4 Summary

In this chapter, results have shown that extrusion thermal dynamics measured on a small scale single screw extruder differed significantly to those measured on a large scale single screw extruder, providing quantification of the effect of extruder scale on thermal measurements. Melt temperature homogeneity was found to be less dependent upon selection of set processing conditions and extruder screw geometry and this was significantly better than that measured in the large scale single screw extruder. On the contrary, process energy consumption measured on the small scale extrusion process was found to be higher at all conditions.

CHAPTER SIX

6 INFRARED THERMOMETRY

6.1 Infrared measurements using a 63.5 mm diameter single screw extruder

The aim of this section is to assess the suitability of infra-red thermometry to quantify the thermal dynamics of single screw extrusion. The non-intrusive sensor was located in the barrel of the 63 mm diameter single screw extruder, positioned such that it provided a measurement of melt temperature in the channel of the metering section of the extruder screw. The rapid response of the technique enabled melt temperature within the extruder screw channel to be monitored in real time, allowing quantification of the thermal stability of the extrusion process. Here, measured data from the IR sensor is presented for LDPE and the medium viscosity grade HD6007 using three extruder screw geometries and set temperatures at a range of screw speeds. Therefore, the effects of extruder screw geometry, screw rotation speed, set temperature and polymer type on measured temperature were investigated.

In addition, IR results were compared to those obtained with a thermocouple grid sensor in the extruder die to evaluate the level of detailed information available using the non-invasive infrared technique and the related suitability for use in an industrial extruder.

Infrared measurements using a large scale single screw extruder

Melt temperature measurements made using the IR sensor located at the metering section of the 63 mm screw channel are shown in Figure 6.1-Figure 6.3, for HD6007 with the tapered compression screw at screw rotation speeds of 10, 50 and 90 rpm.

In each case, IR measurements were collected over a period of five screw rotations and are presented here to demonstrate the periodic nature of melt temperature at this location.

A disruption was seen to occur once per screw rotation due to the action of the extruder flight passing the tip of the IR sensor. This effect of the screw flight was observed in all measurements, manifested either as a periodic dip or peak in temperature. To aid visual interpretation, the data in Figure 6.1-Figure 6.3 have been highlighted to differentiate between regions of melt (screw channel) and screw flight. Figure 6.1 shows that at 10 rpm, measured temperatures across the width of the screw channel were periodic in nature and close to the set temperature of 200°C. Temperature was seen to decrease gradually by around 1°C during each screw rotation before dropping sharply due to the screw flight disruption.

The effect of screw speed on IR temperatures is shown in Figure 6.2 and Figure 6.3. Temperature measurements were less repeatable in nature and were less consistent as screw speed increased due to the melting instabilities which have been previously reported at the same extrusion conditions, as shown in section 4.3.4, Figure 4.29 and Figure 4.30. Melt temperature across the channel was found to vary significantly between screw rotations.

Variations in melt temperature of up to 12°C were observed between the screw flights for the tapered compression screw during the measurement period (Figure 6.3). At 50 and 90 rpm, screw flight disruptions were evidenced by a sharp peak in temperature, suggesting that the temperature of the melt was lower than the screw temperature at these conditions (Figure 6.2 and Figure 6.3).

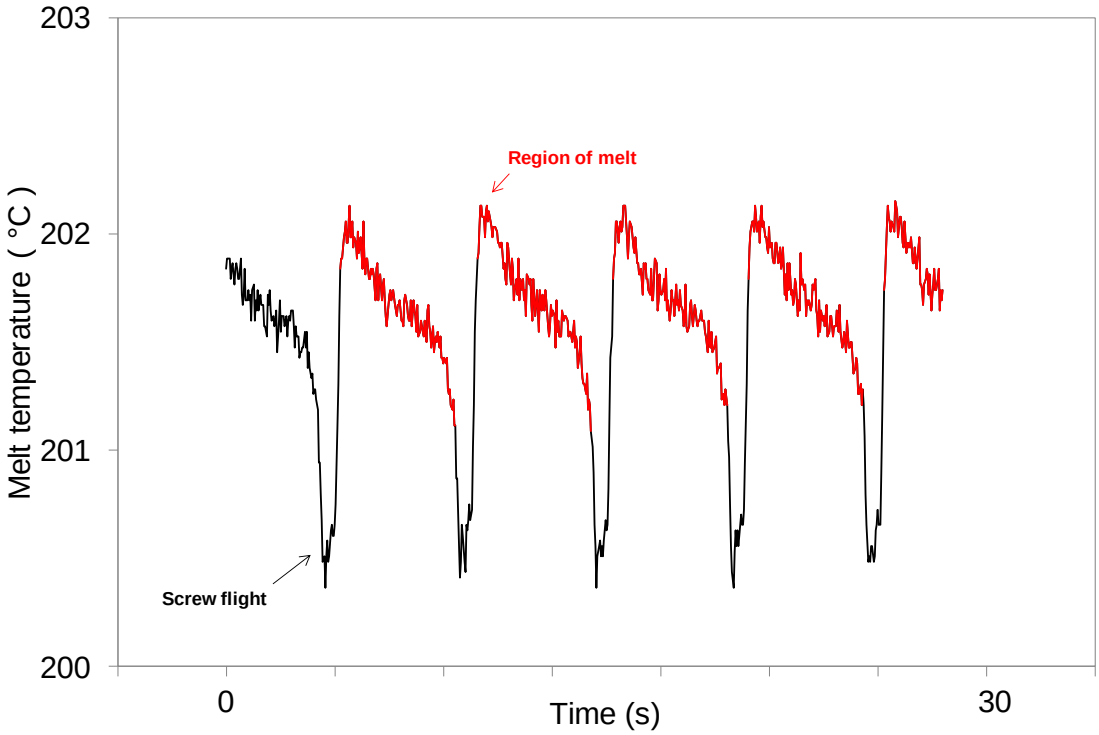

Figure 6.1 Measured infrared melt temperature for HD6007 in the channel of the metering section of the extruder screw; set die temperature 200°C and tapered compression screw at 10rpm, over a period of 30 seconds (red lines represent melt temperature and black lines screw flight)

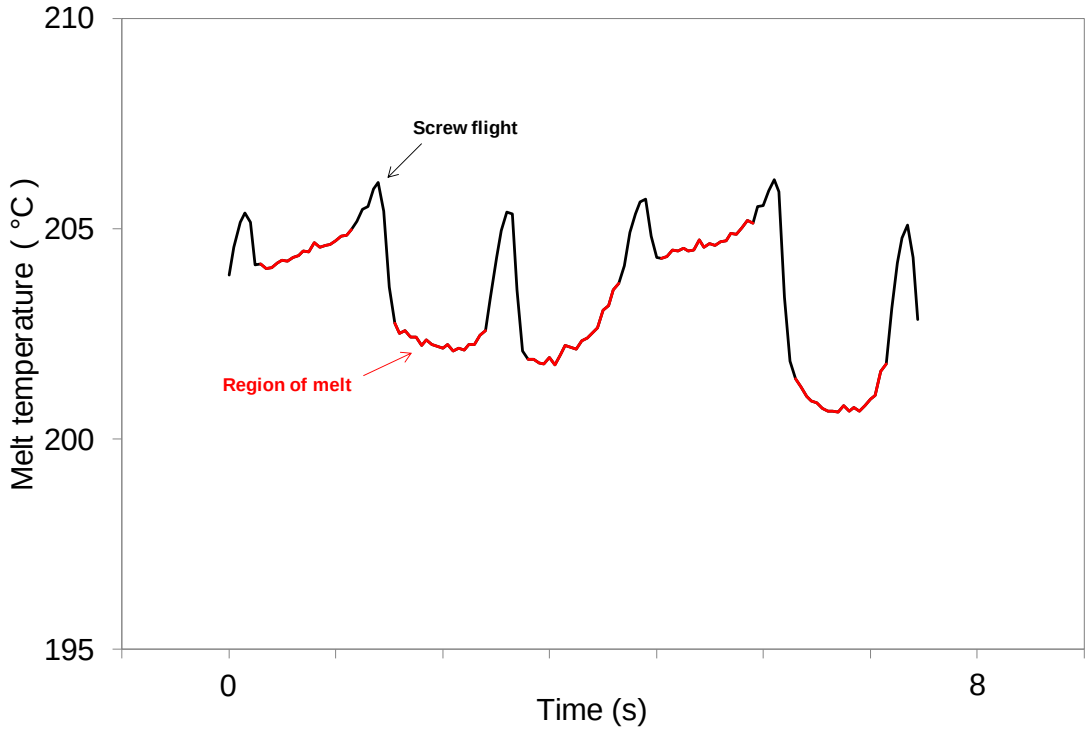

Figure 6.2 Measured infrared melt temperature for HD6007 in the channel of the metering section of the extruder screw; set die temperature 200°C and tapered compression screw at 50rpm, over a period of 30 seconds (red lines represent melt temperature and black lines screw flight)

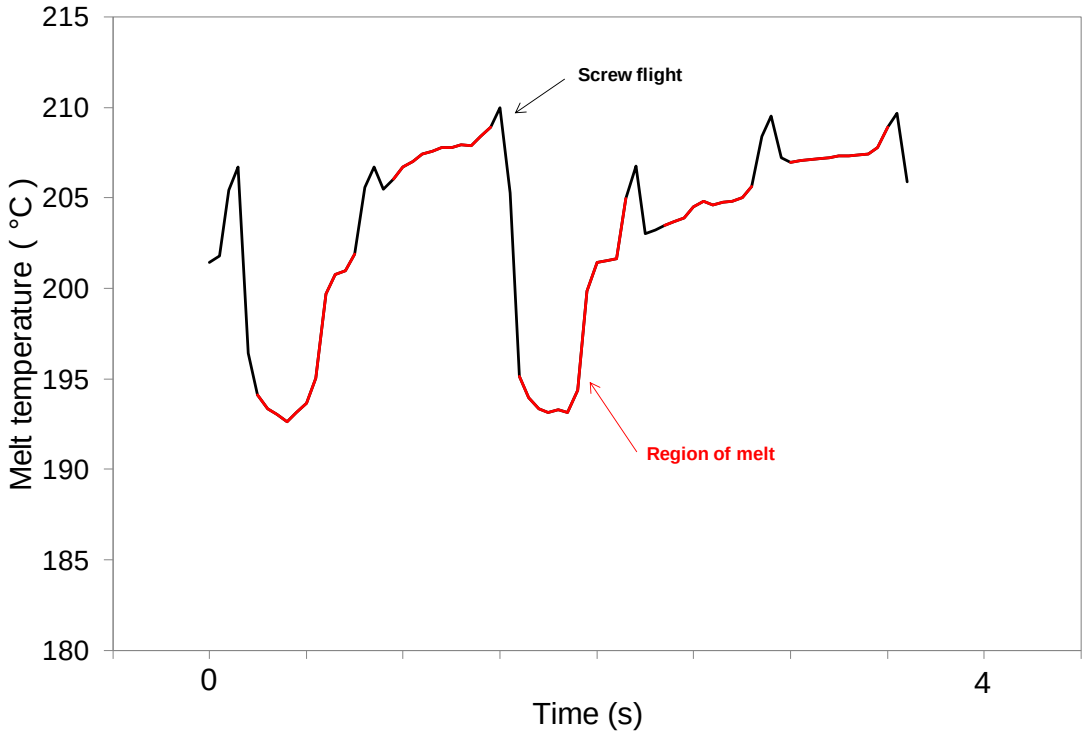

Figure 6.3 Measured infrared melt temperature for HD6007 in the channel of the metering section of the extruder screw; set die temperature 200°C and tapered compression screw at 90rpm, over a period of 30 seconds (red lines represent melt temperature and black lines screw flight)

These results show that the screw flight data has a significant influence on the temperature measured using infrared sensors in the screw channel. In order to examine melt temperature only, flight disruption data was removed using custom designed analysis software. This enabled a more representative assessment of melt temperature across the screw channel. The resulting temperature data were calculated by averaging a set of normalised transient temperature profiles over a measurement period of 30 seconds to generate representative temperature profiles across the width of the screw channel. These profiles are shown in Figure 6.4 and Figure 6.5 for both polymers to highlight the effect of screw speed and screw geometry on melt temperature. It was noted that for HD6007 with the barrier flighted screw, melt temperatures increased as screw rotation speed increased, from 200°C at 10 rpm to 208°C at 90 rpm, and that the profiles were flat in shape, suggesting that temperature was relatively constant across the width of the screw channel (Figure 6.4).

For single flighted screws, measured temperatures profiles initially increased with increasing screw speed but then decreased above a critical screw speed, typically 30 rpm. At higher screw speeds, profiles were less flat in shape, increasing gradually across the width of the screw channel. This inhomogeneity in melt within the screw channel is thought to result from the melt pool forming at the back of the channel, i.e. in front of the trailing flight, during melting. The inherent limitations of single flighted extruder screws can lead to the solid bed of polymer (behind the leading flight) to become fully melted only close to the die end of the extruder screw.

With LDPE (Figure 6.5) temperature decreased as extruder screw speed was increased, especially for the two single flighted screws. This reflects the lower shear viscosity of the LDPE compared to HD6007, and therefore a lower capacity for viscous shear heating. The effect of set temperature on IR temperature measurements is shown for LDPE in more detail in Figure 6.6, to reflect that more viscous energy dissipation via shearing was observed at the lowest set temperature profile of 180°C, as shown in section 4.3.2, Figure 4.5 and Figure 4.6 for LDPE at identical extrusion conditions with use of the thermocouple mesh.

These results demonstrate that the IR technique was sensitive to differences in melt temperature related to polymer type, screw geometry, set temperature and screw rotation speed. The lower shear viscosity of the LDPE used here (see section 4.1, Figure 4.1) is likely to result in less viscous shear heating compared to HD6007, leading to the lower observed melt temperatures at high screw speeds. High screw rotation speeds lead to a shorter residence time of the polymer inside the extruder barrel and therefore it is more difficult to transfer sufficient heat into the polymer to achieve a homogeneous melt.

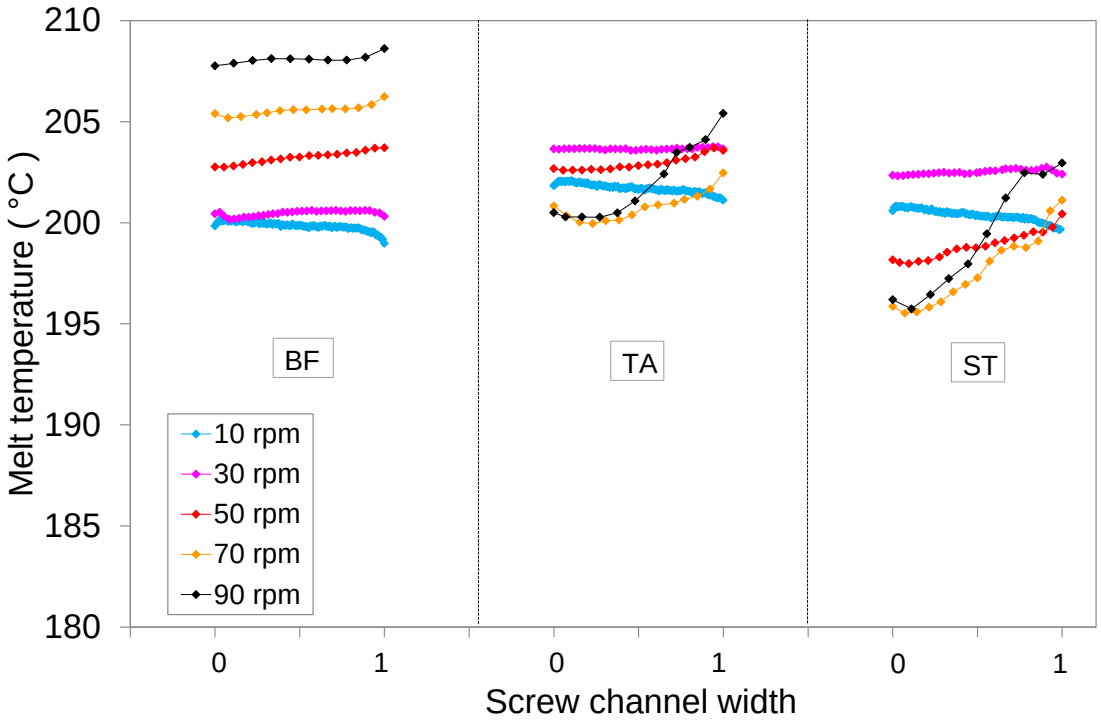

Figure 6.4 Average melt temperature profiles across the width of the screw channel for HD6007 at the end of the metering zone; set die temperature 200°C, measured over a 30 second period

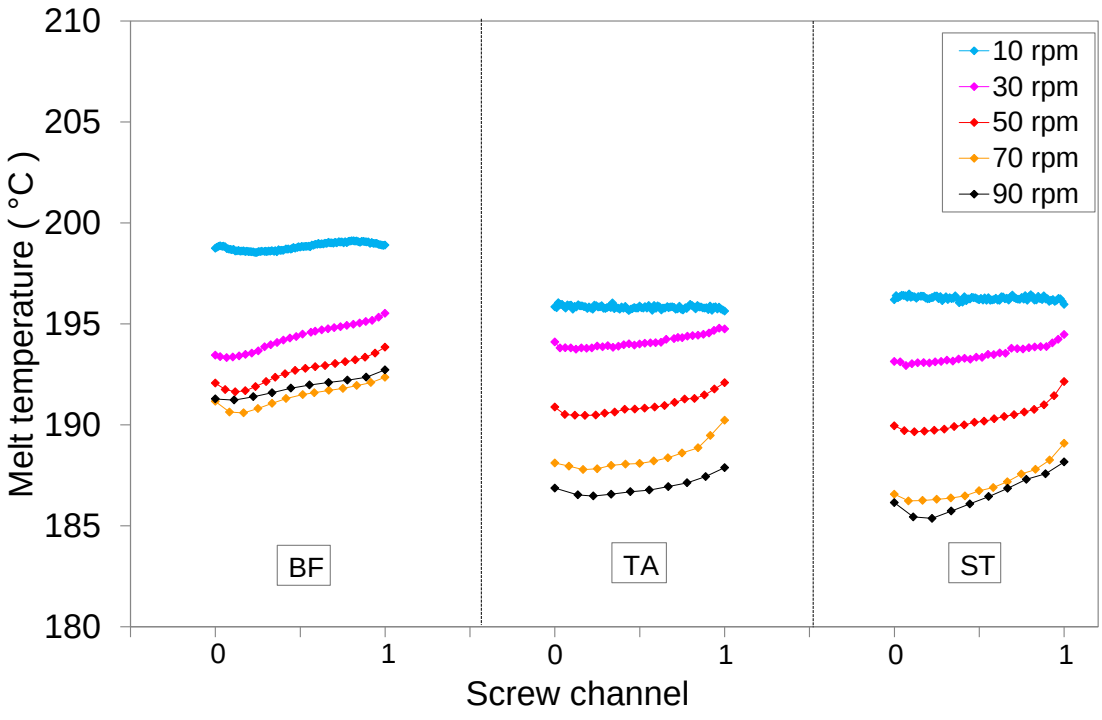

Figure 6.5 Average melt temperature profiles across the width of the screw channel for LDPE at the end of the metering zone; set die temperature 200°C, measured over a 30 second period (BF: Barrier Flighted Screw; TA: Tapered Compression Screw; ST: Stepped Compression Screw)

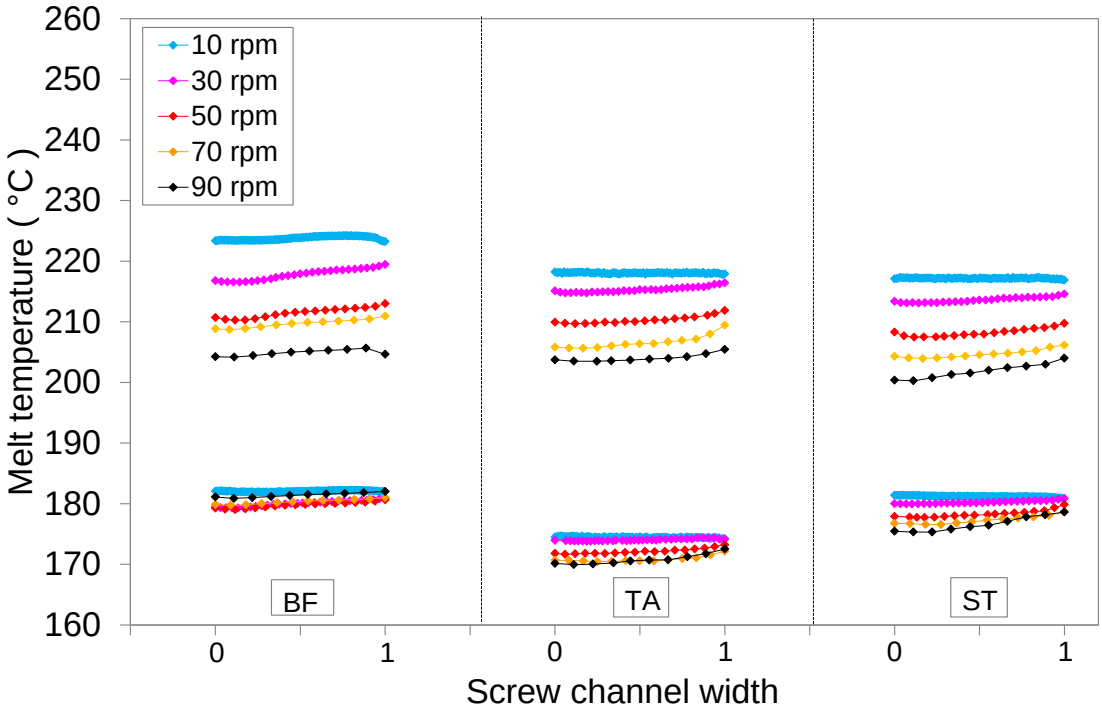

Figure 6.6 Effect of set temperature on melt temperature profiles across the width of the screw channel for LDPE at the end of the metering zone; measured over a 30 second period at 180°C and 220°C (BF: Barrier Flighted Screw; TA: Tapered Compression Screw; ST: Stepped Compression Screw)

In order to provide a comparison to infrared data, radial melt temperature profiles measured using the thermocouple grid (averaged over a period of 30 seconds) are displayed in Figure 6.7 and Figure 6.8 for each material at set process conditions identical to those shown in Figure 6.4 and Figure 6.5.

These data represent melt temperature measurements made at the entrance to the extruder die and were used to provide a reference to the measured IR temperature within the extruder screw channel. Figure 6.7 and Figure 6.8 show that the barrier flighted screw generated melt temperature profiles with lower levels of radial variation across the flow path than both single flighted screws. This provides qualitative agreement with the IR data displayed in Figure 6.4 and Figure 6.5, which also showed higher levels of variation in single flighted screws across the width of the screw channel, especially at high screw rotation speeds. For HD6007 (Figure 6.7) melt temperature in the centre of the flow increased with increasing screw speed, whereas for LDPE (Figure 6.8) melt temperature in the centre of the flow decreased as screw speed increased.

This also demonstrated a qualitative agreement between the two measurement techniques and reflects the lower melt viscosity of LDPE, causing less viscous shear heating to be generated during extrusion, compared to extrusion of HD6007 at identical conditions.

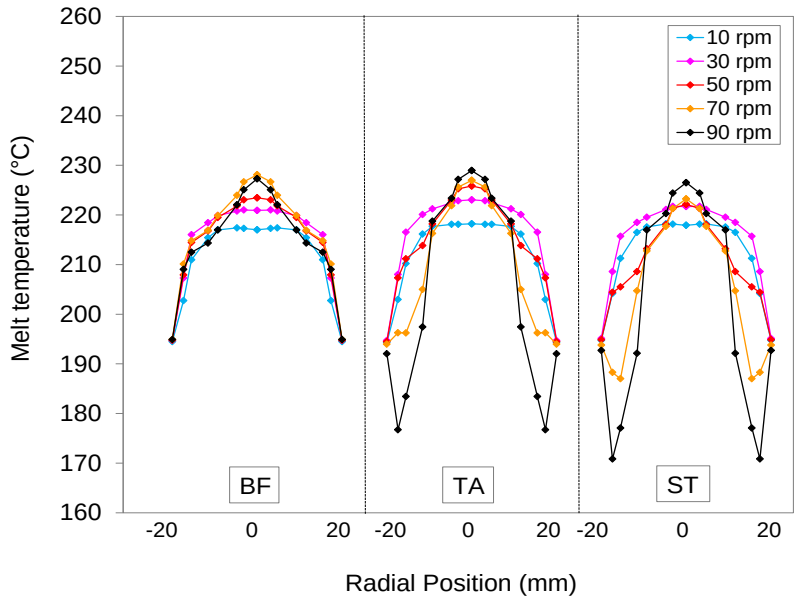

Figure 6.7 Radial melt temperatures in the die section for HD6007; set die 200°C over a period of 30 seconds (BF: Barrier Flighted Screw; TA: Tapered Compression Screw; ST: Stepped Compression Screw)

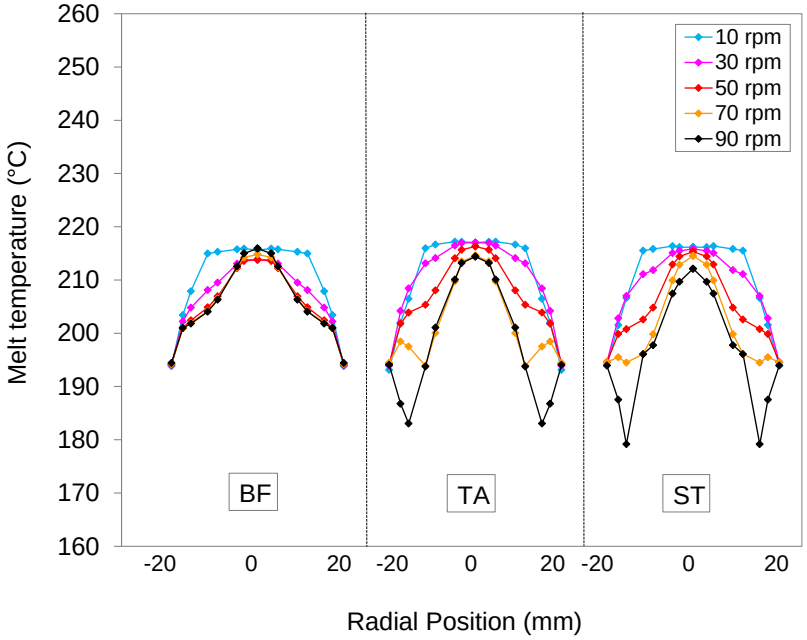

Figure 6.8 Radial melt temperatures in the die section for LDPE; set die 200°C over a period of 30 seconds (BF: Barrier Flighted Screw; TA: Tapered Compression Screw; ST: Stepped Compression Screw)

To provide a quantitative comparison between both measurement techniques, the bulk melt temperature and level of fluctuation from the infrared data are compared directly to corresponding measurements from the thermocouple grid in Figure 6.9 and Figure 6.10. The relationship between bulk temperature and temperature variation and extruder screw speed exhibited similar trends for both measurement techniques although measurements made using the IR sensor were lower in magnitude at all conditions. This is likely to result from the measurement volume of the infrared sensor being more influenced by polymer melt close to the barrel wall, thus having a lower temperature than the bulk. However, these results suggest that the IR sensor could be used to give a good indication of the consistency of melt temperature in the die. In addition, both techniques clearly revealed the pronounced effect of screw speed and screw type on measured temperature. For single flighted screws, especially for HD6007, the data clearly indicates a critical screw speed at which the melting mechanism breaks down causing a decrease in melt temperature (Figure 6.9). This reflects the inefficient melting ability of these screws and is linked to solid bed break up, whereby polymer in the melting section of the screw melts unevenly or not sufficiently.

For the barrier flighted screw this critical point was not evident, and measured melt temperature continued to rise with increasing screw speed, verifying the higher melting capability provided by the barrier screw geometry. For the same screw, low levels of melt temperature variation were measured by both techniques as seen in Figure 6.10. Higher levels of fluctuation above the critical screw speed were observed for single flighted screws which suggest a break down in the effectiveness of the melting process associated with a corresponding decrease in melt homogeneity. Data from both measurement techniques exhibited similar trends; fluctuations increased in magnitude with increasing screw speed.

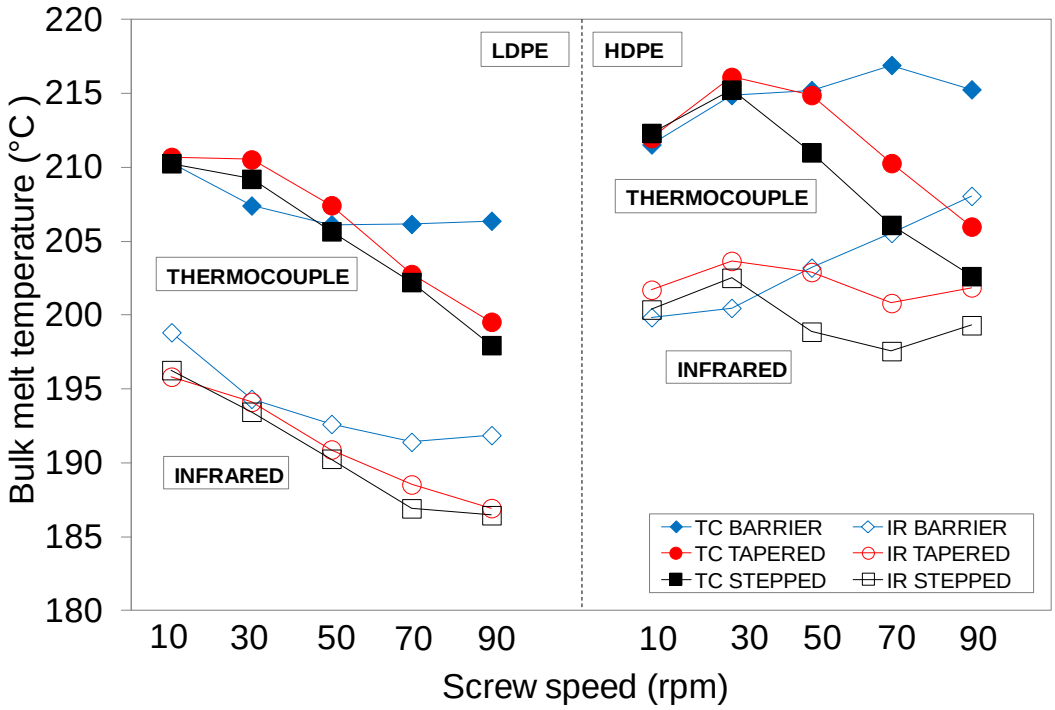

Figure 6.9 Comparison of bulk melt temperature (averaged over a 30 second period) at 200°C from IR and TC grid techniques

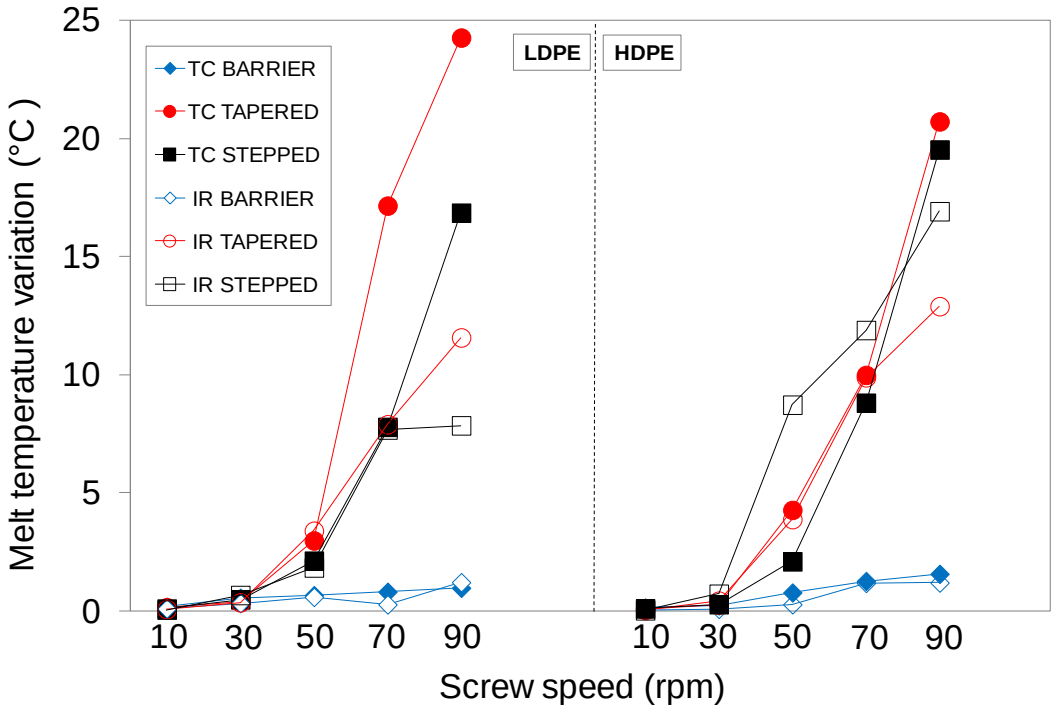

Figure 6.10 Comparison of variation of melt temperature (defined as the difference between maximum and minimum values over a 30 second period) at 200°C from IR and TC grid techniques

Measured IR melt temperatures are displayed in more detail in Figure 6.11- Figure 6.13, to highlight the effects of polymer type and screw geometry on the shape and periodicity of the temperature profile. At a set screw rotation speed of 10rpm (Figure 6.11) the measured temperatures for HD6007 with each screw geometry were similar in nature, exhibiting a periodic decrease in temperature across each screw rotation and then a sharp dip in temperature related to the passing of the screw flight. Corresponding measurements for LDPE showed a slight difference in the shape of the profile, which was more constant across the channel width. Melt temperatures for LDPE were lower in all cases than corresponding values for HD6007 due to the differences in shear heating described earlier.

At screw speeds of 50 and 90 rpm (Figure 6.12 and Figure 6.13) measured melt temperature generated by the two single flighted screws exhibited significant levels of variation. At the same conditions however, the barrier flighted screw exhibited repeatable periodic traces which indicated a relatively stable melt consistency.

Mean values of temperature (averaged over the time to complete one revolution) are displayed in Figure 6.14 for HD6007 to highlight the quality of the melt and its dependence on screw geometry at the highest set screw speed of 90 rpm over a number of screw rotations. The enhanced performance of the barrier flighted screw was clearly shown with lower variation in melt temperature observed. Mean temperatures for both single flighted screws exhibited significantly more variation with temperature changes of up to 16°C observed between subsequent screw rotations, as reflected earlier by the thermocouple mesh data (Figure 6.7).

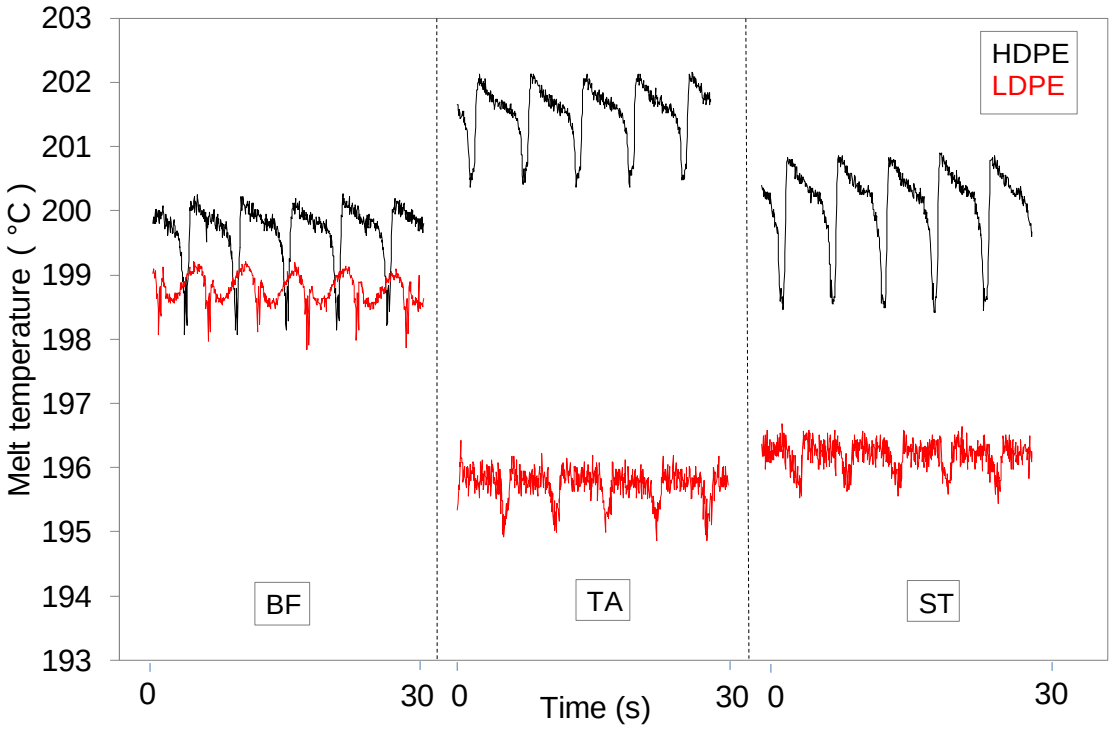

Figure 6.11 Effect of screw type and screw rotation speed on measured infrared temperature at 10 rpm; set die 200°C over a period of 30 seconds

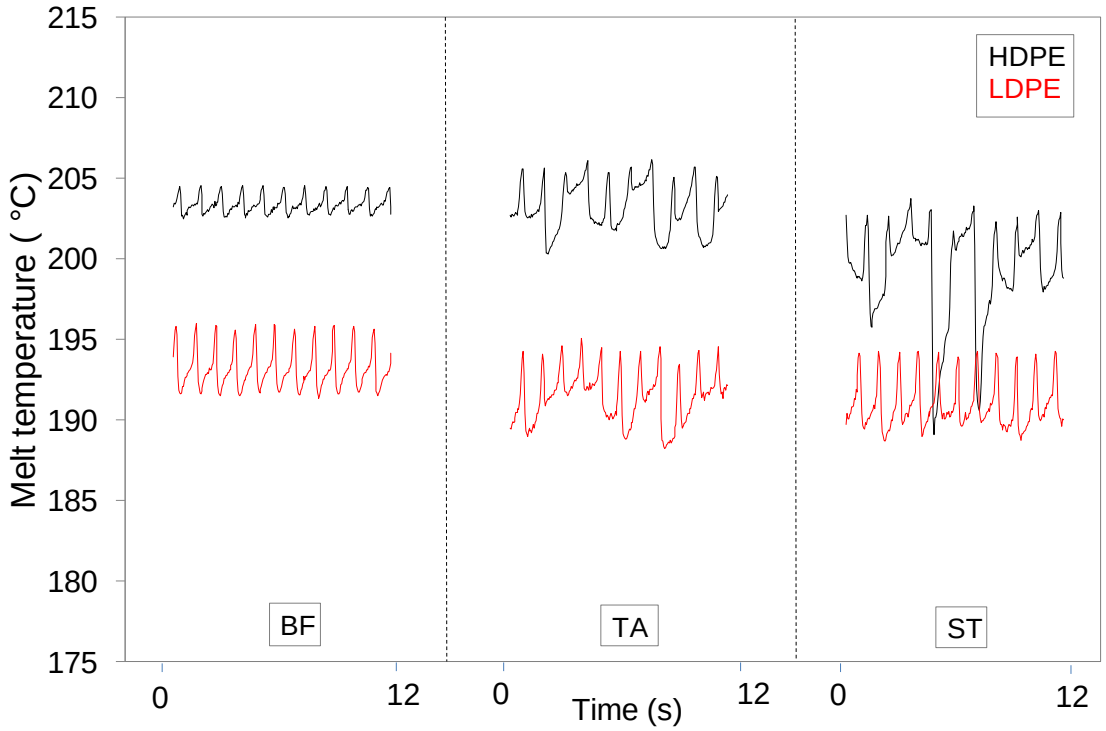

Figure 6.12 Effect of screw type and screw rotation speed on measured infrared temperature at 50 rpm; set die 200°C over a period of 30 seconds

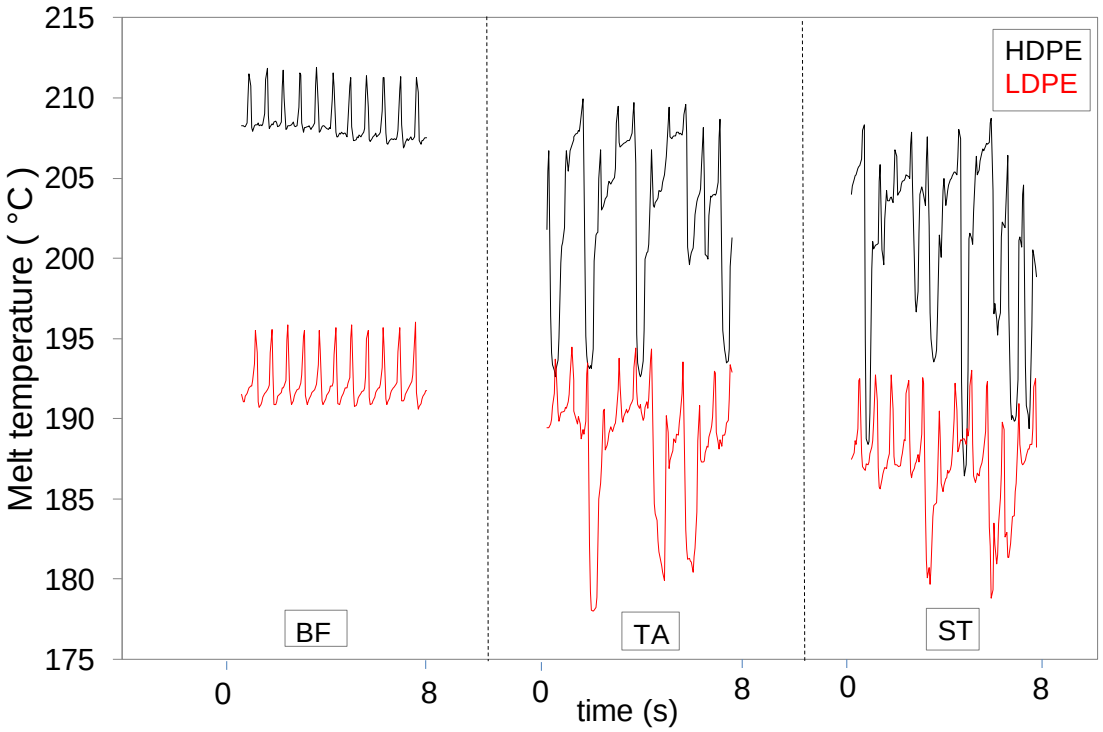

Figure 6.13 Effect of screw type and screw rotation speed on measured infrared temperature at 90 rpm; set die 200°C over a period of 30 seconds

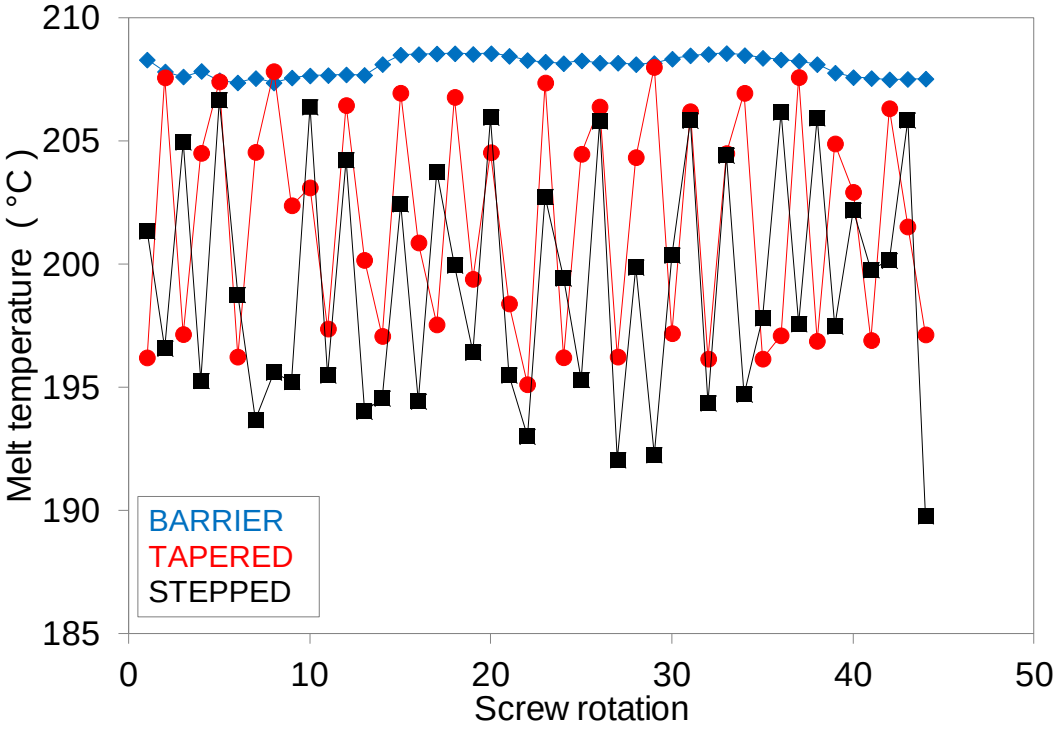

Figure 6.14 Mean values of temperature at each screw rotation; HDPE, set die temperature 200°C and 90rpm

6.2 Infrared measurements using a 38mm diameter single screw extruder

This section aims to examine the effect of extruder scale on the thermal dynamics of the process employing infra-red thermometry. The same IR sensor used in the large extruder was then flush mounted at the end of the 38mm extruder barrel. Here, IR data was generated using HD5050, three screw geometries and set temperatures to provide an examination of the effect of set processing conditions on the measured temperature. Additionally, an intrusive thermocouple grid sensor was located at the entrance to the die enabling quantitative comparison between both measurement techniques.

Infrared measurements using a small scale single screw extruder

Averaged melt temperature profiles for HD5050 across the width of the screw channel at the end of the metering zone are shown in Figure 6.15. Results revealed that temperature profiles generated by each extruder screw at three set temperatures were very similar; flat in shape and increasing in magnitude with increasing speed.
These results were in agreement with radial melt temperature profiles measured using the thermocouple grid (Figure 6.16), reflecting the improved homogeneity of the melt achieved with the 38 mm diameter extrusion process and its lower dependence on screw geometry, as earlier discussed in section 5.2

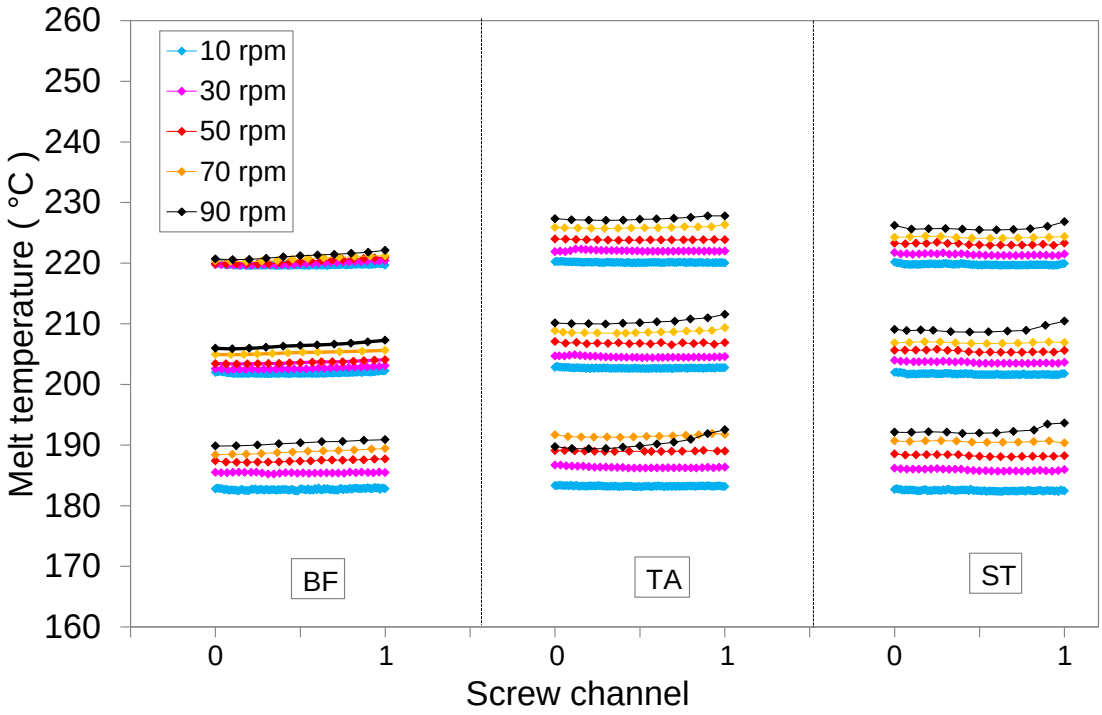

Figure 6.15 Averaged melt temperature profiles for HD5050 across the width of the screw channel at the end of the metering zone; measured over a 30 second period at three set temperatures (220, 200 and 180°C) and (BF: Barrier Flighted Screw; TA: Tapered Compression Screw; ST: Stepped Compression Screw)

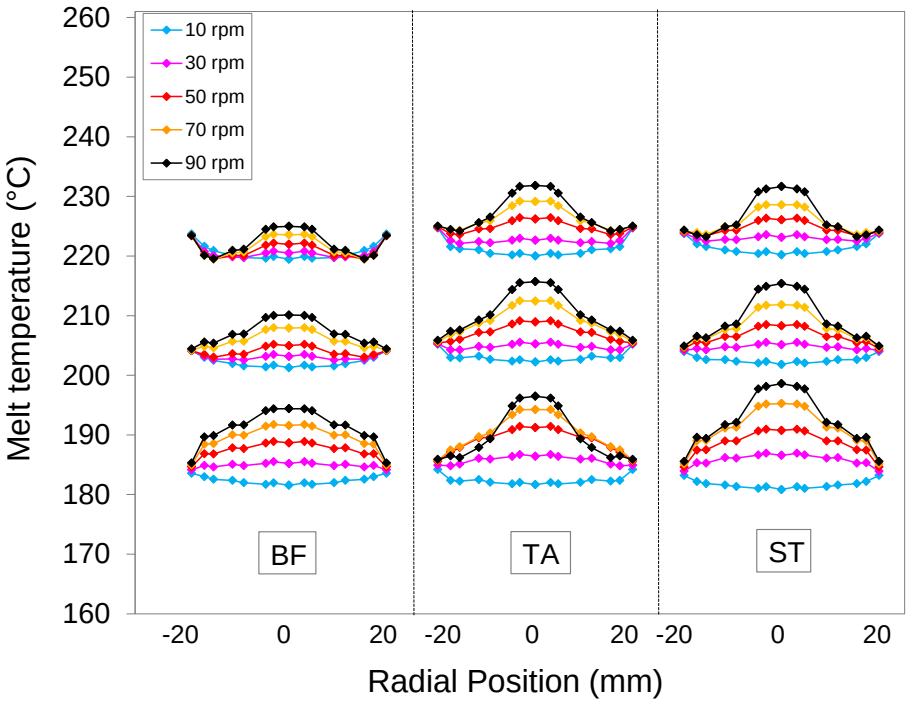

Figure 6.16 Radial melt temperatures measured for HD5050 using three screw geometries and three set temperatures (220, 200 and 180°C) and (BF: Barrier Flighted Screw; TA: Tapered Compression Screw; ST: Stepped Compression Screw)

Figure 6.17 displays bulk melt temperature measured using both techniques, reflecting that the two measured temperatures exhibited identical trends. These results suggested that the IR sensor gave an indication of the bulk melt temperature in the die. Moreover, as shown in Figure 6.18, fluctuations in melt temperature measured from the IR sensor were found to exhibit similar trends to those measured from the thermocouple grid, giving a good indication of the homogeneity of the melt and its corresponding dependence on screw geometry and screw rotation speed.

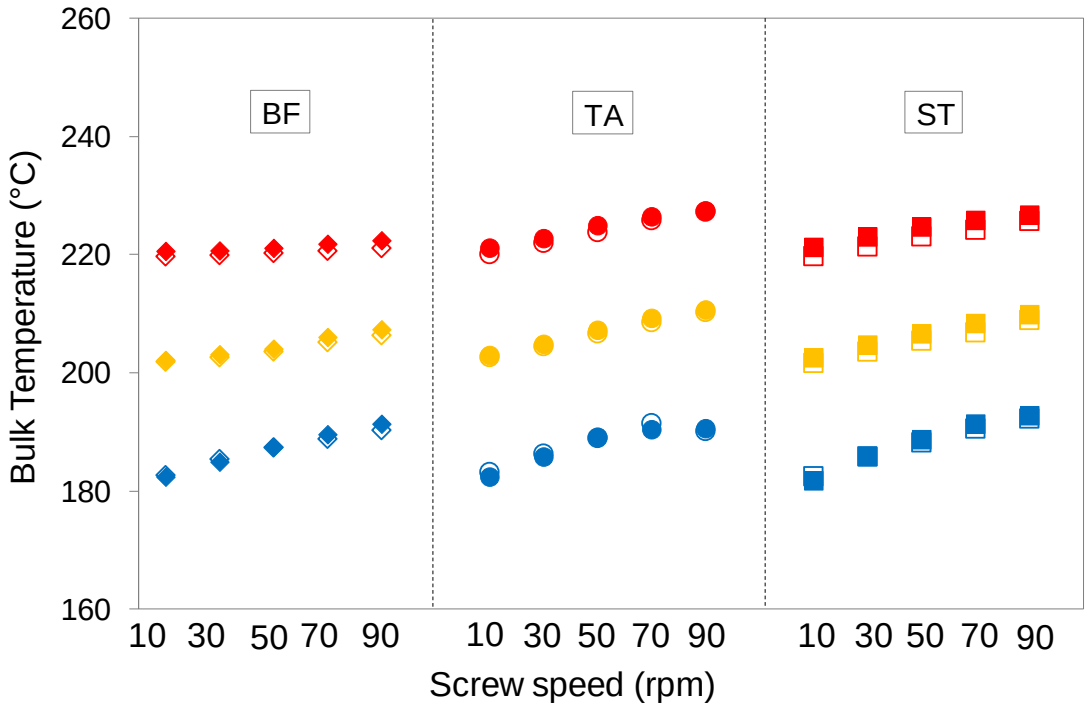

Figure 6.17 Comparison of bulk melt temperature (averaged over a 30 second period) at 220, 200 and 180°C from IR and TC grid techniques (solid fill represents TC data and no fill represents IR data) and (BF: Barrier Flighted Screw; TA: Tapered Compression Screw; ST: Stepped Compression Screw)

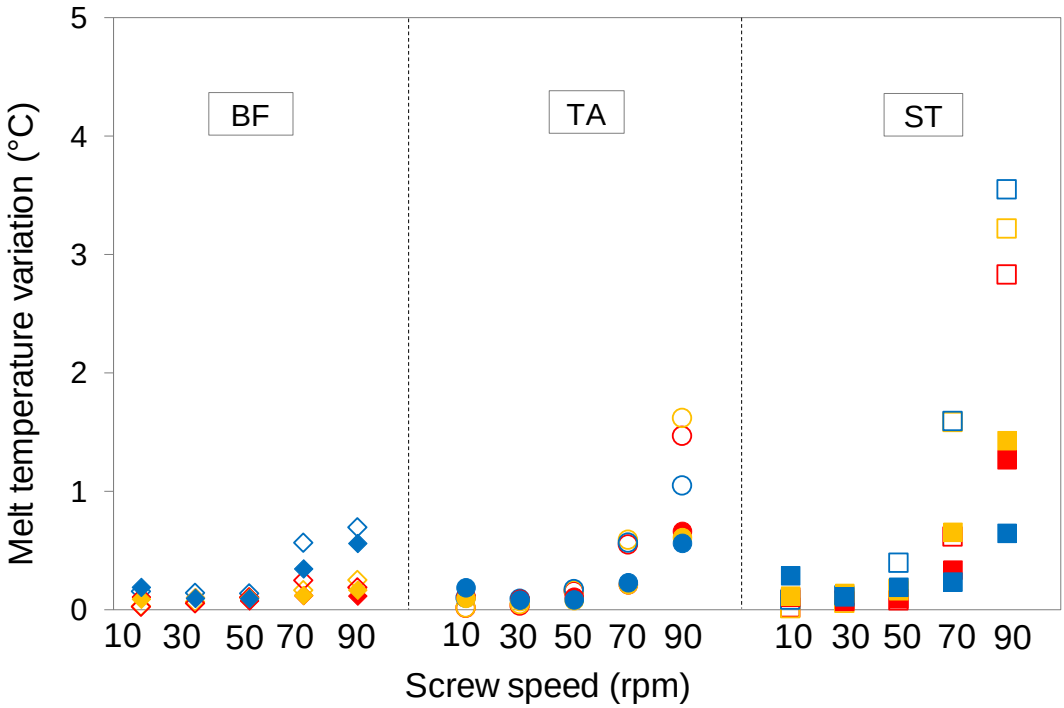

Figure 6.18 Comparison of variation of melt temperature (defined as the difference between maximum and minimum values over a 30 second period) at 220 (red), 200(yellow) and 180°C(blue) from IR and TC grid techniques (solid fill represents TC data and no fill represents IR data) and (BF: Barrier Flighted Screw; TA: Tapered Compression Screw; ST: Stepped Compression Screw)

6.3 Summary

This chapter has shown that infrared thermometry can be used to provide real time quantification of the thermal homogeneity of single screw extrusion. Data generated by the IR sensor were found to be highly sensitive to thermal fluctuations caused by melting instabilities and its corresponding dependence on screw geometry and set processing conditions. Comparisons made with an intrusive thermocouple grid sensor located in the extruder die suggested that the infrared technique provided bulk melt temperature measured at the entrance to the extruder die, especially in a small scale single screw extruder.

CHAPTER SEVEN

7 GENERAL DISCUSSION

The major findings of the experimental work can be summarised as follows:

Extrusion data for LDPE were presented in section 4.3.2. Data revealed that thermal dynamics were affected by screw geometry. Radial melt temperature profiles were found to be more consistent for the barrier flighted screw, with no areas of low temperature being observed near to the die walls as compared to single flighted screws (see Figure 4.5 and Figure 4.6). Interestingly, despite the low levels of temperature variation measured across the flow channel, radial melt temperatures tended to decrease with increasing screw speed, especially for the two single flighted screws. These results suggested that LDPE had a lower capacity of viscous shear heating generated during extrusion which is in agreement with the rheological behaviour observed. The shear viscosity of LDPE was found to be the lowest among the polyethylenes at identical extruder conditions, which could explain that melt temperature did not increase at higher throughputs, highlighting the important role that rheology plays on extrusion performance.

These results quantified that internal shear heat generation had a significant effect on extrusion thermal dynamics. Extruder performance for LLDPE was examined in section 4.3.3. Measured temperatures for LLDPE revealed that now radial melt temperatures increased with increasing screw speed and these were not strongly dependent upon selection of extruder screw geometry. Melt temperature profiles generated by each screw were found to be similar at all conditions (section 4.3.3, Figure 4.14 and Figure 4.15). Similarly, these results suggested that polymer rheology also helped to explain the observed differences between the thermal dynamics of LLDPE and LDPE. Agreeing with (Dealy & Wissbrun, 1999), it was also found that shear viscosity of LLDPE remained higher than LDPE at higher throughputs due to the fact that short chain branching made the LLDPE less sensitive to shear (see section 4.1 and Figure 4.1). This was essential for understanding the results.

The higher viscosity exhibited by LLDPE and its lower sensitivity to shear caused more viscous heating which led to increased melt temperature profiles across the flow path, especially at higher screw speeds. In section 4.1, it was shown that the power law index for LLDPE was higher than LDPE. According to section 2.10.2.2, equation (2.25), LLDPE caused more viscous heating than LDPE. In addition, the internal heat generated enhanced the melting performance achieved with each of the three extruder screws and therefore lower variations in melt temperature were measured for LLDPE than LDPE (Figure 4.8 and Figure 4.17), with a corresponding low dependence of homogeneity on screw geometry.

However, despite the higher throughputs measured for LLDPE, as a result of enhanced melting performance and higher die pressure measured, the extrusion process energy demand was found to be higher than LDPE, especially at higher throughputs (see Figure 4.10 and Figure 4.19). This could be explained by the increased specific energy consumption from the motor measured as a result of major torque requirements to process this polymer that exhibited higher viscosities at identical extrusion conditions (Figure 4.11 and Figure 4.20).

Clearly, these results suggested that melt viscosity was a key variable in polymer extrusion which should be investigated to facilitate an understanding of the thermal dynamics and energy consumption in single screw extrusion. In section 4.3.4 extrusion data for three different molecular weight grades of HDPE was presented to carry out a thorough analysis of the effect of melt viscosity and set process conditions on the thermal efficiency of the process. In terms of thermal dynamics, results reflected that the magnitude of temperature fluctuations across the die flow path increased with increasing melt viscosity, highlighting a high dependence of homogeneity on screw geometry. Single flighted extruder screws exhibited poorer temperature homogeneity and larger fluctuations than the barrier flighted screw, corresponding to the extrusion data for LDPE and LLDPE.

According to (Dealy & Wissbrun, 1999), it was found that single flighted screws become less efficient when the extruder was operated at higher screw speeds, especially during extrusion of high molecular weight grades of HDPE.

For the three grades of HDPE a critical screw speed was evidenced at which the melting mechanism breaks down causing a corresponding decrease in melt quality. Melt quality (thermal homogeneity) was clearly ordered as follows: HD5050 > HD6007 > HD5411 (Figure 4.30).

Moreover, die pressure increased with increasing melt viscosity and pressure variations reflected the poorer processing capability of these screw geometries for the highest viscosity grade HD5411, which could also explain the lowest mass throughputs observed (Figure 4.24). Specific energy consumption was found to be predominantly dependent upon polymer melt viscosity (Figure 4.32).

In general, energy consumption increased with increasing melt viscosity due to the dependence of viscous shear heating on molecular weight and its distribution (see section 4.1 and Figure 4.2).

In section 2.7, equations (2.4) and (2.5), it was shown that the rate of melting is strongly dependent upon the thermal and rheological properties of the polymer. Based on Tadmor´s model, the rate of melting is shown to increase with higher viscosity melts. However, in section 2.5.2 it was shown that melting is highly affected by screw geometry. Single flighted screws were shown to be less efficient in terms of thermal homogeneity at higher throughputs when the melting rate in the extruder is not large enough, and therefore, the solid bed becomes unstable and prematurely breaks up (Myers & Barr, 2002).

In order to show the dependence of melting on screw geometry, reflecting the role of PE rheology on extrusion performance, variations of melt temperature for the five grades of polyethylene are plotted against melt viscosity for single flighted screws in Figure 7.1 and the barrier flighted screw in Figure 7.2. Clearly, variations in melt temperature, that highly affect process stability and product quality, were higher with the two single flighted screws and these increased with increasing PE viscosity, especially for the three grades of HDPE. According to (Myers & Barr, 2002) these results confirmed the improved melting performance provided by the barrier flighted screw, as shown in Figure 7.2

Additionally, energy consumption was found to be significantly affected by melt viscosity, and this was shown to increase with highly viscous materials (see section 2.9.2, equations (2.14) and (2.15)-(2.17). Figure 7.3 shows a clear dependence of energy consumption on melt viscosity, which increased with increasing PE melt viscosity. At screw speeds above 10 rpm it was found that measured specific energy consumption for all PEs and set conditions followed a relatively linear dependence upon melt viscosity, irrespective of set temperature and screw geometry (Figure 7.4).

This finding suggest that melt viscosity could be used as a simple method of predicting or benchmarking specific energy consumption for a particular grade of polymer such as PE.

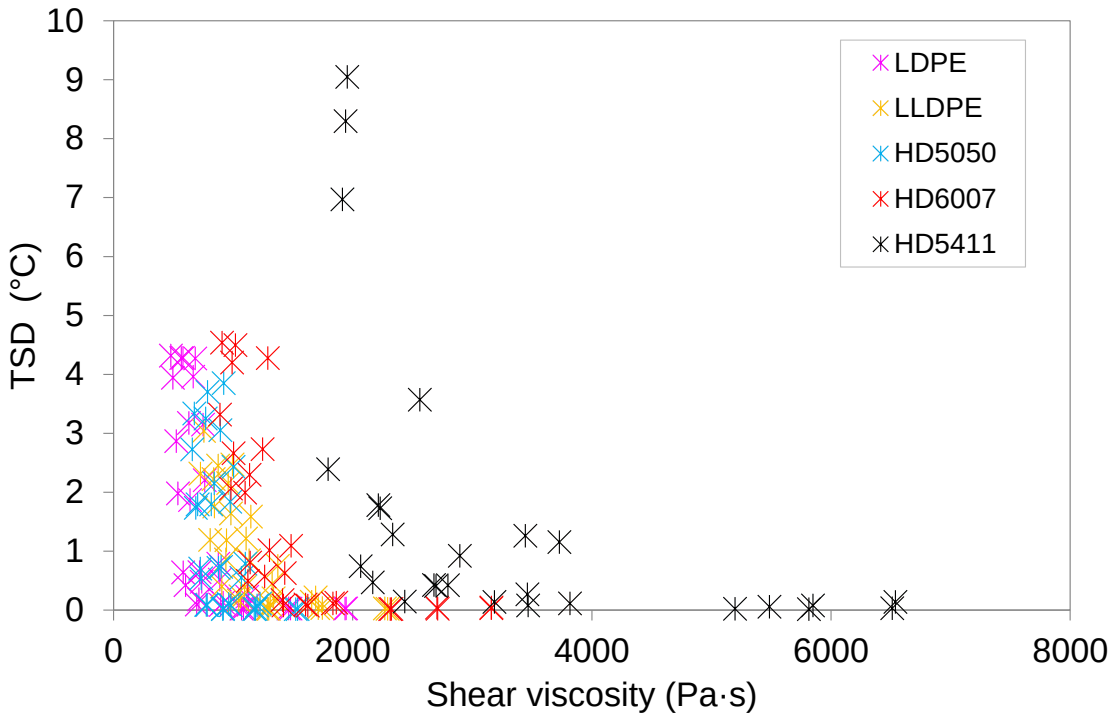

Figure 7.1 Standard deviation of temperature measurements for five grades of PE using two single flighted screws at three set temperatures (220, 200 and 180°C) and (TSD: Standard deviation of temperature measurements over a period of 1 min calculated by taking an average of the standard variation at each individual position)

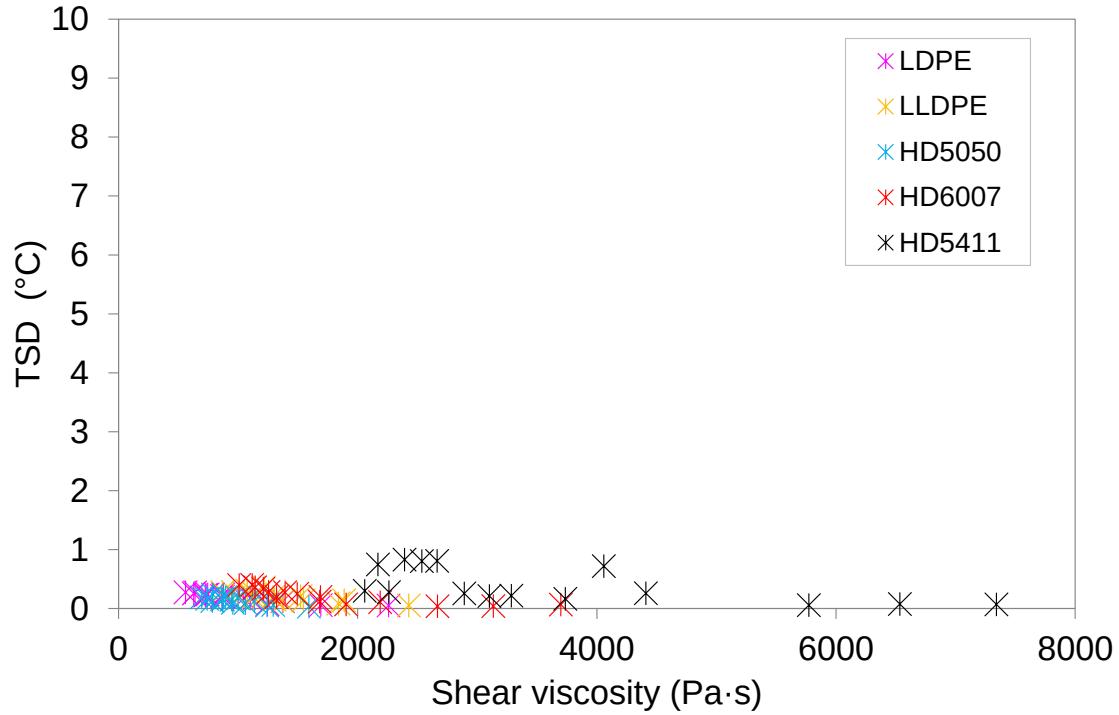

Figure 7.2 Standard deviation of temperature measurements for five grades of PE using a barrier flighted screw at three set temperatures (220, 200 and 180°C) and (TSD: Standard deviation of temperature measurements over a period of 1 min calculated by taking an average of the standard variation at each individual position)

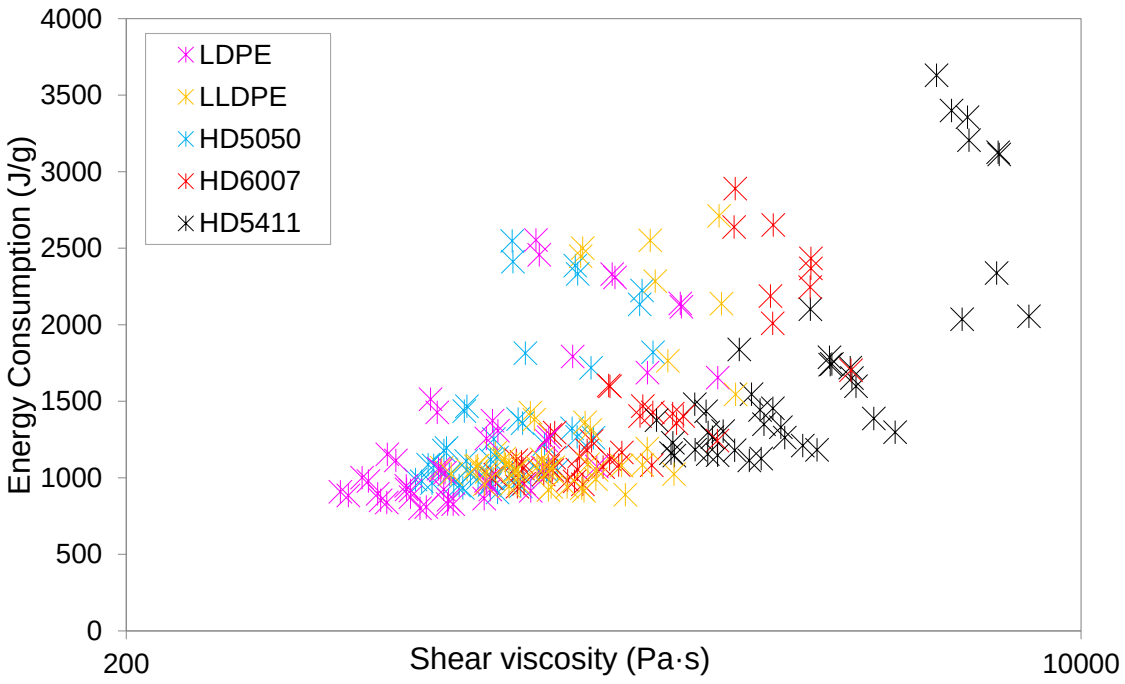

Figure 7.3 Effect of shear viscosity on process energy demand, representing five grades of PE for three screw geometries and set temperatures

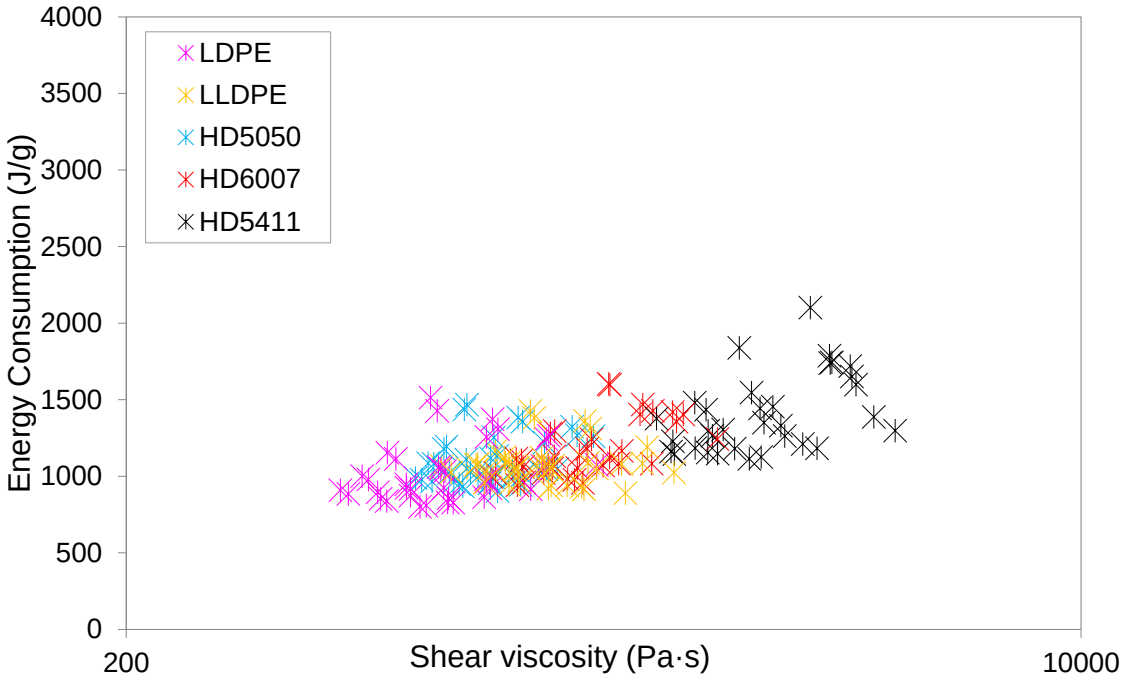

Figure 7.4 Effect of shear viscosity on process energy demand, representing five grades of PE for three screw geometries and set temperatures (from 30 to 90 rpm)

Extrusion measurements for PP were presented in section 4.3.5 to highlight the importance of careful selection of processing conditions and its effect on thermal dynamics and energy efficiency of the extrusion process. Despite the higher melting point measured for PP compared to polyethylenes and polystyrene (see section 4.2, Table 4.2), extrusion set temperature profiles were not tailored to suit its thermal properties and as a result identical extrusion conditions were used. However, this provided valuable information concerning melting performance and its dependence on screw design. Clearly, the thermal homogeneity of the extrusion process was highly dependent upon extruder screw design. This confirmed the limited melting ability of single flighted screws when the extruder is operated at high throughputs. Based on Tadmor´s model (see section 2.7, equation (2.5)), the rate of melting is highly dependent upon the difference between the melting point of the polymer and the initial temperature of the solid bed. With PP, therefore, there was not sufficient time for the volume of polymer within the screw channel to be melted homogeneously.

In this section, the difference in melting observed between the two single flighted screws and its effect on melt temperature was more pronounced, highlighting the poorest thermal homogeneity exhibited by the stepped compression screw. This could be explained by the higher levels of pressure variation measured at identical set temperatures profiles of 220 and 200°C at 90 rpm (see Appendix C), suggesting that a poorer effectiveness of the melting process is associated with an increase in pressure deviation (see Appendix C, Figure C4) and a decrease in melt homogeneity, corresponding with the large temperature drops near to the die walls shown in Figure 4.34 and Figure 4.35. Furthermore, the higher levels of pressure variation indicated that the melting mechanism broke down causing a decrease in melt quality as shown predominantly with the highest viscosity grade HD5411 (see Figure 7.1).

Despite the fact that the barrier flighted screw provided improved melt consistency at the extruder die, throughputs from this screw were lower than those achieved with the two single flighted screws. This is in agreement with throughputs measured for HD5050 at 180°C and the highest viscosity grade HD5411 (Figure 4.22 and Figure 4.24), reflecting the poorer processing capability of this screw when the polymer is not sufficiently molten to flow over the barrier flight. Here, the selection of not tailored barrel set temperatures profiles to suit the thermal properties of PP (melting point) led to the lowest throughputs measured among the polymers used throughout the experiments, especially for the barrier flighted screw where achieving melting is more challenging (Figure 4.33).

This caused the highest values of specific energy consumption measured for this geometry at identical processing conditions due to the poorest melting performance achieved during extrusion of PP (see Figure 4.39). Clearly, this was reflected by the highest values of motor power consumption observed (Figure 4.40), which were found to be non-linearly dependent upon screw speed and highly affected by set temperature.

Extrusion data for PS were displayed in section 4.3.6. This enabled examination of the thermal efficiency for single screw extrusion of an amorphous thermoplastic, including any differences in measured temperature and energy consumption with respect to semi-crystalline thermoplastics, at identical extrusion conditions. For this amorphous material, extrusion thermal dynamics were found to be dependent upon screw geometry and strongly affected by set temperature. At the lowest set temperature profile of 180°C, radial melt temperatures for all three extruder screws were seen to increase significantly with screw speed (Figure 4.44). Agreeing with (Giles et al., 2005), shear viscosity for PS was found to be highly affected by set temperature and shear rate, highlighting its viscous behaviour sensitive to both temperature and shear. At 180°C it was noticed that shear viscosity differed significantly to that measured at 220°C, leading to the highest difference observed among the polymers used throughout the studies (see Figure 4.1 and Figure 4.3). These results suggested that PS had a major capacity for viscous shear heating at 180°C, causing the temperature to rise due to viscous dissipation. This was also reflected by the die pressure measurements which were strongly affected by extrusion set temperature (Figure 4.47).

On the other hand, it has been reported that semi-crystalline polymers have a higher heat capacity than amorphous polymers (Kühnle & Grünschloss, 1999). Grünschloss & Noriega, (2012) argued that semi-crystalline polymers would be expected to require more energy to reach the molten state than amorphous thermoplastics, which do not have crystalline structures being destroyed in the melt phase. According to them, the demand of energy required by the heaters/cooling fans for PS was found to be the lowest (Figure 4.50), highlighting the dependence of energy consumption on the polymer's thermal properties.

The lowest contribution from the heaters/cooling fans to the total energy consumption appeared here to cause a reduction in energy that led to the lowest process energy consumption being measured among the polymers used throughout the experiments (Figure 4.48).

From the motor energy consumption shown in Figure 4.49, it was revealed that the high sensitivity of PS to temperature had a significant impact on energy consumption. A strong dependence of motor energy consumption on melt viscosity was shown due to its temperature dependence, leading to a large difference in energy measured between the lowest and the highest set temperature profiles of 180 and 220°C.

In section 4.3.7 it was found that the processing capability in terms of throughput of these screw geometries was highest for PET, corresponding with the lowest values of viscosity measured in section 4.1, Figure 4.3. Similarly to PP, barrel set temperature profiles were not optimised to suit the thermal properties of PET; these temperatures were increased to facilitate the extrusion process since the melting point of PET is significantly higher than polyethylenes, polystyrene and polypropylene (section 4.2, Table 4.2).

In addition, PET was dried before processing due its hygroscopic nature. However, these results clearly highlighted the dependence of throughput on shear viscosity, which could explain the highest extrusion outputs produced with PET, as shown in Figure 4.51. These results also revealed that in those extrusion processes where the polymer exhibited lower shear viscosity, as shown with LDPE, LLDPE and the three grades of HDPE (Figure 4.4, Figure 4.13, Figure 4.22 and Figure 4.24), the barrier flighted screw provided higher throughputs than the two single flighted screws due to its greater free volume. Moreover, it was also observed here that at the lowest set temperature profile of 280°C, temperature profiles generated with the barrier flighted screw were more sensitive to viscous shear heating than those measured with single flighted screws, providing improved melt consistency at the extruder exit, as shown with LDPE, HD5050, PP and PS at 180°C (see Figure 4.15, Figure 5.20, Figure 4.44 and Figure 4.35, respectively). This is thought to result from the complex geometry of the barrier flighted screw that exposes the polymer to higher shear stresses (Rauwendaal, 2012) .

In terms of energy consumption PET would be expected to consume more energy from the heaters/cooling fans due the selection of higher barrel set temperature profiles. However, extruder throughputs were shown to be the highest among the polymers studied and therefore these two competing effects appeared here to be mutually cancelling. As a result process energy demand was similar to that measured for PS from 30 to 90 rpm (see Figure 4.57 and Figure 4.48, respectively). At 10 rpm, it was shown that PS required the lowest levels of energy consumption due to its amorphous nature.

These results suggested that PET extrusion process can result in major costs than those required for polyethylenes, polystyrene and polypropylene as a result of the large quantities of extra energy required to dry and heat the polymer before processing (Michaeli & Schmitz, 2004). Additionally, it was revealed that due to its viscous behaviour being highly sensitive to temperature (see section 4.1, Figure 4.3), this polymer required a constant temperature during the feeding stage to ensure that this did not incur in large variations in specific motor energy consumption, as shown in Figure 4.58. The effect of extruder scale on extrusion performance using similar extruders and employing identical screw geometries and set processing conditions was examined in chapter 5. Overall, the improved thermal homogeneity achieved with the small scale extruder was clearly revealed.

Bulk temperatures rose with increasing screw speed and did not show a critical screw speed at which the melting mechanism breaks down causing a decrease in melt temperature (see Figure 5.7 and Figure 5.21). Variations of melt temperature of up to 0.4°C were measured for HD5050 and LDPE in the small extruder (Figure 5.8 and Figure 5.22), which were significantly lower than those measured in the large extruder (Figure 5.9 and Figure 5.23), highlighted that melting performance and its effect on melt homogeneity was less dependent upon screw geometry.

In section 2.7.2, according to the melting theory proposed by (Lindt, 1985) although the solid bed is melted by conduction from the barrel and screw surface, most of the melting occurs in the upper melt film where the barrel heaters are placed and intensive viscous heat generation takes place. As shown in Table 7.1, the shear rate along the screw channel in the small extruder is significantly higher than the large extruder and therefore higher levels of viscous shear were generated during the small scale extrusion process, which led to enhanced melting performance. This was noticed in Figure 5.7, where bulk temperature for LDPE measured on the small scale extruder tended to rise with increasing screw speed. Agur, (1986) examined the effect of extruder scale in twin screw extrusion and argued that with larger diameter screws, the ratio of heat transfer area (at the barrel surface) to screw channel volume decreases, leading to a lower heat transfer capability achieved with the large scale. Furthermore, this confirms that the improved melting ability provided by the extruder screws at smaller scale resulted in an increased quality of the melt.

Table 7.1 Shear rate in the screw channel

TA	**Large extruder** (D=63.5mm h_d=10.53mm) FEED $\dot{\gamma}(s^{-1})$	**Large extruder** (D=63.5mm h_d==3.46mm) METERING $\dot{\gamma}(s^{-1})$	**Small extruder** (D=38mm h_d =5.99mm) FEED $\dot{\gamma}(s^{-1})$	**Small extruder** (D=38mm h_d =1.95mm) METERING $\dot{\gamma}(s^{-1})$
rpm				
10	3.15	9.60	5.24	16.11
30	9.47	28.82	15.73	48.33
50	15.78	48.04	26.22	80.55
70	22.10	67.26	36.71	112.77
90	28.41	86.48	47.20	144.99

Although L/D ratio remained constant (having length to diameter ratios of 24:1), experimental data cannot be directly compared to the scale-up methods given in section 2.12, due to the fact that channel depths in the metering sections of the large screws does not satisfy the commonly accepted square root rule. However, according to (Fenner & Williams, 1971), results have shown that melt homogeneity decreases in large scale extruders, especially when the process involves the use of plastics with high viscosity.

Most notably, in terms of energy consumption data have shown that measured energy in the small scale extruder enables prediction of a process window from lab to industrial scale. From Figure 5.12 and Figure 5.26, the relationship between energy consumption and screw speed and its dependence on screw geometry was similar in both extrusion processes.

In chapter 6 extrusion thermal dynamics were assessed using a non-intrusive infrared temperature sensor located in the barrel of the 63.5 mm diameter single screw extruder. Overall these measurements showed that the data generated by the IR sensor was highly sensitive to thermal fluctuations relating to the melting performance of the extruder screw, polymer type and set processing conditions. The level of information provided by the IR sensor was comparable to that generated by a thermocouple mesh located at the entrance to the extrude die, suggesting that the IR technique could be used to investigate and optimise the melting performance of extrusion processes without disrupting the melt flow.

Similarly to section 6.1, the same infrared sensor was located in the barrel of a 38 mm single screw extruder in an attempt to examine the effect of extruder scale on the thermal dynamics of the process. Measured data from the IR sensor were also compared to temperature results obtained with a thermocouple mesh sensor in the extruder die. Infra-red data was clearly shown to be sensitive to screw speed, extruder screw geometry and barrel set temperature profiles. Here, magnitudes in melt temperature from both techniques exhibited identical trends (Figure 6.17) and levels of temperature fluctuation between the two measurements were shown to differ in less than 3°C at all conditions (Figure 6.18). Clearly, infrared thermometry was sensitive to melt homogeneity, reflecting the improved melt quality achieved with the small extruder, as shown in Figure 6.15 where melt temperature profiles were flat across the width of the screw channel and did not exhibit inhomogeneity in melt as shown with HD6007 (Figure 6.4). Moreover, these results suggested that melt homogeneity and penetration depth can affect significantly the measurement of the sensor. The IR sensor provided more accurate temperature measurements due the homogeneity of the temperature in the measurement region and the shallower channel depths in the metering sections of the small extruder screws (see section 3.4.2, Figure 3.7).

CHAPTER EIGHT

8 CONCLUSIONS AND RECOMMENDATIONS FOR FURTHER WORK

8.1 Conclusions

In-process measurement techniques have been used to investigate the thermal homogeneity and energy efficiency of single screw extrusion of polymers. The aims of the project were to quantify the effects of process conditions, polymer rheology, screw geometry and extruder scale on melt temperature and specific energy consumption. The conclusions derived from the experimental work are as follows:

I. Extrusion thermal dynamics

- Melt temperature homogeneity measured on the large scale single screw extruder was found to be more dependent upon extruder screw geometry at higher throughputs. In general, at screw speeds above 50 rpm, single flighted screws exhibited poorer temperature homogeneity than a barrier flighted screw with a spiral mixer.

- The effect of PEs rheology on measured melt temperature across the die flow path was clearly evidenced. For the three grades of HDPE studied, levels of variation in radial melt temperatures were found to increase with increasing melt viscosity.

- Melt temperature homogeneity for LDPE was shown to be poorer than LLDPE due to its higher sensitivity to shear and corresponding low capacity for viscous shear heating generated.

- Bulk temperature for LLDPE was found to be strongly affected by screw speed due to the dependence of melt viscosity on viscous energy dissipation via shearing. Bulk temperature for PS, however, was shown to be highly dependent upon set temperature reflecting a viscous behaviour sensitive to both shear and temperature.

- Thermal homogeneity measured on the small scale single screw extruder was found to be less dependent upon polymer rheology, set processing conditions and extruder screw geometry. Both single flighted screws and a barrier flighted screw with a spiral mixer provided similar levels of temperature variation, reflecting the higher melt homogeneity achieved with the small scale extrusion process.

II. Extrusion performance in terms of throughput

- Extruder throughput was found to be more dependent upon extruder screw geometry, set temperature and polymer type when the extruder was operated at high screw speeds.

- Set temperature appeared to have a major effect on throughput for the barrier flighted screw when the polymer being processed exhibited greater shear viscosities. With lower viscosity grades, the barrier flighted screw produced higher throughputs than the two single flighted screws due to its higher free volume.

- An inadequate selection of set process conditions was found to adversely affect mass throughputs, especially for the barrier flighted screw as shown with PP.

III. Melting performance

- For both single flighted screws a break down in the effectiveness of the melting process in the large scale extrusion process was shown to be associated with a decrease in melt homogeneity and a corresponding increase in melt pressure variations, as shown with the highest viscosity grades of polyethylene and polypropylene.

- Melting performance for the small scale extrusion process did not exhibit a critical screw speed at which the melting mechanism began to break down deteriorating the quality of the melt. The effect of melting on extrusion thermal performance was found to be less dependent upon extruder screw geometry.

IV. Specific energy consumption

- In general, the highest levels of total specific energy consumption in the large scale single screw extruder were measured at the lowest screw speed of 10 rpm for all screw geometries, set conditions and polymers being used. At this particular screw speed, the difference in measured energy between the barrier flighted screw and the two single flighted screws was found to be the highest. Above 10 rpm, measured energy values decreased with increasing screw speed, becoming less dependent upon screw geometry and extruder set temperature.

- Total specific energy consumption was found to be lower for the barrier flighted screw. However, with PP it was shown that an inadequate selection of set processing conditions led to the highest energy consumption measured due to the dependence of specific energy consumption on melting performance, especially for the barrier flighted screw.

- For all polyethylenes studied, total specific energy consumption was shown to be predominantly dependent upon polymer melt viscosity. Energy consumption was found to increase with increasing melt viscosity due to the dependence of viscous shear on melt viscosity. At screw speeds above 10 rpm, the measured specific energy consumption was shown to follow a relatively linear dependence upon melt viscosity, irrespective of set temperature and screw geometry, suggesting that melt viscosity could be used as a simple method of predicting or

benchmarking specific energy consumption for single screw extrusion of polyethylene.

- Specific energy consumption for the motor was also found to be strongly affected by the viscous behaviour of the polymer being processed and the effect of set temperature. In general, lowest specific motor energy consumption was measured at the lowest set temperature profile due to the dependence of melt viscosity on temperature. With LLDPE, it was shown that lower shear sensitivity caused an increase in motor energy consumption. With PS, it was found that motor energy consumption was significantly affected by set temperature due to a viscous behaviour highly sensitive to temperature and shear. With PET, it was shown that motor energy consumption could vary depending upon feeding temperature due to a viscous behaviour predominantly sensitive to temperature.

- In general, specific energy consumption from heaters/cooling fans was found to gradually decrease with decreasing set temperature being lower as screw speed increased. Specific energy consumption was shown to be more favourable with PS, highlighting the amorphous nature of this polymer. Compared to semi-crystalline thermoplastics, extrusion of PS was shown to consume less energy from the heaters/cooling fans, leading to the lowest extrusion process energy demand.

- Specific energy consumption measured on the small scale single screw extruder was found to be higher than that measured in the large scale extrusion process at all conditions, especially at 10 rpm. The relationship between specific energy consumption and processing conditions and extruder screw geometry was found to be similar in both extrusion processes, allowing prediction of a process window from lab to industrial scale within which energy efficiency can be optimised.

V. Summary

- While it is recognised that melt quality and associated product quality is the first priority in extrusion, extrusion data measured on the large scale single screw extruder have indicated an acceptable process window within which melt quality is high. By judicious selection of extruder screw geometry, set process temperature conditions and appropriate screw speeds, energy efficiency can be optimised without any reduction in melt quality.

  For the polymers used in this work (LDPE, LLDPE, HDPE, PP, PS and PET), low screw rotation speeds (10 and 30 rpm) were found to consume higher levels of specific energy, whereas for single flighted screws an intermediate screw rotation speed of 50 rpm was found to produce the best balance between melt quality and energy consumption. A barrier flighted screw with spiral mixer, however, was found to provide the best melt quality over a greater screw speed range (50 to 90 rpm). In addition, this work highlighted that an evaluation of the motor energy allows more sensitive examination of the effect of processing conditions on melt viscosity and thermal properties on energy measurements.

- Extrusion data measured on the small scale single screw extruder indicated a wider process window (50 to 90 rpm), within which melt quality and energy consumption produced the best balance irrespective of screw geometry. Above 10 rpm, screw design had less impact on extrusion thermal dynamics and energy consumption, leading to a low dependence of the thermal efficiency of the process on processing conditions and screw geometry.

- The ability of infra-red thermometry to provide non-invasive melt temperature measurements in the metering section of the extruder screw was found to be suitable for use in development of extruder screw designs and process optimisation.

8.2 Recommendations for further work

According to the findings of the current study, the following areas have been identified for further research work:

1. It is recommended that a barrier screw without a mixing section be studied for further analysis of the contribution of this section on the effectiveness of the melting process and its corresponding effect on melt temperature homogeneity.

2. Further analysis should be conducted to investigate the effect of internal screw cooling, especially with polymers that exhibit highly viscous behaviour. This may help to observe changes in melting performance and investigate its effect on the extrusion thermal dynamics and specific energy consumption.

3. Further work should be done to assess the effect of filler content on the thermal dynamics and energy consumption of the extrusion process, allowing quantification of temperature variation and melt viscosity.

4. It would be useful to use polyethylene in powder form to investigate whether the melting mechanism varies, causing a significant impact on melt quality and extrusion process energy demand.

5. It would be useful to perform a similar detailed thermal analysis using a twin screw extruder. This would allow investigation of the suitability of thermocouple meshes to assess the twin extrusion thermal dynamics and examine the differences between specific energy consumption.

6. The polymer IRC laboratory at Bradford has a windowed extruder barrel. This could be employed for visualisation studies inside the barrel and carry out non-invasive measurements at different L/D positions. This would allow more accurate examination of the melting process and its effect on temperature homogeneity and pressure variations.

7. Data from this detailed experimental study should be used to develop models which could be used to aid extrusion process control.

References

Abeykoon, C. et al. 2011. A new model based approach for the prediction and optimisation of thermal homogeneity in single screw extrusion. *Control Engineering Practice*. **19**(8),pp.862–874.

Abeykoon, C., Kelly, A.L., Brown, E.C., et al. 2014. Investigation of the process energy demand in polymer extrusion: A brief review and an experimental study. *Applied Energy*. **136**,pp.726–737.

Abeykoon, C., Li, K., et al. 2010. Modelling the Effects of Operating Conditions on Die Melt Temperature Homogeneity in Single Screw Extrusion. *UKACC International Conference on CONTROL 2010*,pp.42–47.

Abeykoon, C., McAfee, M., et al. 2010. Modelling the Effects of Operating Conditions on Motor Power Consumption in Single Screw Extrusion *In*: *Life System Modeling and Intelligent Computing SE - 2*. Lecture Notes in Computer Science. Springer Berlin Heidelberg, pp. 9–20.

Abeykoon, C., Kelly, A.L., Vera-Sorroche, J., et al. 2014. Process efficiency in polymer extrusion: Correlation between the energy demand and melt thermal stability. *Applied Energy*. **135**,pp.560–571.

Acur, E.E. and Vlachopoulos, J. 1982. Numerical simulation of a single-screw plasticating extruder. *Polymer Engineering & Science*. **22**(17),pp.1084–1094.

Agur, E.E. 1986. Extruder Scale-up in a Corotating Twin-Screw Extrusion Compounding Process. *Advances in Polymer Technology*. **6**(2),pp.225–232.

Al-Fouzan, A.M. 2011. Polyethylene terephthalate/clay nanocomposites : compounding, fabrication and characterisation of the thermal, rheological, barrier and mechanical properties of polyethylene terephthalate/clay nanocomposites. PhD, University of Bradford

Anger, K., Potente, H., Schöppner, V., Enns, E., et al. 2009. Dynamic Temperature and Pressure Measurement in Polymer Processing. *Journal of Plastics Technology*. **5**(1),p.31.

Anger, K., Potente, H., Schöppner, V., Hömann, H., et al. 2009. Radial Temperature Modelling inside the Screw Channel for Tempered Single Screws. *Journal of Materials Processing Technology*. **5**(2).

Bagley, E.B. 1957. End Corrections in the Capillary Flow of Polyethylene. *Journal of Applied Physics*. **28**(5).

Bendada, A. and Lamontagne, M. 2004. A new infrared pyrometer for polymer temperature measurement during extrusion moulding. *Infrared Physics & Technology*. **46**(1–2),pp.11–15.

Blaine, R. 2014. *Thermal Application Note - Polymers heat of fusion* [online]. Available from: www.tainstruments.com/library_download.aspx?file.

Brown, E.C. et al. 2000. In line melt temperature measurement during real time ultrasound monitoring of single screw extrusion. *Plastics, Rubber and Composites*. **29**(1),pp.3–13.

Brown, E.C. et al. 2004. Melt temperature field measurement in single screw extrusion using thermocouple meshes. *Review of Scientific Instruments*. **75**(11).

Brown, E.C. et al. 1999. Ultrasound: A Virtual Instrument Approach for Monitoring of Polymer Melt Variables. *Journal of Reinforced Plastics and Composites*. **18**(4),pp.331–338.

Bruker, I. et al. 1987. Numerical Analysis of the Temperature Profile in the Melt Conveying Section of a Single Screw Extruder: Comparison with Experimental Data. *Polymer Engineering and Science*. **27**(7),pp.504–509.

Bur, A.J. et al. 2004. Temperature gradients in the channels of a single-screw extruder. *Polymer Engineering and Science*. **44**(11),pp.2148–2157.

Carley, J.F. and McKelvey, J.M. 1953. Extruder Scale-Up Theory and Experiments. *Industrial & Engineering Chemistry*. **45**(5),pp.989–992.

Carreau, P.J. 1968. Rheological Equations from Molecular Network Theories (Ph.D. Thesis).

Chen, T.-F. et al. 1999. Temperature measurement of polymer extrusion by ultrasonic techniques. *Measurement Science and Technology*. **10**(3),pp.139–145.

Chung, C.I. 1984. On the scale-up of plasticating extruder screws. *Polymer Engineering & Science*. **24**(9),pp.626–632.

Classes of plastics 2006. *Classification of plastics: Microstructure of various plastics and effect of heating and cooling during processing* [online]. Available from: http://www.dc.engr.scu.edu/cmdoc/dg_doc/develop/material/classify/a1000001.htm.

College, C. 2015. *Differential Scanning Calorimetry; First and Second OrderTransitions in PETE* [online]. Available from: http://www.colby.edu/chemistry/PChem/lab/DSCPETE.pdf.

Compuplast Inc 2011. Compuplast Inc,.

Covas, J. and Gaspar-Cunha, A. 2009. Use of Multi-objective Evolutionary Algorithms in Extrusion Scale-Up *In*: *Applications of Soft Computing SE - 9*. Advances in Soft Computing. Springer Berlin Heidelberg, pp. 86–94.

Covas, J. and Stevens, M.J. 1995. *Extruder Principles and Operation* 2nd Ed. Springer.

Cox, A.P.D. et al. 1981. The melting behavior of a low density polyethylene powder in a screw extruder. *Polymer Engineering & Science*. **21**(2),pp.86–92.

Crystallinity in polymers 2014. Crystallinity. Available from: http://www.doitpoms.ac.uk/tlplib/polymerbasics/crystallinity.php.

Cunha, S.M. et al. 2009. Melting of Polymer Blends in Single- Screw Extrusion- An Experimental Study. *International Journal of Material Forming*. **2**(1),pp.729–732.

Dae Han, C. et al. 1991. A Study on the Performance of the Maddock Mixing Head in Plasticating SingleScrew Extrusion. *Polymer Engineering & Science*. **31**(11),pp.818–830.

Dealy, J.M. and Wissbrun, K.F. 1999. *Melt Rheology and Its Role in Plastics Processing: Theory and Applications*. Springer Verlag Gmgh.

Delgadillo-Velazquez, O. et al. 2008. Sharkskin and Oscillating Melt Fracture: Why in Slit and Capillary Dies and Not in Annular Dies? *Polymer Engineering & Science*. **48**(2),pp.405–414.

Deng, J., Li, K., Harkin-Jones, E., Price, M., Karnachi, N., et al. 2014. Energy monitoring and quality control of a single screw extruder. *Applied Energy*. **113**,pp.1775–1785.

Deng, J., Li, K., Harkin-Jones, E., Price, M., Fei, M., et al. 2014. Low-cost process monitoring for polymer extrusion. *Transactions of the Institute of Measurement and Control*. **36**(3),pp.382–390.

Donovan, R.C. 1971. A theoretical melting model for plasticating extruders. *Polymer Engineering & Science*. **11**(3),pp.247–257.

Dray, R. 2002. *How to compare Barrier Screws* [online]. Available from: http://www.ptonline.com/articles/how-to-compare-barrier-screws.

Edmondson, I.R. and Fenner, R.T. 1975. Melting of thermoplastics in single screw extruders. *Polymer*. **16**(1),pp.49–56.

Eslami, H. 2014. *Understanding Screw design for Film Extrusion Process* [online]. Available from: http://www.macroeng.com.

Esseghir, M. and Sernas, V. 1994. On the measurements of the radial temperature distribution in an extruder channel. *Advances in Polymer Technology*. **13**(2),pp.133–140.

Farmer, N. 2013. *Trends in Packaging of Food, Beverages and Other FMCG*. Woodhead Publishing Limited.

Fenner, R.T. and Williams, J.G. 1971. Some melt flow and mechanical design aspects of large extruders. *Polymer Engineering & Science*. **11**(6),pp.474–483.

Forsyth, T.H. and Murphy, N.F. 1969. Experimental Measurement of Temperature Profiles of Molten Flowing Polymers in a Heat Exchanger. *Polymer Engineering and Science*. **9**(1),pp.22–26.

Franca, D.R. et al. 2000. Ultrasonic In-Line Monitoring of Polymer Extrusion. *Polymer Engineering & Science*. **40**(1),pp.82–94.

Fyrillas, M. et al. 1999. A Mechanism for Extrusion Instabilities in Polymer melts. *Polymer Engineering & Science*. **39**(12),pp.2498–2504.

Gammadot 2015. *What is a rheometer?* [online]. Available from: http://www.gammadot.com/index.htm?Theory/What_is_a_Rheometer.htm~mainFrame.

Giles, H.F.J. et al. 2005. *Extrusion The Definitive Processing Guide and Handbook*. William Andrew Publishing/Plastics Design Library.

Grünschloss, E. and Noriega, M.P. 2012. Improved approximations in thermal properties for single screw extrusion *In*: *SPE-ANTEC*., p. 1058.

Haberstroh, E. et al. 2002. Real-Time Monitoring of Reactive Extrusion Processes by Means of In-Line Infrared Spectroscopy and Infrared Temperature Measurement. *Macromolecular Materials and Engineering*. **287**(3),p.203.

Han, C.D. et al. 1996. Plasticating single-screw extrusion of amorphous polymers: Development of a mathematical model and comparison with experiment. *Polymer Engineering & Science*. **36**(10),pp.1360–1376.

Harper, C.A. and Petrie, E.M. 2003. *Plastics Materials and Processes*. John Wiley & Sons, Inc., Hoboken, New Jersey.

Hatzikiriakos, S. et al. 1997. Rheological characterization of polyethylene terephthalate resins using a multimode Phan-Tien-Tanner constitutive relation. *Rheologica Acta*. **36**,pp.568–578.

Hoffman, D.M. and McKinley, B.M. 1985. Crystallinity as a Selection Criterion for Engineering Properties of High Density Polyethylene. *Polymer Engineering & Science*. **25**(9),pp.562–569.

Hsieh, F.H. 2003. Extruder Power Requirements *In*: D. R. HELDMAN, ed. *Encyclopedia of Agricultural,Flood and Biological Engineering*., p. 298.

Huang, H.-X. and Peng, Y.-C. 1993. Theoretical modeling of dispersive melting mechanism of polymers in an extruder. *Advances in Polymer Technology*. **12**(4),pp.343–352.

Judeh, Y.H. 1989. Development of a novel measuring device to assess the temperature profiles of polymers melts flowing in plasticating extruders. PhD thesis, University of Manchester.

Kantor, K.M. 2010. Analizing Extruder Energy Consumption *In*: *SPE-ANTEC.*, pp. 603–609.

Kelly, A.L. et al. 2003. Infrared melt temperature measurement: effect of filler content on penetration depth *In*: *SPE-ANTEC.*, pp. 3306–3310.

Kelly, A.L. et al. 2002. Temperature Measurement Methods for Polymer Processing *In*: *PPS 18th Annual meeting*. Guimaraes, Portugal, p. 122.

Kelly, A.L. et al. 2006. The effect of screw geometry on melt temperature profile in single screw extrusion. *Polymer Engineering & Science*. **46**(12),pp.1706–1714.

Kent, R. 2008. Energy management in plastics processing — framework for measurement, assessment and prediction. *Plastics, Rubber and Composites*. **37**(2-4),pp.96–104.

Kim, H.T. and Collins, E.A. 1971. Temperature Profiles for Polymer Melts in Tube Flow. Part II. Conduction and Shear Heating Corrections. *Polymer Engineering and Science*. **11**(2),pp.83–92.

Kim, S.Y. et al. 1982. Factors affecting the energy efficiency of single screw extruders. *Fibre Science and Technology*. **17**(1),pp.41–61.

Kong, Y. and Hay, J.. 2003. Multiple melting behaviour of poly(ethylene terephthalate). *Polymer*. **44**(3),pp.623–633.

Kühnle, H. and Grünschloss, E. 1999. *"Berechnung der Austragszone von Einschneckenextrudern", Rheologie in der Kunststofftechnik*. Technische Akademie Esslingen, Ostfildern, Germany.

Lai, E. and Yu, D.W. 2000. Modeling of the plasticating process in a single-screw extruder: A fast-track approach. *Polymer Engineering & Science*. **40**(5),pp.1074–1084.

Lee, K.Y. and Han, C.D. 1990. Analysis of the performance of plasticating single-screw extruders with a new concept of solid-bed deformation. *Polymer Engineering & Science*. **30**(11),pp.665–676.

Leeuwen, J. Van 1967. Stock Temperature Measurement in Plastifying Equipment. *Polymer Engineering & Science*. (12),pp.98–109.

Lindt, J.T. 1976. A dynamic melting model for a single-screw extruder. *Polymer Engineering & Science*. **16**(4),pp.284–291.

Lindt, J.T. 1985. Mathematical modeling of melting of polymers in a single-screw extruder a critical review. *Polymer Engineering & Science*. **25**(10),pp.585–588.

Lindt, J.T. 1981. Pressure development in the melting zone of a single-screw extruder. *Polymer Engineering & Science*. **21**(17),pp.1162–1166.

Maddock, B.H. 1959. A visual Analysis of Flow and Mixing in Extruder Screws *In*: *SPE-ANTEC*., pp. 383–389.

Maddock, B.H. 1974. Extruder scale-up by computer. *Polymer Engineering & Science*. **14**(12),pp.853–858.

Mallouk, R.S. and McKelvey, J.M. 1953. Power Requirements of Melt Extruders. *Industrial & Engineering Chemistry*. **45**(5),pp.987–989.

McKelvey, J.M. 1983. Energy Utilization in Extrusion. *Advances in Polymer Technology*. **3**,pp.205–211.

Michaeli, W. and Schmitz, T. 2004. Processing Polyethylene Terephthalate on a Single Screw Extruder without Predrying using Hopper- and Melt Degassing *In*: *SPE-ANTEC.*, pp. 294–298.

Migler, K.B. and Bur, A.J. 1998. Fluorescence Based Measurement of Temperature Profiles During Polymer Processing. *Polymer Engineering and Science*. **38**(1),pp.213–221.

Mondvai, I. et al. 1973. Extrudieren von Thermoplasten II. *Plaste Kautschzik*. **20**,p.630.

Myers, J.A. and Barr, R.A. 2002. Improved Screw Design for Maximium Conductive Melting *In*: *SPE-ANTEC.*, p. 154.

Neagu, R.M. et al. 2000. Electrical conductivity studies in nylon 11. *Journal of Applied Physics*. **88**(11).

Nietsch, T. et al. 1997. Melt Temperatures and Residence Times in an Extruder by Infrared Spectroscopy. *International Polymer Processing*. **12**(4),pp.307–315.

Noriega, M.P. et al. 2004. In line measurement of the polymer melting behavior in single screw extruders. *Journal of Polymer Engineering*. **24**(6),p.557.

Pearson, J.R.A. 1976. Scale-up of Single Screw Extruders for Polymer processing. *Plastics and Rubber:processing*. **1**,pp.113–118.

PlasticsEurope 2013. Plastics – the Facts 2013 An analysis of European latest plastics production , demand and waste data.

Potente, H. 1991. Existing Scale-up Rules for Single-screw Plasticating Extruders. *International Polymer Processing*. **6**(4),pp.267–278.

Potente, H. and Fisher, P. 1977. Model Laws for the Design of Single Screw Plasticating Extruders. *Kunststoffe*. **67**,pp.242–247.

Rasid, R. and Wood, A.K. 2003. Effect of process variables on melt temperature profiles in extrusion process using single screw plastics extruder. *Plastics, Rubber and Composites*. **32**(5),pp.187–192.

Rauwendaal, C. et al. 1998. A New dispersive mixer for Single Screw Extruders *In*: *SPE-ANTEC.*, pp. 277–283.

Rauwendaal, C. 1989. An improved analytical melting theory. *Advances in Polymer Technology*. **9**(4),pp.331–336.

Rauwendaal, C. 2010. *How to get peak performances & efficiency out of your extrusion line, part I.*

Rauwendaal, C. 2001. *Polymer Extrusion* 4th Ed. Hanser Gardner Publications,Inc., Cincinnati, Ohio, USA.

Rauwendaal, C. 1994. *Polymer Extrusion* 3rd Ed. Hanser Gardner Publications, Inc., Cincinnati, Ohio, USA.

Rauwendaal, C. 1987. Scale-up of single screw extruders. *Polymer Engineering & Science*. **27**(14),pp.1059–1068.

Rauwendaal, C. 2012. *The role of screw design in efficient extrusion of medical devices* [online]. Available from: http://www.ptonline.com/articles/the-role-of-screw-design-in-efficient-extrusion-of-medical-devices.

Rauwendaal, C. and Ponzielli, G. 2003. *Temperature development in screw extruders* [online]. Available from: http://www.rauwendaal.com/.

Reliance 2012. *Extrusion Principles* [online]. Mumbai, India. Available from: http://www.ril.com/downloads/pdf/extrusion principles.pdf.

Rios, A.C. et al. 2000. Experimental and numerical study of rhomboidal mixing sections. *International Polymer Processing*. **15**(1),pp.12–19.

Sabota, K.D. et al. 1995. Advanced temperature measurements in polymer extrusion *In*: *SPE-ANTEC.*, p. 2832.

Salminen, P. 2013. Using recycled polyethylene terephthalate (PET) in the production of bottle trays. PhD thesis, Arcada.

Saltuk, I. et al. 1972. Energy transport to molten flowing polymer systems: I. Development of an apparatus to obtain temperature profiles. *Polymer Engineering and Science*. **12**(6),pp.397–401.

Schenkel, G. 1978. Extruder Series with Variable L/D ratios. *Kunststoffe*. **68**,pp.155–162.

Scott.Blair, G.. et al. 1939. The flow of cream through narrow glass tubes. *Journal of Physical Chemistry*. **43**(7),pp.853–867.

Shapiro, J. et al. 1976. Melting in single screw extruders. *Polymer*. **17**(10),pp.905–918.

Shen, X. et al. 1992. An experimental evaluation of melt temperature sensors for thermoplastic extrusion *In*: *SPE-ANTEC*., pp. 918–926.

Steward, E. 2002. Barrier Screws, their history and their function *In*: *SPE-ANTEC*., pp. 69–73.

Street, L.F. 1961. Plastifying extrusion. *International Plastics Engineering*. **1**,pp.289–296.

Tadmor, Z. 1966. Fundamentals of Plasticating Extrusion. *Polymer Engineering and Science*. **6**,pp.185–190.

Tadmor, Z. et al. 1967. Melting in plasticating extuders theory and experiments. *Polymer Engineering & Science*. **7**(3),pp.198–217.

Tadmor, Z. and Gogos, C.G. 2006. *Principles of Polymer Processing* 2nd Ed. (John Wiley & Sons, ed.).

Tadmor, Z. and Klein, I. 1970. *Engineering principles of plasticating extrusion*. Van Nostrand Reinhold Co., New York, USA.

TU Braunschweig 2015. *Differential Scanning Calorimetry (DSC)* [online]. Available from: http://www.itc.tu-bs.de/Abteilungen/Makro/Methods/dsc.htm.

Tutco 2015. Thermocouples. Available from: http://www.tutco.com/temperature_sensors/thermocouples.php.

Verma, R. et al. 1990. Some studies on melt flow behaviour of poly(ethylene terephthalate). *Indian Journal of Fibre & and Textile Research*. **16**,pp.39–45.

Vlachopoulos, J. and Struut, D. 2003. Overview Polymer Processing. *Materials Science and Engineering*. **19**,p.1161.

White, J.L. and Potente, H. 2003. *Screw Extrusion: Science and Technology (Progress in Polymer Processing* (Hanser Gardner Publ, ed.).

Wilczyński, K. 1996. A Computer Model for Single-Screw Plasticating Extrusion. *Polymer-Plastics Technology and Engineering*. **35**(3),pp.449–477.

Wilczyñski, K. 2001. SSEM: a computer model for a polymer single-screw extrusion. *Journal of Materials Processing Technology*. **109**(3),pp.308–313.

Womer, T.W. 2000. Basic Screw geometry "Things your screw designer never told you about screw designs" *In*: *SPE-ANTEC.*, p. 112.

Wong, A.C.-Y. et al. 2000. Visualization studies on the comparison of mixing characteristics of single-screws having different mixing elements. *Advances in Polymer Technology*. **19**(1),pp.1–13.

Wood, A.K. 1996. UK Patent GB2,291,197.

Yang, Y. 2008. Temperature distribution measurement and control of extrusion process by tomography *In*: *IEEE International Workshop on Imaging Systems and Techniques.*, pp. 170–174.

Yasuda, K. 1979. Investigation of the analogies between viscometric and linear viscoelastic properties of polystyrene fluids (Ph.D. Thesis).

Yazbak, G. and Diraddo, R.W. 1993. An inside look at extrusion melt temperatures. *Plastics Technology*. **39**(6),pp.61–66.

Yazbaz, G. and Diraddo, R.W. 1993. An inside look at extrusion melt temperatures. *Plastics Technology*.

Yi, B. and Fenner, R.T. 1976. Scaling up Plasticating Screw Extruders on the Basic of Simular Melting Performances. *Plastics and Rubber Processing*. **1**,pp.119–123.

Zatloukal, M. and Musil, J. 2009. Analysis of entrance pressure drop techniques for extensional viscosity determination. *Polymer testing*. **28**,pp.843–853.

Závadský, E. and Karniš, J. 1985. Mathematical model of a single-screw plasticating extruder. *Rheologica Acta*. **24**(6),pp.556–565.

Zhu, F. and Chen, L. 1991. Studies on the theory of single screw plasticating extrusion. Part I: A new experimental method for extrusion. *Polymer Engineering & Science*. **31**(15),pp.1113–1116.

Appendix A

A.1 Raw Material Data Sheet

A.1.1 LDPE

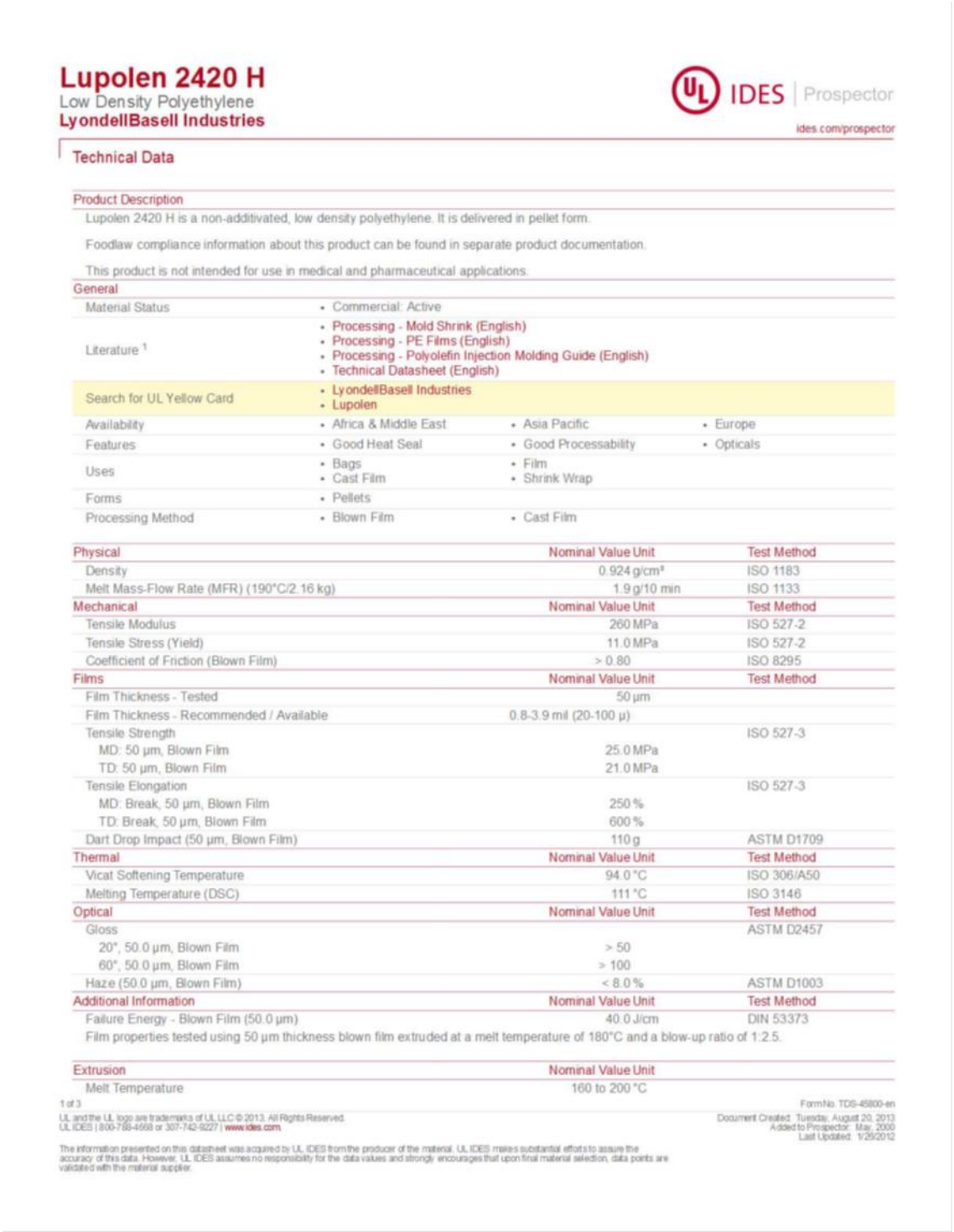

Lupolen 2420 H
Low Density Polyethylene
LyondellBasell Industries

UL IDES | Prospector
ides.com/prospector

Technical Data

Product Description
Lupolen 2420 H is a non-additivated, low density polyethylene. It is delivered in pellet form.
Foodlaw compliance information about this product can be found in separate product documentation.
This product is not intended for use in medical and pharmaceutical applications.

General			
Material Status	• Commercial: Active		
Literature [1]	• Processing - Mold Shrink (English) • Processing - PE Films (English) • Processing - Polyolefin Injection Molding Guide (English) • Technical Datasheet (English)		
Search for UL Yellow Card	• LyondellBasell Industries • Lupolen		
Availability	• Africa & Middle East	• Asia Pacific	• Europe
Features	• Good Heat Seal	• Good Processability	• Opticals
Uses	• Bags • Cast Film	• Film • Shrink Wrap	
Forms	• Pellets		
Processing Method	• Blown Film	• Cast Film	

Physical	Nominal Value Unit	Test Method
Density	0.924 g/cm³	ISO 1183
Melt Mass-Flow Rate (MFR) (190°C/2.16 kg)	1.9 g/10 min	ISO 1133
Mechanical	**Nominal Value Unit**	**Test Method**
Tensile Modulus	260 MPa	ISO 527-2
Tensile Stress (Yield)	11.0 MPa	ISO 527-2
Coefficient of Friction (Blown Film)	> 0.80	ISO 8295
Films	**Nominal Value Unit**	**Test Method**
Film Thickness - Tested	50 µm	
Film Thickness - Recommended / Available	0.8-3.9 mil (20-100 µ)	
Tensile Strength		ISO 527-3
MD: 50 µm, Blown Film	25.0 MPa	
TD: 50 µm, Blown Film	21.0 MPa	
Tensile Elongation		ISO 527-3
MD: Break, 50 µm, Blown Film	250 %	
TD: Break, 50 µm, Blown Film	600 %	
Dart Drop Impact (50 µm, Blown Film)	110 g	ASTM D1709
Thermal	**Nominal Value Unit**	**Test Method**
Vicat Softening Temperature	94.0 °C	ISO 306/A50
Melting Temperature (DSC)	111 °C	ISO 3146
Optical	**Nominal Value Unit**	**Test Method**
Gloss		ASTM D2457
20°, 50.0 µm, Blown Film	> 50	
60°, 50.0 µm, Blown Film	> 100	
Haze (50.0 µm, Blown Film)	< 8.0 %	ASTM D1003
Additional Information	**Nominal Value Unit**	**Test Method**
Failure Energy - Blown Film (50.0 µm)	40.0 J/cm	DIN 53373
Film properties tested using 50 µm thickness blown film extruded at a melt temperature of 180°C and a blow-up ratio of 1:2.5.		

Extrusion	Nominal Value Unit
Melt Temperature	160 to 200 °C

Form No. TDS-45800-en
Document Created: Tuesday, August 20, 2013
Added to Prospector: May, 2000
Last Updated: 1/25/2012

A.1.2 LLDPE

Flexirene® CL 10

Linear Low Density Polyethylene

Versalis S.p.A.

UL IDES | Prospector

ides.com/prospector

Technical Data

Product Description

Flexirene® CL 10 is a butene copolymer linear low density polyethylene (C4-LLDPE), with antioxidants, suitable for cast extrusion of thin film with high optical properties.

Flexirene® CL 10 is recommended for the production of stretch film to be used both in manual and in automatic wrapping machines. In a multilayer film, Flexirene® CL 10 enhances the optical properties of the global formulation; moreover, for its high processability, the resin is recommended whenever high productivity has to be reached.

General			
Material Status	• Commercial: Active		
Literature [1]	• Technical Datasheet (English)		
Availability	• Europe	• North America	
Additive	• Antioxidant		
Features	• Antioxidant • Butene Comonomer	• Copolymer • Fast Molding Cycle	• Food Contact Acceptable • Opticals
Uses	• Film	• Multilayer Film	• Stretch Wrap
Agency Ratings	• EU Food Contact, Unspecified Rating		
Forms	• Pellets		
Processing Method	• Cast Film		

Physical	Nominal Value	Unit	Test Method
Density	0.918	g/cm³	ISO 1183
Melt Mass-Flow Rate (MFR) (190°C/2.16 kg)	2.6	g/10 min	ISO 1133
Mechanical	**Nominal Value**	**Unit**	**Test Method**
Coefficient of Friction			ISO 8295
vs. Itself - Dynamic, Cast Film	> 0.50		
Films	**Nominal Value**	**Unit**	**Test Method**
Film Thickness - Tested	23	µm	
Film Thickness - Recommended / Available	10 to 50	µm	
Tensile Modulus			ISO 527-3
1% Secant, MD: 23 µm, Cast Film	90.0	MPa	
1% Secant, TD: 23 µm, Cast Film	105	MPa	
Tensile Stress			ISO 527-3
MD: Yield, 23 µm, Cast Film	9.00	MPa	
TD: Yield, 23 µm, Cast Film	8.00	MPa	
MD: Break, 23 µm, Cast Film	35.0	MPa	
TD: Break, 23 µm, Cast Film	25.0	MPa	
Tensile Elongation			ISO 527-3
MD: Break, 23 µm, Cast Film	600	%	
TD: Break, 23 µm, Cast Film	800	%	
Dart Drop Impact [3] (23 µm, Cast Film)	100	g	ISO 7765-1
Elmendorf Tear Strength [4]			ISO 6383-2
MD: 23.0 µm	38.0	kN/m	
TD: 23.0 µm	103.0	kN/m	
Thermal	**Nominal Value**	**Unit**	**Test Method**
Brittleness Temperature	< -70.0	°C	ASTM D746
Vicat Softening Temperature	97.0	°C	ISO 306/A
Melting Temperature	121	°C	Internal Method
Optical	**Nominal Value**	**Unit**	**Test Method**
Gloss (45°, 23.0 µm, Cast Film)	91		ASTM D2457
Haze (23.0 µm, Cast Film)	2.0	%	ISO 14782

Form No. TDS-15307-en
Document Created: Tuesday, August 20, 2013
Added to Prospector: November, 1995
Last Updated: 8/9/2011

Extrusion	Nominal Value	Unit
Melt Temperature	220 to 270	°C

Notes

[1] These links provide you with access to supplier literature. We work hard to keep them up to date; however you may find the most current literature from the supplier.

[2] Typical properties: these are not to be construed as specifications.

[3] F50

[4] Cast Film

Form No. TDS-15307-en
Document Created: Tuesday, August 20, 2013
Added to Prospector: November, 1995
Last Updated: 8/9/2011

A.1.3 HD5050

Rigidex® HD5050EA

Product Technical Information

Rigidex® HD5050EA is a high density polyethylene copolymer grade with a narrow molecular weight distribution, specially developed for injection and compression moulding applications requiring high environmental stress cracking resistance

Typical applications

- Caps & closures – non beverages
- Beverages over-caps
- Technical parts
- Bins
- Crates, boxes, household items

Benefits and Features

- Good environmental stress cracking resistance
- High impact strength
- Low warpage
- Slip agent free grade

Properties		Test Methods	Values	Units
Physical				
Density		ISO 1872	950	kg/m³
Melt Flow Rate	2.16 kg load	ISO 1133	4	g/10min
Mechanical				
Tensile Modulus		ISO 527 -1&2 (1B)	1100	MPa
Tensile Strength	@ Yield	ISO 527 -1&2 (1B)	25	MPa
Charpy Impact Strength, 23°C		ISO 179	5.5	kJ/m²
Environmental Stress Cracking Resistance (ESCR)		ASTM 1693, 23°C	170	h

The values given are typical values measured on the product. These values should not be considered as specification

February, 2008

Published by
INEOS Polyolefins

A.1.4 HD6007

Rigidex® HD6007S

Product Technical Information

Rigidex® HD6007S is a medium molecular weight polyethylene grade supplied in pellet form for use in a wide range of blow moulding and extrusion applications.

Typical applications

- Lightweight containers produced at high speeds, e.g. bottles for packaging powders, milk and chemical products which have a low environmental stress cracking activity

Benefits and Features

- Very easy processing
- High rigidity
- Good surface finish

Properties		Test Methods	Values	Units
Physical				
Density (annealed)		ISO 1872	962	kg/m³
Melt Flow Rate	2.16 kg load	ISO 1133	0.6	g/10min
Mechanical				
Tensile Strength @ yield (23°C, Type 2 Speed D)		ISO 527	30.5	MPa
Elongation @ break (23°C, Type 2 Speed D)		ISO 527	> 300	%
Flexural Modulus (23°C @ 100 mm/min)		ISO 178	1700	MPa
Charpy Impact Strength		ISO 179	8	kJ/m²
BTT stress crack resistance (F50 @ 50°C, 100% concentration)		ASTM 1693-97a	20	hours
Bottle stress crack resistance (60°C)		INEOS Method	1	hours

The values given are typical values measured on the product. These values should not be considered as specification

April, 2010

Published by
INEOS Olefins & Polymers Europe

A.1.5 HD5411

Rigidex® HM5411EA

Product Technical Information

Rigidex® HM5411EA is a high molecular weight copolymer grade supplied in pellet form for medium and large blow moulding applications where a combination of high environmental stress cracking resistance and good rigidity is required.

Typical applications

- High performance blow moulded containers typically of 1-60 litres capacity for packaging aggressive products
- Robust industrial and technical mouldings

Benefits and Features

- Very high environmental stress crack resistance
- Good rigidity
- High melt strength
- High impact strength

Properties		Test Methods	Values	Units
Physical				
Density (annealed)		ISO 1872/1-1993	952	kg/m³
Melt Flow Rate	21.6 kg load	ISO 1133-1997 cond. G	10	g/10min
Mechanical				
Tensile Strength @ yield (23°C, Type 2 Speed D)		ISO 527-2:1996	26	MPa
Elongation @ break (23°C, Type 2 Speed D)		ISO 527-2:1996	> 300	%
Flexural Modulus (23°C @ 100 mm/min)		ISO 178-1997	1100	MPa
Charpy Impact Strength		ISO 179-1982	23	kJ/m²
BTT stress crack resistance:				
- 100% Adinol 50°C		ASTM 1693-97a	> 1000	hours
- 10% Adinol 50°C		ASTM 1693-97a	130	hours
Bottle stress crack resistance (60°C)		INEOS Method	50	hours

The values given are typical values measured on the product. These values should not be considered as specification

July, 2008

Published by
INEOS Polyolefins

A.1.6 PP

lyondellbasell

Moplen HP640J

Polypropylene, Homopolymer

Product Description

Moplen HP640J is a nucleated homopolymer for extrusion and thermoforming applications. *Moplen* HP640J exhibits a good stiffness and transparency.
The main applications of *Moplen* HP640J are fruit baskets, trays, transparent drinking cups and containers. *Moplen* HP640J is a developmental grade

Product Characteristics

Status	Commercial: Active
Test Method used	ISO
Availability	Europe, Africa-Middle East
Processing Method	Extrusion Thermoforming
Typical Customer Applications	Housewares

Typical Properties	Method	Value	Unit
Physical			
Density	ISO 1183	0.9	g/cm³
Melt flow rate (MFR) (230°C/2.16Kg)	ISO 1133	3.2	g/10 min
Melt volume flow rate (230°C/2.16Kg)	ISO 1133	4.3	cm³/10min
Mechanical			
Tensile Modulus	ISO 527-1, -2	1600	MPa
Tensile Stress at Yield	ISO 527-1, -2	37	MPa
Tensile Strain at Break	ISO 527-1, -2	>50	%
Tensile Strain at Yield	ISO 527-1, -2	9	%
Impact			
Charpy unnotched impact strength (23 °C, Type 1, Edgewise)	ISO 179	190	kJ/m²
Charpy notched impact strength (23 °C, Type 1, Edgewise, Notch A)	ISO 179	4	kJ/m²
Hardness			
Ball indentation hardness (H 358/30)	ISO 2039-1	78	MPa
Thermal			
Heat deflection temperature B (0.45 MPa) Unannealed	ISO 75B-1, -2	90	°C
Vicat softening temperature (A50 (50°C/h 10N))	ISO 306	154	°C
(B50 (50°C/h 50N))		94	°C
Optical			
Haze (1 mm)	ASTM D 1003	30	%

A.1.7 PS

PRODUCT INFORMATION

STYROLUTION

Styrolution PS 124N

GENERAL PROPERTIES

Styrolution PS 124N is a general purpose polystyrene grade with a good flow characteristic and an improved heat resistance.

PHYSICAL PROPERTIES (TYPICAL VALUES)

Property	Value	Unit	Standard	Method
Volume melt-flow rate MVR	**12**	$cm^3/10$ min	ISO 1133	200 °C/5 kg
Vicat softening temperature VST	**87**	°C	ISO 306	B50/oil
Charpy impact strength at 23 °C	**10**	kJ/m^2	ISO 179	1eU
Tensile stress at break	**50**	MPa	ISO 527-2	50 mm/min
Nominal strain at break	**2**	%	ISO 527-2	50 mm/min
Tensile modulus	**3200**	MPa	ISO 527-2	1 mm/min
Flexural strength	**80**	MPa	ISO 178	2 mm/min
Ball indentation hardness H	**150**	N/mm^2	ISO 2039-1	358 N/30 s
Density	**1040**	kg/m^3	ISO 1183	
Water absorption (after 24 h)	**< 0.1**	%	ISO 62	
Temp. of deflection under load HDT/A	**78**	°C	ISO 75-2	1.8 MPa
Thermal conductivity	**0.16**	W/m·K	DIN 52 612	
Mean therm. coefficient of linear expansion	**$0.8 \cdot 10^{-4}$**	K^{-1}	DIN 53 752	(23 - 80)°C
Processing shrinkage	**0.4-0.6**	%	ISO 294-4	

PROCESSING

Styrolution PS 124N can be processed by all methods normally used for polystyrene. It is well balanced in its flow characteristic and heat resistance and is so used preferably for injection moulding. It can be extruded as a blend component with high impact grades and as a gloss layer of thermoformed foils and sheets.

EXAMPLES OF APPLICATION

Screw caps, cups, containers, sorting boxes, display stands, Petri dishes, cuvettes, pipettes, record and cassette stands.

Styrolution Group GmbH
Info@styrolution.com, www.styrolution.com

Driving Success. Together.

A.1.8 PET

TERGAL INDUSTRIES

POLYESTER POLYMER

T74F9 0.80 / Item code PF00040

CAS: N°25038-59-9

CHARACTERISTICS:

⇒ Product description	White granulates
⇒ Melt point	Approx 252 °C
⇒ Bulk density	Approx 0, 83 g/cm3
⇒ Density	Approx 1, 40 g/cm3

SPECIFICATIONS

			METHODS
⇒	INTRINSIC VISCOSITY (dl/g)	0.80 ± 0.02	05 - Poly. 3K - 310
⇒	COLOR L*	≥ 81	05 - Poly. 3K - 250
⇒	a*	-2≤a≤0	05 - Poly. 3K - 250
⇒	b*	b<1	05 - Poly. 3K - 250
⇒	ACETALDEHYDE (ppm)	≤1	05 - Poly. 3K - 230
⇒	Carboxylic End Groups (meq/t)	≤ 60	05 - Poly. 3K - 140
⇒	Diethylene Glycol (%)	≤ 2	05 - Poly. 3K - 280
⇒	Weight of 100 chips	1, 4 g ± 0, 1	05 - Poly. 3K - 300

CONDITIONING AND TRANSPORT
⇒ Big Bags of 1100kg or road-tanker

STOCKHOLDING
⇒ Keep stock protected from humidity

USES
⇒ Bottles, films, yarns, fibres

HYGIENE AND SAFETY ⇒ This product presents no particular toxic features

TRANSPORT REGULATIONS
⇒ Not applicable

PRODUCTION SITE ⇒ 02 430 GAUCHY / FRANCE

The information contained in this notice is based on the state of our knowledge of the product concerned at the issue date of the notice. The information is given in good faith and does not constitute a guarantee on our part. It is only offered as an indication, except for the actual specifications. It ought not, in any case, to be a substitute for evaluation trials which the user should out to verify, on each situation, its acceptability for the intended end use.
Our services are at your disposal to give you all additional information and offer you our documentation. We reserve the right to carry out technical modifications to the product.

Appendix B

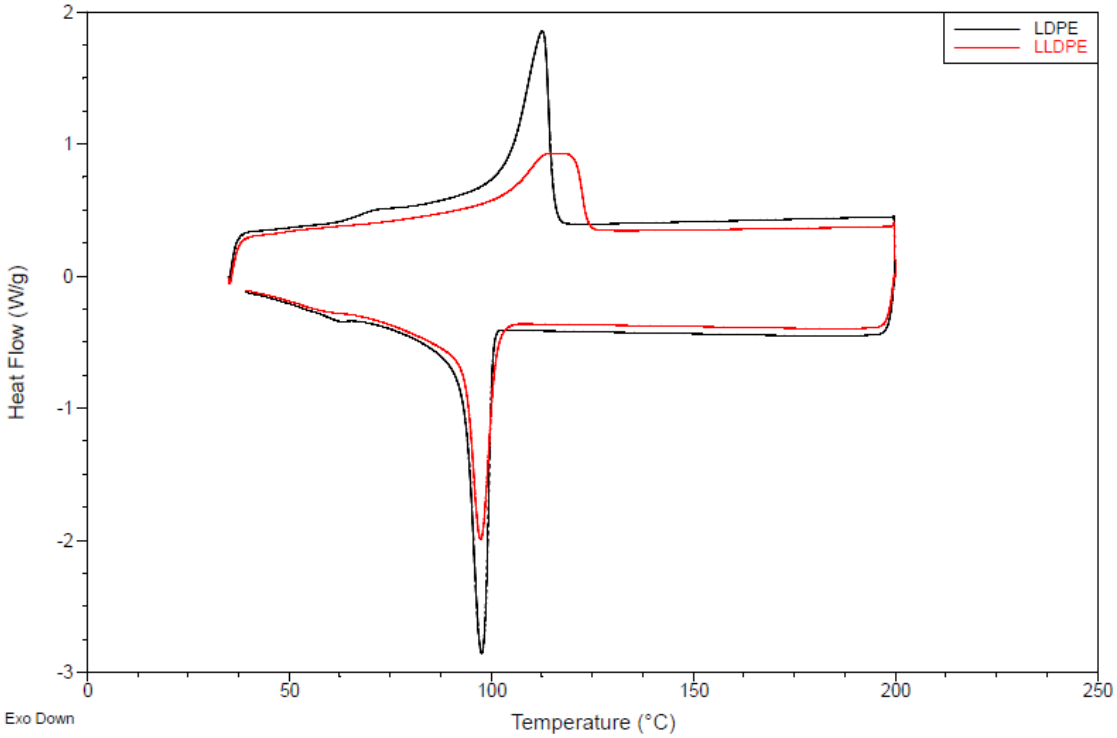

Figure B1 DSC curves for LDPE and LLDPE

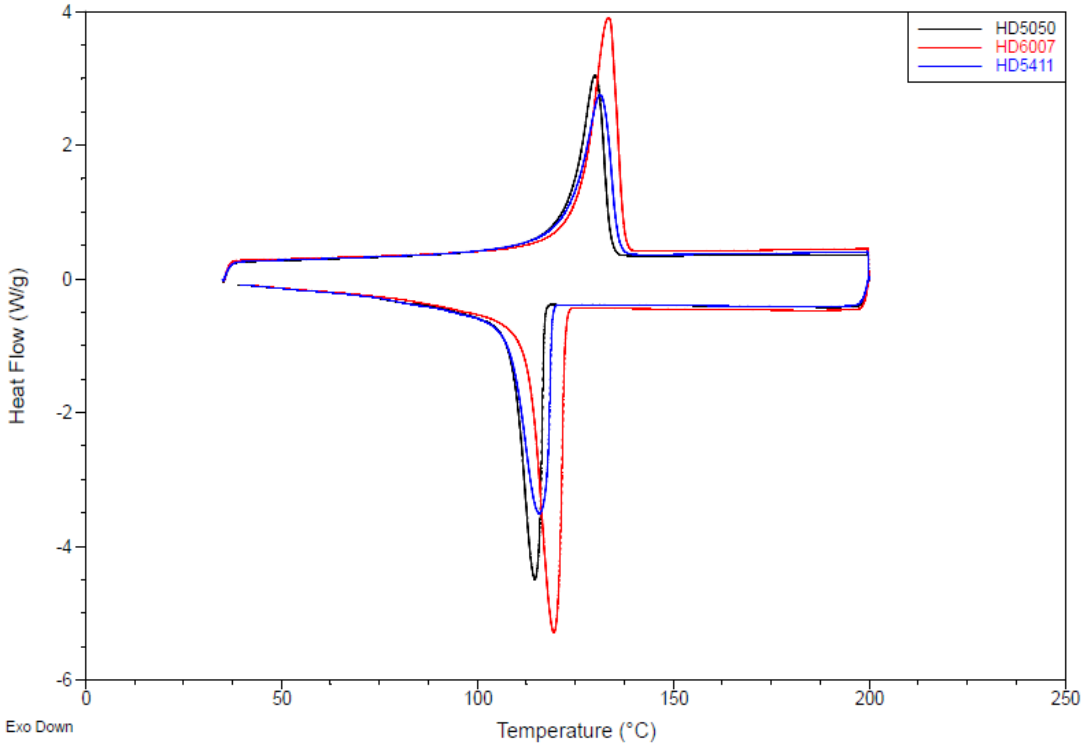

Figure B2 DSC curves for the three grades of HDPE

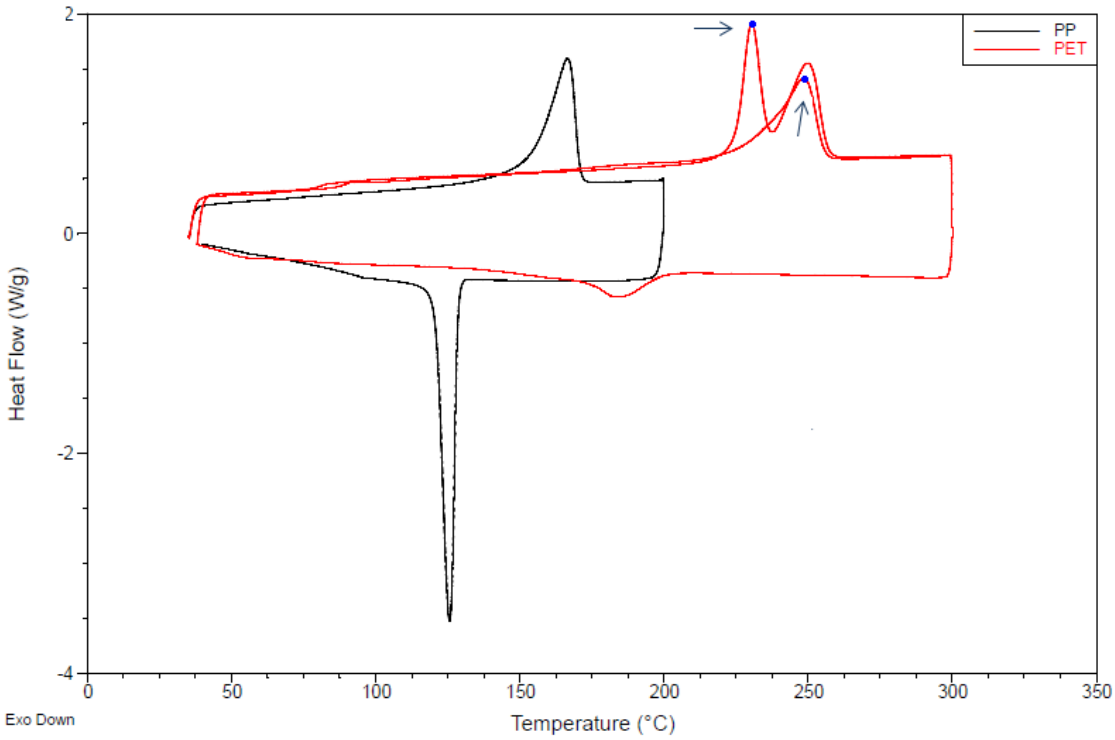

Figure B3 DSC curves for PP and PET (arrows indicate double melting endotherm behaviour)

Appendix C

C.1 Melt pressure variation

C.1.1 LDPE

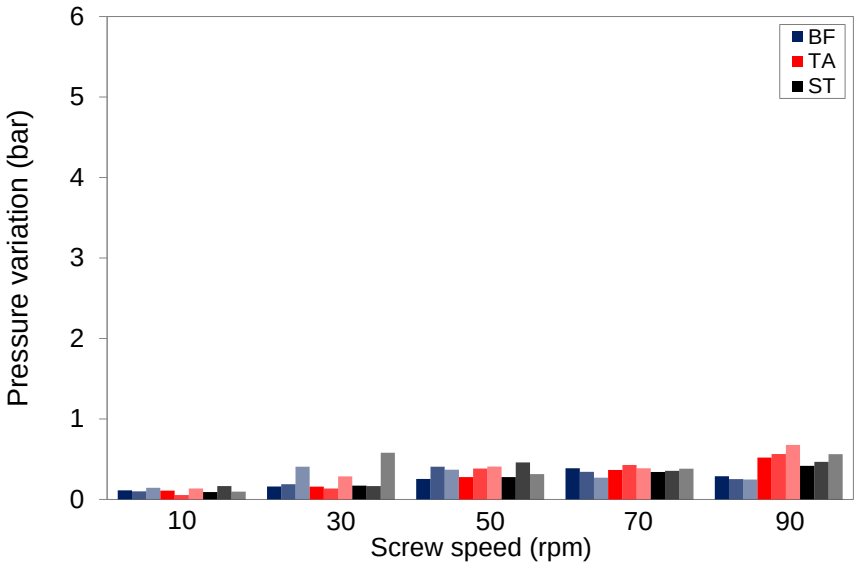

Figure C1 Melt pressure variation (max value-min value) for LDPE (dark colours represent 220°C, medium 200°C and light 180°C) and (BF: Barrier Flighted Screw; TA: Tapered Compression Screw; ST: Stepped Compression Screw)

C.1.2 LLDPE

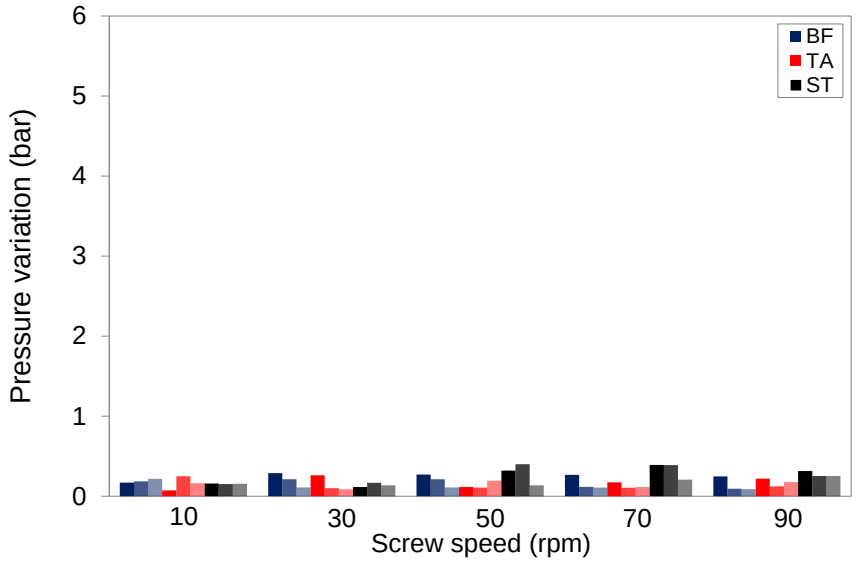

Figure C2 Melt pressure variation (max value-min value) for LLDPE (dark colours represent 220°C, medium 200°C and light 180°C) and (BF: Barrier Flighted Screw; TA: Tapered Compression Screw; ST: Stepped Compression Screw)

C.1.3 HDPE

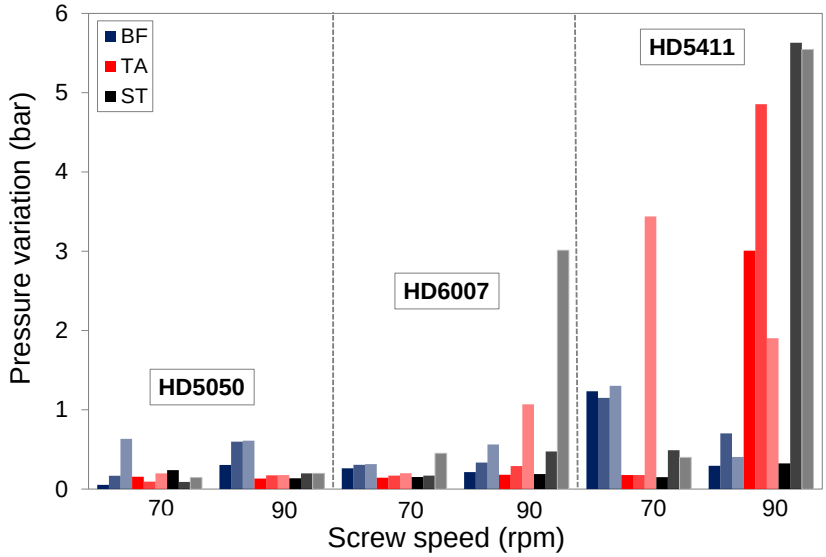

Figure C3 Melt pressure variation (max value-min value) for all grades of HDDPE (dark colours represent 220°C, medium 200°C and light 180°C) and (BF: Barrier Flighted Screw; TA: Tapered Compression Screw; ST: Stepped Compression Screw)

C.1.4 PP

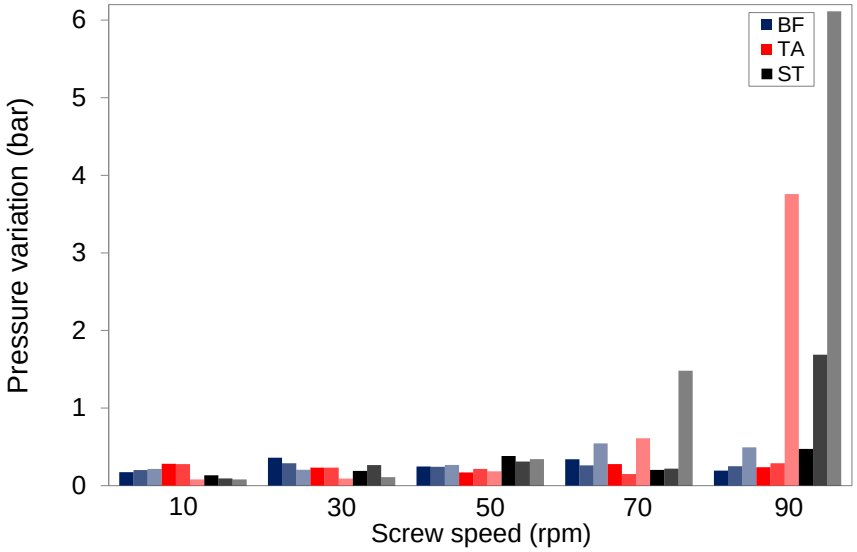

Figure C4 Melt pressure variation (max value-min value) for PP (dark colours represent 240°C, medium 220°C and light 200°C) and (BF: Barrier Flighted Screw; TA: Tapered Compression Screw; ST: Stepped Compression Screw)

C.1.5 PS

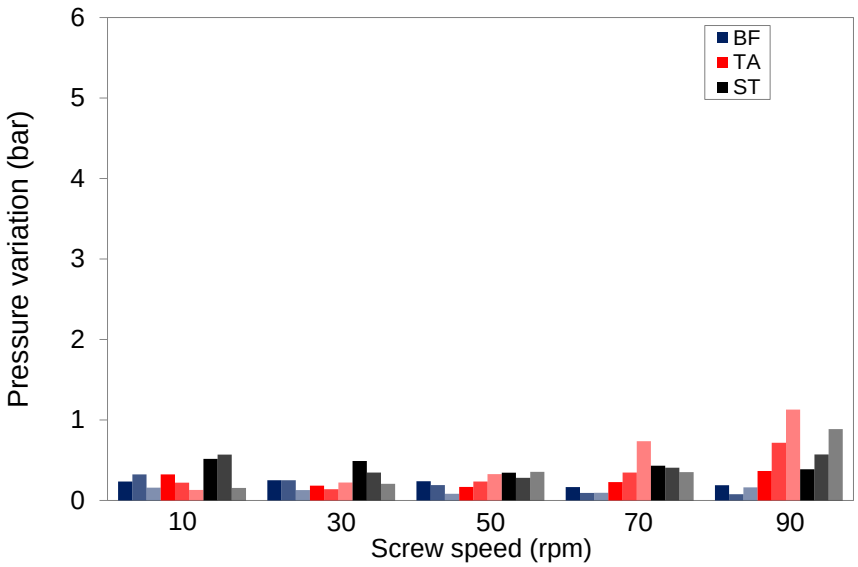

Figure C5 Melt pressure variation (max value-min value) for PS (dark colours represent 220°C, medium 200°C and light 180°C) and (BF: Barrier Flighted Screw; TA: Tapered Compression Screw; ST: Stepped Compression Screw)

C.1.6 PET

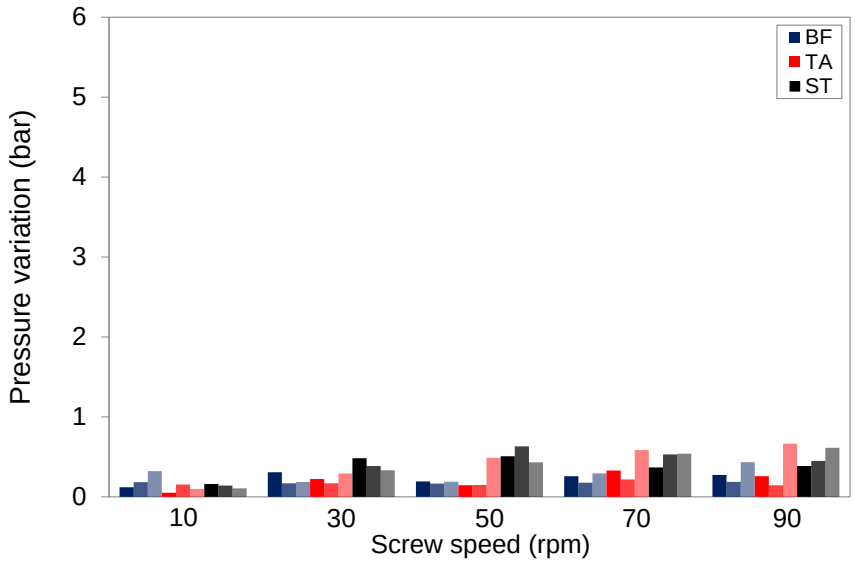

Figure C6 Melt pressure variation (max value-min value) for PET (dark colours represent 220°C, medium 200°C and light 180°C) and (BF: Barrier Flighted Screw; TA: Tapered Compression Screw; ST: Stepped Compression Screw)

Appendix D

D.1 Energy consumption required by the motor for PET

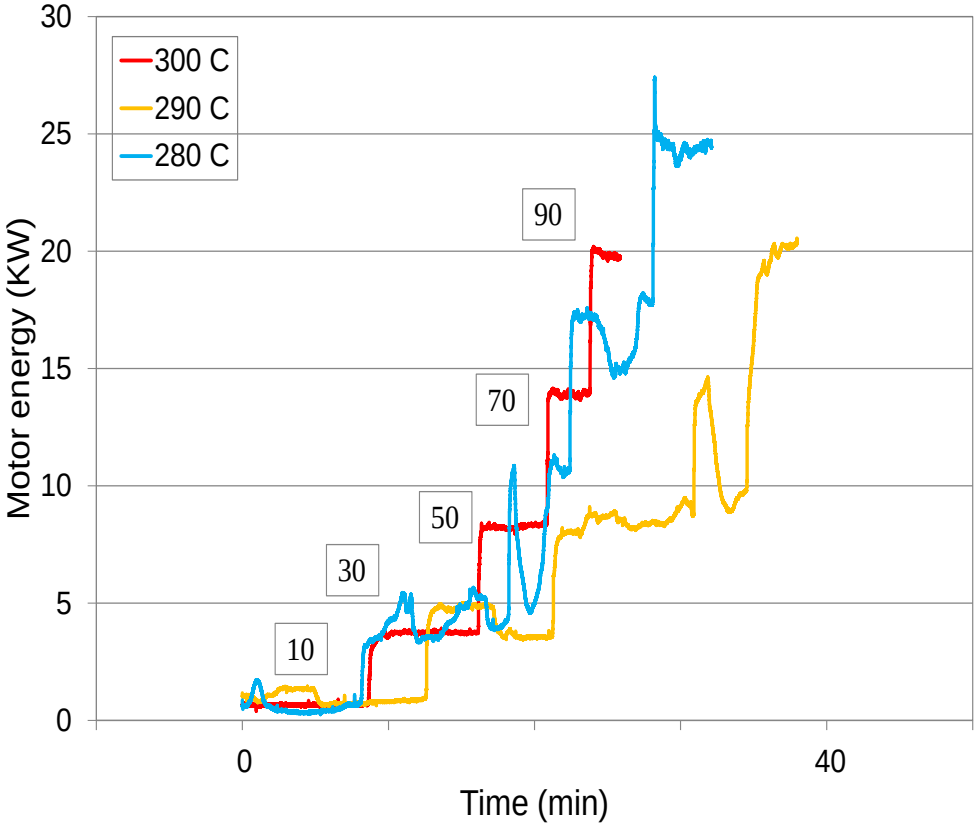

Figure D1 Motor energy consumption for PET (kW)